Synthesis, structural analysis, and assembly of water soluble quinoline-based oligoamide foldamers

Xiaobo Hu

université de BORDEAUX

THÈSE PRÉSENTÉE
POUR OBTENIR LE GRADE DE

DOCTEUR DE
L'UNIVERSITÉ DE BORDEAUX

ÉCOLE DOCTORALE DES SCIENCES CHIMIQUES
SPÉCIALITÉ : CHIMIE ORGANIQUE

Par Xiaobo HU

Synthèse, analyses structurales et assemblage de foldamères oligoamide hydrosolubles à base de quinolines

Sous la direction de : Dr. Ivan HUC

Soutenue le 15 Juin 2017

Membres du jury :

Mme. ALEZRA, Valérie	Maître de Conférences, Université Paris Sud	Rapporteur
M. DAWSON Simon	Consultant, IDBS	Examinateur
Mme. FISCHER, Lucile	Chargée de recherche, CNRS	Examinateur
M. GUICHARD, Gilles	Directeur de recherche, CNRS	Président
M. HUC, Ivan	Directeur de recherche, CNRS	Directeur de these
M. WILSON, Andrew	Professeur, University of Leeds	Rapporteur

Acknowledgement

First I want to thank my supervisor, Dr. Ivan Huc, who has motivated and inspired me in the past years. As a supervisor, he taught me how to lead a project from very beginning the idea germination to the end manuscript preparation. As a guide, he brought me into the field of foldamer chemistry where I learned new knowledge and expanded the scope of my view. As an advisor, he could always give helpful suggestions which encouraged me to overcome those difficulties in the lab. These precious experience and knowledge are truly the best gift to me and, for sure, I will gain a lot from this in my future career.

Then, I'd like to thank my unofficial supervisor, Dr. Simon Dawson, who is special and meaningful to my PhD life. He is also so kind and full of knowledge. He helped me settle down in Bordeaux, guided me to be familiar with lab and projects, taught me thinking and writing, and most importantly he was always my backing. I still remember that year I just arrived Bordeaux and I told my family and friends "don't worry about my living in France". Thanks to Simon, I could always be confident to say so.

I also want to thank my co-supervisor Dr. Lucile Fischer who helped me finish my PhD thesis and gave me suggestions. Thank Dr. Yann Ferrand who helped me a lot and from whom I also learned a lot, especially molecular modeling. Thank Dr. Pradeep Mandal who spent lot of efforts to help me grow crystals and obtain crystal structures of my projects. Thank Dr. Xiang Wang and Dr. Xuesong Li who gave me help, fun and happiness. They all played important roles in my whole PhD life.

Besides, I thank all the members in Huc Group, previous and present, and all the individuals who helped me. Especially, Victor, Eric, Sunbum, Markandeya, Subrata, Panchami, Valentina, Maëlle, Antoine Meunier, Antoine Jacquet, Michal, Mohamed Elsawy, Makoto, Yui, Christos, Laure, Guillaume, Barbara, and Brice, Axelle, Estelle, Frédéric, Loïc, Cameron, and Jinhua, Siyuan, Nan (these Chinese names come last letting you know the last doesn't at all mean the least).

At last, my wife, Yan Cai, without whom I cannot image the life abroad. She sacrificed her time and otherwise a promising career to come with me and has always been accompanying me for the past years in France. She showed her patience and optimism. She gave me with her understanding and supporting. There are always not enough words to express my gratitude and love to my wife.

Contents

Introduction

Foldamer chemistry is a rapidly expanding research field. A main target of this field is to explore the construction of various artificial architectures that mimic the folded structure of biopolymers found in nature. Up to now, many artificial architectures derived from a large variety of backbones are able to adopt secondary structures to mimic those protein secondary structures found in nature, such as α-helices and β-sheets, and also their ability to create other structures not existent in nature, such as knots and tailbiters. Foldamers are a promising class of biological mimics considering not only the ability of mimicking protein secondary structures but also those biological applications achieved in this field, such as acting as protein inhibitors and mimicking enzymes to catalyze a chemical reaction. Moreover, their applications in materials, such as forming nanofibers and liquid crystals, show the ability of foldamers to possess functionalities beyond the scope of nature. All the knowledge from the studies of these artificial objectives is extremely helpful in understanding the similar processes happened in nature.

Quinoline oligoamide foldamers are an important branch of foldamers. They have been shown to possess many desirable features. They are medium sized (0.5-5.0 kDa), resistant to proteolytic degradation, conformationally stable in a wide range of solvents and in particular in water even at high temperatures, and most importantly, they adopt well-defined, predictable conformations. Towards biological functionalizations and mimics, they are able to interact with protein surfaces, afford high affinity for G-quadruplex DNA, possess cell-penetrating properties, and mimic protein tertiary structures. Due to the stability and predictability of quinoline oligoamide foldamer frames, controlled spatial organization of α-amino acid side chains can be achieved by incorporating α-amino acids into quinoline oligoamide foldamers. In addition, based on these quinoline related foldamers, some sophisticated structures are also achieved, including double helix and foldaxanes.

Up to now, most studies of quinoline-based oligoamide foldamers are carried out in organic solvents. This thesis aimed to expand their scope in aqueous medium and presents several methodologies to achieve solubility, folding, side-chain variation, aggregation and crystal growth ability in water. These studies are expected to have a general merit and influence for the further researches of quinoline-based oligoamide foldamers in water.

Chapter one is a short review of aromatic oligoamide foldamers. It briefly introduces the history of foldamer chemistry and focus on the introduction of aromatic oligoamide foldamers. From the general synthetic methodologies to the structure construction strategies, solution phase synthesis, solid phase synthesis (SPS), and different folding principles guided by hydrogen bonding are presented. From various folded conformations to the general structural elucidation techniques, those prevalent secondary structures, one case of tertiary structures, assembled architectures such as foldaxanes and helix bundles, and useful structural elucidation tools including NMR and X-ray analysis are highlighted.

In chapter two, a SPS method is developed to enable the fast access to α-amino acid/quinoline (**X**/**Q**) hybrid oligoamide foldamers. A dimer strategy is also described as a complementary method for the SPS protocol. Several water-soluble hybrid foldamers were synthesized to study their folding behavior and folded conformations in water. Through CD and NMR studies, $(\mathbf{XQ})_n$-type foldamers showed unpredictable folding behavior and ill-defined folding conformations. In contrast, $(\mathbf{XQ_2})_n$-type foldamers could adopt helical conformations and allowed linear arrangement of α-amino acid side chains in space via NMR full assignment and crystallographic analysis.

In chapter three, several short side chains were identified in order to endow aromatic foldamers with both solubility in, and crystal growth ability from water. Several synthetic routes were validated enabling the installation of these side chains onto aromatic monomers. Six quinoline oligoamides displaying these side chains were synthesized as the case study. In all cases but one, crystals were obtained from

aqueous medium. The only case that resisted crystallization was assigned to exceedingly high water solubility. These results validate the idea of using shorter and more rigid side chains to improve crystal growth ability of aromatic foldamers.

In chapter four, emphasis and efforts were put to construct self-assembled aromatic helix bundles in water. Based on hydrophobic effects and electrostatic interactions, several construction strategies were attempted. NMR and crystallographic studies in water indicated that hydrophobic effects are weaker than expected and not strongly conducive of aggregation. The high success rate of crystallization of these foldamers displaying different short side chains developed in chapter three verifies again their ability to endow aromatic foldamers with solubility in, and crystal growth ability from water.

Chapter 1

Aromatic oligoamide foldamers: a review

1. Introduction

Many subjects in chemistry are inspired by nature. The *Foldamer*[1] could be one successful case amongst the others. Since the definition[1b] of foldamer in chemistry by Samuel H. Gellman, it has been two decades. However, the existence of folding and folded structures in nature is as old as the *Origin of Life*, and these normally can be found in the biopolymers which mainly comprise polypeptides, polynucleotides and polysaccharides. In the living organisms, more often than not, folding is the key feature biopolymers have to adopt to control their molecular machinery and further to perform their chemical functions like information storage by nucleic acids and enzymatic catalysis by proteins. Thereby, the primary task of foldamers is to mimic folding processes in nature and eventually achieve functions that could match and even surpass those of nature.

Although the age of foldamer is so young comparing to the history of biopolymers, their development is not at all slow comparing to the evolution of nature. It took hundreds and thousands of years for nature to elect out a certain number of building blocks to construct structures, suitable and stable, to carry out functions. But for foldamers, after a period of twenty years, there already are many structures and functions emerging. This could be attributed to the virtually infinite number of building blocks available and unlimited imagination of humans.

The early discovery and study of foldamers came out as β-peptides.[2] At that time, to find a short-chain β-peptide being able to fold into helical structure was still an unbelievable discovery. But it was proved to be possible by Dieter Seebach and

1. a) For a book, see: S. Hecht, and I. Huc, editors. *Foldamers: structure, properties and applications.* John Wiley & Sons, **2007**. b) For reviews, see: S. H. Gellman, *Acc. Chem. Res.* **1998**, 31, 173; c) D. J. Hill, M. J. Mio, R. B. Prince, T. S. Hughes, and J. S. Moore, *Chem. Rev.* **2001**, 101, 3893; d) I. Huc, *Eur. J. Org. Chem.* **2004**, 17; e) W. S. Horne and S. H. Gellman, *Acc. Chem. Res.* **2008**, 41, 1399; f) I. Saraogi, and A. D. Hamilton, *Chem. Soc. Rev.* **2009**, 38, 1726; g) G. Guichard, and I. Huc, *Chem. Commun.* **2011**, 47, 5933; h) D.-W. Zhang, X. Zhao, J.-L. Hou, and Z.-T. Li, *Chem. Rev.* **2012**, 112, 5271.
2. a) D. Seebach, P. E. Ciceri, M. Overhand, B. Jaun, D. Rigo, L. Oberer, U. Hommel, R. Amstutz and H. Widmer, *Helv. Chim. Acta*, **1996**, 79, 2043; b) D. Seebach, K. Gademann, J. V. Schreiber, J. L. Matthews, T. Hintermann, B. Jaun, L. Oberer, U. Hommel and H. Widmer, *Helv. Chim. Acta*, **1997**, 80, 2033; c) D. H. Appella, L. A. Christianson, I. L. Karle, D. R. Powell, and S. H. Gellman, *J. Am. Chem. Soc.* **1996**, 118, 13071; d) G. P. Dado, and S. H. Gellman, *J. Am. Chem. Soc.* **1994**, 116, 1054.

co-workers.[2a-b] They synthesized a β-peptide hexamer (Figure 1a) and by NMR study found that it could fold into a left-handed helix. According to their model generated from the NMR data in deuterated pyridine, the helix has averagely three β-amino acid residues per turn and contains 14-membered H-bonded rings (3_{14} helix). Then a series of β-peptides including some "mixed" sequences (Figure 1b, only shows one of them as the example) were synthesized by the same group to study folding behavior of β-peptides. The results came out encouraging that most of the sequences folded into helical structures. An even inspiring result was that depending on the sequences they could adopt more than one secondary structure. In other words, like natural α-peptides, β-peptides also have sequence-depended structural variability. At the same time, Samuel H. Gellman group reported the crystal structure of a hexamer of *trans*-2-aminocyclo-hexanecarboxylic acid (*trans*-ACHC, Figure 1c-d)[2c] which gave an unambiguous and direct evidence of the helix formation of β-peptides. Another important aspect of this study is that due to the intrinsic rigidity of the unnatural backbone this hexamer expressed relatively high folding stability comparing to the natural α-peptides.

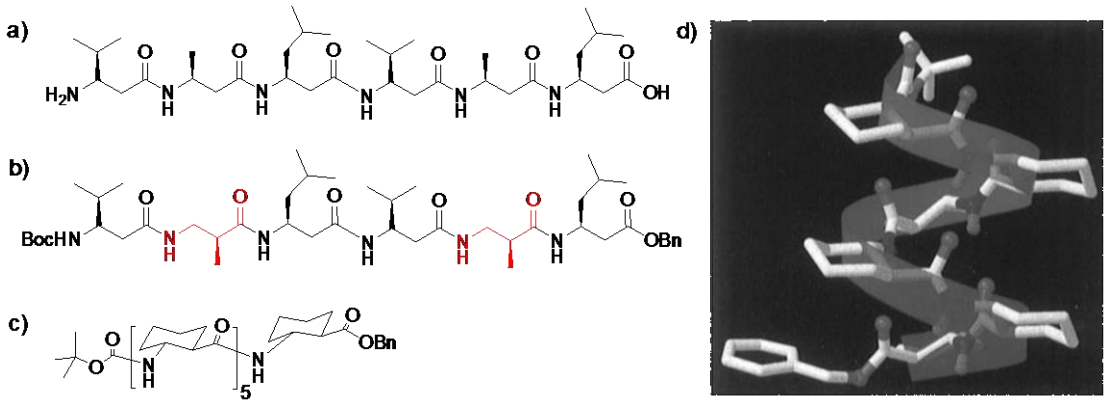

Figure 1. a) Short-chain β-peptide; b) "mixed" β-peptide; c) *trans*-2-aminocyclo-hexanecarboxylic acid hexamer and d) its crystal structure.

After that, the field of foldamers has received a great interest and thereby experienced a fast development. Nowadays, these synthetic polymers have infiltrated into almost all chemical disciplines. The family of foldamers has enlarged from

β-peptides and biotic foldamers[1c,g] to now include γ-, or δ-peptides,[1c,3] abiotic foldamers,[1c,g] and their hybrid foldamers.[1e,g-h] New connecting ways (bonds between non adjacent building blocks)[4] as well as new folding principles also came out. As a consequence, novel backbones and conformations were generated. Among those emerging topics, aromatic oligoamide foldamers,[1d,f,h] a branch of abiotic foldamers, stood out as one of the most promising classes of foldamers. Similar to biopolymers in nature, these aromatic oligoamide foldamers could also fold into different secondary structures, although the dominant conformation usually is helical. Nevertheless, there are several attractive properties making them important and distinct from their bio-analogous: a) high stability of their folded structure including in aqueous solvents, thus b) the predictability of their folding patterns; c) their ready synthetic accessibility, and d) their amenability to modifications. With these unique physical properties and folding modes that natural motifs cannot access, one can expect that they would be able to interact with biomolecules in an unforeseen and interesting way.

In this thesis, the emphasis is on the synthesis and structural study of oligoamide foldamers that are composed of aromatic or aliphatic/aromatic hybrid building blocks. Therefore, the following sections in chapter one will mainly discuss the present synthetic methods and folding structures of aromatic-related oligoamide foldamers.

3. a) D. Seebach, A. K. Beck and D. J. Bierbaum, *Chem. Biodiversity*, **2004**, 1. 1111; b) C. Baldauf, R. Gunther and H. J. Hoffmann, *J. Org. Chem.*, **2005**, 70, 5351; c) L. Szabo, B. L. Smith, K. D. McReynolds, A. L. Parrill, E. R. Morris, and J. Gervay, *J. Org. Chem.* **1998**, 63, 1074; d) X. Zhao, M. X. Jia, X. K. Jiang, L. Z. Wu, Z. T. Li and G. J. Chen, *J. Org. Chem.*, **2004**, 69, 270.
4. a) V. Semetey, D. Rognan, C. Hemmerlin, R. Graff, J.-P. Briand, M. Marraud and G. Guichard, *Angew. Chem., Int. Ed.* **2002**, 41, 1893; b) A. Salaun, M. Potel, T. Roisnel, P. Gall and P. Le Grel, *J. Org. Chem.* **2005**, 70, 6499; c) X. Liand, and D. Yang, *Chem. Commun.* **2006**, 3367.

2. Synthetic approaches of aromatic amide foldamers

2.1 Solution phase synthesis

Unlike peptides chemistry where both solution phase and solid phase synthesis are prevalent, the approach of producing aromatic amide foldamers is mainly in solution phase. Most of the time, the synthesis of aromatic oligomers in solution phase is straightforward (Figure 2a). Chemists usually employ acid chlorides as the activated intermediate to couple with aromatic amines. The carboxylic acids may also be converted to an ester form before coupling with amine. Besides, direct coupling of carboxylic acid with the amine precursors in the presence of coupling reagent is also a usual way. In solution phase synthesis, normally one end of the oligomer (either N-terminus or C-terminus) should be properly protected[5] in order to avoid the potential polymerization of the building blocks. Thus, Boc, CBz, and Fmoc groups are often present as the protection group of amine, or sometimes the N-terminus is directly present as a nitro group. For the carboxylic acid at the C-terminus, to be an ester form is the normal choice.

In order to obtain long oligomers within a limited number of steps, the convergent synthetic strategy is used to serve this purpose. For instance, instead of coupling with monomers thirty-two times, this long oligomer could be achieved by converging two 16mers together while the 16mer through two 8mers and so on. However, when the oligomers get longer, its reactivity becomes lower due to the enhanced intramolecular stacking. The inherent reason of this problem is the secondary structure formation, helical conformation for example, thus the enhanced steric hindrance. Therefore, a higher temperature or/and a longer reaction time may be required to improve the yield. A conformation control strategy was also developed to address this issue.[6] Through this method, folding can be efficiently restrained by

5. a) A. Hoorfar, W. D. Ollis, and J. F. Stoddart, *Tetrahedron Lett.* **1980**, 4211; b) A. Hoofar, W. D. Ollis, J. A. Price, J. S. Stephanatou, and J. F. Stoddart, *J. Chem. Soc., Perkin Trans. 1* **1982**, 8, 1649; c) M. Feigel, G. Lugert, J. Manero, and M. Bremer, *Liebig Ann. Chem.* **1989**, 1089.
6. a) C. J. Creighton, and A. B. Reitz, *Org. Lett.* **2001**, 3, 893; b) A. M. Zhang, J. S. Ferguson, K. Yamato, C. Zheng, and B. Gong, *Org. Lett.* **2006**, 8, 5117.

putting a constraint substituent group onto the backbone. Taking a helical foldamer for example, an acid-labile 2,4-dimethoxybenzyl group (DMB) was installed on the amino group to interrupt otherwise hydrogen bonding. This group would then be removed to allow the helical conformation to take place (Figure 2b).

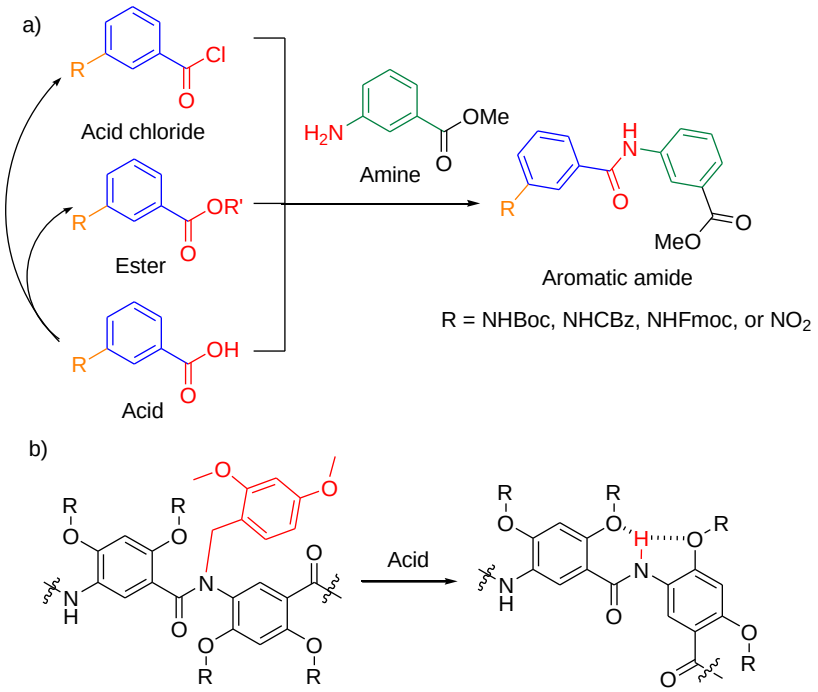

Figure 2. a) Usual activation and protection strategies of producing aromatic amide oligomers. Showing benzene derivatives and the methyl ester as the example. b) Conformation control strategy.

2.2 Solid phase synthesis

While the fast development and wide use of solution phase synthesis strategies for synthesizing aromatic amide foldamers, chemists started to develop the solid phase synthesis (SPS) approach inspired by SPS of peptide.[7] SPS is a very efficient method. It allows rapid access to the desired products. Through SPS, functionalized building blocks can be incorporated stepwise with considerably convenient purification just by filtration for each step. Therefore, one noticeable advantage of SPS for foldamer

7. a) H. M. König, R. Abbel, D. Schollmeyer, and A. F. M. Kilbinger, *Org. Lett.* **2006**, 8, 1819; b) B. Baptiste, C. Douat-Casassus, K. Laxmi-Reddy, F. Godde, and I. Huc, *J. Org. Chem.* **2010**, 75, 7175; c) T.-K. Lee, and J.-M. Ahn, *ACS Comb. Sci.* **2011**, 13, 107; d) X. Hu, S. J. Dawson, Y. Nagaoka, A. Tanatani, and I. Huc, *J. Org. Chem.* **2016**, 81, 1137; e) S. J. Dawson, X. Hu, S. Claerhout, and I. Huc, *Meth. Enzym.* **2016**, 580, 279; f) N. R. Wurtz, J. M. Turner, E. E. Baird, and P. B. Dervan, *Org. Lett.*, **2001**, 3, 1201; g) F. Campbell, J. P. Plante, T. A. Edwards, S. L. Warriner and A. J. Wilson, *Org. Biomol. Chem.*, **2010**, 8, 2344.

synthesis is that it can allow rapidly generating a long sequence without the laborious re-synthesis of intermediates required by a more convergent solution phase approach. This merit would be more remarkable when the sequence becomes complex. Additionally, the oligomers are separately anchored on the polymer material of the resin. Thus the possible reactivity problem due to the aggregation or hybridization (forming double helices for example) of the oligomers could be avoided. These features are attractive for the chemists dealing with aromatic foldamers.

Despite the benefits mentioned above, the introduction of an SPS strategy into aromatic amide foldamer chemistry is not without challenges. An important advantage of SPS, the efficiency mentioned above, mainly relies on the purity (better to be higher than 95%) of the building blocks and the yield (better to be higher than 95%) of each step. The former issue could be solved by pre-purification. However, the later one is totally dependent on the reaction conditions during each coupling. The methodology of SPS is initially standardized for peptide synthesis thus normally uses coupling reagents like HOBt/HBTU. However, unlike aliphatic amine, the inherent low reactivity of aromatic amine (a usual feature of aromatic oligoamide building blocks, also see Figure 2) makes it incompatible with normal coupling reagents (or in other words, the resulting yield is not high enough to be favorable for multiple couplings). Therefore, synthetic strategies involving more active reagents such as acid chlorides were developed to match the requirement of SPS of aromatic amide foldamers. Meanwhile, the assistance of microwave is also required in order to be both rapid and essentially quantitative. But for the hybrid sequences combining both aromatic amine and α-amino acid, it generates another problem that racemization of α-amino acid may occur when it is activated into acid chloride form. Thus a specific protocol, an in situ acid chloride method, was developed to address this issue.[7d-e] This will be discussed in detail in Chapter two. In the same chapter, a dimer SPS strategy is also developed, which comprises solution phase synthesis of dimeric building blocks and then SPS of oligomers. This strategy could be a complement of the in situ acid chloride method.

3. Architectures in aromatic amide foldamers

3.1 Construction strategies --- the design

Constructing an aromatic foldamer usually starts with small pieces of building blocks and eventually comes out as a novel secondary structure or a complex conformation. This design approach was best classified as bottom-up approach. By and large, the design, or in other words the folding principle of aromatic oligoamide foldamers, often takes advantage of the inherent rigidity in aromatic building blocks, various attractive or repulsive non-covalent interactions, and torsional flexibility of the linkers to guide the foldamer to adopt their discrete folded conformations.[8] Followings are some examples based on aromatic amide backbones in which hydrogen bonding is the dominant driving force although there are many cases with the cooperation from other effects.

3.1.1 Hydrogen bonding at the outer rim of the backbone

Bing Gong and co-workers reported a crescent-like oligoamide foldamer.[9] Folding of this kind of architecture is guided by the formation of several discrete three-center hydrogen bonding systems at the outside edge (Figure 3a). Hydrogen bonds formation and thus the crescent shape conformation result from the selectivity of the equilibrium of its diaryl amide motifs (Figure 3b). It is a reasonable assumption that conformer **1a** with two hydrogen bonds will be more stable than **1b** and **1c** which only have one. Moreover, for **1b** and **1c**, they both have the electrostatic repulsion stemming from oxygen atoms on adjacent repeat units. As a consequence, conformer **1d** could be deduced as to be the least favorable conformation, which was validated by the ab initio molecular orbital calculation (in vacuo). Other aromatic amide foldamers adopting this folding strategy were also reported.[10]

8. K. Kirshenbaum, R. N. Zuckermann, and K. A. Dill, *Curr. Opin. Struct. Biol.* **1999**, 9, 530.
9. J. Zhu, R. D. Parra, H. Zeng, E. Skrzypczak-Jankun, X. C. Zeng, and B. Gong, *J. Am. Chem. Soc.* **2000**, 122, 4219.
10. a) B. Gong, *Chem. – Eur., J.* **2001**, 7, 4336; b) H.-P. Yi, X.-B. Shao, J.-L. Hou, C. Li, X.-K. Jiang, and Z.-T. Li, *New J. Chem.* **2005**, 29, 1213; c) X. Wu, G. Liang, G. Ji, H.-K. Fun, L. He, and B. Gong, *Chem. Commun.* **2012**,

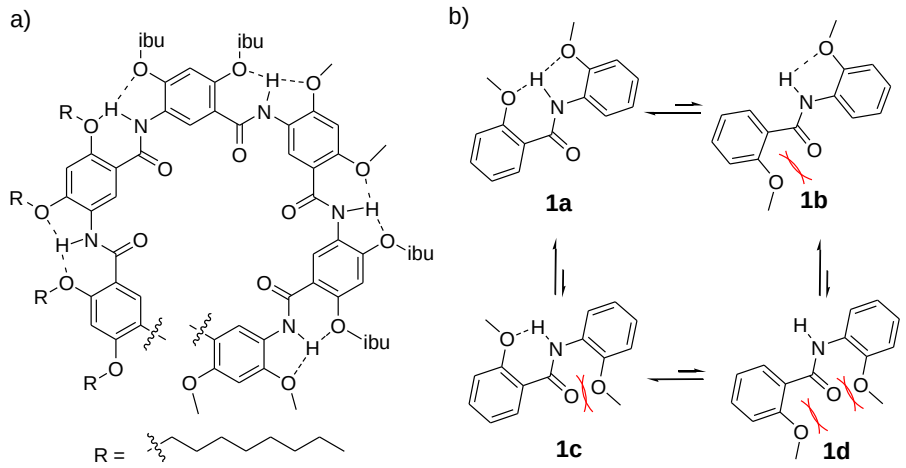

Figure 3. a) Crescent oligoamide and b) equilibrium of diaryl amide oligomers.

3.1.2 Hydrogen bonding at the inner rim of the backbone

Forming hydrogen bonds at inner side of the architecture is a very prevalent pattern in aromatic amide foldamers. There are many famous cases whose folding was mainly driven by this type of hydrogen bonding.[1a,h] The first example, quinoline-based oligoamide foldamers (Figure 4a-b),[11] is from Ivan Huc's group. Quinoline-based oligoamide foldamers are famous for their excellent stability and predictability. One important reason is the formation of hydrogen bond network inside its helical conformation which provides a shield to prevent it from being disturbed by the competitors or other factors from outside. Similarly, the preference of forming three-center hydrogen bond in the equilibrium of quinoline dimer motif (**Q_2**, Figure 4a) together with the electrostatic repulsions and the geometry of amine and acid functions on the quinoline ring determine the formation of the resulting helical conformation. Once the helix is formed, it will be further stabilized by the π-π interactions between each aromatic turn (Figure 4b). This is another reason why this type of foldamer is so rigid.

Another interesting case of this hydrogen bonding class is the pyridine based

48, 2228; d) B. Gong, H. Zeng, J. Zhu, L. Yua, Y. Han, S. Cheng, M. Furukawa, R. D. Parra, A. Y. Kovalevsky, J. L. Mills, E. Skrzypczak-Jankun, S. Martinovic, R. D. Smith, C. Zheng, T. Szyperski, and X. C. Zeng, *Proc. Natl. Acad. Sci. U. S. A.* **2002**, 99, 11583.

11. H. Jiang, J.-M. Leger, and I. Huc, *J. Am. Chem. Soc.* **2003**, 125, 3448.

oligoamide foldamer (Figure 4c).[12] It was found the initially folded helical conformation could be switched into an extended structure by adding an excess of trifluoroacetic acid (TFA). The pyridine units of the backbone could selectively capture protons from relatively mild acid source (TFA). Therefore, the previous hydrogen bonding mode (Figure 4c, see the red box) was disrupted and the new pattern induced the formation of an extended structure. However, when it was exposed to an even stronger acid (triflic acid), all pyridines were protonated so that another helical conformation formed driven by the novel hydrogen bonding system (Figure 4c, see the blue box). The switch of the hydrogen bonding modes and consequently the change of folding behavior emphasize the importance of the hydrogen bonding in foldamer design.

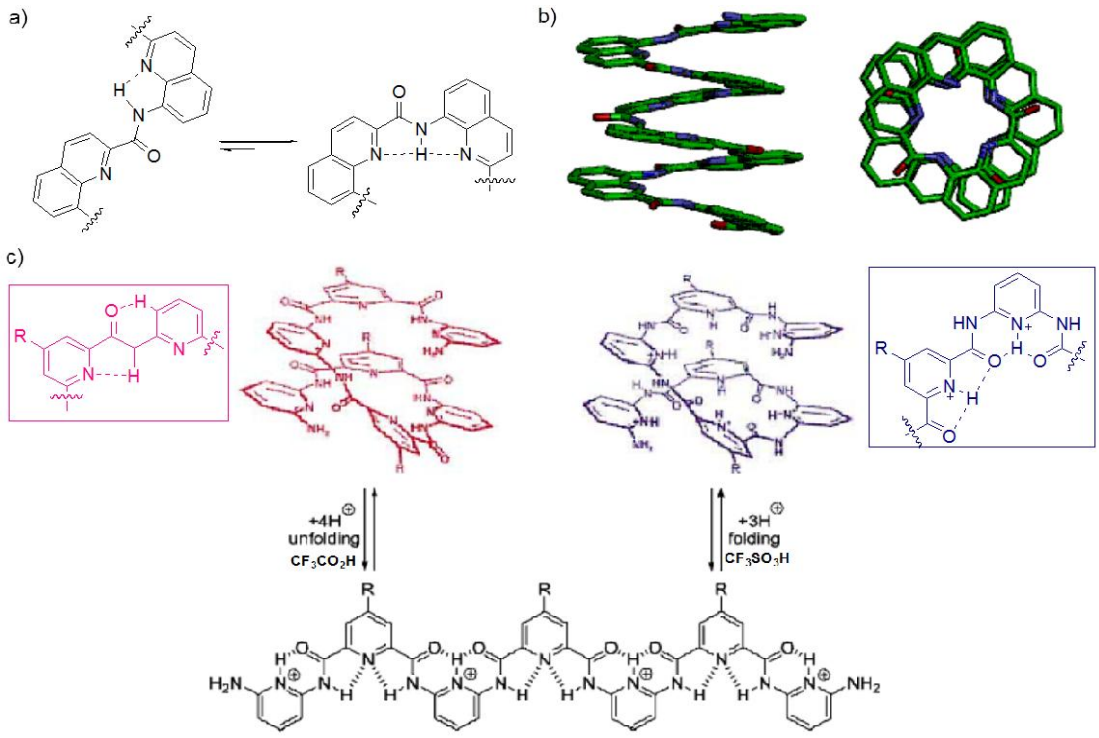

Figure 4. a) Equilibrium of quinoline-amide-based dimer motif ($\mathbf{Q_2}$) and b) crystal structure of a $\mathbf{Q_8}$. c) Folding controled by changing the hydrogen bonding modes.

3.1.3 Hydrogen bonding at both rims of the backbone

Examples of this class are not rich probably due to the complexity of the design.

12. C. Dolain, V. Maurizot, and I. Huc, *Angew. Chem., Int. Ed.* **2003**, 42, 2738.

One example from this class is the aromatic hydrazide-based foldamers.[13] Thanks to the introduction of the hydrazide link, formation of hydrogen bonding at both rims of the backbone is achieved (Figure 5). The hydrogen bonding motifs are similar to that used for amide-based foldamers. The planarity and trans arrangement of the hydrazide moiety, or the amide units, allow the formation of a five-center hydrogen bond at the inner side while at the same time forming a three-center hydrogen bond at the outside. Further study of this series of foldamers indicated that they are rigid and can adopt a helical conformation when the sequence gets longer.

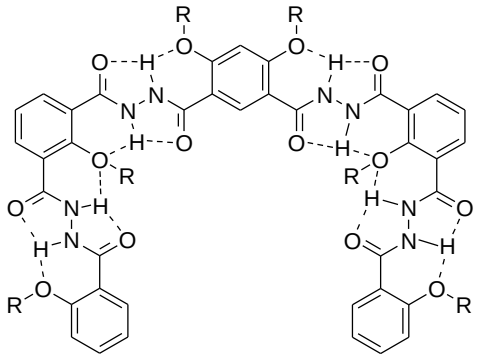

Figure 5. Hydrogen bonding at both rims of the backbone.

3.1.4 Other strategies

There are many other strategies to drive or induce oligomers to fold. Some famous designs were reported. For instance, backbones utilizing bipyridine segments;[14] folding guided by solvophobic effects;[15] and metal[16] or anion[17] induced folding. The discussion of which will not go further here since this thesis mainly studies the folding behavior guided by hydrogen bonding.

13. J.-L. Hou, X.-B. Shao, G.-J. Chen, Y.-X. Zhou, X.-K. Jiang, and Z.-T. Li, *J. Am. Chem. Soc.* **2004**, 126, 12386.
14. a) D. M. Bassani, and J.-M. Lehn, *Bull. Chem. Soc. Fr.* **1997**, *134*, 897; b) D. M. Bassani, J.-M. Lehn, G. Baum, and D. Fenske, *Angew. Chem.,Int. Ed.* **1997**, 1845; c) M. Ohkita, J.-M. Lehn, G. Baum, and D. Fenske, *Chem. Eur. J.* **1999**, *5*, 3471; d) M. Ohkita, J.-M. Lehn, G. Baum, and D. Fenske, *Heterocycles* **2000**,*52*, 103.
15. a) A. Tanatani, H. Kagechika, I. Azumaya, K. Yamaguchi, and K. Shudo, *Chem. Pharm. Bull.* **1996**, *44*, 1135; b) A. Tanatani, H. Kagechika, I. Azumaya, R. Fukutomi, Y. Ito, K. Yamaguchi, and K. Shudo, *Tetrahedron Lett.* **1997**, *38*, 4425; c) A. Tanatani, K. Yamaguchi, I. Azumaya, R. Fukutomi, K. Shudo, and H. Kagechika, *J. Am. Chem. Soc.* **1998**, *120*, 6433; d) R. Fukutomi, A. Tanatani, H. Kakuta, N. Tomioka, A. Itai, Y. Hashimoto, K. Shudo, and H. Kagechika, *Tetrahedron Lett.* **1998**, *39*, 6475; e) H. Kagechika, I. Azumaya, A. Tanatani, K. Yamaguchi, and K. Shudo, *Tetrahedron Lett.* **1999**, *40*, 3423.
16. R. B. Prince, T. Okada, and J. S. Moore, *Angew. Chem., Int. Ed.* **1999**, 38, 233.
17. Y.-X. Xu, X. Zhao, X.-K. Jiang, and Z.-T. Li, *J. Org. Chem.* **2009**, 74, 7267.

3.2 Different conformations and structure elucidation

Up to now, a massive number of synthetic foldamers have been produced. However, if inspecting into these foldamers, one will find the disproportion of the diversity of backbones and the eventual folding conformations (population of the former is far more than this of the later). A suppositional reason could be that most designs are following the limited folding strategies present which normally inherently determinate the final conformations. Nevertheless, there is another possibility in the other hand that the discovery of new conformations is restricted by the means of structure elucidation or, in other words, the complexity of the foldamers. No matter how, some typical conformations are worth to show here and they could be an inspiration for innovation of novel architectures.

3.2.1 Different conformations

Amongst others, the helix is the most often seen conformation in aromatic foldamers. As an inherent property of the helix, they could be either right-handed (P) or left-handed (M) helix. With the help of intermolecular interaction (in particular, π-π interaction and solvophobic interaction), they could also be double helix[18] or multiple helix.[19] Governed by more than one folding behavior, which is normally present in hydrid sequences, helical foldamers could also have shapes other than canonical helix such as a herringbone helix.[20]

Foldamers with sheet-like conformation are much less common. Comparing with a helical conformation, the reason could be the inherent larger conformational surface exposed to the surroundings so that they would have more possibility to undergo aggregation and even precipitation. It is then not hard to imagine there are less reports

18. J. Shang, Q. Gan, S. J. Dawson, F. Rosu, H, Jiang, Y. Ferrand, and I. Huc, *Org. Lett.* **2014**, 16, 4992.
19. a) Y. Ferrand, A. M. Kendhale, J. Garric, B. Kauffmann, and I. Huc, *Angew. Chem. Int. Ed.* **2010**, 49, 1778; b) Q. Gan, C. Bao, B. Kauffmann, A. Grelard, J. Xiang, S. Liu, I. Huc, and H. Jiang, *Angew. Chem. Int. Ed.* **2008**, 47, 1715.
20. N. Delsuc, F. Godde, B. Kauffmann, J.-M. Leger, and I. Huc, *J. Am. Chem. Soc.* **2007**, 129, 11348.

or successful characterization of sheet-like foldamers. Nevertheless, there is an excellent example[21] of this class from Ivan Huc's group. Multi-stranded artificial β-sheets were constructed based on the rational design of hydrogen bonding and the rigid turns (Figure 6). The hydrogen bonds serve for endowing each turn and strand a local stable and flat plane, while the methyl groups on the adjacent ring of the rigid turns enable these strands to arrange upon each other (prevent them from random rotation by stereohindrance effects). They together allowed the strands undergoing well-fitted face-to-face π-π interactions between appended linear aromatic segments to be strong enough for folding in the organic solvent, but weak enough to prevent aggregation and precipitation.

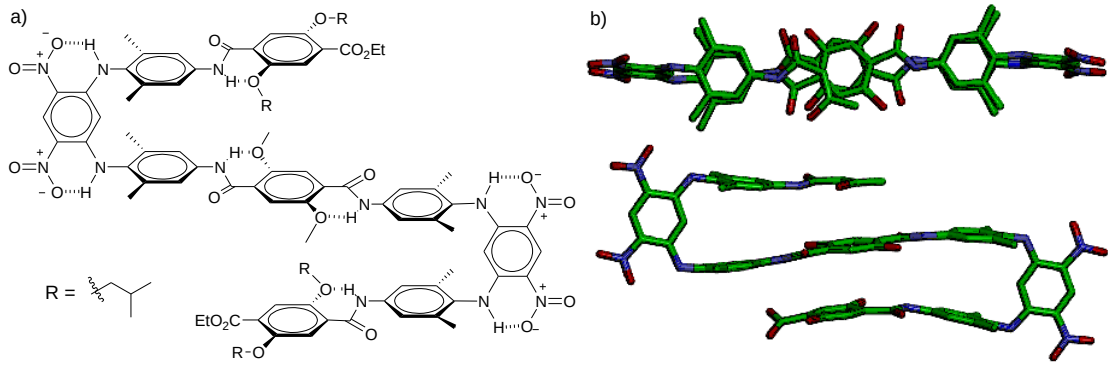

Figure 6. Aromatic oligoamide β-sheet foldamer: a) formula and b) crystal structure.

Other foldamers displaying folded architectures which are unknown or unusual in biopolymers were also reported. Such as pillar-like conformations,[22] non-canonical helices,[20, 23] tailbiters,[24] and knots.[25] One common feature of these peculiar folding is their hybrid backbones, particularly the combination of aromatic and aliphatic elements. This is an important advantage of foldamers in contrast to biopolymers. With the heterogeneous backbones of the hybrid foldamers, unsuspected sectors of the structural and functional space may be reached. Investigation of folding behavior

21. L. Sebaoun, V. Maurizot, T. Granier, B. Kauffmann, and I. Huc, *J. Am. Chem. Soc.* **2014**, 136, 2168.
22. R. S. Lokey and B. L. Iverson, *Nature*, **1995**, 375, 303.
23. D. Seebach, S. Abele, K. Gademann, G. Guichard, T. Hintermann, B. Jaun, J. Mathews, and J. V. Schreiber, *Helv. Chim. Acta*, **1998**, 81, 932.
24. C. A. Hunter, A. Spitaleri, and S. Tomas, *Chem. Commun.*, **2005**, 3691.
25. J. Bruggemann, S. Bitter, S. Muller, W. M. Muller, U. Muller, N. M. Maier, W. Lindner, and F. Vogtle, *Angew. Chem., Int. Ed.*, **2007**, 46, 254.

influenced by more than one type of folding tendencies may yield disordered structures, but may also be the most efficient way to generate novel conformations where homogenous oligomers can hardly reach and thus new and interesting properties and functions. Thus we envisioned the hybrid aromatic/aliphatic amide foldamers would be a field worth to explore more. Detailed investigations are discussed in Chapter two.

3.2.2 Structure elucidation

Since the helix is the most frequently characterized object among aromatic foldamers, the usage of circular dichroism (CD) spectroscopy is prevalent in this field. The advantage of this technique relied on its fast and unambiguous access of helical preference of the target molecule if there are stereogenic factors involved. However, the use of CD is also limited to chiral foldamers because of this reason (otherwise, no signal will arise).

Another important technique is NMR. The investigation of aromatic foldamers will routinely involve intra/inter-molecular assembling relating to the non-covalent bonds. NMR is a very powerful tool to detect or to indicate the existence of this type of interactions in solution phase. For example, comparing with those of the controls (around 8 ppm), a remarkable downfield shifting (to around 11 ppm) of aromatic amide hydrogen atoms is an indication of hydrogen bond formation in the aromatic amide foldamers. For an aromatic helical foldamer with constantly upfield shifting of some signals while its sequence prolonged, it probably means the enhanced π-π interactions and thus more compact helical packing and increased electronic effect of aromatic ring current. Besides, if one wants to obtain the picture of spatial organization of a foldamer in solution phase, 2D NMR can be the right technique to serve this purpose. For example, nuclear overhauser effect (NOE) of NOESY can show a signal (a correlation) between two protons when they are spatially close (normally, it requires distance less than 5 angstrom). Therefore, if there are more

correlations between those structurally remote protons, one can imagine the folding way that a foldamer undergoes or can even build a molecular model via computational chemistry. A detailed example of this is presented in chapter two.

Thanks to the relatively stable and usually well-defined conformations of aromatic foldamers, characterization in solid state by X-ray analysis becomes possible. In fact, in some cases where the conformation is complicated, single-crystal X-ray diffraction probably is the only way to clearly elucidate the spatial organization of their structures in the solid state. For some long oligomers which are usually difficult to crystallize, a combination of X-ray analysis and computational calculation could be helpful. This is based on the assumption that, for the long oligomer consisting of repeated segments, the backbone can be regarded as a combination of defined local conformations. Thus, with the parameters from the crystal structures of its short versions, a molecular model could be built (deduced) to predict the final conformation of the long foldamer.

Even though, the crystal growth is still a big challenge to most aromatic foldamers. Especially for those from water, there are only limited numbers of successful cases reported.[26] To address this issue, we did a systematic case study to improve crystal growth ability of aromatic foldamers, which is presented in chapter three.

3.3 Assembly and protein structure mimics

Towards the bigger and more complex architectures the biopolymers will normally adopt to perform molecular machinery and chemical functions, many sophisticated structures are designed and constructed by foldamer chemists. For aromatic helical foldamers, due to their large size and coplanarity, it was found that

26. a)V. Pavone, S.-Q. Zhang, A. Merlino, A. Lombardi, Y. Wu, and W. F. DeGrado, *Nat. Commun.*, **2014**, 5, 3581; b) C. G. Cummings, and A. D. Hamilton, *Tetrahedron* **2013**, 69, 1663; c) L. A. Estroff, C. D. Incarvito, and A. D. Hamilton, *J. Am. Chem. Soc.*, **2004**, 126, 2.

they may further intertwine to form double and even multiple helices. A heteromeric sequence comprises of 8-amino-2-quinolinecarboxylic acid and 7-amino-8-fluoro-2-quinolinecarboxylic acid (Figure 7) was reported to be able to form double helix in variety of solvents.[27] Self-assembly of double helix was determined by NMR and mass spectrometry and the results showed that the aqueous medium permits and greatly enhances the dimerization of this aromatic oligoamide foldamer.

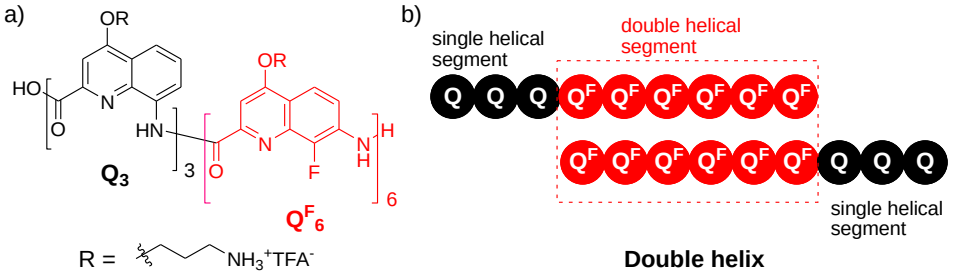

Figure 7. a) Formula of the heteromeric sequence and b) simplified representation of the double helix.

From the same group, a foldaxane was constructed by assembly of an aromatic amide helix and a linear molecule (Figure 8).[28] In this report, they studied the binding behavior of helical foldamers toward linear molecules. Interestingly, the initial self-assembled double helix could undergo dissociation into single helix upon adding a linear guest molecule. This process could then result in generation of a helix-derived [2]foldaxane.

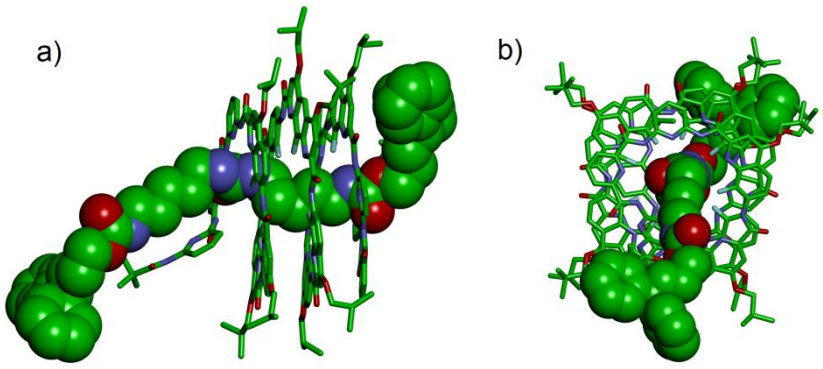

Figure 8. Crystal structure of the foldaxane based on an aromatic foldamer: a) side view and b) top view. The linear guest molecule is highlighted in Space-filling calotte model (also referred to CPK model).

27. J. Shang, Q. Gan, S. J. Dawson, F. Rosu, H. Jiang, Y. Ferrand, and I. Huc, *Org. Lett.* **2014**, 16, 4992.
28. Q. Gan, Y. Ferrand, C. Bao, B. Kauffmann, A. Grélard, H. Jiang, and I. Huc, *Science* **2011**, 331, 1172.

Besides, structures to mimic tertiary and quaternary structures of proteins were also reported. Two helices were bound on purpose by a four-atoms-long linear linker. As the result of this design, a foldamer which can mimic the protein tertiary structure was achieved (Figure 9).[29] Structurally, it was constructed from abiotic (aromatic) building blocks; it possesses considerablely larger size (> 8 kDa) and higher complexity than normal single-molecular foldamers; and it is comparable to a small protein in consideration of the size. Generation of this kind of protein mimics represents novel platforms and thus new strategies to study molecular recognition or enzyme catalysis. Despite the challenges of design, synthesis and structure elucidation, some excellent cases of mimicking quaternary structure of proteins were reported by Samuel H. Gellman, Alanna Schepartz, Gilles Guichard and their co-workers, with the backbone of their foldamers constructed via aliphatic building blocks.[30] However, it is still hard to find good cases from aromatic foldamers. Thus, we were encouraged to develop strategies to access this challenging field with the aromatic building blocks (see chapter four).

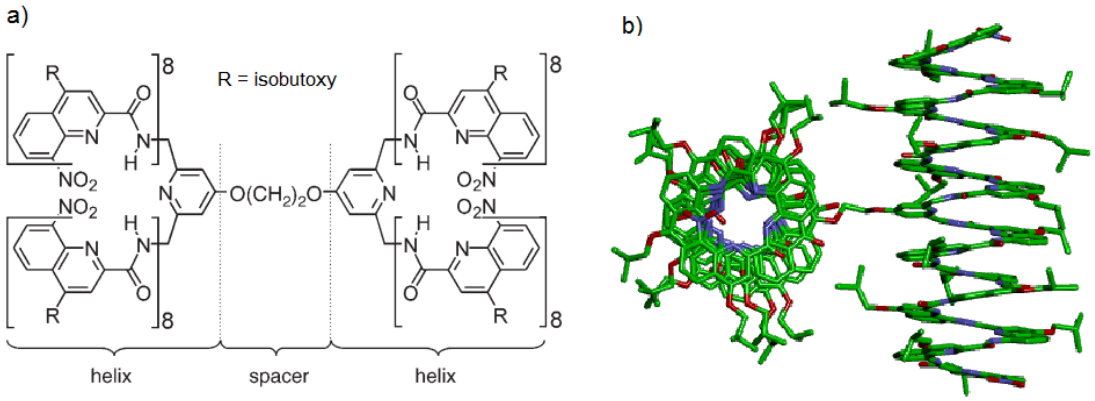

Figure 9. Formula a) and crystal structure b) of the foldamer mimicking tertiary structure of protein.

29. N. Delsuc, J.-M. Léger, S. Massip, and I. Huc, *Angew. Chem., Int. Ed.* **2007**, 46, 214.
30. a) W. S. Horne, J. L. Price, J. L. Keck, and S. H. Gellman, *J. Am. Chem. Soc.* **2007**, 129, 4178; b) J. L. Price, W. S. Horne, and S. H. Gellman, *J. Am. Chem. Soc.* **2010**, 132, 12378; c) M. W. Giuliano, W. S. Horne, and S. H. Gellman, *J. Am. Chem. Soc.* **2009**, 131, 9860; d) J. P. Miller, M. S. Melicher, and A. Schepartz, *J. Am. Chem. Soc.* **2014**, 136, 14726; e) J. L. Goodman, E. J. Petersson, D. S. Daniels, J. X. Qiu, and A. Schepartz, *J. Am. Chem. Soc.* **2007**, 129, 14746; f) M. A. Molski, J. L. Goodman, C. J. Craig, H. Meng, K. Kumar, and A. Schepartz, *J. Am. Chem. Soc.* **2010**, 132, 3658; g) G. W. Collie, K. Pulka-Ziach, C. M. Lombardo, J. Fremaux, F. Rosu, M. Decossas, L. Mauran, O. Lambert, V. Gabelica, C. D. Mackereth, and G. Guichard, *Nat. chem.* **2015** 7, 871.

Other architectures as the result of assembly were also reported. Such as [2]catenanes from Zhan-Ting Li's group,[31] bistable[2]rotaxanes from Zhao's goup,[32] macroscopically vesicles,[33] nanofibers,[34] and liquid crystals.[35] Together with the above mentioned structures, they show that foldamers could access unlimited diversity of conformations and thus many potential applications. All these need, and are also worth, to be further developed.

31. J. Wu, J.-L. Hou, C. Li, Z.-Q. Wu, X.-K. Jiang, Z.-T. Li, and Y.-H. Yu, *J. Org. Chem.* **2007**, 72, 2897.
32. K.-D. Zhang, X. Zhao, G.-T. Zhao, Y. Liu, Y. Zhang, H.-J. Lu, X.-K. Jiang, and Z.-T. Li, *Angew. Chem., Int. Ed.* **2011**, 50, 9866.
33. a) W. Cai, G.-T. Wang, Y.-X. Xu, X.-K. Jiang, and Z.-T. Li, *J. Am. Chem. Soc.* **2008**, 130, 6936; b) L.-Y. You, and Z.-T. Li, *Chin. J. Chem.* **2010**, 28, 1547; c) K.-D. Zhang, G.-T. Wang, X. Zhao, X.-K. Jiang, and Z.-T. Li, *Langmuir* **2010**, 26, 6878.
34. C. Ren, S. Xu, J. Xu, H. Chen, and H. Zeng, *Org. Lett.* **2011**, 13, 3840.
35. G.-T. Wang, X. Zhao, and Z.-T. Li, *Tetrahedron* **2011**, 67, 48.

4. Conclusion

Foldamers are a fast developing field in chemistry. As one of the most promising branches of the foldamer, aromatic amide foldamers possess some attractive properties: a) high stability, b) predictability, c) synthetic accessibility, and d) their amenability to modifications. A variety of backbones were synthesized to investigate their folding behavior and spatial organization. The results came out that there are less diverse structures and in which the canonical helix is the dominated conformation. Besides, constructing quaternary structures as protein mimics is still a challenging subject and remains a blank in aromatic foldamers waiting to be filled.

We envision hybrid foldamers could be interesting and helpful objects to produce novel conformations and thus new functionalities. Particularly, aromatic/aliphatic hybrid sequences may access the area where both homo-biotic and homo-abiotic foldamers can not arrive. The result of folding behavior studies in hybrid foldamers could also be useful for the complex foldamer design. In addition, improving the crystal growth ability of foldamers in water can facilitate structure elucidation and thus the investigations carried out in aqueous medium. As a result, these will open an avenue allowing fast development of functions and applications of foldamers in water. Efforts are also worth to be made to construct self-assembled aromatic helix bundles in water despite the potentially huge challenges. The knowledge from the investigation of self-assembly in water will be particularly useful of understanding these side chain interaction processes occurring in nature, such as hydrophobic effects, aggregation, and electrostatic interactions.

Chapter 2

Solid-Phase Synthesis of Water-Soluble Helically Folded Hybrid α-Amino Acid/Quinoline Oligoamides

(Adapted with permission from X. Hu, S. J. Dawson, Y. Nagaoka, A. Tanatani, and I. Huc, *J. Org. Chem.* **2016**, 81, 1137. Copyright 2017 American Chemical Society)

Contributors:

Dr. Simon J. Dawson supervised the synthesis and analysis; Yui Nagaoka synthesized dimer block; Dr. Mohamed Elsawy did the preliminary exploration of SPS conditions; Dr. Pradeep K. Mandal carried out crystallization and crystal structure determination and refinement.

Objectives:

- Develop an efficient solid phase synthesis method (SPS) for incorporating α-amino acid into quinoline oligoamides.
- Develop a dimer strategy as a complementary protocol to the above SPS method.
- Construct water-soluble α-amino acid/quinoline (**X**/**Q**) hybrid oligoamide foldamers and investigate their folding behavior and folded conformation in water through CD and NMR.
- Structural elucidation of these hybrid foldamers in water via NMR full assignment or crystallography.

1. Introduction

The peptide backbone, consisting of the 20 α-amino acids provided by nature, is the primary structure that endows proteins with their ability to fold and results in their unique properties *in vivo*. In particular, the diverse side chains of α-amino acid building blocks play a crucial role in controlling protein folding,[1] protein–protein interactions,[2] and protein–ligand interfaces.[3] They are thus critical in allowing proteins to perform their wide variety of functions, among others, enzyme catalysis,[4] cellular signaling,[5] and molecular transport.[6] However, in isolation, short α-peptides are typically structurally unstable,[7] meaning side-chain orientations are spatially disorganized. This to a great extent complicates their potential use in biological applications.

Various strategies have been explored to overcome the conformational instability of α-peptides with particular emphasis on developing sequences that can form helical structures. These include analogues incorporating β-, γ-, or δ-amino acids,[7a,7c,8] sterically restricted residues,[9] chiral directing groups,[10] and urea bonds,[11] or the

1. a) M. J. Gething, and J. Sambrook, *Nature* **1992**, 355, 33; b) A. Nicholls, K. A. Sharp, and B. Honig, *Proteins: Struct., Funct., Genet.* **1991**, 11, 281.
2. S. Jones, J. M. Thornton, *Proc. Natl. Acad. Sci. U. S. A.* **1996**, 93, 13.
3. a) J. P. Xiong, T. Stehle, R. Zhang, A. Joachimiak, M. Frech, S. L. Goodman, and M. A. Arnaout, *Science* **2002**, 296, 151; b) M. Wilchek, E. A. Bayer, and O. Livnah, *Immunol. Lett.* **2006**, 103, 27.
4. a) S. J. Benkovic, and S. Hammes-Schiffer, *Science* **2003**, 301, 1196; b) A. J. Russell, and A. R. Fersht, *Nature* **1987**, 328, 496.
5. R. S. Syed, S. W. Reid, C. Li, J. C. Cheetham, K. H. Aoki, B. Liu, H. Zhan, T. D. Osslund, A. J. Chirino, J. Zhang, J. Finer-Moore, S. Elliott, K. Sitney, B. A. Katz, D. J. Matthews, J. J. Wendoloski, J. Egrie, and R. M. Stroud, *Nature* **1998**, 395, 511.
6. a) H. Luecke, and F. A. Quiocho, *Nature* **1990**, 347, 402; b) L. F. Nagle, and H. J. Morowitz, *Proc. Natl. Acad. Sci. U. S. A.* **1978**, 75, 298.
7. a) T. Hintermann, K. Gademann, B. Jaun, and D. Seebach, *Helv. Chim. Acta* **1998**, 81, 983; b) J. A. Vila, D. R. Ripoll, and H. A. Scheraga, *Proc. Natl. Acad. Sci. U. S. A.* **2000**, 97, 13075; c) J. Frackenpohl, P. I. Arvidsson, J. V. Schreiber, and D. Seebach, *ChemBioChem* **2001**, 2, 445.
8. a) W. F. DeGrado, J. P. Schneider, and Y. Hamuro, *J. Pept. Res.* **1999**, 54, 206; b) S. H. Gellman, *Acc. Chem. Res.* **1998**, 31, 173; c) D. Seebach, and J. L. Matthews, *Chem. Commun.* **1997**, 2015; d) C. Baldauf, R. Gunther, and H. J. Hofmann, *J. Org. Chem.* **2006**, 71, 1200; e) Baldauf, C.; Gunther, R.; Hofmann, H. J. *J. Org. Chem.* **2004**, 69, 6214; f) T. Hintermann, K. Gademann, B. Jaun, and D. Seebach, *Helv. Chim. Acta* **1998**, 81, 983; g) S. Hanessian, X. Luo, R. Schaum, and S. Michnick, *J. Am. Chem. Soc.* **1998**, 120, 8569.
9. a) R. L. Baldwin, and G. D. Rose, *Trends Biochem. Sci.* **1999**, 24, 26; b) P. C. Lyu, J. C. Sherman, A. Chen, N. R. Kallenbach, *Proc. Natl. Acad. Sci. U. S. A.* **1991**, 88, 5317.
10. a) T. J. Sanborn, C. W.Wu, R. N. Zuckermann, and A. E. Barron, *Biopolymers* **2002**, 63, 12; b) C. W. Wu, T. J. Sanborn, K. Huang, R. N. Zuckermann, and A. E. Barron, *J. Am. Chem. Soc.* **2001**, 123, 6778.
11. K. Burgess, K. S. Linthicum, and H. Shin, *Angew. Chem., Int. Ed. Engl.* **1995**, 34, 907.

presence of a covalent linkage between residues remote in a sequence (i.e., "stapling").[12] These peptide analogues can be broadly classified as "biotic" foldamers.[13] In contrast, an alternative strategy to develop a stable and well-defined secondary structure is to utilize backbones and folding modes that differ significantly from those of the biopolymer. Examples of these can be termed "abiotic" foldamers.[13]

To act as appropriate biopolymer mimics, abiotic foldamers must be able to display biotic-like functionality with a spatial organization compatible with biological targets. One key factor in achieving this is the predictability with which side-chain functional groups are arranged on the foldamer backbone. In this way, they can be made to closely mimic their respective placement in a biotic motif, such as a peptide α-helix. Significant progress toward this has been made by the group of Hamilton, using terphenyl-,[14] biphenyldicarboxamide-,[15] terephthalamide-,[16] and benzoylurea-based[17] scaffolds, by Wilson and co-workers with their oligobenzamide template,[18] the Rebek and Konig groups with their respective pyridazine/piperazine[19] and 1,4-dipiperazine benzene-based scaffolds,[20] and the Burgess group with a piperidine-piperidinone scaffold.[21]

Aside from being potential biopolymer mimics, one advantage of abiotic foldamers is precisely that they can afford access to functional group arrangements that are inaccessible to natural motifs, yet may also interact with biomolecules in unforeseen and interesting ways. Helical aromatic oligoamide foldamers consisting of 8-amino-2-quinolinecarboxylic acid having a side chain in position 4 "$\mathbf{Q^{Xxx}}$" (where

12.Y. W. Kim, T. N. Grossmann, and G. L. Verdine, *Nat. Protoc.* **2011**, 6, 761.

13. a) D. J. Hill, M. J. Mio, R. B. Prince, T. S. Hughes, and J. S. Moore, *Chem. Rev.* **2001**, 101, 3893; b) G. Guichard, and I. Huc, *Chem. Commun.* **2011**, 47,5933.

14. B. P. Orner, J. T. Ernst, and A. D. Hamilton, *J. Am. Chem. Soc.* **2001**, 123, 5382.

15. I. Saraogi, and A. D. Hamilton, *Biochem. Soc. Trans.* **2008**, 36, 1414.

16. J. M. Rodriguez, L. Nevola, N. T. Ross, J. I. Lee, and A. D. Hamilton, *ChemBioChem* **2009**, 10, 829.

17. C. G. Cummings, and A. D. Hamilton, *Curr. Opin. Chem. Biol.* **2010**, 14, 341.

18. a) J. P. Plante, T. Burnley, B. Malkova, M. E. Webb, S. L. Warriner, T. A. Edwards, and A. J. Wilson, *Chem. Commun.* **2009**, 5091; b) A. J. Wilson, *Chem. Soc. Rev.* **2009**, 38, 3289; c) A. Barnard, K. Long, H. L. Martin, J. A. Miles, T. A. Edwards, D. C. Tomlinson, A. Macdonald, and A. J. Wilson, *Angew. Chem.* **2015**, 127, 3003; d) V. Azzarito, J. A. Miles, J. Fisher, T. A. Edwards, S. L. Warriner, and A. J. Wilson, *Chem. Sci.* **2015**, 6, 2434.

19. a) A. Volonterio, L. Moisan, J. Rebek, Jr., *Org. Lett.* **2007**, 9, 3733; b) L. Moisan, S. Odermatt, N. Gombosuren, A. Carella, and J. Rebek, Jr., *Eur. J. Org. Chem.* **2008**, 2008, 1673.

20. P. Maity, and B. Konig, *Org. Lett.* **2008**, 10, 1473.

21. D. Xin, L. M. Perez, T. R. Ioerger, and K. Burgess, *Angew. Chem., Int. Ed.* **2014**, 53, 3594.

Xxx refers to three-letter code of analogous α-amino acids bearing the same side chain, when available) do not display side-chains in the same manner as α-helices, yet they feature key properties that make them promising peptidomimetics: they are medium sized (0.5–5.0 kDa), resistant to proteolytic degradation,[22] conformationally stable in a wide range of solvents and in particular in water[23] even at high temperatures, [24] and most importantly, they adopt well-defined, predictable conformations.[25] They have been shown to possess cell-penetrating properties,[22, 26] and side-chain functionality can be tuned to afford high affinity for G-quadruplex DNA[27] or to interact with protein surfaces.[28]

A logical extension from exclusively abiotic peptidomimetics is to incorporate the exact functional groups that mediate protein–protein recognition, i.e., α-amino acids. A single amino acid may for example be added at the extremity of an α-helix mimetic.[18c] When multiple α-amino acids are incorporated in an abiotic sequence to form a hybrid scaffold, the completely different folding principles of biotic and abiotic units may offer access to secondary structures distinct from those of biopolymers or synthetic homo-oligomers.[29] In other cases, the folding of abiotic units may be so effective that it forces α-amino acids to adopt conformations distinct from those found in peptides. We recently reported an example of this kind using helically folded quinoline oligoamides. Hybrid sequences consisting of a repeating motif of a single L-leucine residue (**L**) followed by a quinoline (**Q**) dimer with 4-isobutoxy, leucine-like, side chains (**LQ**$^{\mathbf{Leu}}_{\mathbf{2}}$, Figure 1a) have been found to adopt a right-handed helical conformation in organic solvents. The crystal structure of (**LQ**$^{\mathbf{Leu}}_{\mathbf{2}}$)$_4$ showed a

22. E. R. Gillies, F. Deiss, C. Staedel, J. M. Schmitter, and I. Huc, *Angew. Chem., Int. Ed.* **2007**, 46, 4081.
23. T. Qi, V. Maurizot, H. Noguchi, T. Charoenraks, B. Kauffmann, M. Takafuji, H. Ihara, and I. Huc, *Chem. Commun.* **2012**, 48, 6337.
24. N. Delsuc, T. Kawanami, J. Lefeuvre, A. Shundo, H. Ihara, M. Takafuji, and I. Huc, *ChemPhysChem* **2008**, 9, 1882.
25. a) H. Jiang, J.-M. Léger, and I. Huc, *J. Am. Chem. Soc.* **2003**, 125, 3448; b) C. Dolain, A. Grélard, M. Laguerre, H. Jiang, V. Maurizot, and I. Huc, *Chem. - Eur. J.* **2005**, 11, 6135.
26. J. Iriondo-Alberdi, K. Laxmi-Reddy, B. Bouguerne, C. Staedel, and I. Huc, *ChemBioChem* **2010**, 11, 1679.
27. S. Muller, K. Laxmi-Reddy, P. V. Jena, B. Baptiste, Z. Dong, F. Godde, T. Ha, R. Rodriguez, S. Balasubramanian, and I. Huc, *ChemBioChem* **2014**, 15, 2563.
28. J. Buratto, C. Colombo, M. Stupfel, S. J. Dawson, C. Dolain, B. L. d'Estaintot, L. Fischer, T. Granier, M. Laguerre, B. Gallois, and I. Huc, *Angew. Chem., Int. Ed.* **2014**, 53, 883.
29. R. V. Nair, K. N. Vijayadas, A. Roy, and G. J. Sanjayan, *Eur. J. Org. Chem.* **2014**, 2014, 7763.

similar conformation as that of quinolinecarboxamide homologous sequences despite the absence of features of aliphatic and aromatic building blocks.[30] Nevertheless, variable temperature and solvents NMR studies indicated $(\mathbf{LQ^{Leu}}_2)_4$ can adopt two conformations in different organic solvents. Thus an alternative structure was proposed via calculation. It showed a similar helical conformation as its crystal structure but with different hydrogen bonding mode reminiscent of the hydrogen bonding occurring in an α-helix. This ability of quinoline backbones to dictate folding was also observed with aliphatic blocks other than α-amino acids.[31] In contrast, sequences of a repeating L-leucine-quinoline dimer (**LQ$^{\mathbf{Leu}}$**, Figure 1b) were found to adopt a partially folded zigzag tape conformation with local conformational variability precluding long-range order. In other words, when there are too few quinoline residues to dominate the folding process, hybrid and potentially ill-defined behavior may result.[32] An interesting aspect of the $(\mathbf{LQ^{Leu}}_2)_n$ helices is that the leucine residues are driven to form a linear array of side chain at ~3.5 Å intervals, corresponding to the pitch of an aromatic helix. These arrays of side chains may be of use for the recognition of proteins or nucleic acid structures. In such an approach, a great advantage would lie in the commercial availability of α-amino acids: a wide variety of side chains may be incorporated without resorting to the potentially nontrivial and labor intensive synthesis of differently functionalized abiotic building blocks.

30. M. Kudo, V. Maurizot, B. Kauffmann, A. Tanatani, and I. Huc, *J. Am. Chem. Soc.* **2013**, 135, 9628.

31. a) D. Sánchez-García, B. Kauffmann, T. Kawanami, H. Ihara, M. Takafuji, M.-H. Delville, and I. Huc, *J. Am. Chem. Soc.* **2009**, 131, 8642; b) B. Baptiste, C. Douat-Casassus, K. Laxmi-Reddy, F. Godde, and I. Huc, *J. Org. Chem.* **2010**, 75, 7175.

32. a) P. Prabhakaran, S. S. Kale, V. G. Puranik, P. R. Rajamohanan, O. Chetina, J. A. Howard, H. J. Hofmann, and G. J. Sanjayan, *J. Am. Chem. Soc.* **2008**, 130, 17743; b) D. Srinivas, R. Gonnade, S. Ravindranathan, and G. J. Sanjayan, *J. Org. Chem.* **2007**, 72,7022; c) A. Roy, P. Prabhakaran, P. K. Baruah, and G. J. Sanjayan, *Chem. Commun.* **2011**, 47, 11593; d) M. Kudo, V. Maurizot, H. Masu, A. Tanatani, and I. Huc, *Chem. Commun.* **2014**, 50,10090.

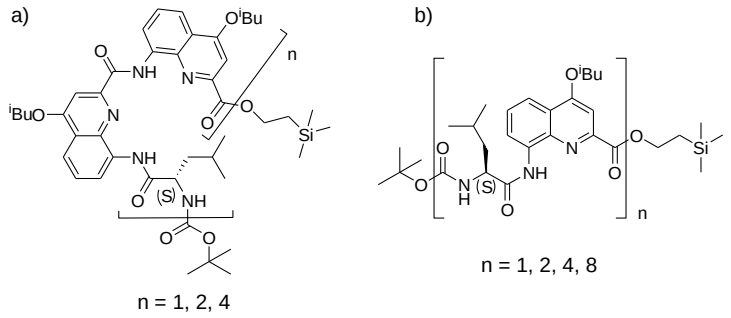

Figure 1. Structures of a) $\mathbf{LQ^{Leu}_2}$ and b) $\mathbf{LQ^{Leu}}$-type sequences.

The purpose of the present investigation was twofold: develop a convenient synthetic methodology of $(\mathbf{XQ_2})_n$ oligomers with varied linear arrays of α-amino acids "**X**" and explore their conformation behavior in water. Because folding of aromatic oligoamide foldamers gives rise to extensive contacts between aromatic rings, it is greatly enhanced by hydrophobic effects.[23] We thus anticipated that the behavior of these hybrid sequences might vary in aqueous conditions. The previously reported solution phase synthesis of $(\mathbf{LQ^{Leu}_2})_n$ oligomers involved the preparation of water insoluble $\mathbf{LQ^{Leu}}$ and $\mathbf{LQ^{Leu}_2}$ intermediates. Synthesizing a variety of sequence analogues would thus be time-consuming, as it would require the production of a number of **XQ** and $\mathbf{XQ_2}$ intermediate building blocks. In contrast, a solid-phase methodology would be ideal in that it offers the advantage of allowing the stepwise incorporation of building blocks, including those that are commercially available.

Drawing on our experience with the solid-phase synthesis (SPS) of quinoline oligoamides,[31b] this chapter describes the development of a corresponding efficient methodology for the SPS of α-amino acid/quinoline hybrid sequences via the use of in situ formed α-amino acid chlorides. We have used this methodology to produce sequences based on **XQ** and $\mathbf{XQ_2}$ repeat motifs and investigated their conformations via CD and NMR studies. Polar side chains introduced on each **Q** unit were expected to diverge from the folded structures and, with the contribution of the main chain carboxylate terminus, to ensure water solubility of oligomers in the millimolar range despite the high aromatic content of the sequences. Our structural investigations include the full structural assignment by NMR of a dodecameric $(\mathbf{XQ_2})_4$ sequence, where four different α-amino acids have been incorporated, and the characterization

of its helical conformation in aqueous medium (by convention, a monomer maybe a quinoline unit or an α-amino acid indifferently; an $(\mathbf{XQ_2})_4$ has 12 units and is thus considered to be a dodecamer). At last, the solid state structural elucidation of an undecameric $\mathbf{FQ_2}$-type sequence via its crystal structure from water is described.

2. Methodology development

2.1 Background

The production of oligomers by SPS is particularly attractive in that it offers a method for rapidly generating sequence analogues where any monomer unit can be substituted for another without the laborious resynthesis of intermediates required by a more convergent solution phase approach. Although solid phase peptide synthesis methods are now widely standardized, the use of an SPS strategy for the production of foldamers based on 8-amino-2-quinolinecarboxylic acid is not without its challenges. The aromatic amine is a relatively poor nucleophile and thus coupling requires activation of monomers as acid chlorides and microwave assistance to be both rapid and essentially quantitative. We therefore anticipated the coupling of α-amino acids to this unit to be difficult. Indeed, in the solution-phase synthesis of $\mathbf{(LQ^{Leu})}_{\boldsymbol{n}}$ and $\mathbf{(LQ^{Leu}{}_2)}_{\boldsymbol{n}}$ oligomers, leucine was required to be activated as the acid fluoride for it to be coupled to an 8-aminoquinoline monomer (Scheme 1). Coupling to a quinoline dimer was found to be unfeasible, as it required heating, long reaction times, and resulted in significant racemization.[30]

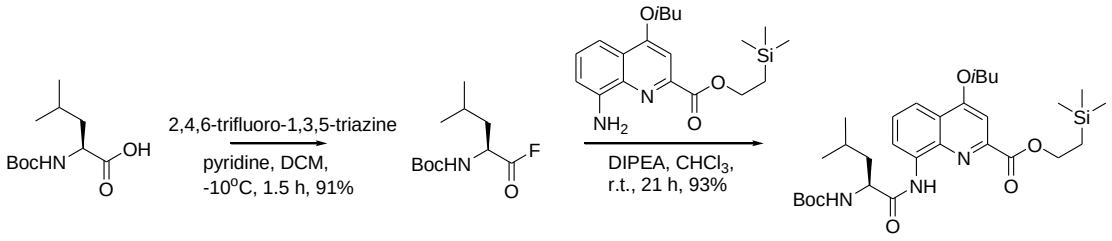

Scheme 1. Coupling leucine to 8-aminoquinoline as the acid fluoride

Although our previous experience with SPS of quinoline oligoamides indicated that acid chlorides would be required for efficient coupling, the disadvantages of activating α-amino acids as their corresponding acid chlorides are widely reported.[33] We thus initially investigated some of the newer generations of coupling

33. a) L. A. Carpino, M. Beyermann, H. Wenschuh, and M. Bienert, *Acc. Chem. Res.* **1996**, 29, 268. b) Bodanszky, M.*Principles of Peptide Synthesis.* Springer-Verlag: Berlin, **1984**. c) E. Falb, T. Yechezkel, Y. Salitra, and C. Gilon, *J. Pept. Res.* **1999**, 53, 507.

reagents, including aminiums (HATU), [34] phosphoniums (PyBroP), [35] propylphosphonic anhydride (T3P), [36] and the cyanuric chloride derivative DMTMM,[37] without success. This was also the case for both preformed acid fluorides (using cyanuric fluoride) and even those formed in situ (using DAST). We therefore returned to investigating the use of acid chlorides, reasoning that, if the activation and coupling process was short enough, it might be permitted without significant racemization. In this respect, the in situ generation of acid chlorides via the trichloroacetonitrile/triphenylphosphine methodology of Jang and co-workers[38] seemed to be an ideal choice; indeed, this procedure has also been subsequently applied to SPS.[39] (Thank Dr. Mohamed Elsawy for the preliminary exploration of these SPS conditions)

2.2 In situ acid chloride solid phase synthesis protocol

Initial trials appeared promising, and we thus carried out a brief study to assess coupling efficiency and compatibility of different side-chain functional groups between α-amino acids and quinolines carrying different side chains (Figure 2). For this, we employed a resin-bound quinoline dimer (Scheme 2) as starting material, which was synthesized using our SPS methodology from Wang-bromide resin.[31b] Fmoc-Lys(Boc)–OH was subsequently coupled using our initial unoptimized conditions: four equivalents of amino acid and four coupling cycles to afford, after resin cleavage, trimer **3c** in approximately 85% yield. Despite this initial success, we were concerned by two factors, the high excess of amino acid required and the possibility of racemization, especially in the case of cysteine.

34. L. A. Carpino, *J. Am. Chem. Soc.* **1993**, 115, 4397.
35. E. Frerot, J. Coste, A. Pantaloni, M. N. Dufour, and P. Jouin, *Tetrahedron* **1991**, 47, 259.
36. A. A. Waghmare, R. M. Hindupur, and H. N. Pati, *Review Journal of Chemistry* **2014**, 4,53.
37. M. Kunishima, C. Kawachi, J. Monta, K.Terao, F. Iwasaki, and S. Tani, *Tetrahedron* **1999**, 55, 13159.
38. D. O. Jang, D. J. Park, and J. Kim, *Tetrahedron Lett.* **1999**, 40, 5323.
39. I. Vágó, and I. Greiner, *Tetrahedron Lett.* **2002**, 43, 6039.

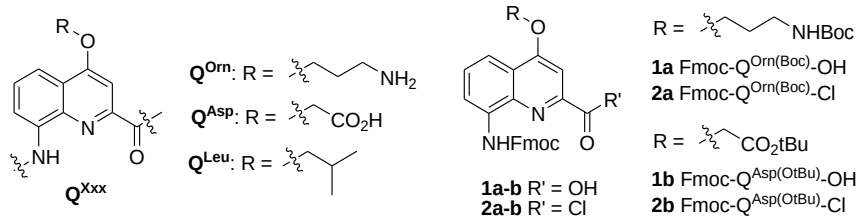

Figure 2. Structures of $\mathbf{Q^{Xxx}}$ and Fmoc-protected quinoline monomers.

We initially dealt with the first concern and were fortunate to discover that a key variable was the excess of triphenylphosphine, which if increased allowed complete coupling in the presence of only two equivalents of amino acid (in this case, the orthogonally protected Fmoc-Lys(Boc)–OH) after only two coupling cycles. This method proved effective with the majority of amino acids tested, although in some cases (e.g., serine), the number of coupling cycles needed to be increased. In all cases apart from α-amino-isobutyric acid (Fmoc-AiB–OH, which will be discussed later), coupling was complete after four cycles. Trimers **3a**–**g** (Fmoc-$\mathbf{XQ_2}$-OH) were thus resynthesized using these conditions, affording crude yields from 50 to 70% and purities >90% by HPLC. These products were also characterized by NMR and MS.

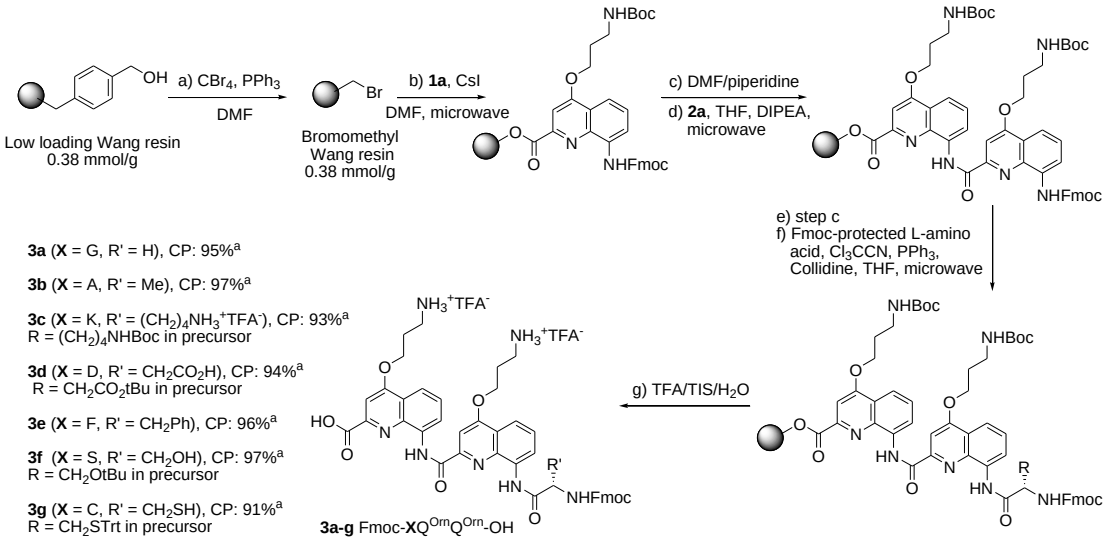

[a] CP stands for crude purity

Scheme 2. Solid phase synthesis of various Fmoc-$\mathbf{XQ_2}$-OH hybrid tripeptides.cc

2.3 Racemization assays

We assessed racemization by the addition of a second chiral center to allow detection of diastereoisomers. To each amino acid coupled to the quinoline amine via

its acid chloride we coupled the same amino acid a second time (via HBTU/HOBt) with both the D and L forms of that amino acid. In each Fmoc-**L**X-**L**X-(**Q**)$_2$ tetramer (**4a-e**) produced, the byproduct resulting from racemization of the first amino acid residue (Fmoc-**L**X-**D**X-(**Q**)$_2$) would be an enantiomer of the Fmoc-**D**X-**L**X-(**Q**)$_2$ tetramer (**5a-e**, with identical HPLC retention time and NMR signals) and vice versa. We considered it unlikely that racemization would occur during coupling of the second amino acid unit because this is not normally associated with aminium coupling reagents.[40] Detection of diastereomeric byproducts in crude Fmoc-(**X**)$_2$-(**Q**)$_2$ tetramers **4a**–**e** and **5a**–**e** was achieved by both RP-HPLC (table 1) and ^{1}H NMR (see **Experimental part**). As expected, chemical shifts and HPLC retention times of the Fmoc-**D**X-**L**X-(**Q**)$_2$ tetramers **5a**–**e** matched well with the putative byproducts of α-amino acid chloride racemization in Fmoc-**L**X-**L**X-(**Q**)$_2$ (**4a-e**), i.e., Fmoc-**L**X-**D**X-(**Q**)$_2$.

Table 1. RP-HPLC racemization analysis of Fmoc-**L**X-**L**X-(**Q**)$_2$ (**4a-e**) and Fmoc-**D**X-**L**X-(**Q**)$_2$ (**5a-e**).

Tetramers	X	Ratio product:by-product[a]
4a	A	98 : 2
4b	K	N/A[b]
4c	D	99 : 1
4d	F	95 : 5
4e	S	98 : 2
5a	A	99 : 1
5b	K	N/A[b]
5c	D	94 : 6
5d	F	99 : 1
5e	S	98 : 2

[a]Determined by RP-HPLC,. [b]Ratio could not be determined by RP-HPLC due to overlaying of the two peaks.

The estimation of racemization was found to be robust and accurate. For example, tetramer **4a** showed approximately 2% byproduct formation by RP-HPLC, the peak of which corresponded well in terms of retention time with tetramer **5a** (Figure 3).

40. D. H. Rich, and J. Singh, *The peptides.* Academic Press: New York, **1979**.

Similarly, tetramer **5a** contained approximately 1% byproduct formation, the peak of which corresponded well with **4a**.

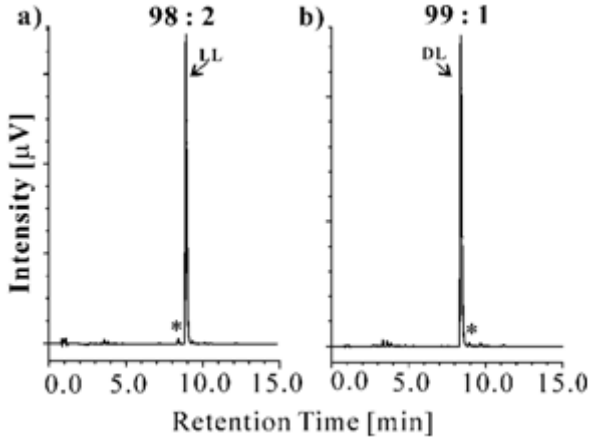

Figure 3. RP-HPLC chromatogram of crude products a) **4a** and b) **5a**. LL = Fmoc-Ala-Ala-$(Q)_2$-OH, DL = Fmoc-DAla-Ala-$(Q)_2$-OH; and * = putative byproduct of racemization during in situ acid chloride coupling.

The incidence of racemization for each amino acid incorporated was similar for the D and L isomers with small differences (<5%) probably resulting from the small scale at which these trials were carried out. For cases in which retention times were too similar to distinguish each diastereomer by C_{18}-RP-HPLC (e.g., **4b** and **5b**), ^{1}H NMR showed them to possess distinct differences in chemical shifts in their aromatic and amide regions (Figure 4). In some cases, no signals associated with the other diastereoisomer were visible, indicating racemization was negligible. Overall, racemization was kept under acceptable levels considering its known occurrence when using acid chloride activation. One exception was cysteine for which racemization was found to be too high to be of practical use (not shown).

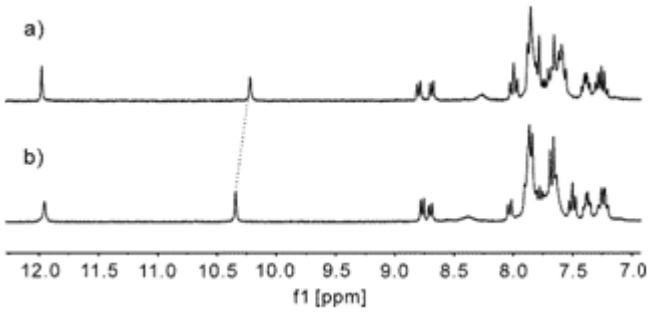

Figure 4. Amide and aromatic region of ^{1}H NMR spectra (300 MHz) of crude a) **4b** and b) **5b** in DMSO-d_6 showing a single set of signals in each instance.

2.4 Dimer strategy

We were keen to develop a methodology to incorporate the α,α-disubstituted AiB residue into hybrid foldamer sequences, as it is well-known for inducing helical folding in α-peptides and might lead to distinct behavior when mixed with an abiotic backbone. Probably due to steric hindrance, in situ acid chloride formation for the introduction of Fmoc-AiB led to incomplete coupling. We thus decided to adopt a fragment condensation methodology for incorporation of this residue. An AiB dimeric block was synthesized from the previously reported methyl 8-amino-4-isobutoxyquinoline-2-carboxylate **6** (Scheme 3). In this case, the isobutoxy side-chain was chosen for its well-documented ability to provide solubility in organic solvents,[41] thus reducing the risk of poor solubility of synthetic intermediates. Fmoc-AiB–OH was converted to its corresponding acid chloride via the use of the Ghosez reagent (1-chloro-*N*,*N*,2-trimethyl-1-propenylamine) and subsequently coupled to amine **6** to afford dimer **7** in 60% yield. The relatively modest yield in this case serves to illustrate the difficulty in coupling even reactive species, such as acid chlorides, to the relatively unreactive quinoline 8-amino group, and thus highlights the utility of microwave assistance during SPS. Conversion of the methyl ester to corresponding acid **8** was carried out in high yield by treatment with LiI, a method which avoids removal or modification of the terminal N^{α}-Fmoc group. (Thank Yui Nagaoka for the synthesis of this dimer block.)

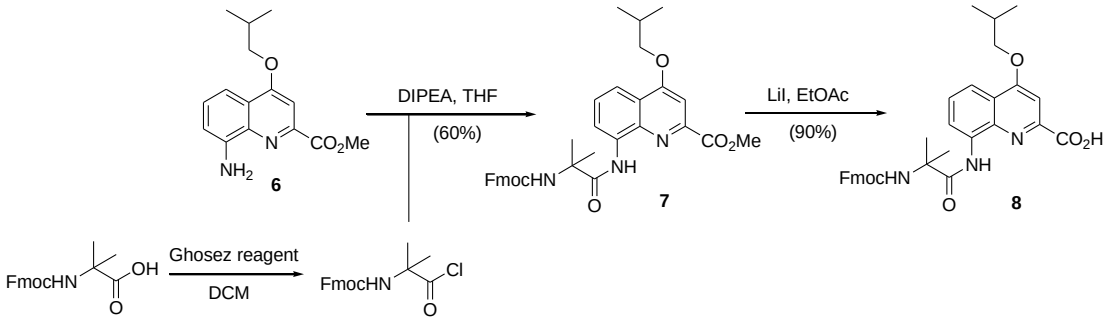

Scheme 3. Synthesis of Fmoc-**AiB**-$\mathbf{Q^{Leu}}$–OH Dimer Building Block **8**

41. B. Baptiste, J. Zhu, D. Haldar, B. Kauffmann, J. M. Léger, and I. Huc, *Chem. - Asian J.* **2010**, 5, 1364.

Preliminary tests with this dimer building block indicated that the HBTU/HOBt system could potentially be used in conjunction with microwave assistance. However, we were concerned that, for longer sequences, coupling efficiency might be reduced, and thus for SPS of the 13mer **9**, we employed our usual conditions[31b] for activation of **8** as the acid chloride followed by microwave-assisted coupling (Scheme 4). This afforded the final product in 39% yield after column chromatography. The fragment condensation approach thus proves useful for those monomers that cannot be coupled in high yield during SPS. However, it was not readily helpful for the particular case of cysteine as even the solution phase coupling to a quinoline monomer led to extensive racemization.

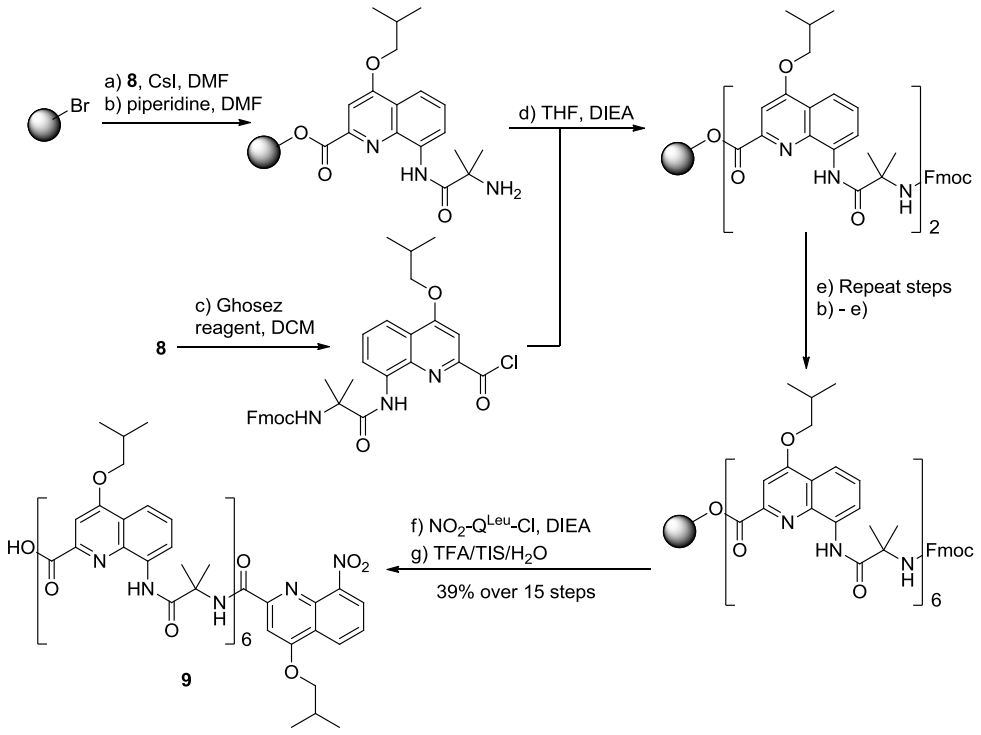

Scheme 4. Microwave assistant SPS of 13mer **9** from dimeric unit **8**.

To summarize, our SPS method for coupling α-amino acids to the quinoline aromatic amine was found to be highly efficient and led in most instances to negligible racemization. To access more difficult hybrid sequences (e.g., containing α-amino acids with higher steric hindrance at the α-carbon), the strategy of using preformed XQ dimer blocks appears to be a viable alternative. Both methods were found to be fully compatible with our microwave-enhanced SPS methodology.

3. Oligoamide synthesis

To confirm the utility of our in situ acid chloride coupling method, we first aimed to synthesize sequences based on a dimeric (**XQ**) repeat motif. Foldamers based on this motif had previously been shown in organic solvents to adopt a partially folded zigzag tape conformation with local conformational variability precluding long-range order.[32d] Considering that hydrophobic effects play a large part in stabilizing the conformations of aromatic oligoamide foldamers in aqueous conditions, we were curious to see if the conformations of fully water-soluble **(XQ)$_n$** sequences were any different from their organic-soluble counterparts.

The first sequence **10** was therefore an **(XQ)$_n$**-type 12mer combining Asp residues with quinolines bearing "Asp-like" side-chains to provide aqueous solubility at neutral or near-neutral pH while minimizing the risk of aggregation associated with mixing side-chains of different charge types (e.g., Asp and Lys). In brief, low-loading (0.38 mmol g^{-1}) Wang resin was converted to its corresponding bromide using the reported procedure[31b] and loaded with the first Fmoc-Q^{Asp} monomer unit (Scheme 5). Fmoc deprotection was carried out using 20% v/v piperidine in DMF at 25 ℃ and Fmoc-Asp(tBu)–OH incorporated via its in situ-formed acid chloride using our optimized methodology. Coupling of the Fmoc-Q^{Asp} monomer unit to the aliphatic amine was carried out through the preformed acid chloride as previously described, and synthesis continued to afford the final sequence. Capping of the N-terminal amine was carried out using acetic anhydride and the crude product (23.5 mg, 51% crude yield; purity by RP-HPLC: 60%) cleaved from the resin using a solution of TFA/TIS/H_2O (95:2.5:2.5 v/v/v). Purification by RP-HPLC afforded the final pure product in a yield of 15% over 27 steps.

We also wanted to extend our methodology to sequences based on the **XQ_2** trimer repeat motif, as an organic soluble analogue was reported to form well-defined helices.[30] However, we anticipated that their sequence might be slightly more of a challenge than with **XQ** repeat motifs due to the incorporation of the additional

coupling between quinoline units. To vary side-chain functionality from sequence **10**, we chose a sequence that combined Lys with quinolines bearing "Orn-like" side-chains.[31b]

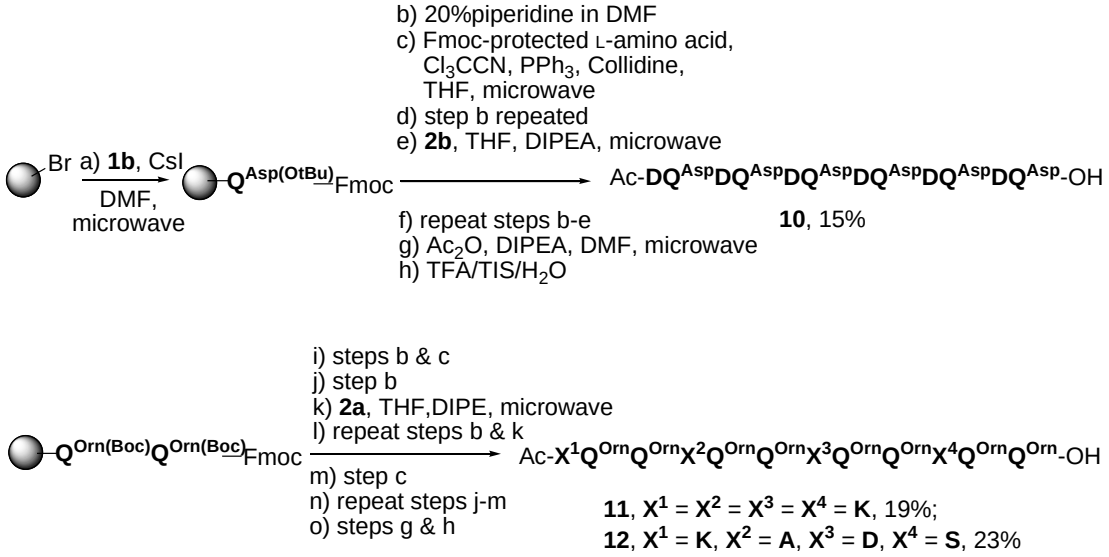

Scheme 5. Solid phase synthesis of water-soluble **XQ** and $\mathbf{XQ_2}$-type hybrid sequences.

Fmoc-$(Q^{Orn})_2$-Wang was synthesized using the methodology as previously described with the Fmoc group deprotected and Fmoc-Lys(Boc)–OH incorporated using our optimized in situ acid chloride method (Scheme 5). The sequence was then continued in the same fashion to produce the 12mer with the terminal Fmoc removed, the resulting amine acetylated, and the product cleaved from the resin in the same manner as for the $\mathbf{(XQ)_n}$ sequence. The resulting crude product was purified by RP-HPLC to afford sequence **11** in a yield of 19% over 27 steps. To further test the reproducibility of our methodology and also to provide a sequence more amenable to full NMR assignment, we also synthesized compound **12**, which incorporated Lys, Ala, Asp, and Ser residues. This sequence was afforded after RP-HPLC purification with a yield of 23% over 27 steps.

4. Structural analysis

4.1 CD study

For **$(XQ)_n$** sequences, we were first interested to see if their backbone flexibility and lower content of aromatic units could be overcome by solvophobic effects in protic solvents, inducing folding into more ordered conformations than observed in organic solvents. For **$(XQ_2)_n$** sequences, we were intrigued to see if protic solvents induced any changes in conformation over that which had been previously seen in the reported crystal structure of **$(LQ^{Leu}{}_2)_4$** from organic solvents. We first turned to CD analysis as a rapid way to detect potential folding behavior. The 12mers **10** and **11** were analyzed as examples of **$(XQ)_n$** and **$(XQ_2)_n$** sequences, respectively. Figure 5 shows that for **11**, the characteristic bands at approximately 380 nm associated with quinoline stacking (and therefore probable helical conformation) are present in both methanol and water. In addition, this CD spectrum also matches well with that reported for **$(LQ^{Leu}{}_2)_4$**, where the positive signal of the band at 380 nm indicates the same right-handed (*P*) helix sense.[30] A similar CD was also recorded for compound **12** (see Experimental part), indicating the low impact of side-chain functionality on this conformational preference. In contrast, we were disappointed to see that the CD spectrum for **10** lacks bands at 380 nm, and its similarity with the CD spectrum of **$(LQ^{Leu})_4$** indicates that this sequence does not appear to fold into a helical conformation even in protic solvents.

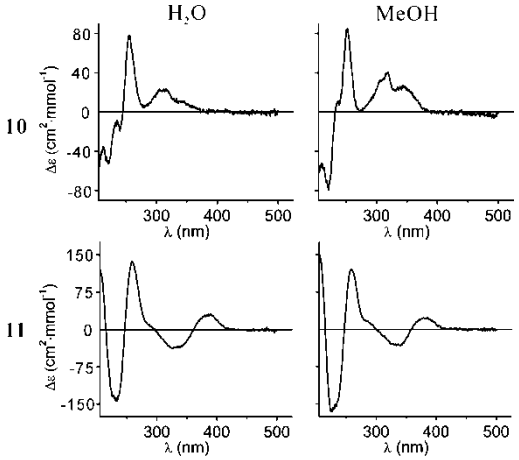

Figure 5. CD spectra of **10** and **11** in H_2O and MeOH at 20 ^oC. (Concentration: 30 μM)

4.2 NMR study and solution phase structure elucidation

4.2.1 ^{1}H NMR study

We then turned to the ^{1}H NMR spectra of **10** and **11** to provide more detailed information about their folding. The aromatic region displayed in Figure 6 shows a single set of sharp signals for compound **11** in both H_2O/D_2O (9:1) and CD_3OH (Figure 6a and 6b, respectively) with resonances spread over a wide chemical shift range and with minimal exchange of amide protons. This indicates that the sequence is in a single well-defined conformation; upfield shifting of some signals also indicates the effect of aromatic π–π stacking associated with helical folding as normally seen in quinoline-based aromatic oligoamide foldamers. Interestingly, the signals of **11** are significantly sharper at 25 ℃ than those of the analogous $\mathbf{(LQ^{Leu}{}_2)_4}$ sequence in solvents such as $CDCl_3$, the spectra of which could only be sharpened by cooling to low temperatures.[30] This difference probably reflects the increased conformational stability of this foldamer type in protic solvents due to the high contribution of hydrophobic effect toward folding and therefore the high impact of solvent on stability of the resulting helix.

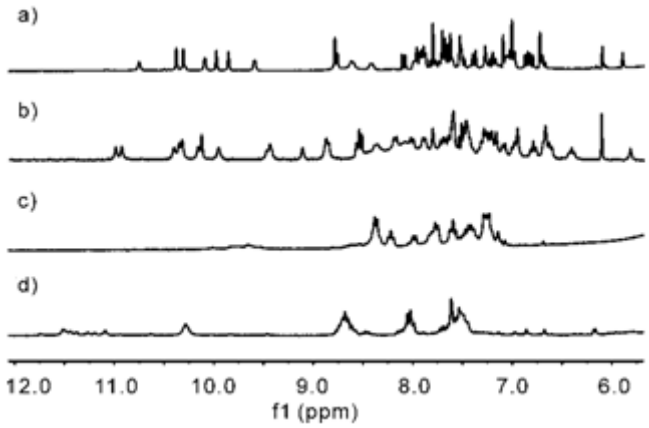

Figure 6. Part of the ^{1}H NMR spectra (300 MHz) of **10** and **11** showing aromatic amide (9 – 12 ppm), aliphatic amide and aromatic proton resonances (6 – 10 ppm) in protic solvents at 25 ℃ for a) **11** in H_2O/D_2O (9:1 v/v), b) **11** in CD_3OH, c) **10** in H_2O/D_2O (9:1 v/v), and d) **10** in CD_3OH.

Furthermore, variable temperature ^{1}H NMR experiments with **11** showed that heating in CD_3OH resulted in signal broadening, whereas in H_2O/D_2O (9:1), this was not observed (Figure 7). This high stability in aqueous conditions also matches well

with our previous experience regarding the solvent dependence of handedness inversion kinetics in quinoline oligoamide foldamers.[42]

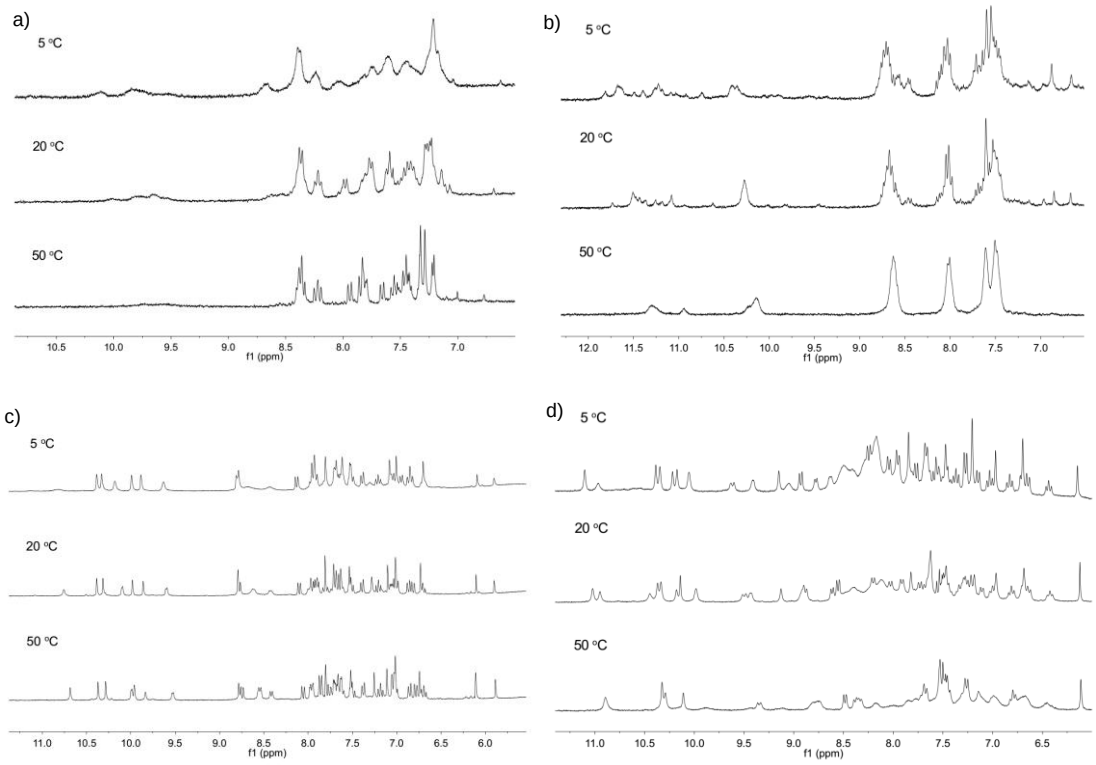

Figure 7. Variable temperature (5 - 50 °C) ^{1}H NMR spectra (amide and aromatic region) of a) **10** in H_2O/D_2O (9:1), b) **10** in CD_3OH, c) **11** in H_2O/D_2O (9:1), and d) **11** in CD_3OH

In contrast, the spectra of **10** show broad signals at 25 ℃ in both H_2O/D_2O (9:1) and CD_3OH (Figure 6c and 6d, respectively) with evident solvent exchange of many amide protons. In addition, the former solvent appears to afford a single set of signals, whereas in the latter, a minor species is apparent. Temperature experiments (Figure 7) revealed that, lower temperatures resulted in signals becoming broader in water and the appearance of additional signals in methanol. Increasing the temperature resulted in convergence of signals. This appearance of additional sets of signals can most likely be attributed to nonspecific aggregation, together with the broadening effect, perhaps indicates the higher availability of hydrophobic surfaces because they are less involved in folding of the sequence. To summarize, the spectra of **10** indicate the

42. S. J. Dawson, A. Mészáros, L. Pethő, C. Colombo, M. Csékei, A. Kotschy, and I. Huc, *Eur. J. Org. Chem.* **2014**, 2014, 4265.

presence of multiple poorly folded and thus solvent accessible conformations with the higher availability of aromatic surfaces permitting nonspecific aggregation.

4.2.2 NMR assignment

To delve further into the solution-state folding behavior of the $\mathbf{(XQ_2)}_{\boldsymbol{n}}$-type foldamers, we carried out a detailed analysis of compound **12** by 2D NMR, a 12mer in which four different amino acid residues had been incorporated. For the convenience of illustrating the assignments, a naming convention was established (Figure 8).

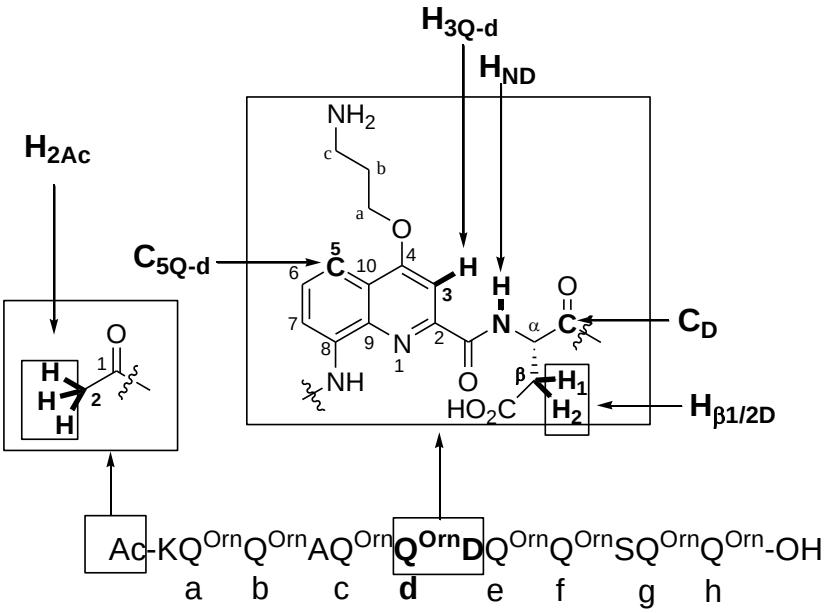

Figure 8. Example of naming convention for 2D NMR assignments.

To begin with, COSY and TOCSY experiments (in H_2O/D_2O (9:1)) were carried out and they permitted assignment of amino acid and quinoline protons as demonstrated in Figure 9. (more examples in Experimental part)

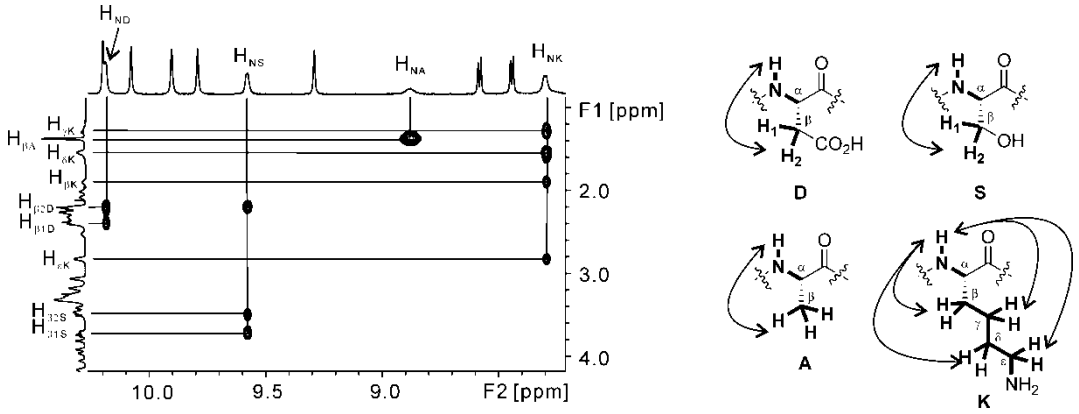

Figure 9. Excerpt from ^{1}H-^{1}H TOCSY spectrum of **12** in H_2O/D_2O (9:1 v/v) at 25 ℃ (700 MHz) indicating the correlations between aliphatic amide proton (H_{NX}) and side-chain methylene protons (H_X) of each amino acid. Double-headed arrows indicate the observed correlations.

Quinoline protons could be separated into eight discrete groups, corresponding to each quinoline unit. HMBC data was then used to establish correlations between each quinoline amide NH with C7 of the ring, which could further provide H5.[25b] In the same manner, H3 could be correlated to C4 and then back to H5. Finally C5 could be correlated to H7. (Examples of these in Experimental part) Once this was completed for each quinoline, it was then correlated with the surrounding amino acid residues to provide sequence information. Figure 10 provides the example of the -DQQS- fragment: the Asp carbonyl carbon (C_D) was correlated to the adjacent quinoline (quinoline 'e') amide NH ($H_{NQ\text{-}e}$), which then provided the quinoline H3 position ($H_{3Q\text{-}e}$) which had been assigned. This could then be correlated to the quinoline carbonyl carbon ($C_{Q\text{-}e}$) and then on to the amide NH of the next quinoline unit ($H_{NQ\text{-}f}$). Correlations continued in the same manner to provide the serine amide NH (H_{NS}). Further details of other correlations are outlined in the Experimental part.

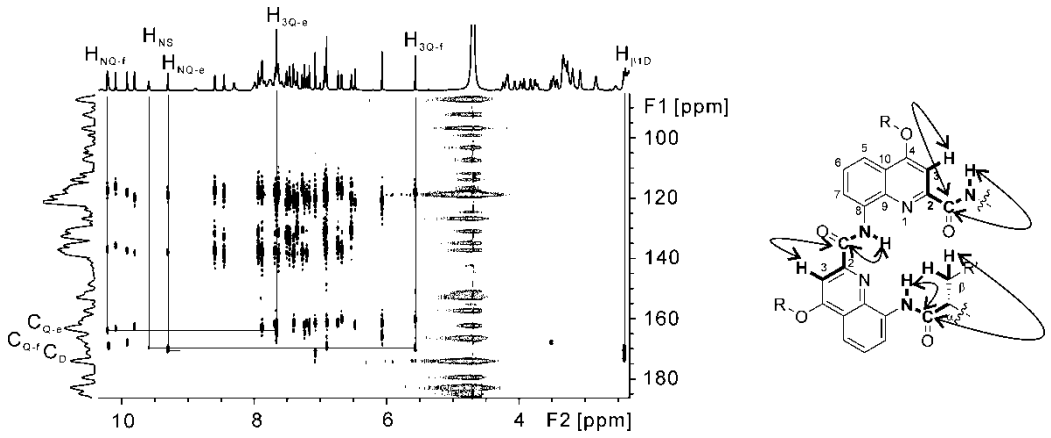

Figure 10. Excerpt from ^{1}H - ^{13}C HMBC spectrum of **12** in H_2O/D_2O (9:1 v/v) at 25 ℃ (700 MHz) indicating the correlations involved in assigning the –DQQS- fragment of the sequence. Double-headed arrows indicate the observed correlations.

4.2.3 Conformational analysis and molecular modeling

Once the sequence was fully assigned, NOESY experiments were used to provide information on the sequence conformation. Important correlations were made between *i* and *i* + 3 quinoline units, and position H3 was particularly useful as a clearly distinguished singlet. For example, correlations can be seen between $H_{3Q\text{-}f}$ with both $H_{3Q\text{-}d}$ and $H_{3Q\text{-}h}$, indicating their closeness in space, and thus suggesting they are stacked in sequence (Figure 11).

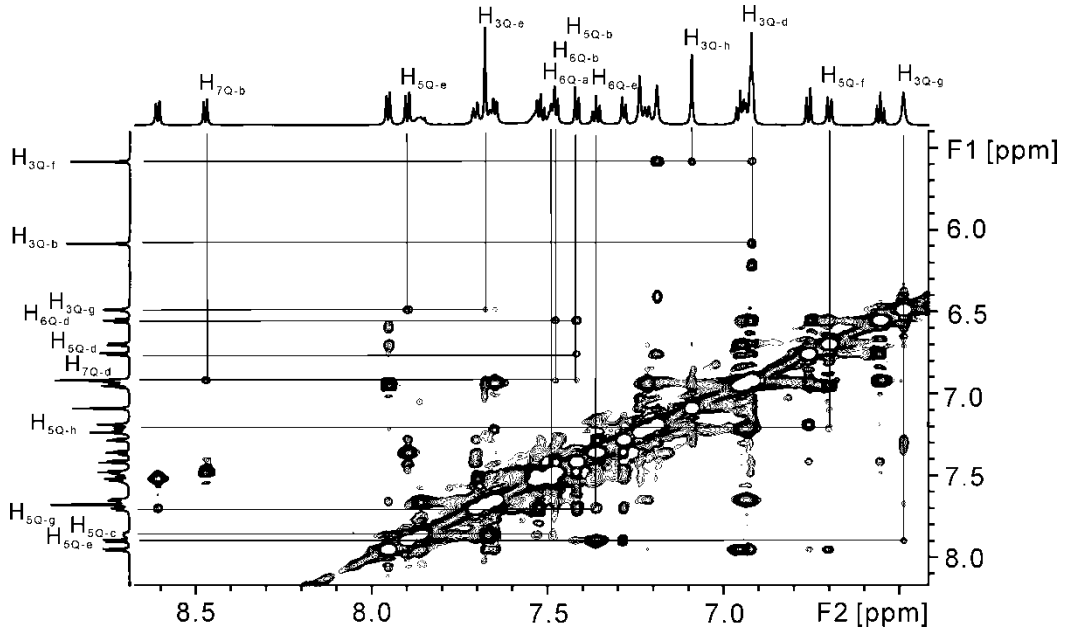

Figure 11. Excerpt from ^{1}H - ^{1}H NOESY spectrum of **12** in D_2O at 25 ℃ (800 MHz) showing the NOE correlations between aromatic protons of quinolines at *i* and *i* + 3.

In a similar manner, methylenes of the quinoline 4-position side-chain proximal to the ether (3.4–4.2 ppm) were also useful in that they were found to have strong correlations with *i* + 3 quinoline ring protons (Figure 12).

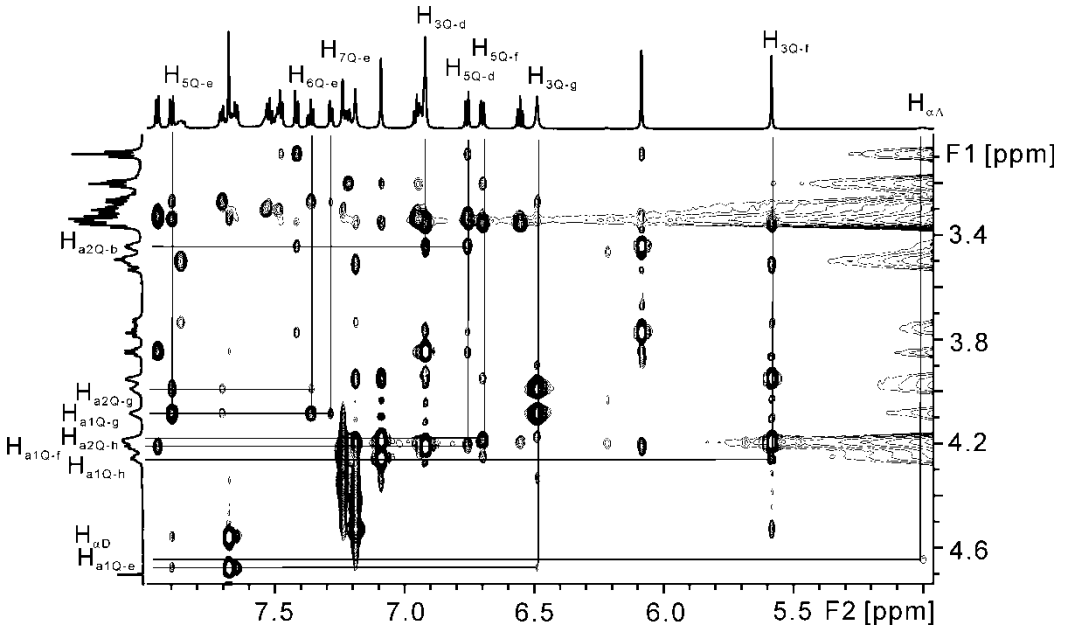

Figure 12. Excerpt from ^{1}H - ^{1}H NOESY spectrum of **12** in D_2O at 25 ℃ (800 MHz) showing the NOE correlations between quinoline side-chain methylene protons and aromatic protons of quinolines at *i* + 3.

Encouraged by the substantial number of NOE correlations that appeared to support a helical conformation, we made the further step to generate a molecular model based on these data. After eliminating overlapping or ambiguous signals, NOE correlations were first integrated and further converted to distance information according to the reported formula.[43] (The list of selected NOE correlations for molecular modeling see Experimental part) Then, an ill-folded structure of **12** with a right-handed helical twist was energy minimized using MacroModel using distance information as constraints. This yielded a first helical structure that was then randomly modified and again minimized by the same method to generate a second molecular model. This process was repeated 19 times to obtain 20 molecular models for superposition and RMSD calculation (see Experimental part). Associated RMSD data show that the sequence backbone demonstrates considerable stability. Panels a–c in Figure 13 show one of the 20 models of compound **12**: in agreement with CD data, it adopts a right-handed

43. E. Ammalahti, M. Bardet, D. Molko, and J. Cadet, *J. Magn. Reson., Ser. A* **1996**, 122, 230.

helical arrangement with close resemblance to the crystal structure of **$(LQ_2)_4$** previously reported.[30] Repeated attempts were made to apply the NOE data to a left-handed structure with no success. Each **XQ_2** unit spans approximately one turn (pitch of 4.1 Å) resulting in an arrangement of the α-amino acid side-chains on one face of the helix. However, rather than being directly overlaid, they are offset from each other by a number of degrees, resulting in a diagonal array of side-chains down the helix axis. The Cα-Cα distances between consecutive α-amino acids starting from the N-terminus are 5.0, 4.4, and 5.0 Å, respectively, which are slightly smaller than the average distance (6.3 Å) in an α-helix. One significant difference from the crystal structure of **$(LQ^{Leu}_2)_4$** is that, in this case, the α-amino acid amide NH groups do not point directly toward the helix axis. Indeed, the NH of alanine appears to form a hydrogen bond with the carbonyl CO of lysine, setting alanine with $\phi = -145.7°$ and $\psi = 40.3°$. It is quite normal for peptides with a secondary structure of β-sheet or right-handed α-helix to have such high negative ϕ values. However, the coordinate falls (combining the small positive ψ value) in the allowed area of β-sheet according to Ramachandran plot. This tilting of the α-amino acid amide function to planes parallel to the helix axis was previously suggested by an energy-minimized molecular model of **$(LQ^{Leu}_2)_4$** that was slightly different from its crystal structure.[30] However, this model suggested that the amide NHs would tilt down in the direction of the C-terminus, forming hydrogen bonds with the quinoline $i + 2$ amide carbonyl. In the model of **12**, it can be seen that the α-amino acid amide NHs are instead tilted upward toward the N-terminus (apart from the NH of lysine, which due to being at the N-terminus appears to be involved in a hydrogen bond with the CO of alanine). In the case of serine, this effect is severe enough that it results in a slight distortion of the backbone π–π stacking, increases the serine ϕ angle to −78.4°, and results in the NH proton being in close proximity (3.0 Å) to H3 of the neighboring quinoline unit 'f' ($H_{3Q\text{-}f}$). This distance was confirmed by analysis of the appropriate correlations via further ROESY experiments (Figure 13d). This distortion is assumedly compensated by the formation of three hydrogen bonds: between the carbonyl of quinoline 'f' with $i + 2$ and $i + 3$ quinoline amide NHs and the C-terminal carboxylic acid.

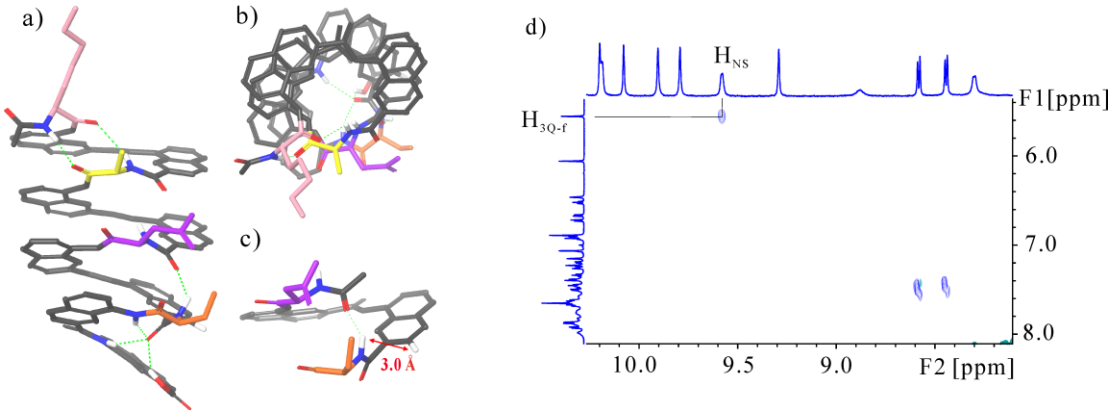

Figure 13. An NOE data based molecular model: a) side view; b) top view; c) segment showing distance between H_{NS} and $H_{3Q\text{-}f}$ of **12**; and d) part of ROESY spectrum of **12** in H_2O/D_2O (9:1 v/v) at 25 ℃ (700 MHz) showing the corresponding correlation between the amide NH of Ser (H_{NS}) and H3 of the neighboring quinoline 'f' ($H_{3Q\text{-}f}$) observed in the molecular model. Key N, O and H atoms are shown in blue, red and white, respectively. Lys, Ala, Asp and Ser residues are shown in pink, yellow, purple, and orange, respectively. Quinolines are shown in grey, with side-chains removed for clarity. Putative hydrogen bonds are shown as dashed green lines. Double-headed arrow in red indicates the distance between H_{NS} and $H_{3Q\text{-}f}$.

Variable temperature NMR experiments with the organic-soluble analogue **$(LQ^{Leu}{}_2)_4$** previously demonstrated the existence of two nonaggregated, concentration-independent and solvent-dependent helical states of similar handedness equilibrating slowly on an NMR time scale, which were assigned to the state observed in the crystal and another suggested by molecular modeling.[30] Our study of water-soluble **12** shows that only one species prevails in water and provides direct evidence for a helical conformation slightly differing from that observed in the solid state. In particular, in water, a number of different hydrogen bond arrangements are possible other than the *i*/*i* – 1 hydrogen bonding network seen in the crystal structure of **$(LQ_2)_4$**.

4.3 Crystallography

Only recently we obtained a crystal structure of this **XQ_2**-type hybrid foldamer from water, an undecameric **FQ_2**-type foldamer (compound **13**). The synthesis and crystallization are based on the quinoline monomers with carboxymethyl side chain which will show in chapter three in detail. Moreover, the design initially was aimed at

constructing a helix bundle in water (see chapter four). Thus, there are some differences of the structure (but should not affect the analysis and result here, Figure 14a).

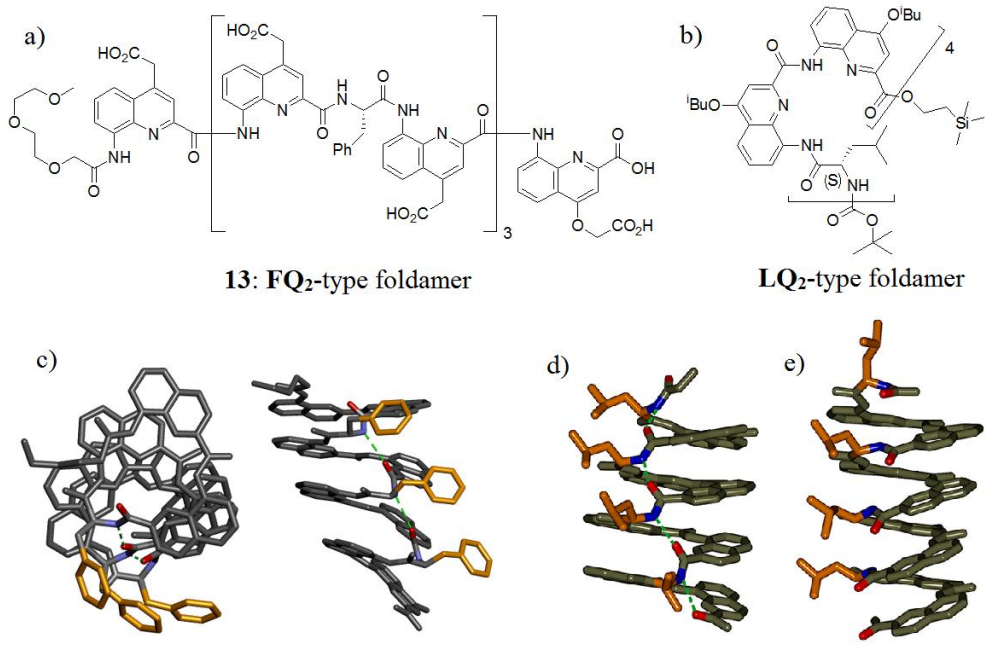

Figure 14. Structures of a) **13** and b) the dodecameric **LQ$_2$**-type foldamer. c) Crystal structure of **13**. d) A proposed molecular model of an alternative structure of the dodecameric **LQ$_2$**-type foldamer. e) Crystal structure of the dodecameric **LQ$_2$**-type foldamer. Phenylalanine and Leucine N atoms and side chains are shown in blue and gold, respectively. Some quinoline or carbamate carbonyl O atoms are shown in red. Some key hydrogen bonds are shown as dashed green lines. Included solvent molecules, quinoline side chains, TMSE groups, *tert*-butyl groups, and H atoms have been omitted for clarity. Crystal structure of **13** is not yet fully refined.

Synthesis of **13** was accomplished using the same SPS method as **11** and **12**. Compared to the structures of **11** and **12**, foldamer **13** has some desired features to facilitate crystallization from water. Instead of using Orn-like side chain on these quinoline motifs, **13** bears these much shorter and more rigid carboxymethyl side chains. However, the C-terminal quinoline residue is **Q^{Asp}** in order to avoid decarboxylation taking place. For detailed discussion of the crystal growth ability and decarboxylation process of this carboxymethyl side chain see chapter three. The diethylene glycol-like tail at the N-terminus is incorporated to disturb the potential head-to-head aggregation (also see chapter four).

An X-ray quality crystal of **13** was obtained by the standard hanging-drop technique. The resulting floppy powder of **13** after lyophilization was dissolved in pure water to obtain a solution with a concentration of 2 mM. Then, the aqueous drops were prepared by mixing 1.0 μL of the foldamer solution with an equal volume of the crystallization reagent (30% PEG 4000, 50 mM TRIS, pH = 8.5, 150 mM NH_4Cl, 10 mM $CaCl_2$). Crystal growth was carried out at 20 ^oC and the crystallization took place while water of the drop diffused (also see chapter three). (Thank Dr. Pradeep K. Mandal for the crystallization of **13** and the following crystal structure determination and refinement.)

Similar to the molecular model of **12**, crystal structure of **13** (Figure 14c) also shows a right-handed helical conformation and linear arrangement of these amino acid (here is phenylalanine) side chains on one side of the helix. An important feature of this crystal structure is the linear array of hydrogen bonding occurred between these amide bonds. Instead of forming hydrogen bond with nearby quinoline motif, these amide NHs tilt down in the direction of the C-terminus to form a linear array of hydrogen bonding with themselves in the planes parallel to the helix axis. This crystal structure unambiguously proves the existence of this type of hydrogen bonding mode in $\mathbf{XQ_2}$-type foldamers and thus verifies our previously proposed molecular model of $(\mathbf{LQ^{Leu}_2})_4$ (Figure 14d, and also shows its formula, 14b, and its crystal structure, 14e, to compare against).[30] Besides, it also inspires us to revise the molecular model of **12** which has only one amide bond adopting the tilted local conformation. After carefully checking the NMR data and those molecular models, we found the present molecular model is still the most possible conformation of **12** in water amongst others. In fact, we also identified one rare (once out of twenty trials) case that the amide bond of Asp residue tilts instead of that of Ser residue. But it also has only one amide bond tilts and the orientation of amide NH is pointed to the N-terminus as well. We also tried the manipulation of the starting conformation for molecular modeling directly as a helical conformation with the linear array of hydrogen bonding between amide bonds similar to these of the crystal structure of **13**. The result came out a twisted local

conformation of Asp residue (its side chain is embedded into the helix) which indicated the given conformation from the crystal structure should not be the prevalent one in water (at least for compound **12**). However, if the manipulated hydrogen bonding array had its amide NHs pointed to the N-terminus (the reversed orientation), it could result a normal helical conformation implying the possible correctness of the orientation of amide NH in molecular model of **12**. Anyhow, crystal structure is only one snapshot of the conformation and it may not be the dominant species in solution. In addition, we have yet not enough knowledge of this $\mathbf{XQ_2}$-type foldamer. Depending on the side chain and solvent, the conformation and folding behavior maybe different from each other. Therefore, the molecular model based on NMR is probably the right (or the dominant) conformation in solution phase.

5. Conclusion and perspectives

An efficient microwave-assisted solid phase methodology has been developed allowing the incorporation of a range of α-amino acids into quinoline oligoamide sequences with negligible racemization (<2%) in most cases. For difficult cases such as AiB, an alternative segment condensation strategy was also validated. Both methods are fully compatible with our existing strategy for SPS of quinoline oligoamides. CD and NMR analysis demonstrated that, even in protic solvents, sequences based on an **XQ** dimer repeat unit do not fold into a single defined conformation with the associated solvent-accessibility of the hydrophobic aromatic surfaces appearing to drive nonspecific aggregation at lower temperatures. In contrast, sequences based on an $\mathbf{XQ_2}$ trimer repeat unit demonstrate folding into a single well-defined conformation in protic solvents at a range of temperatures with no evidence of aggregation behavior. A dodecameric $\mathbf{XQ_2}$-type foldamer containing four different amino acid residues (Lys, Ala, Asp, and Ser) was fully assigned by NMR in aqueous medium, and calculated distances were used to generate a molecular model. This demonstrated that the sequence adopts a right-handed helical arrangement with the four amino acid residues projecting side chains in an array on one face of the helix. Putative hydrogen bonds were shown to be different from those seen in the crystal structure of the organic-soluble analogue $\mathbf{(LQ^{Leu}{}_2)_4}$ and shed further light on conformational preferences of these hybrid sequences under different conditions. The crystal structure of an undecameric $\mathbf{FQ_2}$-type foldamer showed an different helical conformation with a linear array of hydrogen bonding of these amino acid amide bonds which validated our previously proposed molecular model of $\mathbf{(LQ^{Leu}{}_2)_4}$.

Further work will focus on diversifying side-chain functionality of the $\mathbf{(XQ_2)_{\mathit{n}}}$-type hybrid foldamers and then exploring their application toward targeting biological systems such as:

- Protein recognition. The linear arrangement of amino acid side chains on one side of the helical conformation of $\mathbf{(XQ_2)_{\mathit{n}}}$-type foldamer is useful of recognizing

protein surface. By targeting the specific side chains in some protein pockets, these **$(XQ_2)_n$**-type foldamers could potentially act as a protein inhibitor.

- Cell-penetration. Playing with the diversity of side chains, cell-penetration of these **$(XQ_2)_n$**-type foldamers could be achieved. Further studies on the factors affecting cell uptake, such as the length, amphiphilicity, charge preferences and charge distributions of the foldamer, will be helpful for understanding cell-penetration mechanism.

- Helix bundle. The facial polarity of **$(XQ_2)_n$**-type foldamers could be used to lead self-assembly and thus achieve the construction of a helix bundle.

6. Experimental part

6.1 Racemization assessment supported by RP-HPLC and ^{1}H NMR

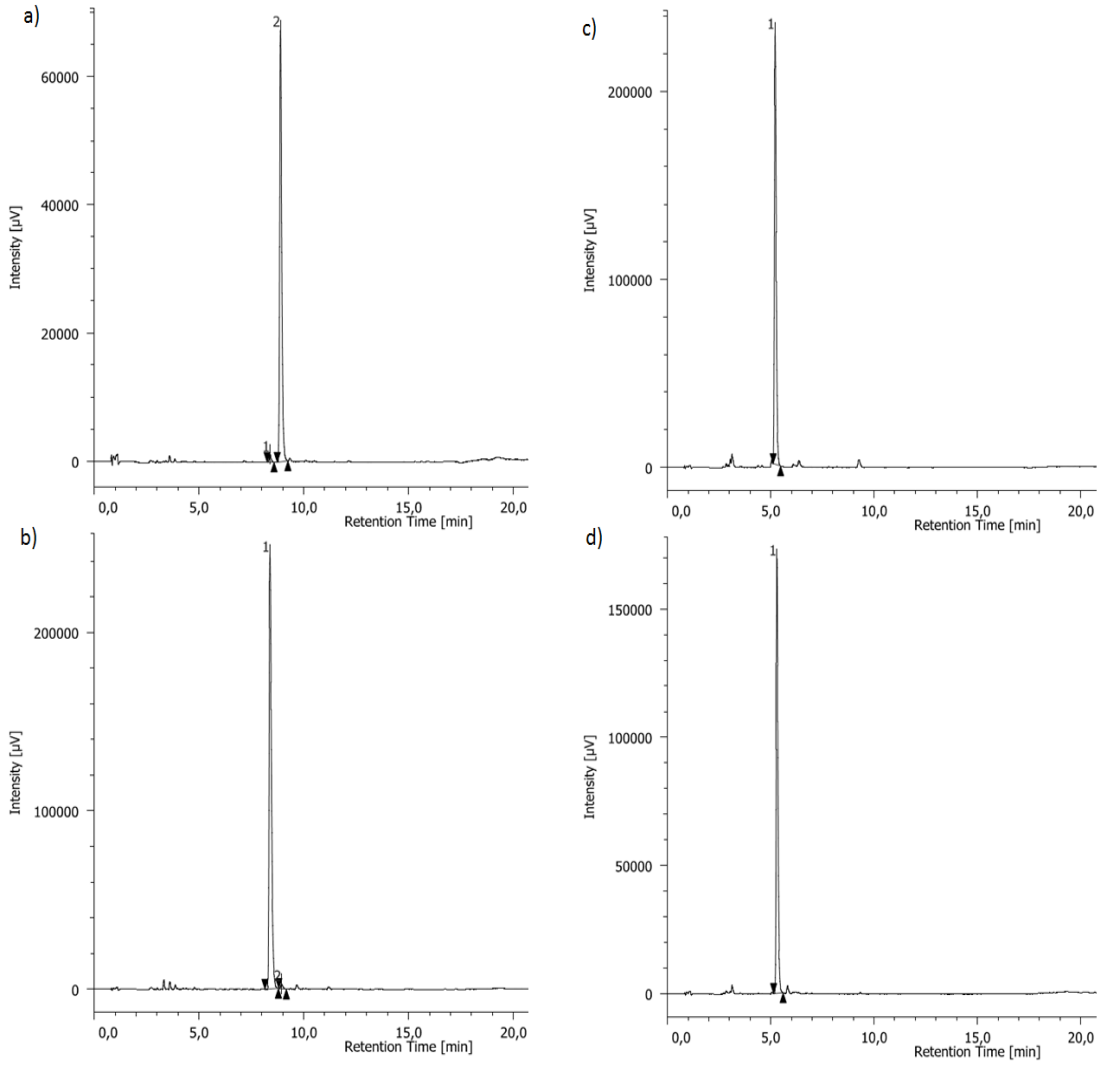

Figure 15. RP-HPLC chromatograms of crude a) **4a**, b) **5a**, c) **4b**, and d) **5b**.

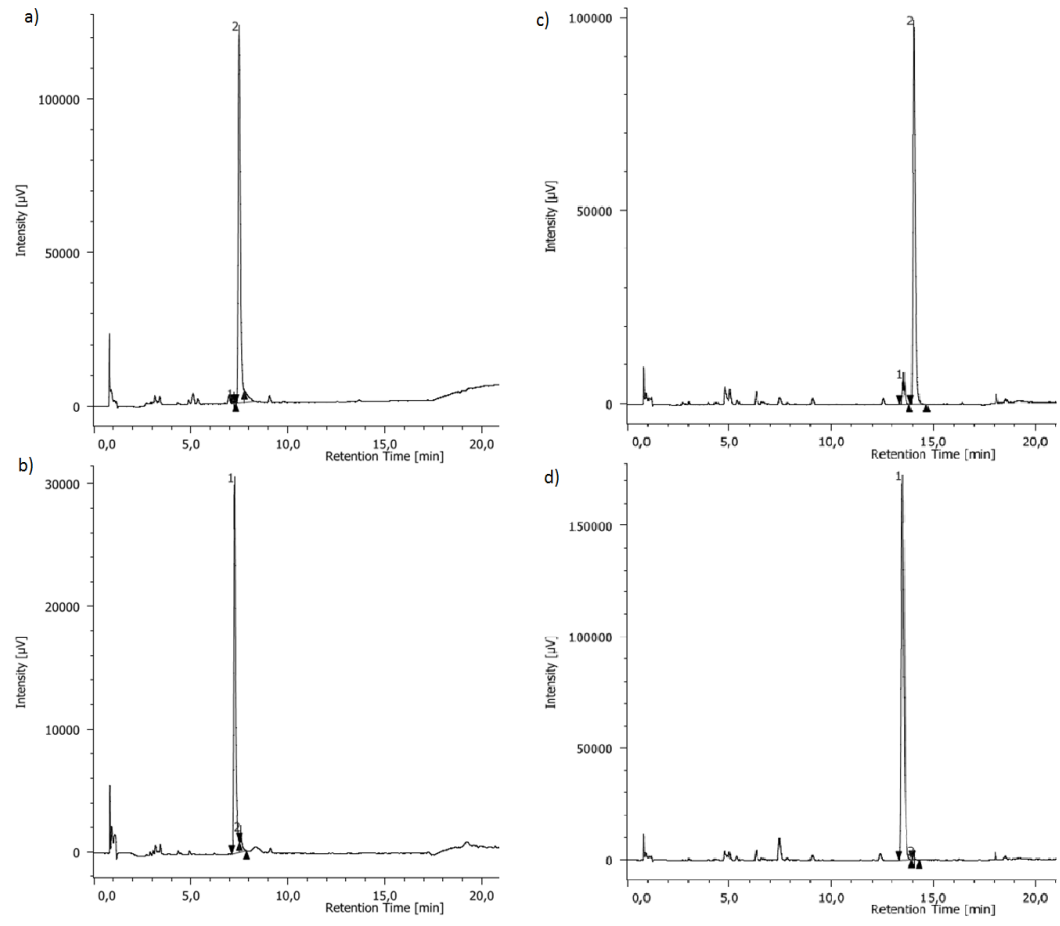

Channel & Peak Information Table
Chromatogram Name h96r2-CH3 Compound 4c
Sample Name
Channel Name CH3

#	Peak Name	CH	tR [min]	Area [µV·sec]	Height [µV]	Area%	Height%	Quantity	NTP	R
1	Unknown	3	7,208	4429	784	0,444	0,648	N/A	35037	
2	Unknown	3	7,483	993842	120243	99,556	99,352	N/A	19982	

Chromatogram Name h97-Asp-DL-CH3 Compound 5c
Sample Name
Channel Name CH3

#	Peak Name	CH	tR [min]	Area [µV·sec]	Height [µV]	Area%	Height%	Quantity	NTP	R
1	Unknown	3	7,250	202505	29995	94,086	95,338	N/A	30300	
2	Unknown	3	7,575	12729	1467	5,914	4,662	N/A	N/A	

Channel & Peak Information Table
Chromatogram Name h98-Phe-LLr-CH3 Compound 4d
Sample Name
Channel Name CH3

#	Peak Name	CH	tR [min]	Area [µV·sec]	Height [µV]	Area%	Height%	Quantity	NTP	Re
1	Unknown	3	13,542	42894	5916	5,258	5,725	N/A	84089	
2	Unknown	3	14,050	772928	97412	94,742	94,275	N/A	76436	

Chromatogram Name h99-Phe-DL-CH3 Compound 5d
Sample Name
Channel Name CH3

#	Peak Name	CH	tR [min]	Area [µV·sec]	Height [µV]	Area%	Height%	Quantity	NTP	Re
1	Unknown	3	13,492	1420167	169000	99,747	99,702	N/A	61330	
2	Unknown	3	14,100	3601	505	0,253	0,298	N/A	98651	

Figure 16. RP-HPLC chromatograms of crude a) **4c**, b) **5c**, c) **4d**, and d) **5d**.

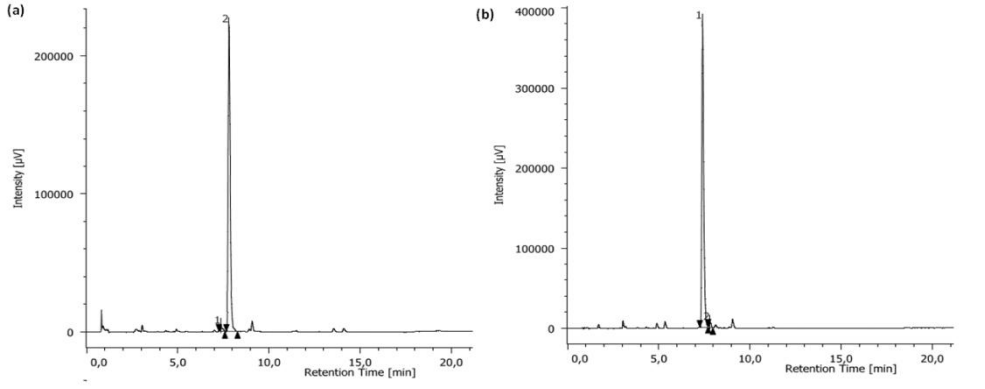

Channel & Peak Information Table
Chromatogram Name 100-Ser-LLr-CH3 Compound 4e
Sample Name
Channel Name CH3

#	Peak Name	CH	tR [min]	Area [µV·sec]	Height [µV]	Area%	Height%	Quantity	NTP	Res
1	Unknown	3	7,358	35287	4125	2,076	1,820	N/A	10318	
2	Unknown	3	7,808	1664122	222468	97,924	98,180	N/A	26041	

Chromatogram Name h101-Ser-DL-CH3 Compound 5e
Sample Name
Channel Name CH3

#	Peak Name	CH	tR [min]	Area [µV·sec]	Height [µV]	Area%	Height%	Quantity	NTP	Res
1	Unknown	3	7,392	2852998	382848	98,354	98,244	N/A	23196	
2	Unknown	3	7,817	47736	6843	1,646	1,756	N/A	30320	

Figure 17. RP-HPLC chromatograms of crude a) **4e** and b) **5e**,

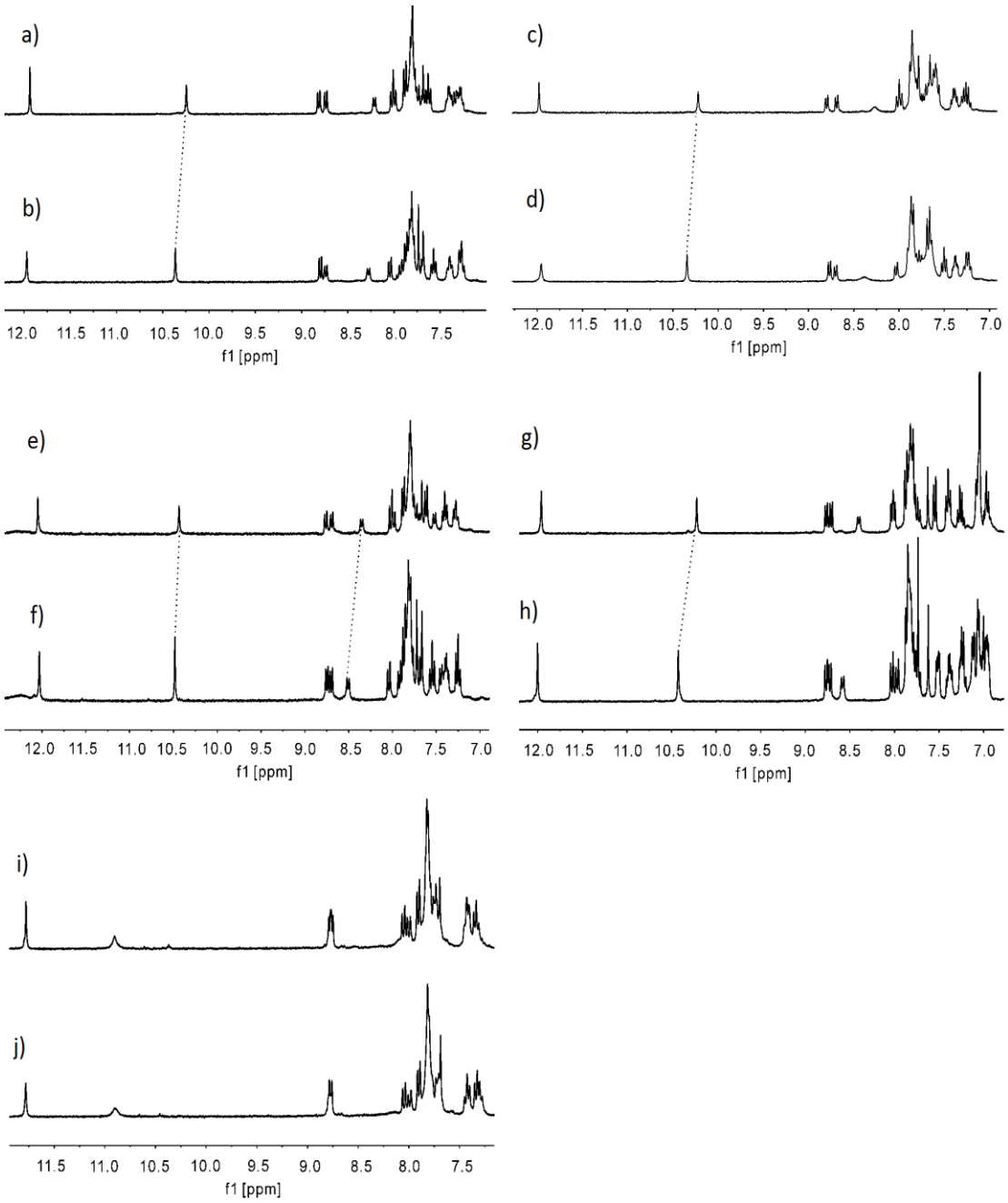

Figure 18. Amide and aromatic region of ^{1}H NMR (300 MHz) spectra of crude a) **4a**, b) **5a**, c) **4b**, d) **5b**, e) **4c**, f) **5c**, g) **4d**, h) **5d** i) **4e**, and j) **5e** in DMSO-d_6 at room temperature.

6.2 CD and UV spectra

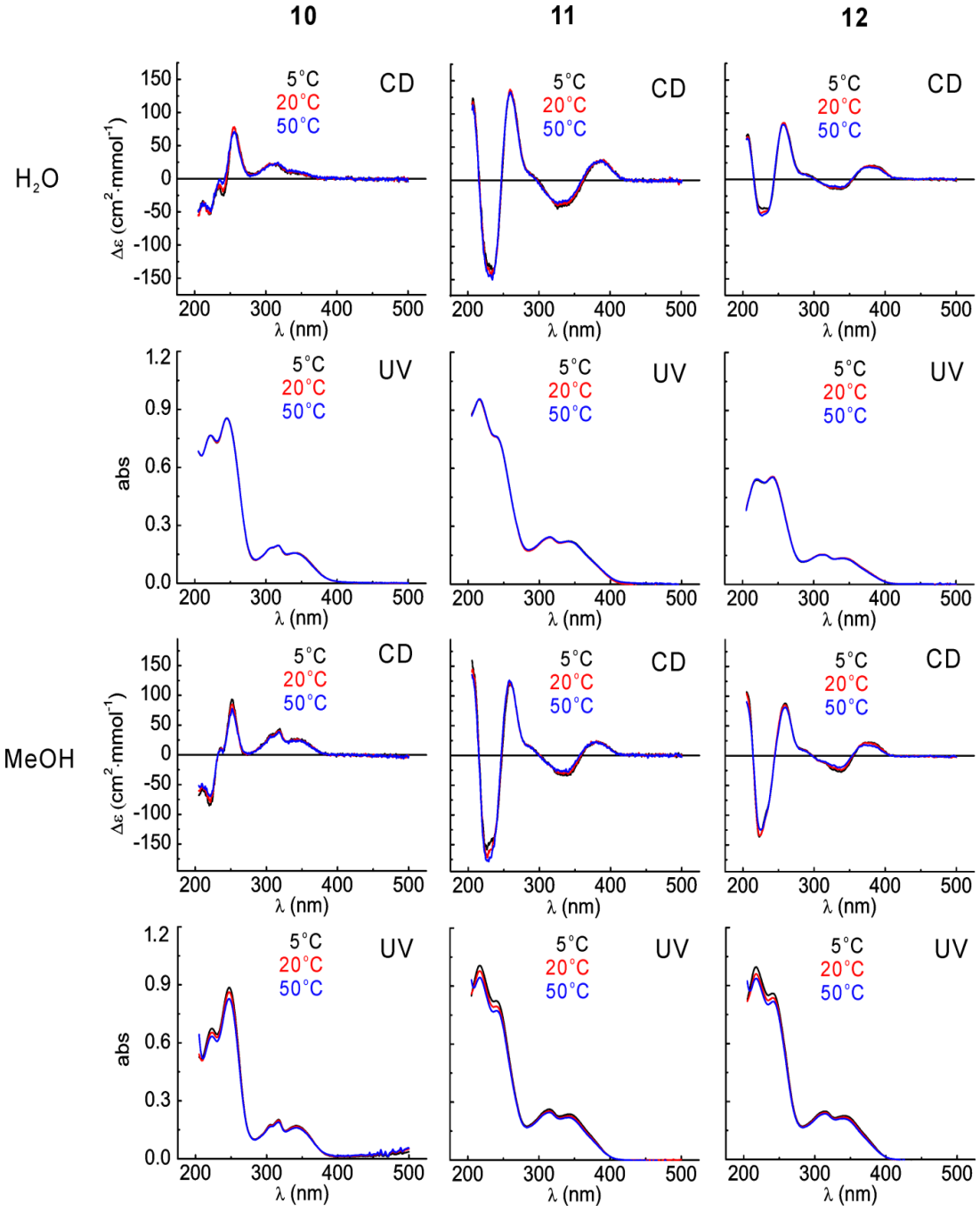

Figure 19. CD and UV (5 – 50 °C) spectra of **10**, **11** and **12** in water and MeOH. (Concentrations: 30 μM)

6.3 2D NMR spectra and assignments

6.3.1 Methods for NMR spectroscopy

Spectra were recorded on four different NMR spectrometers: (1) a Bruker Avance II NMR spectrometer operating at 300 MHz for ^{1}H observation and 75 MHz for ^{13}C observation by means of a 5 mm direct BBO H/X probe with Z gradient capabilities; (2) a Bruker Avance DPX spectrometer operating at 400 MHz for correlation spectroscopy (COSY) experiment by means of a 5 mm QNP $^{1}H/^{13}C/^{19}F/^{31}P/^{2}H$ probe with Z gradient capabilities; (3) a Bruker Avance III spectrometer operating at 700 MHz for total correlation spectroscopy (TOCSY), heteronuclear single quantum coherence (HSQC), heteronuclear multiple bond correlation (HMBC) and rotating-frame overhauser effect spectroscopy (ROESY) experiments by means of a 5 mm TXI $^{1}H/^{13}C/^{15}N/^{2}H$ probe with Z gradient capabilities; and (4) a Bruker Avance III spectrometer operating at 800 MHz for nuclear overhauser effect spectroscopy (NOESY) experiments by means of a 5 mm TCI $^{1}H/^{13}C/^{15}N/^{2}H$ probe with Z gradient capabilities. Data processing was performed with Topspin software. COSY acquisition was performed with a time domain size of 2048 (F2) × 256 (F1), 48 scans per increment, a pulse program of cosydfgpph19, and water suppression using 3-9-19 pulse sequence. TOCSY acquisition was performed with a time domain size of 2048 (F2) × 128 (F1), 80 scans per increment, a pulse program of dipsi2esgpph, a mixing time of 150 ms, and water suppression using excitation sculpting. HSQC acquisition was performed with a time domain size of 2048 (F2) × 131 (F1), 128 scans per increment, and a pulse program of hsqcedetgp. HMBC acquisition was performed with a time domain size of 2048 (F2) × 128 (F1), 128 scans per increment, a pulse program of hmbcgplpndprqf, a coupling constant of 7 Hz, and water suppression using presaturation. NOESY acquisition was performed with a time domain size of 2048 (F2) × 475 (F1), 64 scans per increment, a pulse program of noesyesgpph, a mixing time of 300 ms, and water suppression using excitation sculpting. ROESY acquisition was performed with a time domain size of 2048 (F2) × 128 (F1), 128

scans per increment, a pulse program of roesyesgpph, a mixing time of 200 ms, and water suppression using excitation sculpting.

6.3.2 Spectra and assignments

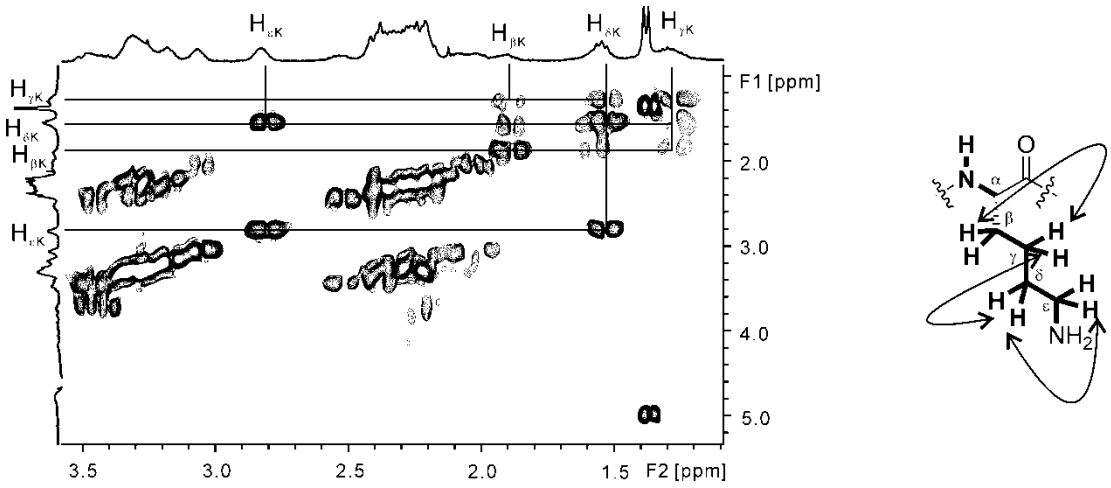

Figure 20. Exerpt from COSY spectrum of **12** in H_2O/D_2O (9:1) at room temperature (400 MHz) indicating the correlations between side-chain methylene protons of the Lys residue. Double-headed arrows indicate observed correlations.

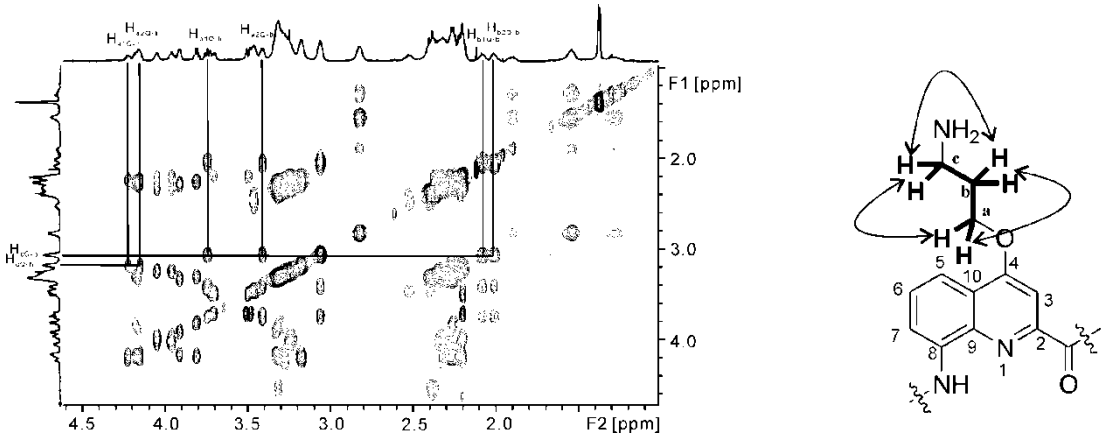

Figure 21. Exerpt from TOCSY spectrum of **12** in H_2O/D_2O (9:1) at room temperature (700 MHz) indicating the correlations between side-chain methylene protons of the same quinoline unit. Double-headed arrows indicate the observed correlations.

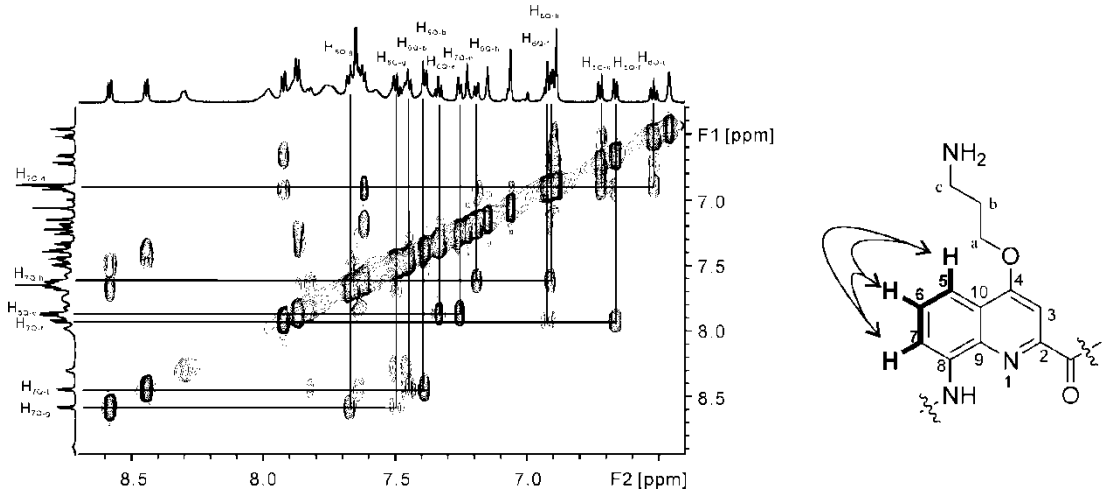

Figure 22. Exerpt from TOCSY spectrum of **12** in H_2O/D_2O (9:1) at room temperature (700 MHz) indicating the correlations between aromatic protons of the same quinoline unit. Double-headed arrows indicate the observed correlations.

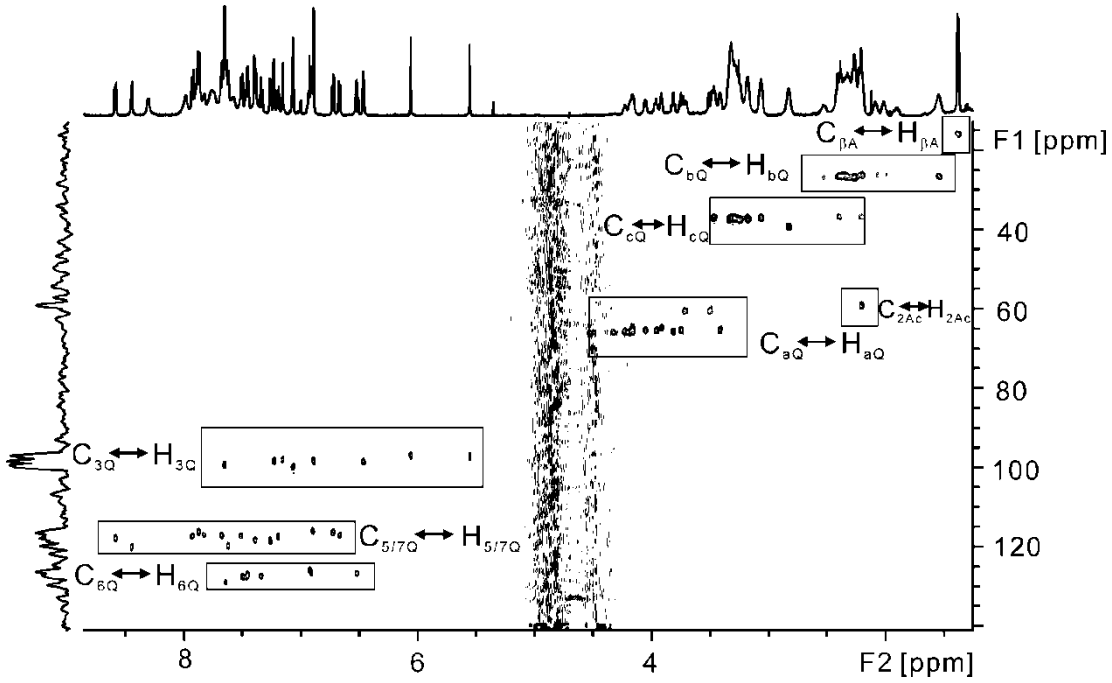

Figure 23. Exerpt from HSQC spectrum of **12** in H_2O/D_2O (9:1) at room temperature (700 MHz) indicating the location of each type of carbon-proton correlation.

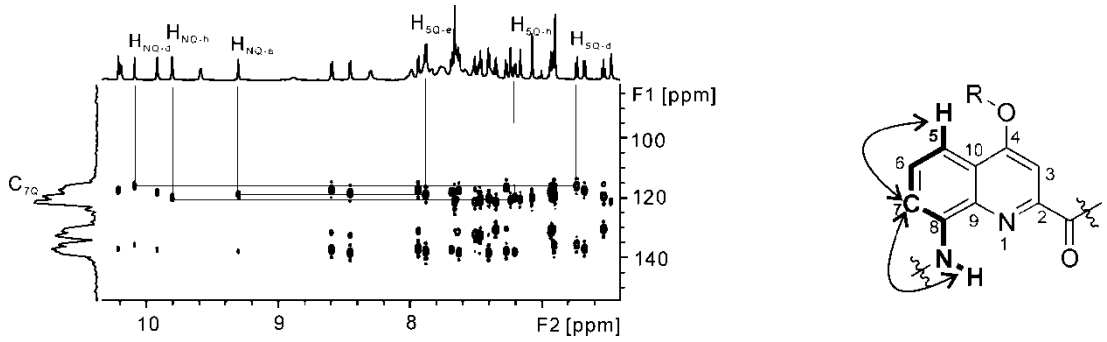

Figure 24. Excerpt from HMBC spectrum of **12** in H_2O/D_2O (9:1) at room temperature (700 MHz) indicating the correlations from aromatic amide proton (H_{NQ}) to aromatic carbon (C_{7Q}) to aromatic proton (H_{5Q}). Double-headed arrows indicate the observed correlations (in bold).

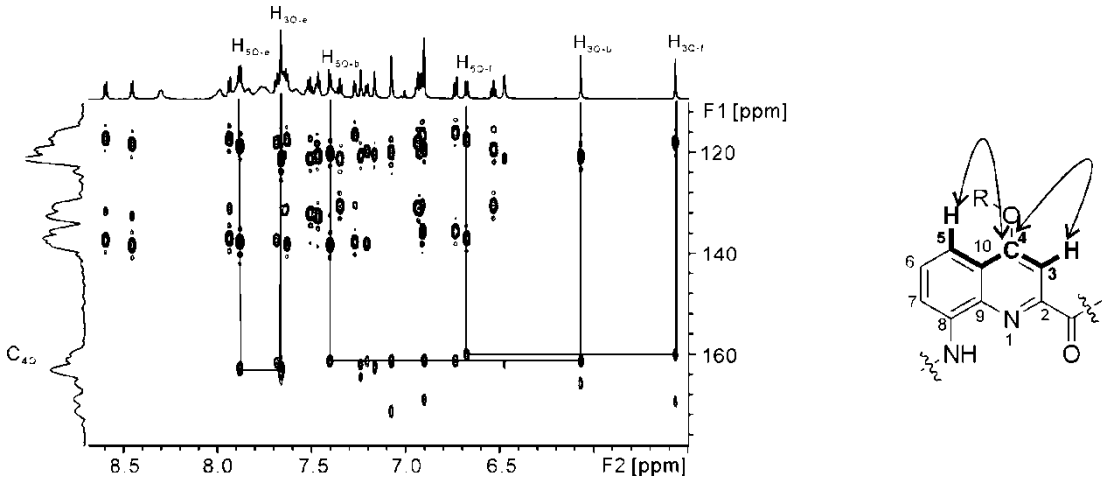

Figure 25. Excerpt from HMBC spectrum of **12** in H_2O/D_2O (9:1) at room temperature (700 MHz) indicating the correlations from aromatic proton (H_{5Q}) to aromatic carbon (C_{4Q}) to aromatic proton (H_{3Q}). Double-headed arrows indicate the observed correlations (in bold).

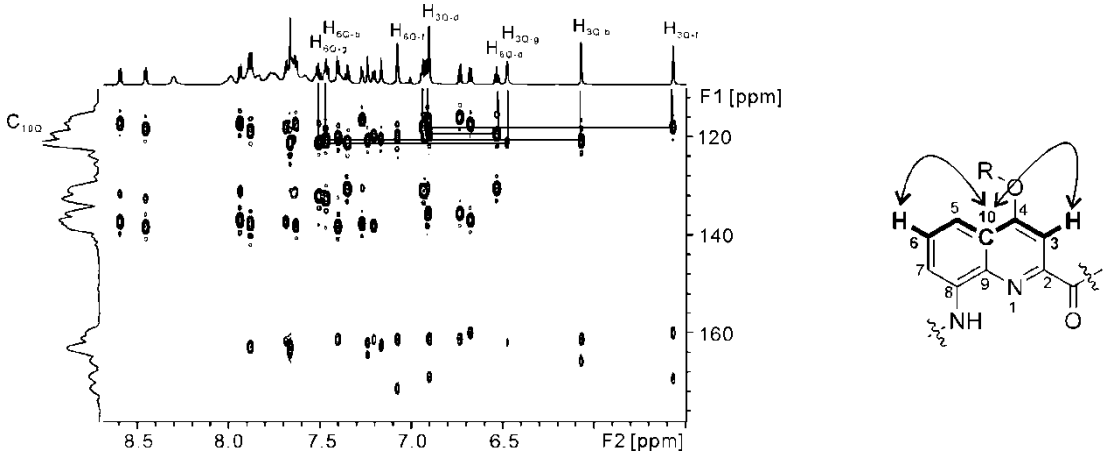

Figure 26. Excerpt from HMBC spectrum of **12** in H_2O/D_2O (9:1) at room temperature (700 MHz) indicating the correlations from aromatic proton (H_{6Q}) to aromatic carbon (C_{10Q}) to aromatic proton (H_{3Q}). Double-headed arrows indicate the observed correlations (in bold).

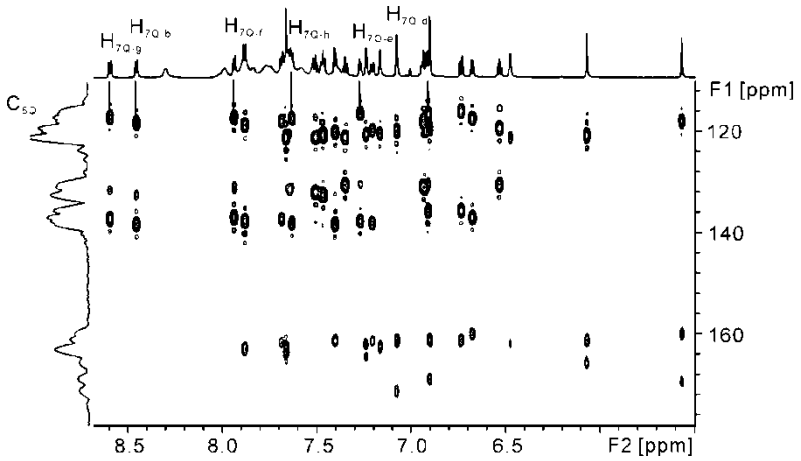

Figure 27. Excerpt from HMBC spectrum of **12** in H_2O/D_2O (9:1) at room temperature (700 MHz) indicating the correlations between aromatic proton (H_{7Q}) and aromatic carbon (C_{5Q}). Double-headed arrows indicate the observed correlations (in bold).

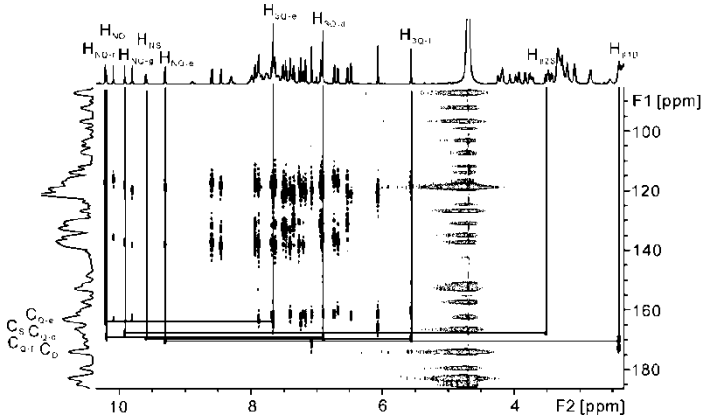

Figure 28. Excerpt from HMBC spectrum of **12** in H_2O/D_2O (9:1) at room temperature (700 MHz) indicating the correlations between methylene proton ($H_{\beta X}$) of the α-amino acid side-chain and its carbonyl carbon (C_X), then to the adjacent aromatic amide proton (H_{NQ}). Also shown the correlation between aromatic proton (H_{3Q}) to aromatic carbon (C_Q) then to the aromatic amide proton (H_{NQ}) from the adjacent quinoline. Double-headed arrows indicate the observed correlations (in bold).

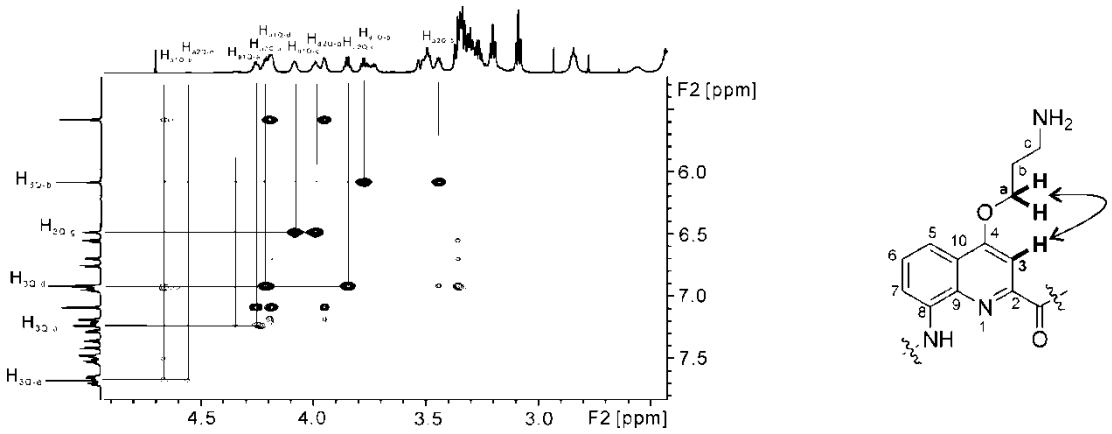

Figure 29. Excerpt from NOESY spectrum of **12** in D_2O at room temperature (800 MHz) showing the NOE correlations between methylene proton ($H_{\alpha Q}$) of the quinoline side-chain and aromatic proton (H_{3Q}) from the same quinoline. Double-headed arrows indicate the observed correlations (in bold).

6.4 Molecular modeling

Methods for molecular modeling. MacroModel version 8.6 (Schrödinger Inc.) was used for building all of the molecular models. The minimization conditions: force field, MMFFs; solvent, none; cutoff, extended; method, TNCG; and maximum iterations, 500) are constant throughout the calculations. To begin, an ill-folded structure of **12** with a left-handed or right-handed helical twist was employed to perform energy minimization by importing the distances information calculated from the selected NOE data (table 2) as the constrained distances. After trying several different starting points, all of the ill-folded structures with a left-handed twist failed to generate any uniform conformation (each time giving a different irregular conformation) after energy minimization. In contrast, the ill-folded structures with a right-handed twist formed a helical structure, which was consistent with CD data. With the first molecular model in hand, another 19 molecular models were obtained to estimate their stability. To access the following 19 molecular models, the first molecular model was randomly released to an ill-folded structure again. Then, energy minimization was carried out via the same method to afford the second molecular model. This process was repeated 18 times to obtain all 20 molecular models. Root-mean-square deviation data was generated in PyMOL. (table 3)

Table 2. Selected NOE correlations for molecular modeling.

Hydrogen from F1 [a]	**Hydrogen from F2**	**Distance (Å)** [b]	**Deviation (Å)** [c]
$H_{\alpha K}$	$H_{\beta K}$	3.19973	0.5
$H_{a2Q\text{-}a}$	$H_{3Q\text{-}a}$	1.94531	0.5
$H_{a2Q\text{-}b}$	$H_{3Q\text{-}b}$	2.3018	0.5
$H_{a2Q\text{-}b}$	$H_{3Q\text{-}d}$	3.25054	0.5
$H_{a2Q\text{-}b}$	$H_{5Q\text{-}d}$	3.49173	0.5
$H_{3Q\text{-}b}$	$H_{3Q\text{-}d}$	3.69805	0.5
$H_{3Q\text{-}b}$	$H_{5Q\text{-}d}$	4.61571	0.5

H_{7Q-b}	H_{3Q-a}	5.22173	0.5
$H_{\alpha A}$	H_{3Q-b}	5.32525	0.5
$H_{\alpha A}$	$H_{\beta 2D}$	3.78279	0.5
$H_{\beta A}$	$H_{\beta K}$	3.1578	0.5
H_{a2Q-c}	H_{3Q-c}	2.38686	0.5
H_{5Q-c}	H_{7Q-a}	3.66457	0.5
H_{5Q-c}	H_{6Q-a}	3.46546	0.5
H_{a2Q-d}	H_{3Q-d}	2.25344	0.5
H_{a2Q-d}	H_{5Q-f}	4.60226	0.5
H_{7Q-d}	H_{7Q-b}	3.95138	0.5
H_{7Q-d}	H_{6Q-b}	4.08377	0.5
H_{7Q-d}	H_{5Q-b}	4.24452	0.5
H_{6Q-d}	H_{7Q-b}	4.8063	0.5
H_{6Q-d}	H_{6Q-b}	3.94681	0.5
H_{6Q-d}	H_{5Q-b}	3.75709	0.5
H_{5Q-d}	H_{6Q-b}	4.66655	0.5
H_{5Q-d}	H_{5Q-b}	4.0246	0.5
$H_{\alpha D}$	$H_{\alpha A}$	3.89396	0.5
$H_{\alpha D}$	H_{3Q-d}	4.4833	0.5
$H_{\alpha D}$	$H_{\beta 2D}$	2.89176	0.5
$H_{\alpha D}$	H_{7Q-e}	4.46797	0.5
$H_{\beta 2D}$	H_{7Q-g}	3.19973	0.5
H_{a1Q-e}	H_{3Q-e}	2.25887	0.5
H_{a1Q-e}	H_{a2Q-g}	4.38112	0.5
H_{a1Q-e}	H_{3Q-g}	4.37361	0.5
H_{7Q-e}	H_{7Q-g}	4.8666	0.5
H_{5Q-e}	H_{3Q-g}	4.1869	0.5
H_{a1Q-f}	H_{5Q-d}	3.58458	0.5

H_{a1Q-f}	H_{3Q-f}	2.21616	0.5
H_{3Q-f}	H_{3Q-d}	3.92193	0.5
H_{3Q-f}	H_{3Q-h}	4.0383	0.5
H_{5Q-f}	H_{7Q-h}	5.41958	0.5
$H_{\beta 2S}$	H_{7Q-g}	4.37735	0.5
H_{a2Q-g}	H_{7Q-e}	4.44251	0.5
H_{a2Q-g}	H_{6Q-e}	3.93158	0.5
H_{a2Q-g}	H_{5Q-e}	3.4995	0.5
H_{a2Q-g}	H_{3Q-g}	2.32557	0.5
H_{3Q-g}	H_{3Q-e}	3.59866	0.5
H_{3Q-g}	H_{5Q-e}	3.83445	0.5
H_{5Q-g}	H_{7Q-e}	3.52767	0.5
H_{5Q-g}	H_{6Q-e}	3.53602	0.5
H_{a1Q-h}	H_{3Q-f}	3.79646	0.5
H_{a1Q-h}	H_{5Q-f}	3.81548	0.5
H_{5Q-h}	H_{7Q-f}	4.29165	0.5
H_{5Q-h}	H_{5Q-f}	3.8495	0.5

[a] The correlated hydrogen from F1; [b] Experimental distance calculated from the integral volume of the corresponding correlation; [c] Fixed deviation of the experimental distance set for energy minimization.

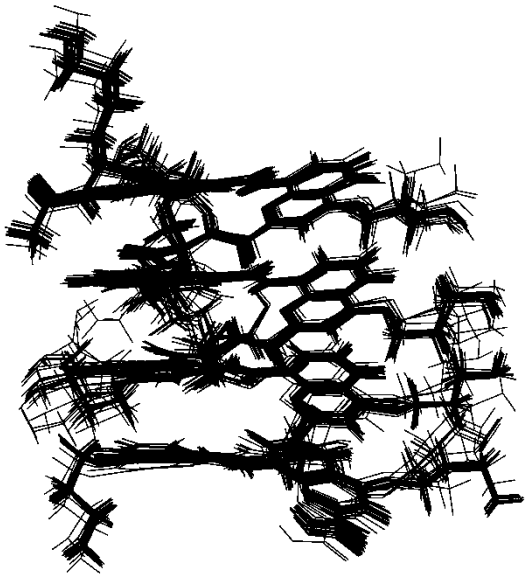

Figure 30. Superposition of 20 structures calculated from different starting structures.

Table 3. Root-mean-square Deviation of the superposed 20 structures

	1	2	3	4	5	6	7	8	9	10	11	12	13	14	15	16	17	18	19	20
1	0	0.186	0.166	0.215	0.207	0.204	0.188	0.249	0.416	0.143	0.194	0.347	0.445	0.433	0.352	0.411	0.435	0.338	0.27	0.486
2	0.186	0	0.163	0.076	0.23	0.229	0.131	0.139	0.276	0.149	0.293	0.28	0.476	0.444	0.296	0.337	0.347	0.17	0.153	0.454
3	0.166	0.163	0	0.256	0.187	0.209	0.131	0.24	0.34	0.049	0.268	0.353	0.493	0.263	0.369	0.418	0.435	0.213	0.221	0.528
4	0.215	0.076	0.256	0	0.298	0.296	0.237	0.281	0.318	0.247	0.252	0.057	0.516	0.406	0.128	0.167	0.279	0.238	0.214	0.407
5	0.207	0.23	0.187	0.298	0	0.058	0.224	0.073	0.285	0.031	0.054	0.279	0.442	0.212	0.301	0.358	0.37	0.24	0.209	0.45
6	0.204	0.229	0.209	0.296	0.058	0	0.224	0.12	0.298	0.112	0.053	0.275	0.45	0.224	0.3	0.358	0.365	0.262	0.21	0.432
7	0.188	0.131	0.131	0.237	0.224	0.224	0	0.068	0.357	0.109	0.28	0.352	0.522	0.271	0.373	0.425	0.44	0.24	0.201	0.54
8	0.249	0.139	0.24	0.281	0.073	0.12	0.068	0	0.226	0.233	0.223	0.238	0.471	0.205	0.249	0.301	0.318	0.211	0.198	0.43
9	0.416	0.276	0.34	0.318	0.285	0.298	0.357	0.226	0	0.351	0.369	0.227	0.52	0.482	0.126	0.218	0.237	0.172	0.277	0.417
10	0.143	0.149	0.049	0.247	0.031	0.112	0.109	0.233	0.351	0	0.255	0.348	0.487	0.267	0.368	0.42	0.434	0.23	0.204	0.517
11	0.194	0.293	0.268	0.252	0.054	0.053	0.28	0.223	0.369	0.255	0	0.242	0.496	0.164	0.271	0.339	0.352	0.321	0.257	0.435
12	0.347	0.28	0.353	0.057	0.279	0.275	0.352	0.238	0.227	0.348	0.242	0	0.492	0.387	0.067	0.124	0.123	0.263	0.26	0.305
13	0.445	0.476	0.493	0.516	0.442	0.45	0.522	0.471	0.52	0.487	0.496	0.492	0	0.703	0.504	0.536	0.524	0.5	0.447	0.471
14	0.433	0.444	0.263	0.406	0.212	0.224	0.271	0.205	0.482	0.267	0.164	0.387	0.703	0	0.397	0.421	0.428	0.27	0.259	0.517
15	0.352	0.296	0.369	0.128	0.301	0.3	0.373	0.249	0.126	0.368	0.271	0.067	0.504	0.397	0	0.071	0.101	0.258	0.277	0.306
16	0.411	0.337	0.418	0.167	0.358	0.358	0.425	0.301	0.218	0.42	0.339	0.124	0.536	0.421	0.071	0	0.068	0.286	0.328	0.303
17	0.435	0.347	0.435	0.279	0.37	0.365	0.44	0.318	0.237	0.434	0.352	0.123	0.524	0.428	0.101	0.068	0	0.316	0.34	0.257
18	0.338	0.17	0.213	0.238	0.24	0.262	0.24	0.211	0.172	0.23	0.321	0.263	0.5	0.27	0.258	0.286	0.316	0	0.18	0.478
19	0.27	0.153	0.221	0.214	0.209	0.21	0.201	0.198	0.277	0.204	0.257	0.26	0.447	0.259	0.277	0.328	0.34	0.18	0	0.449
20	0.486	0.454	0.528	0.407	0.45	0.432	0.54	0.43	0.417	0.517	0.435	0.305	0.471	0.517	0.306	0.303	0.257	0.478	0.449	0

6.5 Methods for chemical synthesis

6.5.1 General procedures

These General Procedures are also suitable for the following chapters unless otherwise specified. All of the reagents and solvents were obtained from commercial sources, including Fmoc-protected amino acids, low loading Wang resin, and Ghosez reagent (1-chloro-*N*,*N*,2-trimethyl-1-propenylamine). *N*,*N*-Diisopropylethylamine (DIPEA) was distilled over calcium hydride. Analytical grade organic solvents were used for solid phase synthesis. Anhydrous THF and DCM for solution and solid phase synthesis were dispensed from a solvent purification system. HPLC grade acetonitrile and Milli-Q water were used for RP-HPLC analyses and purification. SPS was carried out manually at atmospheric pressure using a CEM Discover microwave oven and SPS station and in the proprietary reactor vessels. The temperature of microwave-assisted reactions was controlled by an optical fiber probe internal to the reaction mixture linked to an IR detector. ^{1}H NMR spectra were recorded at 300, 400, 700, or 800 MHz; 2D NMR spectra were recorded at 400, 700, or 800 MHz, and ^{13}C{^{1}H}NMR spectra were recorded at 300 MHz. Chemical shifts are reported in ppm relative to the residual solvent signal of DMSO-d_6 (δ 2.50), CD_3OH (δ 3.31), $CDCl_3$ (δ 7.26, 77.2), or to the reference signal of TMS (δ 0.00) from 10 μM 3-(trimethylsilyl)-1-propanesulfonic acid sodium salt in CD_3OH, D_2O, or H_2O/D_2O (9:1). Abbreviations used for signal multiplicities are s, singlet; d, doublet; t, triplet; q, quartet; m, multiplet or overlapped signals; and br, broad. All coupling constants are reported in hertz (Hz). Silica gel chromatography was performed with Si 60 and thin layer chromatography with Si 60 F254 plates. RP-HPLC analyses were carried out on a C_{18} gravity column (4.6 × 100 mm, 3 μm) at 1.5 mL/min with running solvents: Milli-Q water containing 0.1% v/v TFA (solvent A), CH_3CN containing 0.1% v/v TFA (solvent B), 12.5 mM NH_4Ac-NH_4OH in Milli-Q water, adjusted to pH 8.5 (solvent C), and CH_3CN (solvent D). Gradients for analytical RP-HPLC were as follows: 20–50% B over 15 min (System A); 20–40% B over 10 min (System B);

30–50% B over 10 min (System C); 13–18% B over 10 min (System D); and 8–13% D over 10 min (System E). Systems A–D used solvent A as aqueous component, and System E used solvent C as aqueous component. Column effluent was monitored by UV detection at 214, 254, and 300 nm with a diode array detector. Purification of oligoamides was performed at 4 mL/min on a C_{18}column (21 mm × 125 mm, 5 μm) by semipreparative RP-HPLC. The running solvents of semipreparative RP-HPLC were the same as analytical RP-HPLC. Gradients for semipreparative RP-HPLC were as follows: 15–20% B over 20 min (System F) and 10–15% D over 20 min (System G). System F used solvent A as the aqueous component, and System G used solvent C as the aqueous component. Monitoring was performed by UV detection at 254 and 300 nm with a diode array detector. High resolution electrospray ionization time-of-flight (ESI-TOF) mass spectra were measured in the positive ion mode on a TOF spectrometer.

6.5.2 Synthetic Methods

Fmoc-$Q^{Orn(Boc)}$–OH, Fmoc-$Q^{Asp(OtBu)}$–OH, H_2N-Q^{Leu}-OMe, and O_2N-Q^{Leu}–OH were synthesized as previously reported.[22,26,31b,44] Procedures for resin loading, Fmoc removal, quinoline acid chloride activation and couplings, and resin cleavage were also carried out as previously reported.[31b]

General Method for Coupling with HOBt/HBTU. The corresponding H_2N-oligomer-Wang resin (exemplified by 0.0038 mmol scale, 1 equiv) was washed with anhydrous DMF and then suspended in 0.3 mL of anhydrous DMF, to which was added a solution of Fmoc-protected amino acid or dimer block (0.0114 mmoL, 3 equiv), HBTU (0.0114 mmoL, 3 equiv), HOBt (0.0114 mmoL, 3 equiv), and anhydrous DIEA (0.0114 mmoL, 3 equiv) in anhydrous DMF (0.3 mL). The mixture was then treated with microwaves (25 W, 70 ℃, 10 min). The resin was washed briefly with anhydrous DMF, and the process was repeated once.

44. T. Qi, T. Deschrijver, and I. Huc, *Nat. Protoc.* **2013**, 8, 693.

General Method for N-Terminal Acetylation. The corresponding H_2N-oligomer-Wang resin (exemplified by 0.0038 mmol scale, 1 equiv) was washed briefly with anhydrous DMF and then suspended in 0.3 mL of anhydrous DMF, to which was added anhydrous DIEA (0.076 mmol, 20 equiv) and acetic anhydride (0.038 mmol, 10 equiv) in that order. The mixture was then stirred at 25 ℃ for 20 min. The resin was washed briefly with anhydrous DMF, and the process was repeated once.

General Method for in Situ Acid Chloride Coupling of α-Amino Acids using TCAN/PPh_3 As Exemplified by Synthesis of Compound 3a H_2N-$Q^{OrnBoc}Q^{OrnBoc}$-Wang resin was synthesized on a 0.0076 mmol scale (20 mg of Wang resin, loading 0.38 mmol/g) via the previously reported SPS methodology.[31b] NH_2-$Q^{OrnBoc}Q^{OrnBoc}$-Wang resin was washed briefly with anhydrous THF and then suspended in 0.5 mL anhydrous THF followed by adding 8.7 μL of 2,4,6-Collidine (0.066 mmol, 8.7 equiv). Fmoc-Gly-OH (4.5 mg, 0.015 mmol, 2.0 equiv), PPh_3 (21.9 mg, 0.084 mmol, 11 equiv), and TCAN (6.6 μL, 0.066 mmol, 8.7 equiv) were suspended in 0.5 mL of anhydrous THF in that order and added to the resin immediately, which was then treated with microwaves (50 W, 50 ℃, 15 min). The resin was then washed thoroughly with DMF, DCM, and DCM/MeOH (1:1), dried, and desiccated. Cleavage of the resin (TFA/TIS/H_2O, 95:2.5:2.5, 2 h, 25 ℃) afforded 5.6 mg (75%) crude product (95% purity as determined by RP-HPLC). RP-HPLC (System A) R_t = 9.37 min. ^{1}H NMR (300 MHz, DMSO-d_6): δ 12.01 (s, 1 H), 10.39 (s, 1 H), 8.72–8.80 (m, 2 H), 8.00 (d, J = 7.8 Hz, 1 H), 7.60–7.90 (m, 14 H, -NH_3^+ included), 7.26–7.45 (m, 4 H), 7.08–7.25 (m, 2 H), 4.50–4.60 (m, 2 H), 4.40–4.50 (m, 2 H), 3.50–4.10 (m, 5 H), 3.00–3.20 (m, 4 H), 2.10–2.30 (m, 4 H). HRMS: calcd for $C_{43}H_{42}N_7O_8$ $[M + H]^+$ 784.3095; found 784.3127.

Compound 3b. The same procedure as described for the synthesis of **3a** was applied with the exception that the coupling with TCAN/PPh_3 was repeated once to obtain 5.0 mg (66%) of crude product (97% purity as determined by RP-HPLC). RP-HPLC (System A) R_t = 9.30 min. ^{1}H NMR (300 MHz, DMSO-d_6): δ 11.96 (s, 1

H), 10.50 (s, 1 H), 8.78 (d, *J* = 7.8 Hz, 1 H), 8.64 (d, *J* = 7.5 Hz, 1 H), 7.99 (d, *J* = 8.4 Hz, 1 H), 7.70–7.85 (m, 12 H, -NH_3^+ included), 7.65 (s, 1 H), 7.60 (t, *J* = 8.1 Hz, 1 H), 7.25–7.35 (m, 4 H), 7.05–7.20 (m, 2 H), 4.50–4.60 (m, 3 H), 4.38–4.47 (m, 2 H), 3.43–3.75 (m, 3 H), 3.03–3.18 (m, 4 H), 2.12–2.26 (m, 4 H), 1.37 (d, *J* = 6.9 Hz, 3 H). HRMS: calcd for $C_{44}H_{44}N_7O_8$ $[M + H]^+$ 798.3251; found 798.3260.

Compound 3c. The same procedure as described for the synthesis of **3a** was applied with the exception that the coupling with TCAN/PPh_3 was repeated once to obtain 5.1 mg (58%) of crude product (93% purity as determined by RP-HPLC). RP-HPLC (System B) R_t = 5.30 min. ^{1}H NMR (300 MHz, DMSO-d_6): δ 11.93 (s, 1 H), 10.57 (s, 1 H), 8.78 (d, *J* = 7.8 Hz, 1 H), 8.62 (d, *J* = 7.5 Hz, 1 H), 7.99 (d, *J* = 8.4 Hz, 1 H), 7.55–7.87 (m, 17 H, -NH_3^+ included), 7.25–7.35 (m, 2 H), 7.00–7.22 (m, 4 H), 4.30–4.60 (m, 5 H), 3.40–3.70 (m, overlapped with water peak), 3.05–3.16 (m, 4 H), 2.68–2.77 (m, 2 H), 2.12–2.26 (m, 4 H), 1.85–2.06 (m, 1 H), 1.75 (br), 1.42–1.62 (m, 2 H), 1.27–1.40 (m, 2 H). HRMS: calcd for $C_{47}H_{51}N_8O_8$ $[M + H]^+$ 855.3830; found 855.3853.

Compound 3d. The same procedure as described for the synthesis of **3a** was applied with the exception that the coupling with TCAN/PPh_3 was repeated once to obtain 4.4 mg (56%) crude product (94% purity as determined by RP-HPLC). RP-HPLC (System B) R_t = 8.18 min. ^{1}H NMR (300 MHz, DMSO-d_6): δ 11.95 (s, 1 H), 10.67 (s, 1 H), 8.73 (d, *J* = 7.8 Hz, 1 H), 8.54 (d, *J* = 7.5 Hz, 1 H), 7.99 (d, *J* = 7.5 Hz, 1 H), 7.69–7.93 (m, 12 H, -NH_3^+ included), 7.63 (s, 1 H), 7.54 (t, *J* = 8.1, 1 H), 7.05–7.35 (m, 6 H), 4.80–4.91 (m, 1 H), 4.47–4.57 (m, 2 H), 4.35–4.45 (m, 2 H), 3.29–3.70 (m, overlapped with water peak), 3.00–3.20 (m, 4 H), 2.81–2.91 (m, 1 H), 2.58–2.71 (m, 1 H), 2.14–2.29 (m, 4 H). HRMS: calcd for $C_{45}H_{44}N_7O_{10}$ $[M + H]^+$ 842.3150; found 842.3165.

Compound 3e. The same procedure as described for the synthesis of **3a** was applied with the exception that the coupling with TCAN/PPh_3 was repeated once to obtain 4.7 mg (58%) of crude product (96% purity as determined by RP-HPLC). RP-HPLC (System C) R_t = 7.18 min. ^{1}H NMR (300 MHz, DMSO-d_6): δ 11.92 (s, 1

H), 10.64 (s, 1 H), 8.80 (d, *J* = 7.5 Hz, 1 H), 8.62 (d, *J* = 7.8 Hz, 1 H), 7.99 (d, *J* = 8.4 Hz, 1 H), 7.70–7.87 (m, 12 H, -NH_3^+ included), 7.55–7.65 (m, 2 H), 7.25–7.35 (m, 2 H), 6.97–7.21 (m, 9 H), 4.65–4.80 (m, 1 H), 4.47–4.57 (m, 2 H), 4.35–4.45 (m, 2 H), 3.50–3.65 (m, 1 H), 2.85–3.20 (m, 5 H), 2.12–2.25 (m, 4 H). HRMS: calcd for $C_{50}H_{48}N_7O_8$ $[M + H]^+$874.3564; found 874.3583.

Compound 3f. The same procedure as described for the synthesis of **3a** was applied with the exception that the coupling with TCAN/PPh_3 was repeated three times to obtain 4.0 mg (52%) of crude product (97% purity as determined by RP-HPLC). RP-HPLC (System B) R_t = 8.58 min. ^{1}H NMR (300 MHz, DMSO-d_6): δ 11.78 (s, 1 H), 10.87 (s, 1 H), 8.80 (dd, *J* = 7.5, 0.9 Hz, 1 H), 8.65 (d, *J* = 7.5 Hz, 1 H), 7.99 (dd, *J* = 8.4, 1.2 Hz, 1 H), 7.61–7.91 (m, 13 H, -NH_3^+ included), 7.53 (d, *J* = 8.1, 1 H), 7.30–7.48 (m, 4 H), 7.15–7.28 (m, 2 H), 4.49–4.59 (m, 3 H), 4.38–4.48 (m, 2 H), 3.65–3.91 (m, overlapped with water peak), 3.01–3.23 (m, 4 H), 2.17–2.29 (m, 4 H). HRMS: calcd for $C_{44}H_{44}N_7O_9$ $[M + H]^+$ 814.3201; found 814.3210.

Compound 3g. The same procedure as described for the synthesis of **3a** was applied with the exception that the coupling with TCAN/PPh_3 was repeated twice to obtain 3.6 mg (46%) of crude product (97% purity as determined by RP-HPLC). RP-HPLC (System B) R_t = 11.33 min. ^{1}H NMR (300 MHz, DMSO-d_6): δ 11.97 (s, 1 H), 10.57 (s, 1 H), 9.32 (br, 1 H), 8.77 (dd, *J* = 7.8, 1.2 Hz, 1 H), 8.65 (d, *J* = 7.8 Hz, 1 H), 8.02 (d, *J* = 7.5, 1 H), 7.62–7.89 (m, 14 H, -NH_3^+ included), 7.28–7.41 (m, 4 H), 7.13–7.22 (m, 2 H), 4.49–4.70 (m, 3 H), 4.37–4.49 (m, 2 H), 3.67–3.82 (m, 1 H), 3.45–3.65 (m, overlapped with water peak), 3.03–3.18 (m, 5 H), 2.84–2.98 (m, 1 H), 2.12–2.26 (m, 4 H). HRMS: calcd for $C_{44}H_{44}N_7O_8S$ $[M + H]^+$ 830.2972; found 830.2985.

Compound 4a. Synthesis started from Wang resin on a 3.8 μmol scale (10 mg resin with manufacturer's loading: 0.38 mmol g^{-1}) to obtain 2.3 mg of crude product. RP-HPLC (System A) R_t = 8.39 min (corresponding to DL byproduct, 2% total peak area), 8.89 min (corresponding to LL product, 98% total peak area). ^{1}H NMR (300 MHz, DMSO-d_6): δ 11.92 (s, 1 H), 10.23 (s, 1 H), 8.79 (d, *J*= 7.5 Hz, 1 H), 8.72

(d, *J* = 7.8 Hz, 1 H), 8.19 (d, *J* = 6.6 Hz, 1 H), 7.93–8.06 (m, 2 H), 7.57–7.89 (m, 14 H, -NH_3^+ included), 7.16–7.46 (m, 5 H), 4.60–4.73 (m, 1 H), 4.36–4.58 (m, 4 H), 4.07–4.16 (m, 2 H), 3.83–3.96 (m, 1 H), 3.50–4.65 (m, overlapped with water peak), 3.03–3.17 (m, 4 H), 2.12–2.26 (m, 4 H), 1.37 (d, *J* = 6.9 Hz, 3 H), 0.98 (d, *J* = 7.2 Hz, 3 H). HRMS: calcd for $C_{47}H_{49}N_8O_9$ $[M + H]^+$ 869.3617; found 869.3644.

Compound 4b. Synthesis started from Wang resin on a 3.8 μmol scale (10 mg resin with manufacturer's loading: 0.38 mmol g^{-1}) to obtain 2.5 mg of crude product. RP-HPLC (System A) R_t = 5.21 min (diastereoisomers could not be separated by RP-HPLC). ^{1}H NMR (300 MHz, DMSO-d_6): δ 11.98 (s, 1 H), 10.22 (s, 1 H), 8.80 (d, *J* = 7.8 Hz, 1 H), 8.69 (d, *J* = 7.5 Hz, 1 H), 8.26 (br, 1 H), 7.95–8.07 (m, 2 H), 7.55–7.89 (m, 20 H, -NH_3^+ included), 7.19–7.46 (m, 5 H), 4.31–4.70 (m, 5 H), 3.68–4.23 (m, 4 H), 3.05–3.16 (m, 4 H), 2.60–2.70 (m, 2 H), 2.50–2.60 (m, overlapped with DMSO peak), 2.07–2.25 (m, 4 H), 1.84–2.06 (m, 1 H), 1.63–1.83 (m, 1 H), 1.16–1.58 (m, 10 H). HRMS: calcd for $C_{53}H_{63}N_{10}O_9$ $[M + H]^+$ 983.4774; found 983,4804.

Compound 4c. Synthesis started from Wang resin on a 3.8 μmol scale (10 mg resin with manufacturer's loading: 0.38 mmol g^{-1}) to obtain 2.3 mg of crude product. RP-HPLC (System A) R_t = 7.21 min (corresponding to DL byproduct, 1% total peak area), 7.48 min (corresponding to LL product, 99% total peak area). ^{1}H NMR (300 MHz, DMSO-d_6): δ 12.03 (s, 1 H), 10.42 (s, 1 H), 8.74 (d, *J*= 7.8 Hz, 1 H), 8.68 (d, *J* = 8.1 Hz, 1 H), 8.33 (d, *J* = 7.5 Hz, 1 H), 7.94–8.07 (m, 2 H), 7.47–7.88 (m, 15 H, -NH_3^+ included), 7.21–7.45 (m, 4 H), 4.88–5.11 (m, 1 H), 4.31–4.62 (m, 4 H), 4.01–4.26 (m, 4 H), 3.04–3.18 (m, 4 H), 2.75–2.90 (m, 1 H), 2.50–2.65 (m, overlapped with DMSO peak), 2.15–2.25 (m, 4 H). HRMS: calcd for $C_{49}H_{49}N_8O_{13}$ $[M + H]^+$ 957.3414; found 957.3434.

Compound 4d. Synthesis started from Wang resin on a 3.8 μmol scale (10 mg resin with manufacturer's loading: 0.38 mmol g^{-1}) to obtain 2.0 mg of crude product. RP-HPLC (System A) R_t = 13.54 min (corresponding to DL byproduct, 5% total peak area), 14.05 min (corresponding to LL product, 95% total peak area). ^{1}H NMR (300

MHz, DMSO-d_6): δ 11.94 (s, 1 H), 10.20 (s, 1 H), 8.74 (d, *J*= 7.5 Hz, 1 H), 8.69 (d, *J* = 6.9 Hz, 1 H), 8.38 (d, *J* = 7.8 Hz, 1 H), 7.68–7.87 (m, 11 H, -NH_3^+included), 7.61 (s, 1 H), 7.49–7.56 (m, 2 H), 7.32–7.43 (m, 3 H), 7.18–7.29 (m, 2 H), 6.84–7.11 (m, 10 H), 4.90–5.03 (m, 1 H), 4.34–4.61 (m, 4 H), 3.85–4.23 (m, 3 H), 2.99–3.23 (m, 7 H), 2.76–2.87 (m, 1 H), 2.50–2.65 (m, overlapped with DMSO peak), 2.13–2.25 (m, 4 H). HRMS: calcd for $C_{59}H_{57}N_8O_9$ $[M + H]^+$ 1021.4249; found 1021.4274.

Compound 4e. Synthesis started from Wang resin on a 3.8 μmol scale (10 mg resin with manufacturer's loading: 0.38 mmol g^{-1}) to obtain 2.0 mg of crude product. RP-HPLC (System A) R_t = 7.36 min (corresponding to DL byproduct, 2% total peak area), 7.81 min (corresponding to LL product, 98% total peak area). ^{1}H NMR (300 MHz, DMSO-d_6): δ 11.76 (s, 1 H), 10.89 (s, 1 H), 8.69–8.82 (m, 2 H), 8.03 (d, *J* = 8.4 Hz, 1 H), 7.98 (d, *J* = 8.4 Hz, 1 H), 7.86–7.93 (m, 2 H), 7.64–7.85 (m, 13 H, -NH_3^+ included), 7.24–7.46 (m, 5 H), 4.70–4.85 (m, 1 H), 4.43–4.56 (m, 4 H), 4.02–4.30 (m, 4 H), 3.50–3.79 (m, 4 H), 3.07–3.16 (m, 4 H), 2.13–2.26 (m, 4 H). HRMS: calcd for $C_{47}H_{49}N_8O_{11}$ $[M + H]^+$ 901.3515; found 901.3540.

Compound 5a. Synthesis started from Wang resin on a 3.8 μmol scale (10 mg resin with manufacturer's loading: 0.38 mmol g^{-1}) to obtain 2.6 mg of crude product. RP-HPLC (System A) R_t = 8.38 min (corresponding to LL product, 99% total peak area), 8.94 min (corresponding to DL byproduct, 1% total peak area). ^{1}H NMR (300 MHz, DMSO-d_6): δ 11.95 (s, 1 H), 10.34 (s, 1 H), 8.78 (d, *J* = 7.8 Hz, 1 H), 8.72 (d, *J* = 7.2 Hz, 1 H), 8.26 (d, *J* = 7.5 Hz, 1 H), 8.02 (d, *J* = 8.4 Hz, 1 H), 7.60–7.97 (m, 14 H, -NH_3^+ included), 7.20–7.59 (m, 6 H), 4.63–4.80 (m, 1 H), 4.37–4.57 (m, 4 H), 3.50–4.10 (m, 4 H), 3.04–3.17 (m, 4 H), 2.12–2.25 (m, 4 H), 1.36 (d, *J* = 6.9 Hz, 3 H), 0.98 (d, *J*= 6.9 Hz, 3 H). HRMS: calcd for $C_{47}H_{49}N_8O_9$ $[M + H]^+$ 869.3617; found 869.3636.

Compound 5b. Synthesis started from Wang resin on a 3.8 μmol scale (10 mg resin with manufacturer's loading: 0.38 mmol g^{-1}) to obtain 2.8 mg of crude product. RP-HPLC (System A) R_t = 5.29 min (diastereoisomers could not be separated by RP-HPLC). ^{1}H NMR (300 MHz, DMSO-d_6): δ 11.96 (s, 1 H), 10.34 (s, 1 H), 8.77

(d, *J* = 7.2 Hz, 1 H), 8.69 (d, *J* = 7.8 Hz, 1 H), 8.38 (br, 1 H), 8.03 (d, *J* = 8.4, 1 H), 7.60–7.92 (m, 19 H, -NH_3^+ included), 7.32–7.55 (m, 4 H), 7.18–7.31 (m, 3 H), 4.55–4.71 (m, 1 H), 4.31–4.53 (m, 4 H), 3.64–4.10 (m, 4 H), 3.07–3.16 (m, 4 H), 2.53–2.75 (m, 4 H), 2.13–2.25 (m, 4 H), 1.85–2.06 (m, 1 H), 1.67–1.83 (m, 1 H), 1.16–1.59 (m, 10 H). HRMS: calcd for $C_{53}H_{63}N_{10}O_9$ $[M + H]^+$ 983.4774; found 983,4797.

Compound 5c. Synthesis started from Wang resin on a 3.8 μmol scale (10 mg resin with manufacturer's loading: 0.38 mmol g^{-1}) to obtain 1.5 mg of crude product. RP-HPLC (System A) R_t = 7.25 min (corresponding to LL product, 94% total peak area), 7.58 min (corresponding to DL byproduct, 6% total peak area). ^{1}H NMR (300 MHz, DMSO-d_6): δ 12.01 (s, 1 H), 10.46 (s, 1 H), 8.73 (d, *J* = 7.2 Hz, 1 H), 8.68 (d, *J* = 7.8 Hz, 1 H), 8.49 (d, *J* = 7.8 Hz, 1 H), 8.02 (d, *J* = 8.4 Hz, 1 H), 7.63–7.93 (m, 13 H, -NH_3^+ included), 7.48–7.58 (m, 2 H), 7.31–7.46 (m, 3 H), 7.18–7.28 (m, 2 H), 4.92–5.14 (m, 1 H), 4.36–4.59 (m, 4 H), 3.62–4.23 (m, 3 H), 3.35–3.50 (m, overlapped with water peak), 3.06–3.16 (m, 4 H), 2.74–2.95 (m, 1 H), 2.40–2.70 (m, overlapped with DMSO peak), 2.30–2.37 (m, 1 H), 2.10–2.25 (m, 4 H). HRMS: calcd for $C_{49}H_{49}N_8O_{13}$ $[M + H]^+$957.3414; found 957.3436.

Compound 5d. Synthesis started from Wang resin on a 3.8 μmol scale (10 mg resin with manufacturer's loading: 0.38 mmol g^{-1}) to obtain 2.2 mg of crude product. RP-HPLC (System A) R_t = 13.49 min (corresponding to LL product, 99% total peak area), 14.10 min (corresponding to DL byproduct 1% total peak area). ^{1}H NMR (300 MHz, DMSO-d_6): δ 11.98 (s, 1 H), 10.41 (s, 1 H), 8.75 (d, *J* = 7.8 Hz, 1 H), 8.70 (dd, *J* = 7.5, 0.9 Hz, 1 H), 8.56 (d, *J* = 7.5 Hz, 1 H), 8.01 (dd, *J* = 8.4, 0.9 Hz, 1 H), 7.95 (dd, *J* = 8.4, 0.9 Hz, 1 H), 7.68–7.86 (m, 11 H, -NH_3^+ included), 7.60 (s, 1 H), 7.45–7.54 (m, 2 H), 7.32–7.42 (m, 2 H), 7.16–7.27 (m, 3 H), 6.88–7.16 (m, 10 H), 4.89–5.06 (m, 1 H), 4.34–4.59 (m, 4 H), 3.85–4.16 (m, 3 H), 3.20–3.35 (m, overlapped with water peak), 2.91–3.20 (m, 6 H), 2.28–2.46 (m, 3 H), 2.12–2.25 (m, 4 H). HRMS: calcd for $C_{59}H_{57}N_8O_9$ $[M + H]^+$1021.4249; found 1021.4273.

Compound 5e. Synthesis started from Wang resin on a 3.8 μmol scale (10 mg resin with manufacturer's loading: 0.38 mmol g^{-1}) to obtain 2.0 mg of crude product. RP-HPLC (System A) R_t = 7.39 min (corresponding to LL product, 98% total peak area), 7.82 min (corresponding to DL byproduct, 2% total peak area). ^{1}H NMR (300 MHz, DMSO-d_6): δ 11.76 (s, 1 H), 10.88 (s, 1 H), 8.67–8.89 (m, 2 H), 7.93–8.08 (m, 2 H), 7.85–7.93 (m, 2 H), 7.63–7.84 (m, 13 H, -NH_3^+ included), 7.35–7.47 (m, 2 H), 7.23–7.35 (m, 3 H), 4.69–4.83 (m, 1 H), 4.44–4.55 (m, 4 H), 4.02–4.28 (m, 4 H), 3.44–3.81 (m, 4 H), 3.07–3.16 (m, 4 H), 2.16–2.26 (m, 4 H). HRMS: calcd for $C_{47}H_{49}N_8O_{11}$ $[M + H]^+$ 901.3515; found 901.3522.

Compound 7. To a solution of **6** (2.44 g, 7.5 mmol, 1.5 equiv) in anhydrous DCM under N_2 was added 1-chloro-*N*,*N*,2-trimethyl-1-propenylamine (1.5 mL, 11.25 mmol, 2.25 equiv). The solution was allowed to stir at rt for 2 h. The solvent was then removed on a vacuum manifold (equipped with liquid N_2 solvent trap), and the resulting solid was further dried in this manner for another 3 h to give the corresponding acid chloride (without further purification) in quantitative yield. The resulting acid chloride (2.58 g, 7.5 mmol, 1.5 equiv) in anhydrous THF (30 mL) was added to a solution of methyl 8-amino-4-isobutoxyquinoline-2-carboxylate (1.4 g, 5.0 mmol, 1.0 equiv) in anhydrous THF (30 mL). Anhydrous DIEA (1.3 mL, 7.5 mmol, 1.5 equiv) was added, and the mixture was stirred for 12 h at rt under N_2. The reaction mixture was concentrated and purified by silica gel chromatography (cyclohexane/EtOAc = 1:1) to afford the title compound as a yellow solid (1.75 g, 60%). ^{1}H NMR (300 MHz, $CDCl_3$): δ 10.73 (s, 1H), 8.73 (d, *J* = 7.5 Hz, 1 H), 7.93 (dd, *J* = 8.4, 0.9 Hz, 1 H), 7.71 (br, 2 H), 7.50–7.65 (m, 4 H), 7.15–7.40 (m, overlapped with chloroform peak), 5.92 (br, 1 H), 4.41 (d, *J* = 6.3, 2 H), 4.22 (br, 1 H), 4.06 (d, *J* = 6.3 Hz, 2 H), 3.98 (s, 3 H), 2.22–2.38 (m, 1 H), 1.76 (s, 6 H), 1.15 (d, *J* = 6.9 Hz, 6 H). ^{13}C{^{1}H}NMR (300 MHz, $CDCl_3$): δ 173.07, 165.72, 163.28, 155.23, 146.79, 144.06, 141.38, 139.02, 134.94, 128.50, 127.71, 127.09, 125.21, 122.15, 120.00, 117.66, 115.90, 101.31, 75.39, 66.92, 58.07, 53.03, 47.38, 28.32, 25.69, 19.37. HRMS: calcd for $C_{34}H_{36}N_3O_6$ $[M + H]^+$ 582.2604; found 582.2608.

Compound 8. Compound **7** (1.75 g, 3.0 mmol, 1.0 equiv) was dissolved in ethyl acetate (30 mL), and lithium iodide (3.2 g, 24 mmol, 8 equiv) was added. The mixture was stirred at reflux for 12 h and then cooled to rt. The mixture was diluted with ethyl acetate (120 mL) and washed with water three times and brine once. The organic layer was dried with Na_2SO_4, filtered, and concentrated under reduced pressure. The crude product was purified by silica gel chromatography (DCM/MeOH = 20:1) to afford the title compound as a yellow solid (1.56 g, 92%). ^{1}H NMR (300 MHz, $CDCl_3$): δ 11.54 (s, 1 H), 8.84 (dd, *J* = 7.8, 1.2 Hz, 1 H), 7.95 (dd, *J* = 8.4, 1.2 Hz, 1 H), 7.72 (d, *J* = 7.5 Hz, 2 H), 7.67 (s, 1 H), 7.53–7.64 (m, 3 H), 7.31 (t, 7.2 Hz, 2 H), 7.20 (td, *J* = 7.5, 0.9 Hz, 2 H), 5.15 (s, 1 H), 4.64 (d, *J* = 6.3, 2 H), 4.20 (t, 1 H), 4.08 (d, *J* = 6.6 Hz, 2 H), 2.22–2.39 (m, 1 H), 1.68 (s, 6 H), 1.14 (d, *J* = 6.6 Hz, 6 H). ^{13}C{^{1}H}NMR (300 MHz, $CDCl_3$): δ 172.71, 165.60, 163.92, 157.22, 145.99, 143.40, 141.46, 138.05, 135.88, 128.72, 127.83, 127.24, 125.01, 122.67, 120.07, 118.63, 116.11, 99.98, 75.63, 67.33, 58.68, 47.37, 28.26, 25.94, 19.32. HRMS: calcd for $C_{33}H_{34}N_3O_6$ $[M + H]^+$ 568.2448; found 568.2447.

Compound 9. The title compound was synthesized from dimer block **8** on a 19 μmol scale (50 mg of Wang resin with manufacturer's loading: 0.38 mmol g^{-1}) by using the general SPS methodologies mentioned above and those previously published.[31b] The crude product was purified by silica gel chromatography (DCM/MeOH = 20:1) to afford the title compound as a white solid (16.7 mg, 39%). ^{1}H NMR (300 MHz, $CDCl_3$): δ 12.30 (s, 1 H), 11.78 (s, 1 H), 11.63–11.74 (m, 3 H), 11.58 (s, 1 H), 9.64 (s, 1 H), 9.61 (s, 1 H), 9.50–9.58 (m, 3 H), 8.73–8.93 (m, 7 H), 8.50 (dd, *J* = 8.4, 1.2 Hz, 1 H), 8.18 (dd, *J* = 7.2, 1.2 Hz, 1 H), 8.10 (s, 1 H), 7.84–7.99 (m, 6 H), 7.82 (s, 1 H), 7.78 (s, 1 H), 7.75 (s, 1 H), 7.74 (s, 1 H), 7.71 (s, 1 H), 7.47–7.67 (m, 8 H), 4.27 (d, *J* = 6.3 Hz, 2 H), 4.22 (d, *J* = 6.0 Hz, 2 H), 4.04–4.16 (m, 8 H), 3.95 (d, *J* = 5.7 Hz, 2 H), 2.10–2.43 (m, 7 H), 1.94–2.06 (m, 36 H), 1.20 (d, *J* = 6.6 Hz, 6 H), 1.15 (d, *J* = 6.6 Hz, 6 H), 1.12 (d, *J* = 6.6 Hz, 6 H), 1.03–1.10 (m, 18 H), 0.95 (d, *J* = 6.6 Hz, 6 H). HRMS: calcd for $C_{122}H_{141}N_{20}O_{23}$ $[M + H]^+$2255.0512; found 2255.0527.

Compound 10. The title compound was synthesized on a 19 μmol scale (50 mg of Wang resin with manufacturer's loading: 0.38 mmol g^{-1}) by using the general SPS methodologies mentioned above and those previously published.[31b] The crude product was purified by semipreparative RP-HPLC (System G) to afford the title compound as a white solid (6.9 mg, 15%, purity by RP-HPLC: 97%). RP-HPLC (System E) R_t = 10.20 min. ^{1}H NMR (300 MHz, DMSO-d_6): δ 11.53–11.99 (m, 3 H), 11.43 (s, 1 H), 11.32 (s, 1 H), 10.90 (br, 1 H), 10.32 (br, 2 H), 10.16 (s, 1 H), 10.03 (s, 1 H), 9.07 (s, 1 H), 8.45–8.77 (m, 6 H), 7.73–7.95 (m, 6 H), 7.43–7.65 (m, 11 H), 7.39 (s, 1 H), 6.67 (br), 5.56–5.49 (m, 5 H), 4.48–4.85 (m, 13 H), 2.80–3.10 (m, overlapped with water peak), 2.30–2.70 (m, overlapped with DMSO peak), 1.91–2.15 (m, 1 H), 1.86 (s, 3 H). HRMS: calcd for $C_{98}H_{84}N_{18}O_{44}$ $[M + 2H]^{2+}$ 1108.7461; found 1108.7501.

Compound 11. The title compound was synthesized on a 19 μmol scale (50 mg of Wang resin with manufacturer's loading: 0.38 mmol g^{-1}) by using the general SPS methodologies mentioned above and those previously published.[31b] The crude product was purified by semipreparative RP-HPLC (System F) to afford the title compound as a yellow solid (13.3 mg, 19%, purity by RP-HPLC: 98%). RP-HPLC (System D) R_t = 7.23 min. ^{1}H NMR (300 MHz, CD_3OH): δ 10.99 (s, 1 H), 10.93 (s, 1 H), 10.05–10.48 (m, 3 H), 10.06–10.22 (m, 2 H), 9.95 (s, 1 H), 9.33–9.58 (m, 2 H), 9.11 (s, 1 H), 8.74–8.95 (m, 2 H), 6.55–8.65 (m, 53 H, -NH_3^+ included), 6.25–6.49 (s, 1 H), 6.11 (s, 1 H), 5.82 (s, 1 H), 3.68–4.55 (m, 4 H), 2.70–3.60 (m, overlapped with CH_3OH peak), 2.00–2.68 (m, 31 H), 1.23–1.92 (m, 39 H). HRMS: calcd for $C_{130}H_{160}N_{32}O_{22}$ $[M+4H]^{4+}$ 630.5605; found 630.5629.

Compound 12. The title compound was synthesized on a 19 μmol scale (50 mg of Wang resin with manufacturer's loading: 0.38 mmol g^{-1}) by using the general SPS methodologies mentioned above and those previously published.[31b] The crude product was purified by semipreparative RP-HPLC (System F) to afford the title compound as a pale yellow solid (14.4 mg, 23%, purity by RP-HPLC: 98%). RP-HPLC (System D) R_t = 12.77 min. ^{1}H NMR (800 MHz, 10%D_2O/H_2O v/v %): δ 11.10 (br, 1 H), 10.61 (s, 1 H), 10.44 (br, 1 H), 10.28–10.38 (m, 2 H), 10.23 (s, 1 H), 10.05 (s, 1 H),

9.94 (s, 1 H), 9.72 (s, 1 H), 9.44 (s, 1 H), 9.02 (br, 1 H), 8.73 (d, *J* = 8.0 Hz, 1 H), 8.59 (d, *J* = 8.0 Hz, 1 H), 8.44 (s, 1 H), 7.00–8.24 (m, 41 H, -NH_3^+ included), 6.70 (d, *J* = 8.8 Hz, 1 H), 6.81 (d, *J* = 8.0 Hz, 1 H), 6.67 (t, *J* = 8.0 Hz, 1 H), 6.61 (s, 1 H), 6.21 (s, 1 H), 5.70 (s, 1 H), 4.60–5.20 (m, overlapped with water peak), 3.74–4.59 (m, 11 H), 3.54–3.67 (m, 4 H), 3.27–3.49 (m, 17 H), 3.19–3.24 (m, 2 H), 2.91–3.03 (m, 2 H), 2.68 (br, 1 H), 2.33–2.56 (m, 19 H), 1.99–2.25 (m, 4 H), 1.69 (br, 1 H), 1.40–1.55 (m, 5 H). HRMS: calcd for $C_{122}H_{138}N_{29}O_{25}$ $[M + 3H]^{3+}$803.3484; found 803.3515.

Compound 13. The title compound was synthesized on a 19 μmol scale (50 mg of Wang resin with manufacturer's loading: 0.38 mmol g^{-1}) by using the general SPS methodologies mentioned above and those previously published.[31b] The crude product was purified by semipreparative RP-HPLC (15-25% D over 10 min) to afford the title compound as a pale yellow solid (9.5 mg, 20%, purity by RP-HPLC: 97%). RP-HPLC (15-25% D over 7 min) R_t = 6.73 min. ^{1}H NMR (300 MHz, 10%D_2O/H_2O v/v %): δ 11.18 (s, 4H), 8.62 (s, 4H), 8.42 (br, 4H), 8.15 - 6.59 (m, overlapped with NH_4^+ signals, 87H), 4.16 – 3.85 (m, 6H), 3.30 – 2.50 (m, 30H). HRMS: calcd for $C_{130}H_{106}N_{19}O_{33}$ $[M + H]^+$ 2460.7195; found 2460.7225.

Chapter 3

Optimizing side chains for crystal growth from water: case study of aromatic amide foldamers

(Adapted with permission from X. Hu, S. J. Dawson, P. K. Mandal, X. de Hatten, B. Baptiste, and I. Huc, *Chem. Sci.* **2017**, DOI: 10.1039/C7SC00430C. Copyright 2017 Royal Society of Chemistry)

Contributors:

Dr. Pradeep K. Mandal carried out crystallization and crystal structure determination and refinement; Dr. Simon J. Dawson supervised the synthesis; Dr. Xavier de Hatten, Dr. Simon J. Dawson and Dr. Benoit Baptiste synthesized monomer **19** and tetraamide **3**, and crystallized tetraamide **3**; Dr. Victor Dos Santos and Dr. Marine Stupfel made preliminary contributions for the synthesis of **31** and **21**, respectively.

Objectives:

- Indentify short side chains which are able to endow aromatic foldamers with both solubility in, and crystal growth ability from water.
- Explore the synthetic routes for installing these side chains onto quinoline monomers and then develop the corresponding Fmoc protected quinoline monomers for SPS of quinoline oligoamides.
- Synthesize quinoline oligoamides displaying these side chains as a case study.
- Solubility and crystal growth ability evaluation of these quinoline oligoamides in water and obtain their crystal structures for the detailed crystallographic study.

1. Introduction

Structure elucidation is a necessary step to understand structure-property relationships and the design of functions at the molecular level. Among other techniques, X-ray crystallographic analysis provides unsurpassed accuracy and stands out as a direct way to gather structural information and to make further design possible. The first and main difficulty of crystallographic analysis is crystal growth. In particular, there is a perception – possibly a misperception – by organic chemists that growing crystals from water is difficult, despite the availability of multiple methods, commercial kits and additives that have been developed to crystallize complex biomacromolecules[1] and metallo-organic structures.[2] Water is a most relevant medium in which to elicit molecular and supramolecular functions. Indeed, there is a notable trend in supramolecular chemistry and host-guest chemistry to shift from traditional organic solvents to protic media including water.[3] If the main structure elucidation method was indeed complicated in water due to difficult crystallogenesis, this would constitute a true bottle neck. In the following of this chapter, we show our own difficulties in growing crystals of aromatic amide foldamers suitable for x-ray crystallographic analysis from water and how we successfully overcame them through the design of short and polar side chains that promote both high solubility in water and high crystal growth ability. This work constitutes a case study focused on aromatic helical foldamers, but it certainly has a general value for the crystallization

1. a) A. McPherson, *Introduction to Macromolecular Crystallography*, Hoboken, Wiley-Blackwell, 2nd edn, **2009**; b) R. Giegé, B. Lorber, and A. Théobald-Dietrich, *Acta Crystallogr., Sect. D: Biol. Crystallogr.*, **1994**, 50, 339; c) A. Ducruix, and R. Giegé, in *Crystallization of Nucleic Acids and Proteins. A Practical Approach*, ed. A. Ducruix and R. Giegé, Oxford, IRL Press/Oxford Univ. Press, **1992**..
2. a) T. Sawada, M. Yoshizawa, S. Sato, and M. Fujita, *Nat. Chem.*, **2009**, 1, 53; b) C. Zhao, Q.-F. Sun, W. M. Hart-Cooper, A. G. Di Pasquale, F. D. Toste, R. G. Bergman, and K. N. Raymond, *J. Am. Chem. Soc.*, **2013**, 135, 18802; c) J. L. Bolliger, T. K. Ronson, M. Ogawa, and J. R. Nitschke, *J. Am. Chem. Soc.*, **2014**, 136, 14545; d) J. R. Nitschke, D. Schultz, G. Bernardinelli, and D. Gerard, *J. Am. Chem. Soc.*, **2004**, 126, 16538; e) S. S.-Y. Chui, S. M.-F. Lo, J. P. H. Charmant, A. G. Orpen, and D. Williams, *Science*, **1999**, 283, 1148; f) R. Carballo, B. Covelo, N. Fernandez-Hermida, E. Garcia-Martinez, A. B. Lago, M. Vazquez, and E. M. Vazquez-Lopez, *Crystal Growth & Design*, **2006**, 6, 629.
3. a) E. A. Kataev, and C. Müller, *Tetrahedron*, **2014**, 70, 137; b) A. Dalla Cort, G. Forte, and L. Schiaffino, *J. Org. Chem.*, **2011**, 76, 7569; c) A. P. Davis, *Nature*, **2010**, 464, 169; d) S. Kubik, *Chem. Soc. Rev.*, **2009**, 38, 585; e) G. V. Oshovsky, D. N. Reinhoudt, and W. Verboom, *Angew. Chem., Int. Ed.*, **2007**, 46, 2366; f) E. A. Meyer, R. K. Castellano, and F. Diederich, *Angew. Chem., Int. Ed.*, **2003**, 42, 1210; g) T. J. Mooibroek, J. M. Casas-Solvas, R. L. Harniman, C. M. Renney, T. S. Carter, M. P. Crump, and A. P. Davis, *Nat. Chem.*, **2016**, 8, 69.

from water of innumerable aromatic molecular and supramolecular systems across various fields of chemistry.

In the past two decades, aromatic foldamers and in particular aromatic amide foldamers have emerged as a new class of folded molecular architectures distinct from peptidic and nucleotidic structures.[4] As discussed in chapter one, aromatic amide foldamers have been designed to adopt a variety of shapes, including helices,[5] macrocycles,[6] sheets,[7] linear and zig-zag[8] ribbons, as well as bundle-like architectures (tertiary structure mimics).[9] They give access to structures beyond the reach of biopolymers and find applications in e.g. molecular recognition.[10] By and large, aromatic amide foldamer structures have been characterized in organic solvents from which they crystallize well. Crystal growth ability of these systems, including some of the largest non-biological molecules ever crystallized,[9,11] is assigned to their high conformational stability in organic solvents and to the use of appropriate side chains. In particular, the isobutoxy side chain has proven extremely useful in that it endows foldamers with both high solubility in organic medium and a high crystal

4. a) I. Huc, *Eur. J. Org. Chem.*, **2004**, 1, 17; b) D.-W. Zhang, X. Zhao, J.-L. Hou, and Z.-T. Li, *Chem. Rev.*, **2012**, 112, 5271; c) G. Guichard, and I. Huc, *Chem. Commun.*, **2011**, 47, 5933.
5. a) J. Zhu, R. D. Parra, H. Zeng, E. Skrzypczak-Jankum, X. C. Zeng, and B. Gong, *J. Am. Chem. Soc.*, **2000**, 122, 4219; b) H. Jiang, J.-M. Léger, and I. Huc, *J. Am. Chem. Soc.*, **2003**, 125, 3448; c) H.-P. Yi, C. Li, J.-L. Hou, X.-K. Jiang, and Z.-T. Li, *Tetrahedron*, **2005**, 61, 7974; d) Z.-Q. Hu, H.-Y. Hu, and C.-F. Chen, *J. Org. Chem.*, **2006**, 71, 1131; e) B. Baptiste, J. Zhu, D. Haldar, B. Kauffmann, J.-M. Léger, and I. Huc, *Chem. – Asian J.*, **2010**, 5, 1364; f) Y. Ferrand, A. M. Kendhale, J. Garric, B. Kauffmann, and I. Huc, *Angew. Chem., Int. Ed.*, **2010**, 49, 1778; g) Q. Gan, C. Bao, B. Kauffmann, A. Grelard, J. Xiang, S. Liu, I. Huc, and H. Jiang, *Angew. Chem., Int. Ed.*, **2008**, 47, 1715.
6. a) S. Ferguson, K. Yamato, R. Liu, L. He, X. C. Zeng, and B. Gong, *Angew. Chem., Int. Ed.*, **2009**, 48, 3150; b) H. Fu, Y. Liu, and H. Zeng, *Chem. Commun.*, **2013**, 49, 4127; c) Y.-Y. Zhu, C. Li, G.-Y. Li, X.-K. Jiang, and Z.-T. Li, *J. Org. Chem.*, **2008**, 73, 1745; d) H. Jiang, J.-M. Léger, P. Guionneau, and I. Huc, *Org. Lett.*, **2004**, 6, 2985.
7. a) L. Sebaoun, V. Maurizot, T. Granier, B. Kauffmann, and I. Huc, *J. Am. Chem. Soc.*, **2014**, 136, 2168; b) L. Sebaoun, B. Kauffmann, T. Delclos, V. Maurizot, and I. Huc, *Org. Lett.*, **2014**, 16, 2326.
8. a) Y. Hamuro, S. J. Geib, A. D. Hamilton, *J. Am. Chem. Soc.*, **1996**, 118, 7529; b) J. T. Ernst, J. Becerril, H. S. Park, H. Yin, and A. D. Hamilton, *Angew. Chem., Int. Ed.*, **2003**, 42, 535; c) E. Kolomiets, V. Berl, I. Odriozola, A.-M. Stadler, N. Kyritsakas, and J.-M. Lehn, *Chem. Commun.*, **2003**, 7, 2868; d) Z.-Q. Wu, X.-K. Jiang, S.-Z. Zhu, and Z.-T. Li, *Org. Lett.*, **2004**, 6, 229.
9. a) N. Delsuc, J.-M. Léger, S. Massip, and Ivan Huc, *Angew. Chem., Int. Ed.*, **2007**, 46, 214; b) N. Delsuc, S. Massip, J.-M. Léger, B. Kauffmann, and Ivan Huc, *J. Am. Chem. Soc.*, **2011**, 133, 3165.
10. a) N. Chandramouli, Y. Ferrand, G. Lautrette, B. Kauffmann, C. D. Mackereth, M. Laguerre, D. Dubreuil, and I. Huc, *Nat. Chem.*, **2015**, 7, 334; b) Y. Hua, Y. Liu, C.-H. Chen, and A. H. Flood, *J. Am. Chem. Soc.* **2013**, 135, 14401; c) K.-J. Chang, D. Moon, M. S. Lah, and K.-S. Jeong, *Angew. Chem., Int. Ed.*, **2005**, 44, 7926; d) H. Juwarker, J.-M. Suk, and K.-S. Jeong, *Chem. Soc. Rev.*, **2009**, 38, 3316.
11. X. Li, T. Qi, K. Srinivas, S. Massip, V. Maurizot, and I. Huc, *Org. Lett.*, **2016**, 18, 1044.

growth ability.[5b,5d-g,6d,7,9,10a,11] This observation can be related to the numerous crystal structures of lipophilic peptides and pseudo peptides that often contain short branched side chains such as leucine or valine residues.[12]

Aromatic amide foldamers may be composed of diverse units including benzene, pyridine or anthracene based monomers as mentioned in chapter one. Among them, oligoamides of 8-amino-2-quinolinecarboxylic acids (**Q**) as those shown in Figure 1 form very stable helices spanning two turns every five units that have been characterized in solution[13] and in the solid state.[5b] Intrigued by the potential use of these medium-sized objects in a biological context, we and others have started to explore their interactions with nucleic acids[14] and proteins[15] as well as their cell penetration properties.[16] In parallel, other groups have focused on rod-like architectures for protein surface recognition.[17] A first step was to endow **Qn** oligomers, a priori very hydrophobic molecules, with high (millimolar range) solubility in water. This was successfully achieved by introducing cationic ($\mathbf{Q^{Orn}}$) or

12. a) G. W. Collie, K. Pulka-Ziach, and G. Guichard, *Chem. Sci.*, **2016**, 7, 3377; b) K. Basuroy, B. Dinesh, N. Shamala, and P. Balaram, *Angew. Chem., Int. Ed.*, **2013**, 52, 3136; c) K. Basuroy, B. Dinesh, N. Shamala, and P. Balaram, *Angew. Chem., Int. Ed.*, **2012**, 51, 8736.
13. C. Dolain, A. Grélard, M. Laguerre, H. Jiang, V. Maurizot, and I. Huc, *Chem. –Eur. J.*, **2005**, 11, 6135.
14. a) S. Muller, K. Laxmi-Reddy, P. V. Jena, B. Baptiste, Z. Dong, F. Godde, T. Ha, R. Rodriguez, S. Balasubramanian, and I. Huc, *ChemBioChem*, **2014**, 15, 2563; b) P. K. Mandal, B. Baptiste, B. L. d'Estaintot, B. Kauffmann, and I. Huc, *ChemBioChem*, **2016**, 17, 1911.
15. a) J. Buratto, C. Colombo, M. Stupfel, S. J. Dawson, C. Dolain, B. L. d'Estaintot, L. Fischer, T. Granier, M. Laguerre, B. Gallois, and I. Huc, *Angew. Chem., Int. Ed.* **2014**, 53, 883; b) M. Jewginski, L. Fischer, C. Colombo, I. Huc, and C. D. Mackereth, *ChemBioChem*, **2016**, 17, 727; c) S. Kumar, and A. D. Miranker, *Chem. Commun.*, **2013**, 49, 4749; d) S. Kumar, M. Birol, D. E. Schlamadinger, S. P. Wojcik, E. Rhoades, and A. D. Miranker, *Nat. Commun*., **2016**, 7, 11412.
16. a) E. R. Gillies, F. Deiss, C. Staedel, J.-M. Schmitter, and I. Huc, *Angew. Chem., Int. Ed.*, **2007**, 46, 4081; b) J. Iriondo-Alberdi, K. Laxmi-Reddy, B. Bougueme, C. Staedel, and I. Huc, *ChemBioChem*, **2010**, 11, 1679.
17. a) J. A. Hebda, I. Saraogi, M. Magzoub, A. D. Hamilton, and A. D. Miranker, *Chem. Biol.*, **2009**, 16, 943; b) I. Saraogi, J. A. Hebda, J. Becerril, L. A. Estroff, A. D. Miranker, and A. D. Hamilton, *Angew. Chem., Int. Ed*., **2010**, 49, 736; c) S. Kumar, D. E. Schlamadinger, M. A. Brown, J. M. Dunn, B. Mercado, J. A. Hebda, I. Saraogi, E. Rhoades, A. D. Hamilton, and A. D. Miranker, *Chem. Biol.*, **2015**, 22, 369; d) B. P. Orner, J. T. Ernst, and A. D. Hamilton, *J. Am. Chem. Soc.*, **2001**, 123, 5382; e) H. Yin, G. Lee, K. A. Sedey, O. Kutzki, H. S. Park, B. P. Orner, J. T. Ernst, H.-G. Wang, S. M. Sebti, and A. D. Hamilton, *J. Am. Chem. Soc*., **2005**, 127, 10191; f) H. Yin, G. Lee, H. S. Park, G. A. Payne, J. M. Rodriguez, S. M. Sebti, and A. D. Hamilton, *Angew. Chem., Int. Ed.*, **2005**, 44, 2704; g) J. M. Rodriguez, A. D. Hamilton, *Angew. Chem., Int. Ed*., **2007**, 46, 8614; h) J. P. Plante, T. Burnley, B. Malkova, M. E. Webb, S. L. Warriner, T. A. Edwards, and A. J. Wilson, *Chem. Commun.*, **2009**, 5091; i) J. M. Rodriguez, N. T. Ross, W. P. Katt, D. Dhar, G. Lee, and A. D. Hamilton, *ChemMedChem.*, **2009**, 4, 649; j) W. E. Martucci, J. M. Rodriguez, M. A. Vargo, M. Marr, and A. D. Hamilton, K. S. Anderson, *Med. Chem. Commun.*, **2013**, 4, 1247; k) V. Azzarito, J. A. Miles, J. Fisher, T. A. Edwards, S. L. Warriner, and A. J. Wilson, *Chem. Sci.* **2015**, 6, 2434.

anionic side chains ($\mathbf{Q}^{\mathbf{Asp}}$),[16,18] as well as neutral oligoethylene glycol side chains ($\mathbf{Q}^{\mathbf{Teg}}$).[19] Remarkably, we found that the helical conformations were considerably more stable in water than in organic solvents, presumably due to the hydrophobic component associated with aromatic stacking in water.[19a] This property should have been an advantage for growing crystals, but a considerable number of attempts all proved unsuccessful. Regardless of their length, neither anionic, nor cationic or zwitteranionic helical sequences yielded crystals suitable for x-ray analysis. This was despite the use of multiple screens and a great deal of experience including success at solving difficult cases.[20] In the best scenarios, crystals were obtained that could be shown to be of the foldamers but that did not diffract sufficiently or were polycrystalline. Eventually, crystal structures of the helical foldamers were obtained from water when these were bound to the surface of a protein or a nucleic acid.[14b,15a] In the case of linear aromatic foldamers, crystallization from water has been achieved through the assistance of transition metal coordination.[21] A few other structures of water soluble oligomers have been reported.[22]

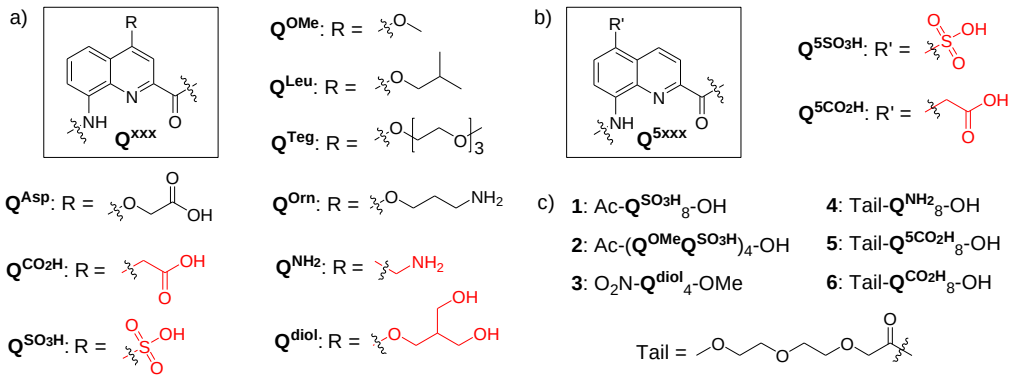

Figure 1. Structures of a) $\mathbf{Q}^{\mathbf{Xxx}}$ and b) $\mathbf{Q}^{\mathbf{5Xxx}}$ amino acid monomers, and summary of c) aromatic amide foldamer sequences **1 - 6**. New side chains developed in this study are shown in red. The terminal 8-nitro group of oligomer **3** replaces the terminal NH function.

18. a) B. Baptiste, C. Douat-Casassus, K. Laxmi-Reddy, F. Godde, and I. Huc, *J. Org. Chem.*, **2010**, 75, 7175; b) S. J. Dawson, X. Hu, S. Claerhout, and I. Huc, *Methods in Enzymology*, **2016**, 580, 279.
19. a) T. Qi, V. Maurizot, H. Noguchi, T. Charoenraks, B. Kauffmann, M. Takafuji, H. Ihara, and I. Huc, *Chem. Commun.*, **2012**, 48, 6337; b) C. Tsiamantas, S. J. Dawson, and I. Huc, *C. R. Chimie*, **2016**, 19, 132.
20. P. K. Mandal, B. Kauffmann, H. Destecroix, Y. Ferrand, A. P. Davis, and I. Huc, *Chem. Commun.*, **2016**, 52, 9355.
21. V. Pavone, S.-Q. Zhang, A. Merlino, A. Lombardi, Y. Wu, and W. F. DeGrado, *Nat. Commun.*, **2014**, 5, 3581.
22. a) C. G. Cummings, and A. D. Hamilton, *Tetrahedron* **2013**, 69, 1663; b) L. A. Estroff, C. D. Incarvito, and A. D. Hamilton, *J. Am. Chem. Soc.*, **2004**, 126, 2.

We hypothesized that the reason for these failures might be the relative flexibility of the side chains of $\mathbf{Q}^{\mathbf{Asp}}$ and $\mathbf{Q}^{\mathbf{Orn}}$. Flexible groups create an entropic barrier to crystallization. They give rise to disorder within the crystal lattice and may perturb long range order. This phenomenon is known to protein crystallographers who have developed surface entropy reduction mutagenesis, targeting mainly side chains such as lysine and glutamates.[23] This chapter describes the design and synthesis of new $\mathbf{Q}^{\mathbf{Xxx}}$ monomers bearing short and more rigid water solubilizing side chains, their incorporation into octameric or tetrameric helical sequences, and the successful growth of crystals suitable for x-ray diffraction analysis. We find that a single atom removal from each side chain may lead to dramatic changes in crystal growth behaviour.

23. Z. S. Derewenda, and P. G. Vekilov, *Acta Cryst.* **2006**, D62, 116.

2. Monomer design and synthesis

2.1 Monomer design

Four new side chains for **Q** monomers were considered in position 4 and, for two of them, in position 5 as well. For the purpose of the subsequent solid supported synthesis (i.e. SPS)[18] of the oligoamide sequences, each new monomer was produced as an Fmoc-protected amine having a free carboxylic acid function. Furthermore, in anticipation that the targeted monomers would serve both the purpose of solubility and crystal growth, and thus that their incorporation in foldamer sequences could become frequent, multigram scale syntheses were developed.

2.2 Monomers bearing sulfonic acid side chain

Sulfonic acid was identified as a desirable target due to the rich background of crystal structures afforded from aryl sulfonates[2d, 24] including in complex with proteins.[25] It is short, rigid, very polar, and anionic over a wide pH range. Among several possible synthetic approaches, two appeared to be suitable to introduce a sulfonic acid on 8-amino-2-quinoline carboxylic quinoline monomers: thiol oxidation or direct sulfonation. Synthesis was first successful with the latter route thanks to a short and simple synthetic protocol (Scheme 1a). Only three steps were needed from commercially available methyl 8-aminoquinoline-2-carboxylate to monomer **9** which has a sulfonic acid group in position 5 (overall yield 60%). Sulfonation is made easy by the donor effect of the amine in the *para* position. Unfortunately, this eventually

24. a) M. Selkti, A. W. Coleman, I. Nicolis, N. Douteau-Guével, F. Villain, A. Tomas, and C. de Rango, *Chem. Commun.*, **2000**, 161; b) S. J. Dalgarno, M. J. Hardie, M. Makha, and C. L. Raston, *Chem. Eur. J.*, **2003**, 9, 2834; c) S. J. Dalgarno, M. J. Hardie, J. L. Atwood, J. E. Warren, and C. L. Raston, *New J. Chem.*, **2005**, 29, 649; d) P. Mal, B. Breiner, K. Rissanen, and J. R. Nitschke, *Science*, **2009**, 324, 1697.
25. a) R. E. McGovern, A. A. McCaerthy, and P. B. Crowley, *Chem. Commun.*, **2014**, 50, 10412; b) L. Jiao, S. Ouyang, M. Liang, F. Niu, N. Shaw, W. Wu, W. Ding, C. Jin, Y. Peng, Y. Zhu, F. Zhang, T. Wang, C. Li, X. Zuo, C.-H. Luan, D. Li, and Z.-J. Liu, *J. Virology*, **2013**, 87, 6829; c) A. Schuetz, J. Min, T. Antoshenko, C.-L. Wang, A. Allali-Hassani, A. Dong, P. Loppnau, M. Vedadi, A. Bochkarev, R. Sternglanz, and A. N. Plotnikov, *Structure*, **2007**, 15, 377; d) H. P. Morgan, I. W. McNae, M. W. Nowicki, W. Zhong, P. A. M. Michels, D. S. Auld, L. A. Fothergill-Gilmore, and M. D. Walkinshaw, *J. Biol. Chem.*, **2011**, 286, 31232.

turned into a disadvantage: the reciprocal electron withdrawing effect of the sulfonic acid on the amine dramatically reduced its reactivity. Even under harsh coupling conditions (60 °C, DBU, 9 equiv of acid chloride, repeated couplings), chain extension from the amine was too inefficient for SPS and the use of **9** was limited to that of an N-terminal monomer.

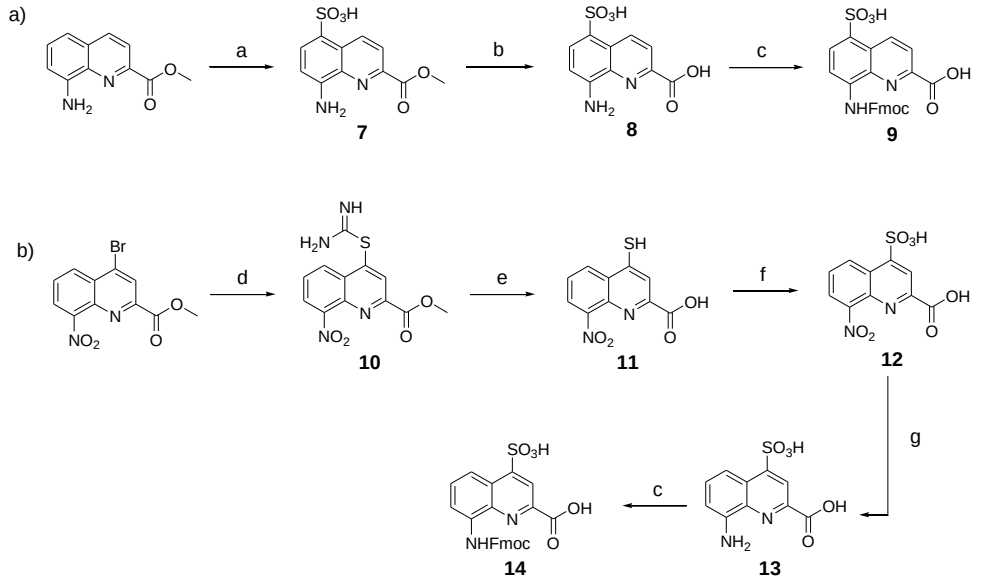

Scheme 1. Synthesis of a) Fmoc-$\mathbf{Q^{5SO_3H}}$-OH (**9**) and b) Fmoc-$\mathbf{Q^{SO_3H}}$-OH (**14**). Reagents and conditions: (a) $ClSO_3TMS$, dioxane, 100 °C, overnight; (b) NaOH, THF/H_2O, r.t., 1h; (c) Fmoc-Cl, $NaHCO_3$, dioxane/H_2O, 0 °C to r.t., overnight; (d) Thiourea, acetone, reflux, overnight; (e) NaOH, MeOH/THF, r.t., 3h; (f) 30% H_2O_2, formic acid, 0 °C, 2h; (g) H_2, Pd/C, MeOH, r.t., 1d.

The synthesis of monomer **14** was then planned (Scheme 1b) with the expectation that a sulfonic acid in position **4** should not alter much the reactivity of the amine function. The starting 4-bromo-quinoline[15a] was first substituted by thiourea. Subsequent hydrolysis yielded quinoline mercaptan **11**. After oxidation of the thiol and hydrogenation of the nitro group, Fmoc protection was installed to afford monomer **14**. Particular care must be taken to control temperature during the oxidation step with hydrogen peroxide because of the inherent risk of explosion associated with this reagent, in particular on large scales. All reactions proceeded efficiently, yet the overall yield was not as high as expected. This was mainly because of the high polarity and water solubility of the sulfonic acid intermediates, which impeded the use of classical work-ups such as extraction or column chromatography.

For example, water solubility was surprisingly high for the Fmoc-protected final product **14** which proved difficult to extract and even harder to isolate by chromatography. Isolation was eventually achieved by direct precipitation from the reaction mixture but, by this method, high purity was possible only by collecting only part of the material.

We initially thought that sulfonic acid protection would be necessary during SPS, but this proved not to be the case. This was fortunate because our trials to make sulfonate esters were all unsuccessful. Thus, the activation of **14** into a carbonyl chloride and its coupling to amines proceeded normally. The SPS procedure nevertheless required some slight changes: once one or more monomer **14** has been added to a sequence, the sulfonic acid may retain some of the piperidine used for subsequent Fmoc deprotections, even after several solvent washes. Being a secondary amine, piperidine may consume part of the acid chlorides added in the next steps, causing a drop in yield that we found to be disastrous when multiple sulfonic acids were present. To address this problem, an additional DIPEA wash after Fmoc deprotection was introduced in the SPS protocol to exchange piperidine with DIPEA.

2.3 Monomer bearing neutral side chain

The extraordinary success of the isobutoxy group at promoting both solubility in, and crystallization from organic solvents,[5b,5d-g,6d,7,9,10a,11] guided the design of monomer **19** (Scheme 2). It was hoped that the branching along with two hydroxyl functions of a side chain derived from 2-hydroxymethyl-1,3-propanediol may result in similar properties in aqueous media. The identification of a protecting group suitable for SPS proved to be delicate. Acetals were found to be too acid labile (cleavage during acid chloride activation with Ghosez's reagent[18]) or not enough (low lability in presence of TFA). Eventually, the di-tert-butylsilylene (DTBS) group was found to be stable during monomer synthesis and under SPS conditions. It resists TFA treatments normally used for resin cleavage but can conveniently be deprotected in the presence

of TBAF. The preparation of **19** entailed usual protocols for side chain introduction.[5b,15a,16a,18a] Mitsunobu reaction, saponification, hydrogenation and Fmoc installation provided **19** in an overall 45% yield. SPS proceeded normally (see Oligomer synthesis part). (Thank Dr. Xavier de Hatten, Dr. Simon J. Dawson and Dr. Benoit Baptiste for the synthesis of **19**.)

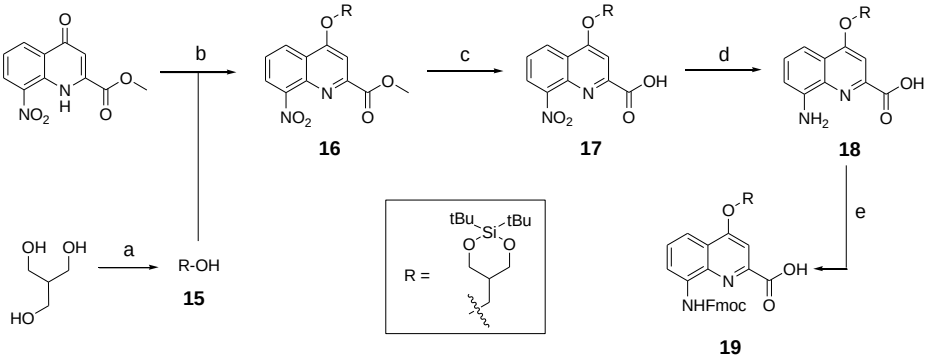

Scheme 2. Synthesis of Fmoc-$\mathbf{Q^{diol(DTBS)}}$-OH (**19**). Reagents and conditions: (a) DTBS ditriflate, anhydrous pyridine, anhydrous THF, -78 °C to r.t., 4h; (b) 15, DIAD, PPh_3, anhydrous THF, 0 °C to 50 °C, 5h; (c) LiOH·H_2O, THF/H_2O, r.t., 1h; (d) H_2, Pd/C, THF, r.t., overnight; (e) Fmoc-Cl, $NaHCO_3$, dioxane/H_2O, 0 °C to r.t., overnight.

2.4 Monomers bearing other polar side chains

2.4.1 Side chain design

The series of polar side chain functionality was further expanded from sulfonic acid (**14**) and diol (**19**) to ammonium (**25**, Scheme 3) and carboxylic acid (**31** and **36**, Scheme 4). The purpose was to cover a range of functionalities and to provide side chains resembling those of $\mathbf{Q^{Asp}}$ and $\mathbf{Q^{Orn}}$ which have proven to be useful in nucleic acid recognition[14] and protein recognition,[15c-d] yet being shorter and therefore more rigid. A novel feature in this chemistry shared by the aminomethyl chain of **25** and the carboxymethyl chains of **31** and **36** is that they are connected to the quinoline ring by a carbon-carbon bond. In the context of biological applications, this linkage may confer a better metabolic stability than hydrolytically cleavable ethers, but the validation of this hypothesis is beyond the scope of the present study.

2.4.2 Monomer bearing aminomethyl side chain

The synthesis of **25**, equipped with a Boc-protected side chain amine and an Fmoc-protected main chain amine, is straightforward (Scheme 3). The yield of each step was above 90% on a multi gram scale. It is noteworthy that the protocol required no column chromatography which should make scale up easy. All six steps of the synthesis and final purification can be achieved in one week with an overall yield as high as 75%. Solid phase synthesis with this monomer proceeded successfully as well (see Oligomer synthesis part). (Thank Dr. Marine Stupfel for the preliminary contributions of synthesizing **21**.**)**

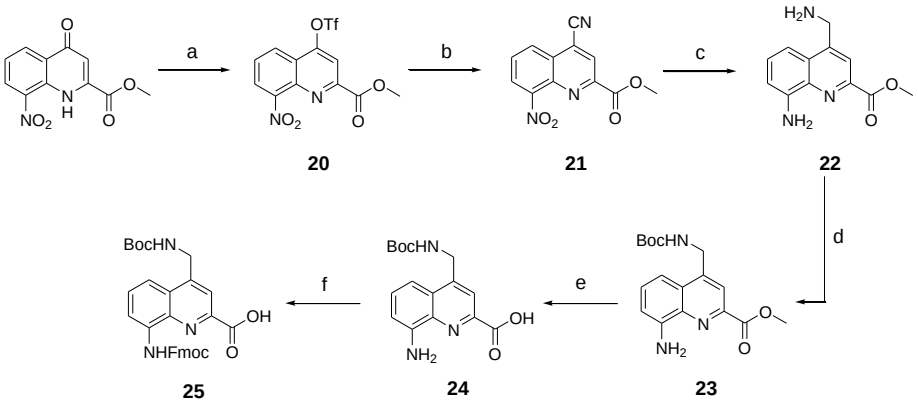

Scheme 3. Synthesis of Fmoc-$\mathbf{Q}^{\mathbf{NH(Boc)}}$-OH (**25**). Reagents and conditions: (a) Tf_2O, anhydrous pyridine, anhydrous DCM, r.t., overnight; (b) KCN, $Pd(PPh_3)_4$, anhydrous toluene/DMF, 100 ^oC, 2h; (c) H_2, Pd/C, AcOH/THF, r.t., overnight; (d) Boc_2O, DIPEA, DCM/CH_3CN, r.t., overnight; (e) LiOH H_2O, THF/H_2O, r.t., 1h; (f) Fmoc-Cl, $NaHCO_3$, dioxane/H2O, 0 ^oC to r.t., overnight.

2.4.3 Monomers bearing carboxymethyl side chain

In contrast, the syntheses of **31** and **36**, which possess a carboxymethyl side chain protected as an acid labile tert-butyl ester, was less easy. The key step is the aryl-alkyl carbon-carbon bond formation via a Pd-catalyzed α-arylation of the zinc enolate of *tert*-butyl acetate.[26] The synthetic route and conditions were first developed and optimized for monomer **31** (Scheme 4a). In order to install the side chain in position 5, the 5-bromo quinoline precursor **28** was prepared in three steps from commercial 5-bromo-2-nitroaniline. The substitution of the bromide by freshly prepared

26. T. Hama, X. Liu, D. A. Culkin, and J. F. Hartwig, *J. Am. Chem. Soc.*, **2003**, 125, 11176.

Reformatsky reagent 2-tert-butoxy-2-oxoethyl zinc (II) bromide is delicate. The key to success was to strictly avoid oxygen. Operating this reaction in a glove box helps ensure a high and reproducible yield and avoids wasting costly catalyst and precursors. The purity of product **29** was found to be crucial to obtain a final Fmoc monomer sufficiently pure (> 97%) for multi-step SPS coupling. Indeed, amino acid **30** and final product **31** are both difficult to purify. When all necessary care is taken, monomer **31** can be prepared on a 10 g scale with a yield of 7% over six steps. (Thank Dr. Victor Dos Santos for the preliminary contributions of synthesizing **31**.)

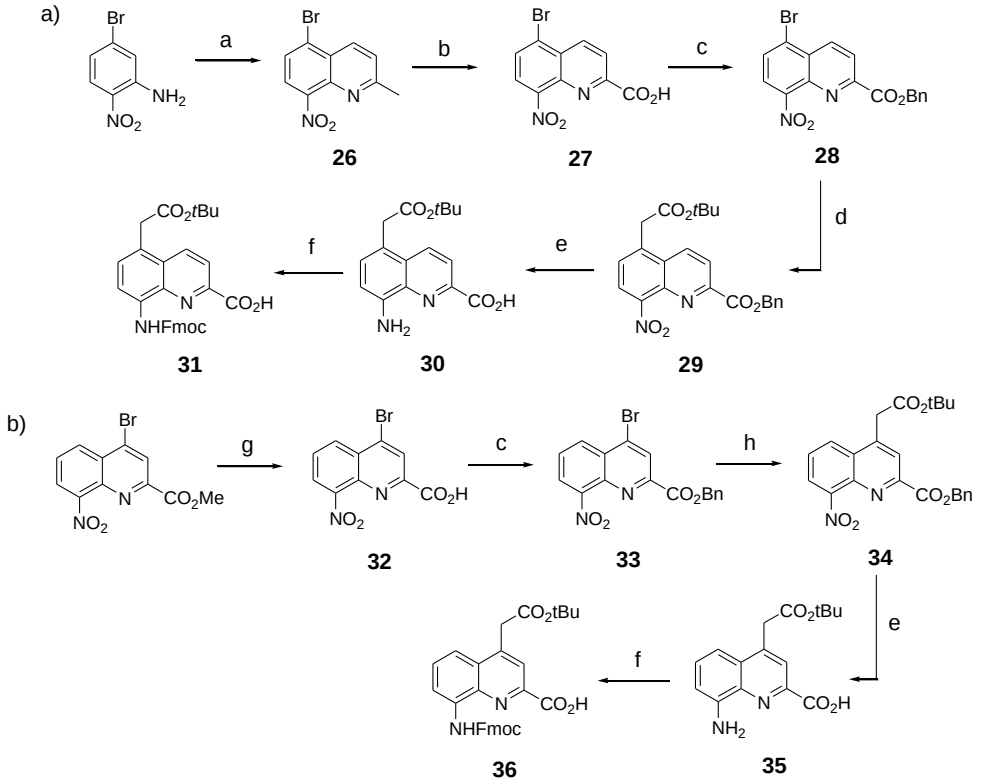

Scheme 4. Synthesis of a) Fmoc-$\mathbf{Q^{5CO_2(tBu)}}$-OH (**31**) and b) Fmoc-$\mathbf{Q^{CO_2(tBu)}}$-OH (**36**). Reagents and conditions: (a) Ethylvinylether, H_2SO_4, AcOH, 70 °C to 120 °C, 30min; (b) SeO_2, pyridine, 80 °C, 2d; (c) Benzyl bromide, K_2CO_3, DMF, r.t., 12h; (d) 2-tert-butoxy-2-oxoethyl zinc (II) bromide, bis(dibenzylidene acetone)-palladium [0], 1,2,3,4,5-pentaphenyl-1'-(di-tert-butylphosphino) ferrocene, THF, 70 °C, 12h; (e) H_2, Pd/C, THF, r.t., 1d; (f) Fmoc-Cl, $NaHCO_3$, dioxane/H_2O, 0 °C to r.t., overnight; (g) LiOH ·H_2O, THF/H_2O, r.t., 1h; (h) 2-tert-butoxy-2-oxoethyl zinc (II) bromide, bis(dibenzylidene acetone)-palladium [0], 1,2,3,4,5-pentaphenyl-1'-(di-tert-butylphosphino) ferrocene, anhydrous THF, r.t., 4h.

Introduction of the same carboxymethyl side chain in position 4 was achieved starting from methyl 4-bromo-8-nitroquinoline-2-carboxylate which was prepared following previously published protocols.[15a] Synthesis was initially considered from

the methyl ester via its subsequent saponification (LiOH) or demethylation (LiI). However, in both cases, purification of the final product **36** was problematic, possibly due to some *tert*-Bu ester cleavage. Instead, the two-step introduction of a benzyl ester proved to be rewarding (Scheme 4b). The subsequent aryl-alkyl cross-coupling, combined benzyl ester hydrogenolysis and nitro group hydrogenation, and final Fmoc introduction all worked as for compound **31**. Monomer **36** was obtained in good purity (RP-HPLC purity > 97%) and good yield (overall 31% after 5 steps) without any column chromatography purification. The synthesis of sequences comprised of this monomer was successful (see the Oligomer synthesis part). However, we found that decarboxylation of the side chain may occur under relatively mild conditions for the C-terminal monomer, for example in pure DMSO at room temperature.[27] We suppose that this decarboxylation is assisted by the neighbour main chain terminal carboxylic acid function (Scheme 5). The use of this monomer is thus fine within an oligoamide sequence but it should be avoided as a C-terminal unit. In principle, such decarboxylation may also occur under UV irradiation.[28] Although we did not encounter any degradation under normal laboratory conditions, protection from UV light is advised.

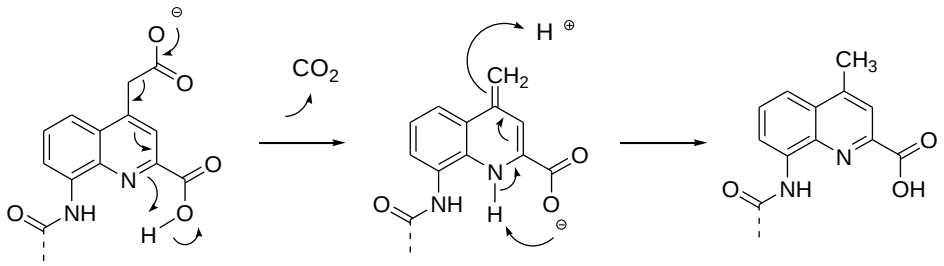

Scheme 5. Possible decarboxylation mechanism.

27. G. R. Jurch, and K. C. Ramey, *Chem. Comm. (London)*, **1968**, 1211b.
28. F. R. Stermitz, and W. H. Huang, *J. Am. Chem. Soc.*, **1971**, 93, 342.

3. Oligomer synthesis and crystallography

3.1 Oligomer synthesis

In order to test the effect of these new side chains on the solubility and crystal growth ability of oligomers in water, oligoamides **1-6** (Figure 1) were synthesized from Fmoc acid monomers **14**, **19**, **25**, **31**, **36** and Fmoc-$\mathbf{Q^{OMe}}$-OH using the previously reported SPS methods[18] (see also Experimental part). As discussed above, the amino group of monomer **9** was too unreactive to elongate an oligoamide sequence. This monomer is only suitable as an N-terminal unit which much limits the scope of its applications. Also, as mentioned above, we have observed decarboxylation of the carboxymethyl side chain in position 4 when placed at the C-terminus of the sequence (as in monomer **36**, see Scheme 5). This degradation is faster in DMSO and in aqueous acidic medium but it does not occur during TFA mediated resin cleavage and side chain deprotection. Fortunately, it is very slow under slightly basic conditions (pH > 8). According to LC-MS monitoring, sequence **6** had undergone less than 5% degradation after six months. The recommendation is nevertheless to avoid placing this monomer at the C-terminus. (Thank Dr. Xavier de Hatten, Dr. Simon J. Dawson and Dr. Benoit Baptiste for the synthesis of **3**.)

3.2 Crystallization

Eventually, all oligomers but sequence **1** produced crystals from aqueous media by a standard hanging drop technique. In order to handle the small amount of oligomers **1-6**, they were prepared as floppy powders by lyophilization technique. All the oligomers could be dissolved in water (oligomer **3** is in water/acetonitrile = 3:1 and thank Dr. Benoit Baptiste crystallized it) to obtain solutions having a final concentration of 2 mM. Crystal growth of oligomers **1-6** were carried out at 20 ^{o}C (temperature was strictly controlled by air conditioning) in 24-well Linbro-style plates. Crystallization took place while water of the drop (the solution containing oligomers,

in a lower concentration of crystallization reagents) diffused into the reservoir solution which had a higher concentration of crystallization reagents (Figure 2, a standard aqueous hanging-drop vapor diffusion technique).

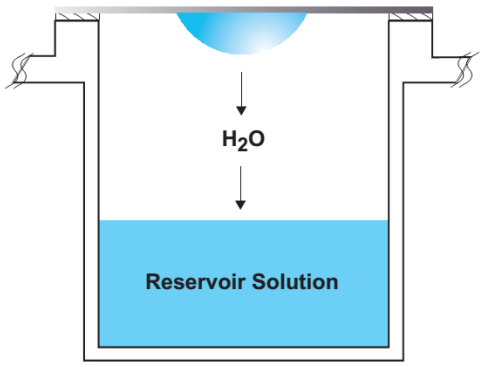

Figure 2. Process of water diffusion

For different sequences, it took different days, from 2 days to a month, to crystallize from water. The aqueous drops were prepared by mixing 0.75 to 1.0 μL of the foldamer solution with an equal volume of the crystallization reagent. After several trials, the proper crystallization conditions are screened out for each oligomer to yield crystals (Figure 3, except oligomer **1** whose water solubility was too high to crystallize before any crystallization reagent). The crystallization conditions which yielded crystals are summarized in Table 1. (Thank Dr. Pradeep K. Mandal for the crystallization and the following crystal structure determination and refinement.)

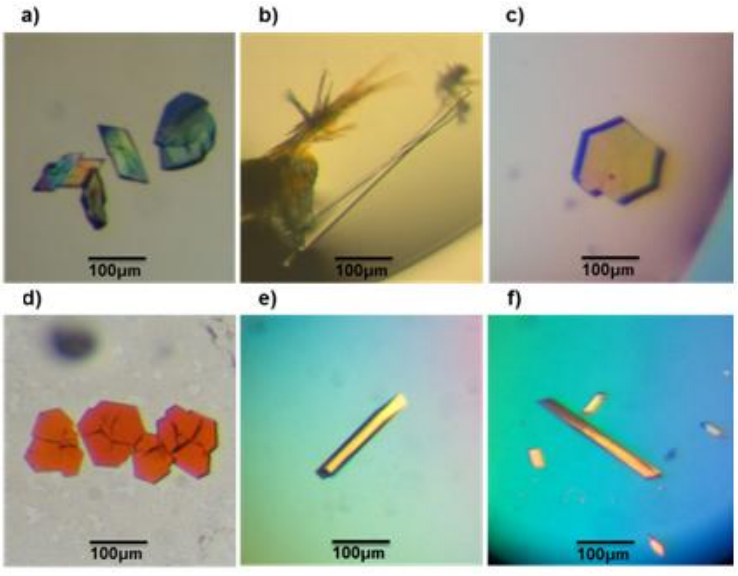

Figure 3: Crystals of water soluble oligomers: a) **2**, b) **3**, c) - d) **4**, e) **5** and e) **6**.

Table 1: Crystallization conditions of the water soluble oligomers

Foldamer	Crystallization reagent	Crystallogenesis	
		Duration	Crystal size
2	100 mM HEPES (pH 7.5), 200 mM $CaCl_2$, 28% v/v PEG 400	21 days	(0.10 x 0.04 x 0.04) mm
3	100 mM HEPES (pH 7.5), 500 mM $(NH_4)_2SO_4$, 30% v/v (+/-) MPD	14 days	(0.50 x 0.01 x 0.01) mm
4	100 mM HEPES (pH 7.0), 200 mM $(NH_4)_2SO_4$, 20 mM $Mg(OAc)_2$, 5% w/v PEG 4000	2 days	(0.15 x 0.15 x 0.03) mm
4	50 mM Imidazole (pH 7.2), 20 mM $ZnSO_4$, 10% w/v PEG 4000	2 days	(0.07 x 0.07 x 0.03) mm
5	100 mM MES (pH 6.5), 200 mM $Ca(OAc)_2$, 28% w/v PEG 8000	5 days	(0.15 x 0.05 x 0.03) mm
6	100 mM MES (pH 6.5), 200 mM $(NH_4)_2SO_4$, 30% w/v PEG 8000	30 days	(0.20 x 0.03 x 0.03) mm

3.3 Crystal structures

Tetraamide **3** derived from the branched neutral diol side chain was synthesized first. SPS as well as side chain deprotection and RP-HPLC purification proceeded smoothly (Figure 4b, for detailed information see Experimental part). The product, however, had a disappointingly low solubility in water, barely reaching 1 mM. This was enough to measure an NMR spectrum, but we inferred that this side chain, while compatible with water, does not confer sufficient water solubility to help dissolve sequences that would also contain hydrophobic residues. Nevertheless, crystals of **3** grew, though not from pure water but from an acetonitrile/aqueous ammonium sulfate mixture. The design that led to propose a branched di-hydroxyl side chain by analogy with the isobutyl group thus proved to be valid. The structure could be solved and is shown in Figure 4c.

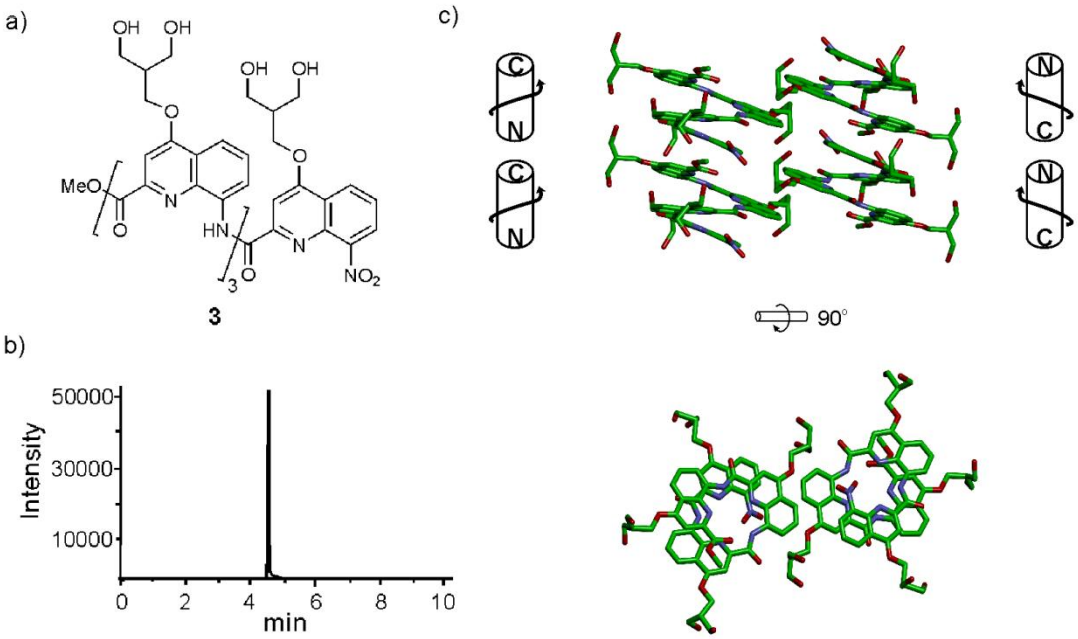

Figure 4. Formula a), RP-HPLC chromatogram b) and crystal structure c) of **3**. Carbon, nitrogen and oxygen atoms are shown in green, blue and red, respectively. Hydrogen atoms have been omitted for clarity. C- and N-termini and helix handedness are indicated in cartoons

Crystal structure of oligomer **3** showed that it is centrosymmetric and thus contains both right-handed (P) and left-handed (M) helices. Helices of each handedness pile-up in head-to-tail infinite stacks. Side chains are projected away from the helices. Inter-helix hydrogen bonds occur directly. Some inter-helix contacts also appear to be mediated by hydrophobic patches of the main chain and side chains (Figure 4c bottom, and Figure 5).

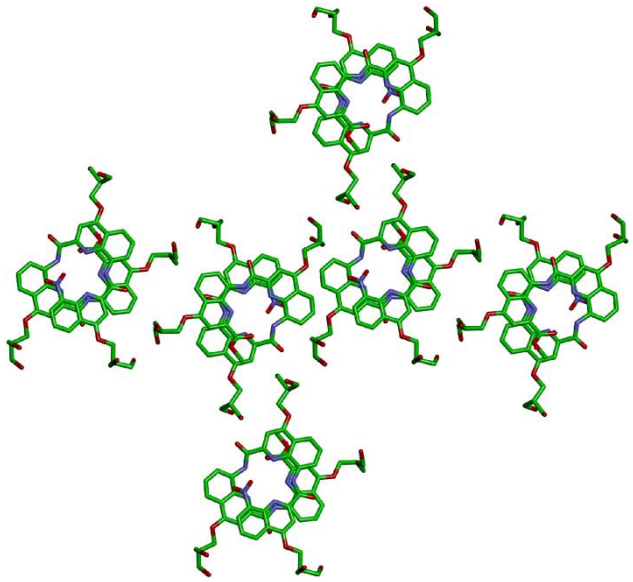

Figure 5. Crystal packing of tetraamide **3**.

Several of the features of the structure of **3** were found to be recurrent in other crystals: the centro-symmetrical nature of the lattice which is common in racemic foldamer helices;[10a,29] and the tendency of the helices to form cylindrical stacks that hide the hydrophobic aromatic cross-sections[30] For oligomers **4-6** (Figure 6), crystals grew easily. Disappointingly, none of the datasets recorded for crystals of cationic octaamide **4** could be solved, even though crystal growth was the fastest for this sequence (3 days) and two differently shaped crystals were obtained (Figure 3c-d). Resolution (at best 1.48 Å) remained too low to solve the structure using ab initio methods and molecular replacement was never successful in our hands despite the availability of high quality models. The diffraction frames (Figure 7) with intense diffraction near 3.5 Å and unit cell dimension unambiguously indicated the presence of the oligoamide in the lattice. We considered this to be sufficient evidence to validate our design approach, and therefore we did not proceed further with efforts to solve the structure of this particular sequence.

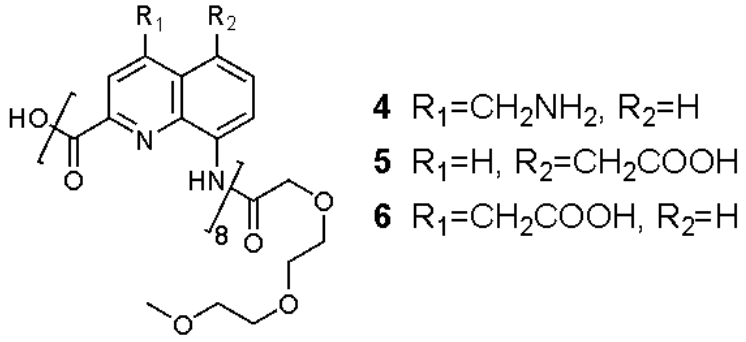

Figure 6. Formulae of octamers **4-6**.

29. a) G. Lautrette, B. Kauffmann, Y. Ferrand, C. Aube, N. Chandramouli, D. Dubreuil, and I. Huc, *Angew. Chem., Int. Ed.*, **2013**, 52, 11517; b) S. Shin, M. Lee, I. A. Guzei, Y. K. Kang, and S. H. Choi, *J. Am. Chem. Soc.*, **2016**, 138, 13390; c) M. Lee, J. Shim, P. Kang, I. A. Guzei, and S. H. Choi, *Angew. Chem., Int. Ed.*, **2013**, 52, 12564; d) J.-H. Eom, R. Jeong, J. Gong, R. W. Driver, and H.-S. Lee, *Bull. Korean Chem. Soc.*, **2015**, 36, 2583; e) D. E. Mortenson, J. D. Steinkruger, D. F. Kreitler, D. V. Perroni, G. P. Sorenson, L. Huang, R. Mittal, H. G. Yun, B. R. Travis, M. K. Mahanthappa, K. T. Forest ,and S. H. Gellman, *Proc. Natl. Acad. Sci.*, **2015**, 112, 13147.
30. See also: H. Zhao, W. Q. Ong, F. Zhou, X. Fang, X. Chen, S. F. Y. Li, H. Su, N.-J. Cho, and H. Zeng, *Chem. Sci.*, **2012**, 3, 2042.

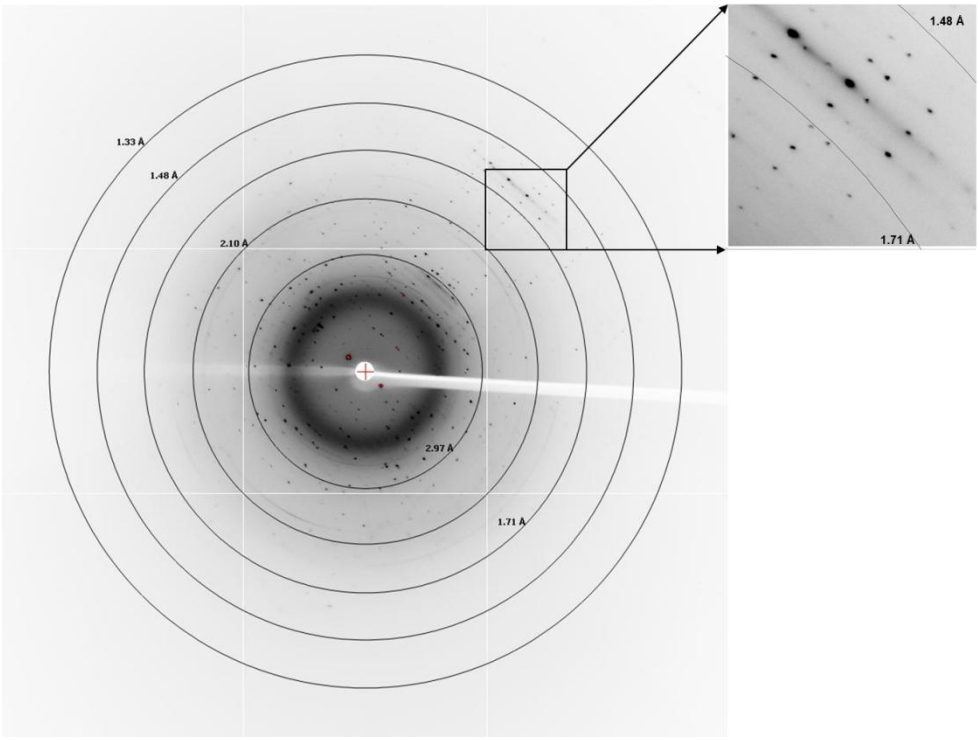

Figure 7. Diffraction pattern of octamer **4**.

Single crystals of octamer **5** suitable for X-ray crystallographic analysis were obtained from a $Ca(OAc)_2$ solution. This time, the arrangement of the helices within the cylindrical stacks were head-to-head, thus creating two distinct interfaces: N-terminus to N-terminus, and C-terminus to C-terminus (Figure 8). This arrangement is held together by calcium bridges involving side chains carboxylates of different helices and a main chain C-terminal carboxylate. In fact, calcium chelates almost all carboxylate functions in the structure, bridging the side chains to other helices or to amide carbonyl groups of the same helix.

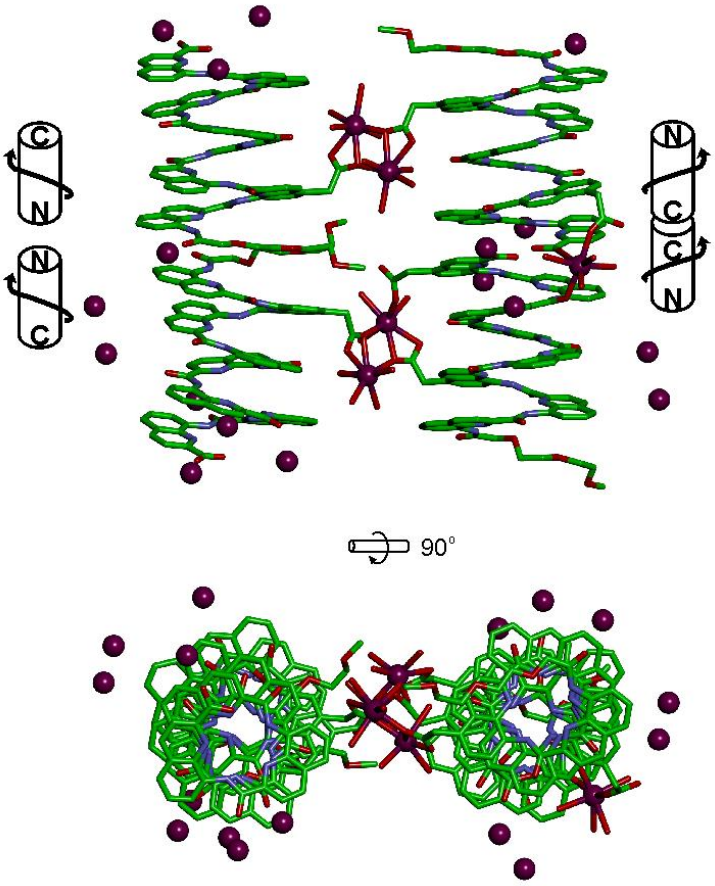

Figure 8. Crystal structures of octamer **5**. Some side chains have been omitted for clarity. Carbon, nitrogen, and oxygen atoms are shown in green, blue, and red, respectively. Calcium is shown as purple balls. Hydrogen atoms have been omitted for clarity. C- and N-termini and helix handedness are indicated in cartoons.

X-ray quality crystals of octamer **6** were obtained under conditions different from those that yielded crystals of octamer **5**, despite the related nature of their side chains (Table 1). This structure was resolved as shown in Figure 9. In the absence of calcium bridges, hydrogen bonds between helices seems to be a prevalent interaction in the crystal lattice, including at the C-terminus/C-terminus aromatic interface within the stacks where hydrogen bonds form between carboxylic acid and quinoline functions (Figure 9b). Other differences between the structures of **5** and **6** include the packing of the helices, which is pseudo-hexagonal in the structure of **6** (Figure 9c), whereas it is square for **5**.

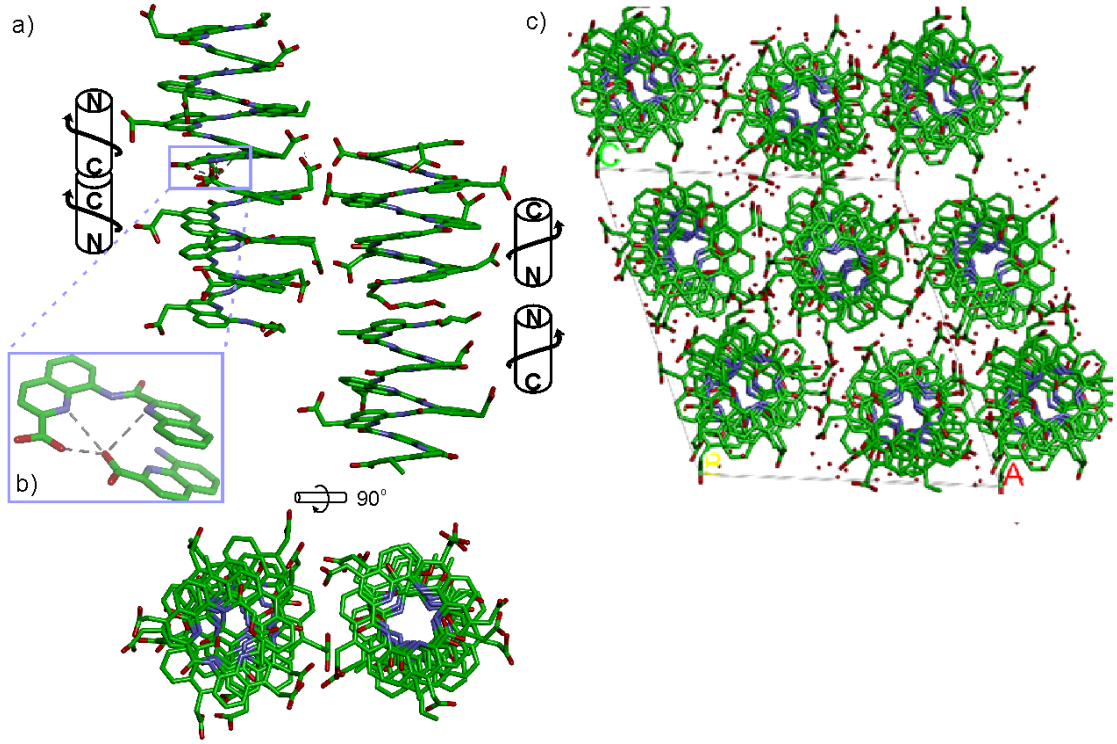

Figure 9. a) Crystal structures of octamer **6**. b) Hydrogen bonds (dashed grey lines) connect two stacked helices of octamer **6** at their C-termini. c) Crystal packing. Carbon, nitrogen, and oxygen atoms are shown in green, blue, and red, respectively. Hydrogen atoms have been omitted for clarity. C- and N-termini and helix handedness are indicated in cartoons.

In the sulfonic acid series, octaamides **1** and **2** bearing eight and four sulfonic acid groups, respectively, were synthesized from monomer **14** and Fmoc-$\mathbf{Q^{OMe}}$-OH. Octamer **1** was synthesized first and, quite disappointingly, did not yield any crystal. Instead, crystals of additives (e.g. salts) recurrently grew from the hanging drops. This observation hinted at a possible high solubility of octamer **1** which we endeavoured to rigorously assess (see Experimental part). Remarkably, solubility in basic and neutral aqueous solutions was so high that we failed to reach saturation with the limited amount of material available. We then measured a maximum solubility of **1** of 108 mM in 0.1 M aqueous HCl. The absence of crystals of **1** was thus not due to direct detrimental effects of sulfonic acid residues but due to enhanced solubility. Oligomer **2** was thus designed in which four sulfonic acid side chains have been replaced by four hydrophobic side chains (-OMe). Oligomer 2 was still well soluble in water, but it eventually crystallized from a $CaCl_2$ aqueous solution after three weeks. Its crystal structure could be solved as shown in Figures 10 and 11. Packing somewhat

resembles the structure of octamer **6** (head-to-head stacks of helices having the same handedness in a pseudo-hexagonal arrangement). Inter-helix interactions are mediated by: (i) aromatic stacking between helix cross-sections; (ii) some hydrophobic contacts between methoxy groups which form a linear array in the crystal lattice (Figures 10b); (iii) intermolecular calcium ions and water mediated bridges between sulfonic acids and main chain amide carbonyl groups (Figure 10b-c).

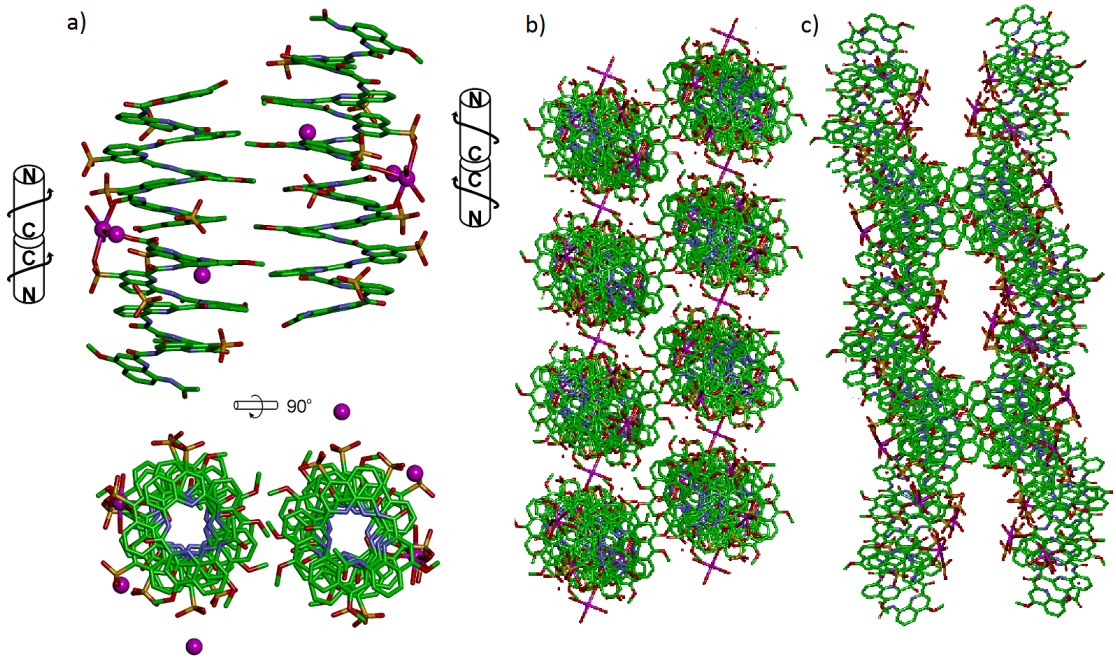

Figure 10. a) Crystal structure of octamer **2**. b) - c) Different views of packing. Carbon, nitrogen, oxygen and sulphur atoms are shown in green, blue, and red, respectively. Calcium is shown as purple balls. Hydrogen atoms have been omitted for clarity. C- and N-termini and helix handedness are indicated in cartoons.

A remarkable aspect of the structure of octamer **2** was its curvature. Oligoamides of 8-amino-2-quinolinecarboxylic acids normally form helices comprised of almost exactly five units per two turns (Figure 11b). This is recurrently observed in crystals grown from organic solvents[5b] and has also been shown in solution.[13] The solid state structures of water soluble oligomers **3**, **5** and **6** described above make no exception. In contrast, the structure of oligomer **2** deviates from this pattern and possesses a slightly larger curvature – i.e. fewer units per turn – revealing a certain degree of flexibility of these helices (Figure 11c-d). It is not clear whether this is the result of the packing interactions mentioned above or a direct outcome of intramolecular

interactions between side chains and the main chain (a related effect was observed upon introduction bromine substituents in position 5[11]).

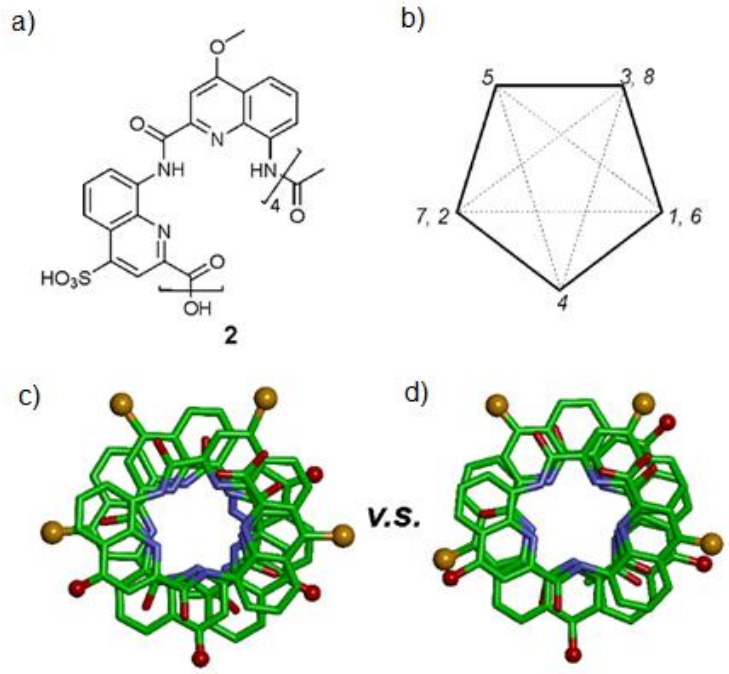

Figure 11. a) Formula of octamer **2**. b) Five-pointed star showing the usual positions of side chains in quinoline-based helices counting monomers from 1 to 8. Top views of the crystal structure of c) octamer **2**, and of d) octamer **6** in which carboxylic acid side chains have been replaced by the side chains of octamer **2**. All side chains are shown as golden (sulfonic acid) or red balls (methoxy).

4. Conclusion and perspectives

In summary, synthetic protocols have been developed to prepare quinoline monomers bearing new short polar – neutral, anionic or cationic – side chains on multigram scales. Side chain protections (or their absence) were made to be compatible with SPS. One tetrameric and five octameric oligoamides displaying these side chains were synthesized and shown to be soluble in water. In all cases but one, crystals were obtained using the hanging drop method, thus validating the initial design principle to combine polarity and rigidity. The only case that resisted crystallization appeared to be due to exceedingly high water solubility endowed by eight sulfonic acid functions. The neutral side chain did provide crystal growth ability from water but contributed poorly to solubility. The difference in crystal growth ability of oligomers **5** and **6** on one hand, and oligomers of $\mathbf{Q}^{\mathbf{Asp}}$ (Figure 1) on the other hand, is striking considering that the side chains of the latter are just one atom longer than those of the former.

The results presented here in the case of helical aromatic amide foldamers may certainly be extrapolated to other aromatic molecular and supramolecular systems. Extrapolation to other short and rigid polar functionalities may also be considered. These developments will be particularly useful to elucidate structures in projects where remarkable properties of foldamers have been observed in aqueous media, including endomolecular recognition and double helix formation.[31] In the future researches, water-soluble aromatic β-sheets would be constructed and solid state structural elucidation of these foldamers can be envisioned by employing these short side chains. Towards protein quaternary structure mimics, water-soluble helix bundles would be constructed through self-assembly of aromatic foldamers in water. With these short side chains armed, the most challenging steps (crystallization and structural elucidation) on the way of approaching helix bundles would be facilitated. The progress of this topic will be shown in chapter four in detail.

31. a) N. Chandramouli, M. F. El-Behairy, G. Lautrette, Y. Ferrand, and I. Huc, *Org. Biomol. Chem.*, **2016**, 14, 2466; b) J. Shang, Q. Gan, S. J. Dawson, F. Rosu, H. Jiang, Y. Ferrand, and I. Huc, *Org. Lett.*, **2014**, 16, 4992.

5. Experimental part

5.1 Methods for X-ray crystallography

5.1.1 Crystallization and X-ray diffraction measurements

For crystallization, lyophilized powders of foldamers **2-6** were dissolved using ultrapure water (for **3**, in water/acetonitrile 3:1) such that the foldamer solutions had a final concentration of 2 mM. Crystallization experiments were performed at 293K using standard aqueous hanging-drop vapor diffusion in 24-well Linbro-style plates. Screening of crystallization conditions was carried out using commercial sparse matrix screen JBScreen Basic 1 to 4, from Jena Biosciences.[32] The aqueous drops composed of 0.75 to 1.0 µL of the foldamer solution and an equal volume of the crystallization reagent. For low temperature diffraction measurements, the crystals were mounted on cryo-loops after quick soaking on Paratone-N oil and flash-frozen. Diffraction measurements were carried out at Proxima-1 beamline (Synchrotron SOLEIL, Paris) using a DECTRIS PILATUS 6M pixel-array detector; at ID29 and BM30A beamlines (ESRF, Grenoble) using ADSC Q315r CCD detector and at IECB x-ray facility (UMS3033) using a micro-focus rotating anode (2.9 kW) Rigaku FRX diffractometer, with Cu Kα radiation and a PILATUS 200K hybrid pixel detector. Diffraction data were processed and scaled using the packages *CrystalClear-SM 1.36*, *XDS* and *CrysAlisPro*.[33]

5.1.2 Structure determination and refinement

All structures were solved by direct method using the charge-flipping program *Superflip*.[34] The phase set calculated allowed identifying most of Foldamers

32. a) J. Jancarik, S.-H. Kim, *J. Appl. Cryst.*, **1991**, 24, 409; b) R. Cudney, S. Patel, K. Weisgraber, Y. Newhouse, A. McPherson, *Acta Crystallogr., Sect. D*, **1994**, 50, 414.
33. a) Rigaku, **2011**, *CrystalClear-SM Expert* and *CrystalStructure*. Rigaku Corporation, Tokyo, Japan; b) W. Kabsch, *Acta Crystallogr., Sect. D*, **2010**, 66, 125; c) Agilent, **2014**, *CrysAlisPRO*. Agilent Technologies Ltd, Yarnton, Oxfordshire, England.
34. L. Palatinus, G. Chapuis, *J. Appl. Cryst.*, **2007**, 40, 786.

(including the N-terminal tails for oligomers **5** and **6**). The structures were refined by full-matrix least-squares method on F^2 with *SHELXL-2014*[35] within the *Olex2* suite.[36] Non-hydrogen atoms for main chains were refined with anisotropic displacement parameters. In case of side chains and solvent molecules, the non-hydrogen atoms were refined with anisotropic or isotropic displacement parameters. Hydrogen atoms were included for the Foldamers in idealized positions using HFIX and refined with a riding model. For solvent molecules, positions of hydrogen atom were not determined. After several attempts to model the disordered water molecules, the PLATON/SQUEEZE[37] procedure was implemented for all structures. DFIX, DELU, SIMU, ISOR, RIGU, AFIX 116, EADP instructions were used to model displacement parameters and the geometry of molecules. The FVAR function was used during refinement of occupancy factors of disordered parts.

The final cif files were checked using IUCR's *checkcif* algorithm. Due to the characteristics of the crystals mentioned above (large volume fractions of disordered solvent molecules and side chains, weak diffraction intensity, incompleteness of data and moderate resolution) a number of A-level and B-level alerts remain in the check cif files. These alerts are explicitly listed below and have been divided into two groups. They are inherent to the data and refinement procedure. They illustrate the limited practicality of the *checkcif* tool for medium sized molecule crystallography. The first group illustrates the weak quality of the data and refinement statistics if compared to that expected for small molecule structures from highly diffracting crystals. The second group is connected with decisions made during refinement and explained below.

Group 1 alerts in crystal structures of **2**, **3**, **5** and **6**:
RFACR01_ALERT_3_A The value of the weighted R factor is > 0.45
THETM01_ALERT_3_A The value of sine(theta_max)/wavelength is less than 0.550
PLAT029_ALERT_3_A _diffrn_measured_fraction_theta_full value Low
PLAT084_ALERT_3_B High wR2 Value (i.e. > 0.25)
PLAT234_ALERT_4_A Large Hirshfeld Difference
PLAT934_ALERT_3_B Number of (Iobs - Icalc)/SigmaW > 10

35. G. M. Sheldrick. *Acta Crystallogr., Sect. C*, **2015**, 71, 3.
36. O. V. Dolomanov, L. J. Bourhis, R. J. Gildea, J. A. K. Howard, and H. Puschmann, *J. Appl. Cryst.*, **2009**, 42, 339
37. A. L. Spek, *Acta Crystallogr., Sect. D*, **2009**, 65, 148.

REFNR01_ALERT_3_B Ratio of reflections to parameters is < 8 for a centrosymmetric structure
PLAT088_ALERT_3_B Poor Data / Parameter Ratio
PLAT341_ALERT_3_B Low Bond Precision on C - C Bonds
PLAT911_ALERT_3_B Missing # FCF Refl Between THmin & STh/L= 0.526

Group 2 alerts for crystal structure **2**:
PLAT306_ALERT_2_B Isolated Oxygen Atom (H - atoms Missing ?)
This alert concerns position of hydrogen atoms not calculated for solvent molecules
PLAT430_ALERT_2_B Short Inter D...A Contact
This alert concerns disordered solvent molecules.

Group 2 alerts for crystal structure **3**:
PLAT245_ALERT_2_A U(iso) H35 Smaller than U(eq) C35 by ... 0.150 AngSq
PLAT312_ALERT_2_A Strange C-O-H Geometry (C-O < 1.25 Ang) .... O2BA Check
PLAT241_ALERT_2_B High 'MainMol' Ueq as Compared to Neighbors of C01U Check
These alerts concern disorder in diol side chains.
PLAT097_ALERT_2_B Large Reported Max. (Positive) Residual Density 1.49 eA-3
This concerns a residual peak in **3** corresponding to symmetry related, partially occupied side chain.

Group 2 alerts for crystal structure **5**:
PLAT201_ALERT_2_B Isotropic non-H Atoms in Main Residue(s) ..... 2 Report
This alert concerns high thermal motion in few side chains or N-terminal tail.
PLAT213_ALERT_2_B Atom N67C has ADP max/min Ratio ..... 4.2 oblate
PLAT213_ALERT_2_B Atom C18C has ADP max/min Ratio ..... 4.6 prolat
PLAT213_ALERT_2_B Atom C26G has ADP max/min Ratio ..... 4.3 prolat
PLAT213_ALERT_2_B Atom C36C has ADP max/min Ratio ..... 4.2 oblate
This alert concerns main chain atoms that were not ideally shaped, however with correct atom type assignment.
PLAT220_ALERT_2_B Non-Solvent Resd 1 C Ueq(max)/Ueq(min) Range 9.4 Ratio
PLAT220_ALERT_2_B Non-Solvent Resd 1 O Ueq(max)/Ueq(min) Range 8.9 Ratio
PLAT241_ALERT_2_B High 'MainMol' Ueq as Compared to Neighbors of O8D Check
PLAT241_ALERT_2_B High 'MainMol' Ueq as Compared to Neighbors of O24H Check
PLAT242_ALERT_2_B Low 'MainMol' Ueq as Compared to Neighbors of Ca02 Check
PLAT242_ALERT_2_B Low 'MainMol' Ueq as Compared to Neighbors of O2E Check
PLAT242_ALERT_2_B Low 'MainMol' Ueq as Compared to Neighbors of C14H Check
PLAT242_ALERT_2_B Low 'MainMol' Ueq as Compared to Neighbors of C22H Check
PLAT242_ALERT_2_B Low 'MainMol' Ueq as Compared to Neighbors of C26D Check
PLAT242_ALERT_2_B Low 'MainMol' Ueq as Compared to Neighbors of C26H Check
These alerts concern thermal motions in side chain or bound Ca^{2+} ions.
PLAT306_ALERT_2_B Isolated Oxygen Atom (H-atoms Missing ?)
This alert concerns position of hydrogen atoms not calculated for solvent molecules
PLAT430_ALERT_2_B Short Inter D...A Contact
This alert concerns disordered solvent molecules.
Group 2 alerts for crystal structure **6**:
PLAT430_ALERT_2_A Short Inter D...A Contact O1 .. O55 .. 2.48 Ang.
PLAT430_ALERT_2_A Short Inter D...A Contact O2 .. O9A .. 2.47 Ang.
PLAT430_ALERT_2_A Short Inter D...A Contact O0AA .. O8BA .. 2.32 Ang.
PLAT430_ALERT_2_A Short Inter D...A Contact O11 .. O9AA .. 2.43 Ang.
PLAT430_ALERT_2_A Short Inter D...A Contact O1DA .. O24 .. 2.41 Ang
This alert concerns disordered solvent molecules.
PLAT201_ALERT_2_B Isotropic non - H Atoms in Main Residue(s)
This alert concerns high thermal motion of side chains or N-terminal tail
PLAT097_ALERT_2_B Large Reported Max. (Positive) Residual Density 1.27 eA-3
This alert concerns a peak that was observed to have short contact with the side chain.
PLAT241_ALERT_2_B High 'MainMol' Ueq as Compared to Neighbors of C7F Check
PLAT242_ALERT_2_B Low 'MainMol' Ueq as Compared to Neighbors of C10H Check
PLAT242_ALERT_2_B Low 'MainMol' Ueq as Compared to Neighbors of C4E Check
PLAT242_ALERT_2_B Low 'MainMol' Ueq as Compared to Neighbors of C11 Check

PLAT242_ALERT_2_B Low 'MainMol' Ueq as Compared to Neighbors of C279 Check
PLAT242_ALERT_2_B Low 'MainMol' Ueq as Compared to Neighbors of C16F Check
PLAT242_ALERT_2_B Low 'MainMol' Ueq as Compared to Neighbors of C82 Check
PLAT242_ALERT_2_B Low 'MainMol' Ueq as Compared to Neighbors of C4K Check
This alert concerns high thermal motion of side chains or N-terminal tail
PLAT306_ALERT_2_B Isolated Oxygen Atom (H-atoms Missing ?)
This alert concerns position of hydrogen atoms not calculated for solvent molecules

Refinement statistics are given in Table 2. Atomic coordinates and structure factors for the crystal structures of **2**, **3**, **5** and **6** have been deposited in the Cambridge Crystallographic Data Centre (CCDC) with accession codes 1521878, 1525865, 1525770 and 1523119 respectively. These data are available free of charge upon request (www.ccdc.cam.ac.uk/).

Table 2: Crystallographic data for the water soluble oligomers.*

Foldamers	2	3	5	6
Formula	$C_{172}H_{112}Ca_2N_{32}O_{11}{}_1S_8$	$C_{56}H_{53..25}N_8O_{17.25}$	$C_{205.5}H_{135.5}Ca_{6.25}N_3{}_2O_{82.50}$	$C_{397}H_{230}N_{64}O_{135}$
M	4539.58	1098.32	4623.43	8056.44
Crystal system	Monoclinic	Triclinic	Orthorhombic	Monoclinic
Z	8	2	8	4
Space group	*C*2/*c*	*P*-1	*Pbca*	$P2_1/n$
a/Å	34.1155 (11)	7.4720 (15)	34.859 (7)	28.255 (4)
b/Å	45.9981 (11)	20.571 (4)	29.286 (6)	51.842 (7)
c/Å	33.3135 (14)	24.604 (5)	51.432 (10)	30.331 (4)
α/°	90	69.40 (3)	90	90
β/°	109.407 (4)	84.50 (3)	90	110.957 (2)
γ/°	90	85.66 (3)	90	90
V/Å^3	49307 (3)	3520.0 (14)	52506 (18)	41490 (10)
T/K	130	100	100	100
ρ/g cm^{-3}	1.277	1.059	1.304	1.290
Color and shape	Yellow rhombohedra	Yellow needles	Yellow orthorhombic	Yellow needles
Size (mm)	0.10 x 0.04 x 0.04	0.50 x 0.01 x 0.01	0.15 x 0.05 x 0.03	0.20 x 0.03 x 0.03
λ/Å	1.54178	0.77492	0.8856	1.54178
μ/mm^{-1}	1.901	0.096	0.383	0.848
Collected reflections	19582	7913	27211	51893

unique data [*Fo>2 σFo*)]	10778	5206	25357	23207
R_{int} %	0.0813	0.0601	0.0389	0.0726
Parameters/restraints	2558/551	728/166	2720/219	4313/3954
R_1, wR_2 ($I > 2\sigma(I)$)	0.1324/0.4119	0.1300/0.4082	0.1568/0.5118	0.1773/0.5229
Goodness of fit	1.480	1.643	2.893	1.688
Total potential solvent accessible void volume from SQUEEZE Å^3	7194.4	1027.5	12657.7	5626
Electron count/cell	2147	311	4648	1526
CCDC number	1521878	1525865	1525770	1523119

* Space group and unit cell for oligomer **4**: $P2_1/n$; a = 19.3860 Å, b = 51.1220 Å, c = 30.5320 Å, α = 90 °, β = 92.318 °and γ = 90 °

5.2 Solubility study

5.2.1 Determination of concentration via NMR

Octamer **1** (2.57 mg) was dissolved in DMSO-d_6 (500 uL) containing 2.0 mM pyridine (figure 12a), to which was added pyridine again to reach 4.0 mM (figure 12b). The concentration of **1** could then be ascertained (2.4 mM) by comparing integral difference of pyridine signals and nearby foldamer signal.

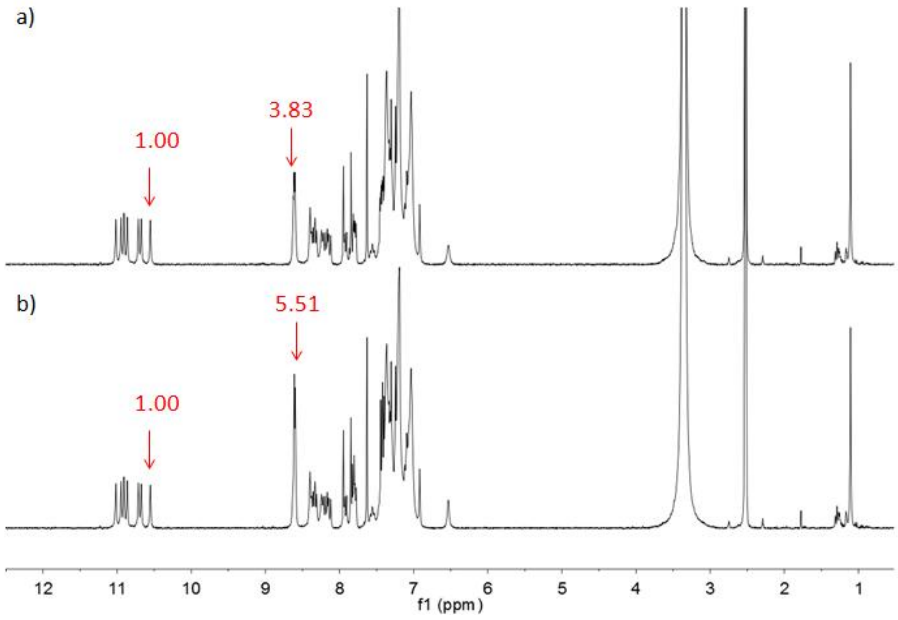

Figure 12: Expansion of ^{1}H NMR spectra of octamer **1** in DMSO-d_6 containing a) 2.0 mM or b) 4.0 mM pyridine. Integrals used are marked (pyridine 2 x CHAr δ: 8.6 ppm). The integral of one foldamer signal was always set to 1.00 as the reference.

5.2.2 Generation of UV calibration curve

The above NMR sample of octamer **1** was then serially diluted with MilliQ-water (containing 0.1 M HCl) and UV absorbance at 370 nm was recorded using a 1 cm path length cuvette. With these data, a calibration curve (Figure 13) was generated. Then, according to the formula Abs = ε·c·l, the extinction coefficient (ε) of **1** at 370 nm was obtained as 20959 L mol^{-1} cm^{-1}.

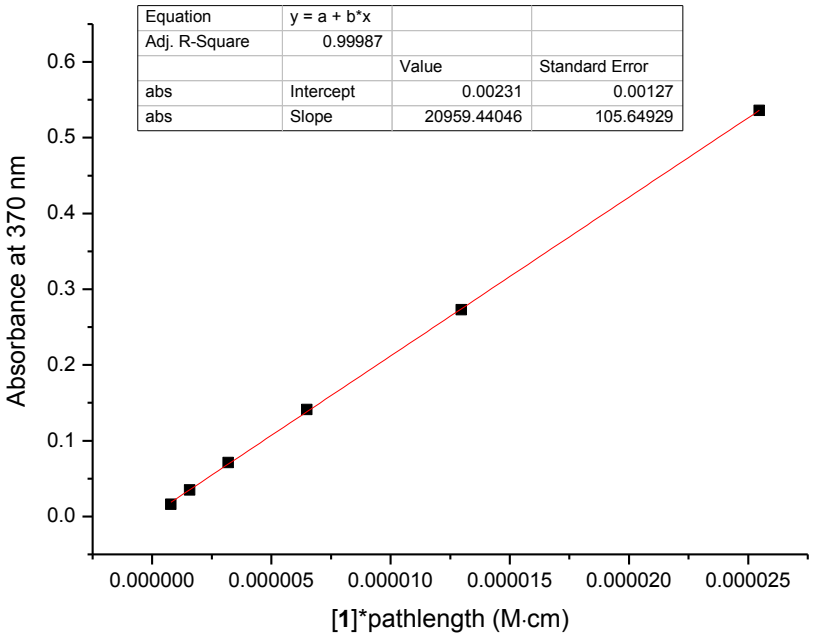

Figure 13: UV absorbance calibration curve affording the extinction coefficient (ε) of octamer **1** at 370 nm as 20959 L mol^{-1} cm^{-1}

5.2.3 Calculation of solubility

A saturated solution of octamer **1** was produced by adding excess solid material (10.4 mg) to MilliQ-water (30 µL, containing 0.1 M HCl) at 20 ℃. The homogeneous suspension was then centrifuged at 6000 rpm for 5 minutes to afford a clear supernatant at the top. An accurately measured volume (2.0 µL) of the supernatant was then removed and diluted to a concentration appropriate for UV absorbance measurement. According to the formula Abs = ε·c·l, the concentration ([**1**] measured,

see table 3) of measured solution could be extrapolated. Thereby, with the known dilution factor, original concentration of saturated solution could also be deduced (experiment was repeated twice, see table 3).

Table 3: Determination of solubility

Experiment	Abs	Volume (μL) [a]	[**1**] measured (mM)	Solubility (mM) [b]
1	0.530	0.24	0.0253	105
2	0.553	0.24	0.0264	110
3	0.543	0.24	0.0259	108
Average	-	-	-	108

[a] Refer to the net (after calculation) volume of original saturated solution. [b] Equal to the concentration of the original saturated solution of octamer **1**.

5.3 Synthetic method

5.3.1 Solid phase synthesis

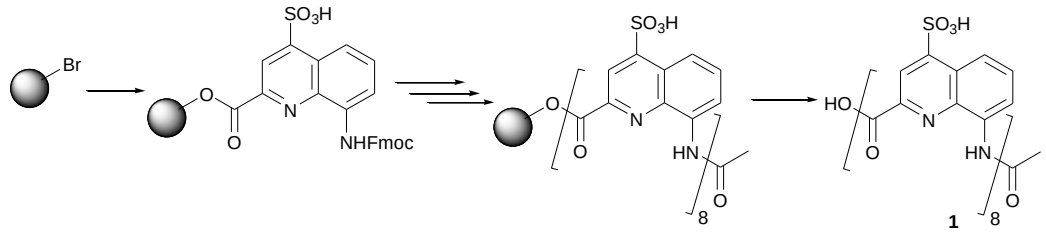

Scheme 6. Solid Phase Synthesis of oligomer **1**.

Oligomer 1: Oligomer **1** was synthesized using the SPS procedures (note: anhydrous THF was used instead of anhydrous DCM during acid chloride activation because of solubility issues) previously reported[18a] on a 41 μmol scale (100 mg of Wang resin, manufacturer's loading 0.41 $mmolg^{-1}$). The crude product was purified by semi-preparative RP-HPLC (0-10% D, over 15 min) to afford the title compound as a yellow solid (14 mg, 17%, purity by RP-HPLC: > 99%). RP-HPLC (0-10% D, over 10 min) R_t =3.8 min. ^{1}H NMR (300 MHz, 10%D_2O/H_2O *v/v* %): δ 11.47 (s, 1H),

11.32 (s, 1H), 11.26 (s, 1H), 11.22 (s, 1H), 10.86 (s, 1H), 10.76 (s, 1H), 10.65 (s, 1H), 9.13 (s, 1H), 8.56 (m, 2H), 8.38-7.38 (m, 28H), 7.22 (d, *J* = 7.5 Hz, 1H), 7.10 (s, 1H), 1.30 (s, 3H). HRMS: calcd. for $C_{82}H_{50}N_{16}O_{34}S_8$ $[M - 2H]^{2-}$ 1029.0226; found 1029.0239.

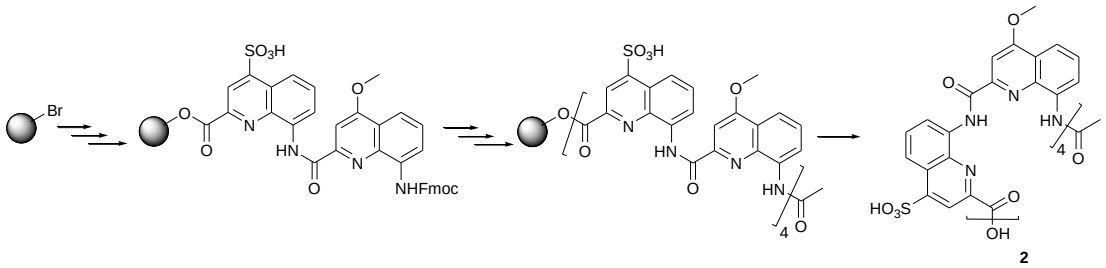

Scheme 7. Solid Phase Synthesis of oligomer **2**.

Oligomer 2: Oligomer **2** was synthesized using the SPS procedures (note: anhydrous THF was used instead of anhydrous DCM during acid chloride activation because of solubility issues) previously reported [18a] on a 10.25 μmol scale (25 mg of Wang resin, manufacturer's loading 0.41 $mmolg^{-1}$). The crude product was purified by semi-preparative RP-HPLC (15-25% D, over 15 min) to afford the title compound as a yellow solid (5 mg, 26%, purity by RP-HPLC: 98%). RP-HPLC (15-25% D, over 10 min) R_t =10.0 min. ^{1}H NMR (300 MHz, DMSO-d_6): δ 11.09 (m, 3H), 10.93 (s, 1H), 10.74 (m, 3H), 8.57 (d, *J* = 8.1 Hz, 1H), 8.34 (m, 4H), 8.03-7.29 (m, 21H), 7.08 (m, 3H), 6.76 (s, 1H), 6.55 (s, 1H), 6.19 (s, 1H), 5.87 (s, 1H), 4.08 (s, 3H), 4.07 (s, 3H), 3.92 (s, 3H), 3.85 (s, 3H), 1.12 (s, 3H). HRMS: calcd. for $C_{86}H_{61}N_{16}O_{26}S_4$ $[M + H]^+$ 1861.2820; found 1861.2889.

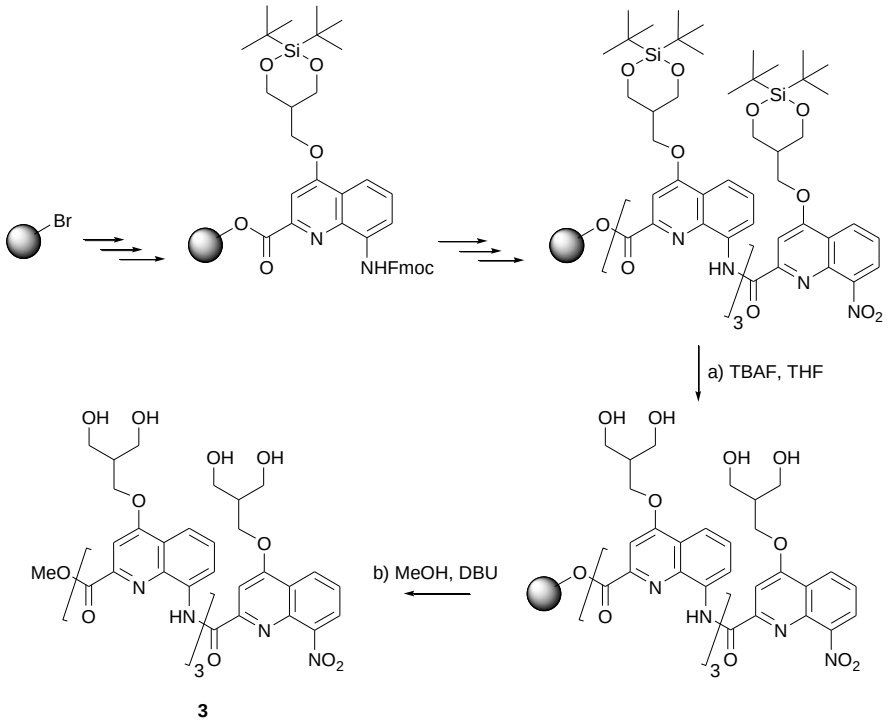

3

Scheme 8. Solution Phase Synthesis of oligomer **3**.

Oligomer 3: Oligomer **3** was synthesized using the SPS procedures (except **steps a** and **b** which are described below) previously reported [18a] on a 10.25 μmol scale (25 mg of Wang resin, manufacturer's loading 0.41 $mmolg^{-1}$). The crude product was purified by semi-preparative RP-HPLC (0-70% B, over 10 min) to afford the title compound as a yellow solid (3.6 mg, 30%, purity by RP-HPLC: > 99%). RP-HPLC (0-70% B, over 10 min, 3 mL/min flow rate) R_t =4.6 min. ^{1}H NMR (300 MHz, DMSO-d_6): δ 12.04 (s, 1H), 11.72 (s, 1H), 11.42 (s, 1H), 9.08 (m, 1H), 8.59 (m, 1H), 8.39 (m, 1H), 8.07-7.52 (m, 10H), 7.37 (s, 1H), 6.90 (s, 1H), 6.69 (s, 1H), 4.74-4.18 (m, 7H), 3.75-2.95 (m, overlapped with water peak), 2.70-2.26 (m, overlapped with DMSO peak). HRMS: calcd. for $C_{57}H_{59}N_8O_{19}$ $[M + H]^+$ 1159.3891; found 1159.3899.

On-resin (di-*tert*-butyl) silyl deprotection (step a): The resin bound quinoline tetramer (started from 25 mg of Wang resin, manufacturer's loading 0.41 $mmolg^{-1}$, 10.25 μmol, 1 equiv) was suspended in 0.9 mL anhydrous THF and a 1 M solution of TBAF in THF (164 μL, 0.164 mmol, 16 equiv) was added. It was then treated with microwaves (50 W, ramp to 50 ℃ over 5 min, then hold at 60 ℃ for 15 min). The resin was washed briefly with anhydrous THF, and the process repeated once. The

resin was then washed thoroughly with DMF and stirred for 2 min at room temperature in DMF. Then washed with DMF, DCM, DCM/MeOH (50/50%, *v/v*%), and MeOH/H_2O (50/50%, *v/v*%) in that order for three cycles.

On-resin methylation (step b): The above resin-bound foldamer was washed with anhydrous THF and transferred to a pressure-resistant glass tube. To the resin were then added 2 mL of anhydrous THF, 2 mL of MeOH and 0.1 mL of 1,8-Diazabicyclo[5.4.0]undec-7-ene (DBU). The mixture was stirred in the sealed pressure-resistant glass tube for 2 h at 80 ^{o}C. The resin was then removed by filtration and the filtrate was concentrated under the reduced pressure. The resulting oily solid was precipitated with Et_2O, triturated, filtered and washed with Et_2O, at last, dried under high vacuum to yield 9 mg of crude product as a yellow solid. This crude product was further purified by semi-preparative RP-HPLC.

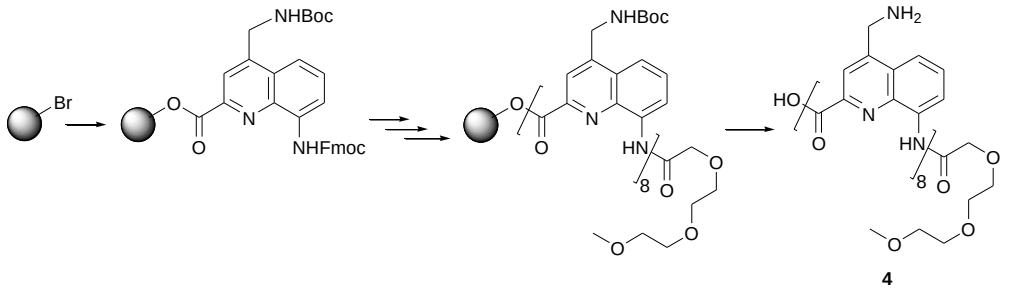

Scheme 9. Solid Phase Synthesis of oligomer **4**.

Oligomer 4: Oligomer **4** was synthesized using the SPS procedures previously reported [18a] on a 10.25 μmol scale (25 mg of Wang resin, manufacturer's loading 0.41 mmolg^{-1}). The crude product was purified by semi-preparative RP-HPLC (5-15% B, over 15 min) to afford the title compound as a yellow solid (7.9 mg, 44%, purity by RP-HPLC: 99%). RP-HPLC (5-15% B, over 10 min) R_t =11.1 min. ^{1}H NMR (300 MHz, DMSO-d_6): δ 11.26 (s, 1H), 11.24 (s, 1H), 11.18 (s, 1H), 11.07 (s, 1H), 11.00 (s, 1H), 10.93 (s, 1H), 10.83 (s, 1H), 9.51 (s, 1H), 8.91-7.88 (m, 22H, containing signals of protonated -NH_2 residues), 7.90-7.06 (m, 33H, containing signals of protonated –NH_2), 4.87-4.08 (m, 19H), 3.50-3.00 (m, overlapped with water peak), 2.64 (s, 3H), 2.60-2.30 (m, overlapped with DMSO peak). HRMS: calcd. for $C_{95}H_{87}N_{24}O_{13}$ [M +

H]$^+$ 1771.6879; found 1771.6925.

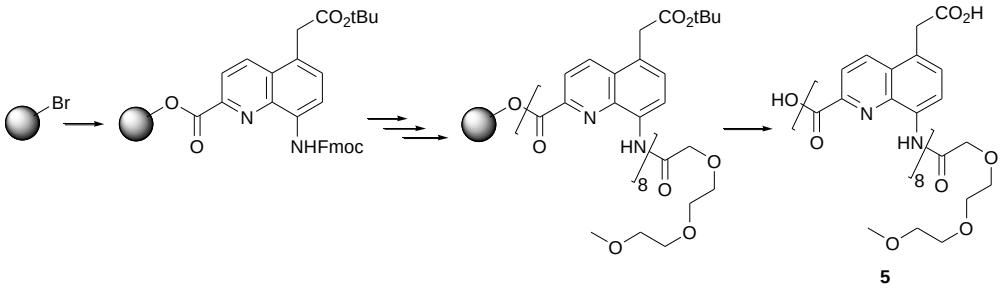

Scheme 10. Solid Phase Synthesis of oligomer **5**.

Oligomer 5: Oligomer **5** was synthesized using the SPS procedures previously reported [18a] on a 10.25 μmol scale (25 mg of Wang resin, manufacturer's loading 0.41 mmolg^{-1}). The crude product was purified by semi-preparative RP-HPLC (0-10% D, over 15 min) to afford the title compound as a yellow solid (6.5 mg, 32%, purity by RP-HPLC: > 99%). RP-HPLC (0-10% D, over 10 min) R_t = 5.0 min. ^{1}H NMR (300 MHz, DMSO-d_6): δ 11.06 (m, 3H), 10.84 (m, 3H), 10.62 (br, 1H), 9.33 (s, 1H), 8.55-6.85 (m, 32H), 4.20-3.10 (m, overlapped with water peak), 2.70 (s, 3H), 2.55 (m, overlapped with DMSO peak), 2.30-1.93 (m, 6H). HRMS: calcd. for $C_{103}H_{80}N_{16}O_{29}$ $[M + 2H]^{2+}$ 1002.7655; found 1002.7680.

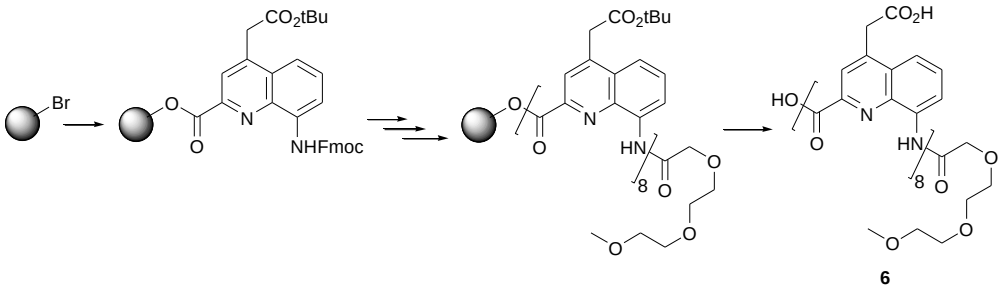

Scheme 11. Solid Phase Synthesis of oligomer **6**.

Oligomer 6: Oligomer **6** was synthesized using the SPS procedures previously reported [18a] on a 10.25 μmol scale (25 mg of Wang resin, manufacturer's loading 0.41 mmolg^{-1}). The crude product was purified by semi-preparative RP-HPLC (0-5% D, over 15 min) to afford the title compound as a yellow solid (9.5 mg, 46%, purity by RP-HPLC: 97%). RP-HPLC (0-5% D, over 10 min) R_t =6.9 min. ^{1}H NMR (300 MHz,

10%D_2O/H_2O *v/v* %): δ 11.41 (s, 1H), 11.40 (s, 1H), 11.25 (s, 1H), 11.19 (s, 1H), 10.77 (s, 1H), 10.65 (s, 1H), 10.59 (s, 1H), 9.70 (s, 1H), 8.08-7.06 (m, 27H), 6.98 (s, 1H), 6.89 (s, 1H), 6.86 (s, 1H), 6.66 (s, 1H), 6.55 (s, 1H),4.30-3.69 (m, overlapped with water), 3.46-3.22 (m, 3H), 2.81 (m, 1H), 2.53 (s, 3H), 2.52-2.11 (m, 5H). HRMS: calcd. for $C_{103}H_{79}N_{16}O_{29}Na$ $[M + H + Na]^{2+}$ 1013.7565; found 1013.7594.

5.3.2 Solution phase synthesis

Compound 7: Methyl 8-aminoquinoline-2-carboxylate (200 mg, 1 mmol, 1 equiv) was dissolved in 10 mL dioxane. Then trimethylsilyl chlorosulfonate (0.23 mL, 1.5 mmol, 1.5 equiv) was added slowly to the solution at room temperature under N_2. The reaction was stirred at 100 ^oC overnight. The resulting mixture was allowed to cool down and DCM added to have a full precipitation. Filtered, washed with DCM and dried to afford the title compound as a grey powder (265 mg, 94%). ^1H NMR (300 MHz, DMSO-d_6): δ 9.22 (d, *J* = 9.0 Hz, 1H), 8.11 (d, *J* = 9.0 Hz, 1H), 7.85 (d, *J* = 8.1 Hz, 1H), 6.93 (d, *J* = 8.1 Hz, 1H), 5.75 (s, DCM), 4.86 (s, H_2O), 3.96 (s, 3H), 3.57 (s, 1,4-dioxane). $^{13}C\{^1H\}$NMR (300 MHz, DMSO-d_6): δ 165.07, 145.56, 138.58, 138.53, 137.55, 137.42, 127.57, 126.16, 121.44, 115.01, 66.40 (1,4-dioxane), 52.80. HRMS: calcd. for $C_{11}H_9N_2O_5S$ $[M - H]^-$ 281.0238; found 281.0236.

Compound 9: Compound **7** (282 mg, 1 mmol, 1 equiv) was dissolved in 20 mL of THF/H_2O (1:1) mixture and stirred at room temperature. NaOH (60 mg, 1.5 mmol, 1.5 equiv) was then added and the mixture stirred for 1 h at room temperature. 1 M HCl was then added to acidify the mixture to approximately pH 4. The resulting mixture was then concentrated to dryness under reduced pressure to afford compound **8** as a brown powder (quantitative) which was used directly in the next step without further purification. Then the above compound **8** was dissolved in 18 mL 10% *w/v* $NaHCO_3$ solution (21 mmol, 21 equiv). To the resulting solution was added a solution of Fmoc-Cl (336 mg, 1.3 mmol, 1.3 equiv) in 10 mL dioxane dropwise over 30 min at 0 ℃. The mixture was then stirred for a further hour at 0 ℃, then at room temperature

overnight. 1 M HCl was added to acidify the mixture to approximately pH 4. The mixture was then washed several times with Et_2O until precipitation occurred. Filtered and washed once with small amount of water and once with DCM. The resulting solid was dried to yield the title compound as a grey powder (315 mg, 64%, purity by RP-HPLC: 98%). RP-HPLC (50-60% B, over 10 min) R_t =5.5 min. ^{1}H NMR (300 MHz, DMSO-d_6): δ 13.61 (br, 1H), 10.48 (s, 1H), 9.38 (d, *J* = 9.0 Hz, 1H), 8.25 (m, 2H), 8.00 (d, *J* = 8.1 Hz, 1H), 7.93 (d, *J* = 7.5 Hz, 2H), 7.90 (d, *J* = 7.2 Hz, 2H), 7.42 (m, 4H), 4.63 (d, *J* = 6.6 Hz, 2H), 4.46 (t, *J* = 6.6 Hz, 1H), 3.33 (s, H_2O). ^{13}C{^{1}H}NMR (300 MHz, DMSO-d_6): δ 165.40, 153.50, 145.04, 143.73, 140.84, 138.23, 137.62, 136.72, 136.39, 127.81, 127.43, 127.26, 125.85, 125.18, 120.50, 120.26, 114.15, 66.54, 46.61. HRMS: calcd. for $C_{25}H_{17}N_2O_7S$ $[M - H]^-$ 489.0762; found 489.0769.

Compound 10: Methyl 4-bromo-8-nitroquinoline-2-carboxylate [15a] (5 g, 16 mmol, 1 equiv) and thiourea (2.4 g, 32 mmol, 2 equiv) were dissolved in 80 mL acetone. The reaction mixture was allowed to reflux under N_2 overnight. After the reaction cooled down, it was filtered and washed with acetone and dried to afford the title compound as a grey powder (4.6 g, 92%). ^{1}H NMR (300 MHz, DMSO-d_6): δ 9.13 (m, 4H), 8.63 (s, 1H), 8.52 (m, 2H), 8.09 (m, 1H), 4.00 (s, 3H), 3.38 (s, H_2O). ^{13}C{^{1}H}NMR (300 MHz, DMSO-d_6): δ 167.07, 163.78, 149.14, 148.86, 138.59, 135.12, 131.34, 130.10, 128.19, 124.94, 53.37. HRMS: calcd. for $C_{12}H_{11}N_4O_4S$ $[M + H]^+$ 307.0496; found 307.0502.

Compound 11: Compound **10** (4.5 g, 14.7 mmol, 1 equiv) was dissolved in 60 mL of MeOH/H_2O (1:3) mixed solvent. NaOH (2.94 g, 73.5 mmol, 5 equiv) was then added and the mixture stirred for 3 h at room temperature. 1 M HCl was then added to acidify the mixture to approximately pH 4 to allow full precipitation. Filtered, washed with THF and dried to afford the title compound as a dark red solid (2.1 g, 60%) which was used directly in the next step without further purification.

Compound 12: The solution of 30% H_2O_2 (1.8 mL, 15 mmol, 5 equiv) in 18 mL formic acid was stirred at room temperature under N_2 for 1 h. It was then cooled down

to 0 ^{o}C and to which was added carefully a suspension of compound **11** (750 mg, 3 mmol, 1 equiv) in 4 mL formic acid. The reaction mixture was stirred at 0 ^{o}C for 2 h under N_2 to form a suspension. It was filtered while it was still cold. The solid was washed with cold water and dried to afford the title compound as a white powder (0.65 g, 72%). (**Note: the filtrate should be quenched carefully.** Dropwise adding the filtrate to 200 mL $Na_2S_2O_3$ (7.1 g, 45 mmol, 15 equiv) aqueous solution was recommended) ^{1}H NMR (300 MHz, DMSO-d_6): δ 8.96 (dd, *J* = 7.8, 1.2 Hz, 1H), 8.27 (s, 1H), 8.14 (dd, *J* = 7.5, 1.2 Hz, 1H), 7.68 (s, 1H), 5.75 (s, DCM). ^{13}C{^{1}H}NMR (300 MHz, DMSO-d_6): δ 165.34, 153.42, 150.56, 148.63, 138.58, 130.96, 127.61, 125.16, 123.65, 119.24. HRMS: calcd. for $C_{10}H_5N_2O_7S$ $[M - H]^-$ 296.9823; found 296.9812.

Compound 13: Compound **12** (0.6 g, 2 mmol) was dissolved in 40 mL MeOH and the flask flushed with N_2. 60 mg (10% by mass) 10% Pd/C was then added and N_2 exchanged with H_2. The mixture was allowed to stir under an H_2 atmosphere at room temperature for one day. The resulting mixture was filtered over celite and solvents were evaporated under reduced pressure to yield the title compound as a bright yellow powder (0.54 g, quant) which was used directly in the next step without further purification.

Compound 14: Compound **13** (540 g, 2 mmol, 1 equiv) was dissolved in 36 mL 10% *w/v* $NaHCO_3$ solution (42 mmol, 21 equiv). To the resulting slurry was added a solution of Fmoc-Cl (672 mg, 2.6 mmol, 1.3 equiv) in 20 mL dioxane dropwise at 0 ℃ over 1 h. The mixture was stirred at 0 ℃ for a further hour, then at room temperature overnight. 1 M HCl was added to acidify the mixture to approximately pH 4. The resulting mixture was washed several times with Et_2O until precipitation occurred. Filtered, solid was washed once with small amount of water and once with DCM. The resulting solid was dried to yield the title compound as a yellow powder (680 mg, 69%, purity by RP-HPLC: > 99%). RP-HPLC (30-60% B, over 10 min) R_t =4.3 min. ^{1}H NMR (300 MHz, DMSO-d_6): δ 13.59 (br, 1H), 10.40 (s, H), 8.48 (m, 2H), 8.32 (br, 1H), 7.93 (d, *J* = 7.2 Hz, 2H), 7.79 (d, *J* = 7.5 Hz, 2H), 7.66 (t, *J* = 8.1

Hz, 1H), 7.37 (m, 4H), 4.61 (d, J = 6.6 Hz, 2H), 4.45 (t, J = 6.6 Hz, 1H). $^{13}C\{^{1}H\}$NMR (300 MHz, DMSO-d_6): δ 165.28, 153.87, 153.52, 145.16, 143.74, 140.84, 137.68, 135.68, 129.16, 127.81, 127.26, 125.29, 125.20, 120.68, 120.27, 117.78, 115.96, 66.47, 46.63. HRMS: calcd. for $C_{25}H_{19}N_2O_7S$ $[M + H]^+$ 491.0908; found 491.0912.

Compound 15: Compound **15** was synthesized by using modified literature protocol.[38] 2-Hydroxymethylpropanediol (1g, 9.43 mmol, 1 equiv) was dissolved in 183 mL anhydrous THF and then anhydrous pyridine (3.3 mL, 40.5 mmol, 4.3 equiv) was added. The mixture was cooled to -78 ℃ and stirred under N_2 in a round bottom flask with dropping funnel attached. Di-*tert*-butylsilyl ditriflate (3.1 mL, 9.43 mmol, 1.0 equiv) was diluted with 37 mL anhydrous THF under N_2, and transferred via a cannula to the dropping funnel, then added dropwise to the 2-hydroxymethylpropanediol solution at -78 ℃ under N_2 over 1 h. The reaction was allowed to slowly reach -30 ℃ over 2 hours, then it was removed from the cooling bath and allowed to reach room temperature over 1 h. A saturated solution of $NaHCO_3$ (90 mL) was added and the mixture stirred at room temperature for a further 30 min. Organic solvents were evaporated under reduced pressure, and the remaining aqueous suspension extracted three times with EtOAc. The combined organic layers were washed once with ice-cold HCl (0.1 M), once with saturated $NaHCO_3$, and once with brine. The organic layer was dried over $MgSO_4$ and then solvents were evaporated under reduced pressure. The resulting oil was purified by column chromatography (100% cyclohexane to cyclohexane/EtOAc = 9/1) to afford the title compound as a pale yellow oil (1.5 g, 65%). ^{1}H NMR (300 MHz, $CDCl_3$): δ 4.18 (m, 2H), 3.92 (m, 2H), 3.51 (d, J = 6.0 Hz, 2H), 2.30 (m, 1H), 1.54 (s, H_2O), 1.04 (s, 9H), 1.02 (s, 9H). $^{13}C\{^{1}H\}$NMR (300 MHz, $CDCl_3$): δ 67.06, 61.43, 42.86, 27.52, 27.37, 22.67, 20.48. HRMS: calcd. for $C_{12}H_{27}O_3Si$ $[M + H]^+$ 247.1724; found 247.1721.

Compound 16: Methyl 8-nitro-(1H)-4-quinolinone-2-carboxylate (735 mg, 2.96 mmol, 1 equiv), compound **15** (1.46 g, 5.93 mmol, 2.0 equiv) and triphenylphosphine

38. W. Zhang, S. Oya, M.-P. Kung, C. Hou, D. L. Maier, and H. F. Kung, *J. Med. Chem.* **2005**, 48, 5980.

(1.0 g, 3.9 mmol, 1.3 equiv) were suspended in 11 mL anhydrous THF and stirred under N_2 at 0 ℃. DIAD (738 µL, 3.9 mmol, 1.3 equiv) was then added to the mixture dropwise at 0 ℃ over 20 min. The resulting slurry was then stirred at room temperature for a further 2 h, and then heated to 50 ℃ under N_2 for 2 h. The mixture was allowed to come to room temperature and solvents evaporated under reduced pressure. The oily residue was triturated in MeOH and the resulting precipitate was left at -18 ℃ for 15 h. Solid was isolated by filtration, washed with ice-cold MeOH and dried to afford the title compound as an off-white powder (1.1 g, 74%). ^{1}H NMR (300 MHz, $CDCl_3$): δ 8.41 (dd, *J* = 8.4, 1.5 Hz, 1H), 8.11 (dd, *J* = 7.5, 1.2 Hz, 1H), 7.68 (m, 1H), 7.63 (s, 1H), 4.37 (m, 2H), 4.18 (m, 4H), 4.04 (s, 3H), 2.78 (m, 1H), 1.09 (s, 9H), 1.08 (s, 9H). ^{13}C{^{1}H}NMR (300 MHz, $CDCl_3$): δ 165.55, 162.24, 151.32, 148.55, 140.08, 126.42, 126.10, 125.25, 123.05, 102.16, 67.76, 66.49, 53.51, 40.01, 27.47, 27.36, 22.65, 20.62. HRMS: calcd. for $C_{46}H_{64}N_4O_{14}Si_2Na$ $[2M + Na]^+$ 975.3856; found 975.3834

Compound 17: Compound **16** (1.1 g, 2.20 mmol, 1 equiv) was dissolved in 80 mL THF/H_2O (4:1) mixed solvent and LiOH·H_2O (139 mg, 3.31 mmol, 1.5 equiv) was added. The reaction mixture was allowed to stir at room temperature for 1 h. 1M HCl was then added to acidify the mixture to approximately pH 4. The resulting mixture was extracted three times with DCM. The combined organic layers were washed twice with H_2O, once with brine, and the aqueous phases back-extracted once with DCM. The combined organic phases were dried over $MgSO_4$. Then solvents were evaporated under reduced pressure to afford the title compound as a pale brown powder (1.0 g, quant). ^{1}H NMR (300 MHz, $CDCl_3$) δ 8.48 (dd, *J* = 8.4, 1.2 Hz, 1H), 8.25 (dd, *J* = 7.5, 1.2 Hz, 1H), 7.76 (m, 1H), 7.72 (s, 1H), 4.39 (m, 2H), 4.24 (d, *J* = 6.3 Hz, 2H), 4.15 (m, 2H), 2.79 (m, 1H), 1.09 (s, 9H), 1.08 (s, 9H). ^{13}C{^{1}H}NMR (300 MHz, $CDCl_3$): δ 163.74, 163.50, 149.39, 147.22, 138.41, 127.04, 126.94, 126.48, 123.45, 100.30, 68.35, 66.36, 39.93, 27.46, 27.37, 22.62, 20.67. HRMS: calcd. for $C_{22}H_{30}N_2O_7SiNa$ $[M + Na]^+$ 485.1720; found 485.1705

Compound 18: Compound **17** (1.03 g, 2.23 mmol) was dissolved in 43 mL THF

and the flask was flushed with N_2. 103 mg (10% by mass) 10% Pd/C was added and N_2 exchanged with H_2. The reaction mixture was allowed to stir at room temperature under an H_2 atmosphere overnight. The resulting mixture was filtered over celite and solvents were evaporated under reduced pressure to yield the title compound as a bright yellow powder (1.01 g, quant) which was used directly in the next step without further purification.

Compound 19: Compound **18** (1.0 g, 2.34 mmol, 1 equiv) was dissolved in 13 mL dioxane and 42 mL of a 10% *w/v* $NaHCO_3$ solution (50 mmol, 21 equiv) was added. To the resulting slurry was added a solution of Fmoc-Cl (786 mg, 3.04 mmol, 1.3 equiv) in 42 mL dioxane dropwise at 0 ℃ over 1 h. The reaction mixture was allowed to stir at 0 ℃ for one hour and then at room temperature overnight. The resulting mixture was diluted with 60 mL H_2O and pH was brought to 2-3 by dropwise addition of 1 M HCl. The mixture was then extracted three times with CH_2Cl_2 and the combined organic phases were washed three times with brine, dried over $MgSO_4$. Solvents were evaporated under reduced pressure. The resulting oily residue was purified by column chromatography (100% CH_2Cl_2 to CH_2Cl_2/MeOH = 9/1) to yield the title compound as a light green powder (930 mg, 61%, purity by RP-HPLC: 98%). RP-HPLC (30-100% B, over 13 min) R_t =16.3 min. ^{1}H NMR (300 MHz, DMSO-d_6): δ 10.35 (br, 1H), 8.33 (br, 1H), 7.93 (m, 2H), 7.77 (m, 3H), 7.59 (m, 2H), 7.39 (m, 4H), 4.60 (d, J = 6.6 Hz, 2H), 4.43 (t, J = 6.6 Hz, 1H), 4.27 (m, 4H), 4.09 (m, 2H), 2.65 (m, 1H), 1.03 (s, 9H), 1.01 (s, 9H). ^{13}C{^{1}H}NMR (300 MHz, DMSO-d_6): δ 166.34, 161.99, 153.33, 143.69, 140.78, 137.48, 135.42, 128.91, 128.03, 127.74, 127.20, 125.11, 121.34, 120.21, 120.01, 116.07, 114.39, 100.72, 66.90, 66.39, 65.93, 46.56, 27.27, 27.06, 22.14, 19.93. HRMS: calcd. for $C_{37}H_{43}N_2O_7Si$ $[M + H]^+$ 655.2834; found 655.2826.

Compound 20: Methyl 8-nitro-(1H)-4-quinolinone-2-carboxylate (3.75 g, 15 mmol, 1 equiv) and fleshly distilled pyridine (4 mL, 50 mmol, 3.3 equiv) were dissolved in 100 mL anhydrous DCM. To the solution was slowly added triflic anhydride (3.75 mL, 22.5 mmol, 1.5 equiv) at 0 ^{o}C, under N_2 atmosphere. The reaction mixture was stirred

at room temperature overnight and then the resulting mixture was neutralized with a saturated solution of NH_4Cl at 0 ℃. The mixture was extracted three times with CH_2Cl_2. The combined organic phases washed with brine, dried over $MgSO_4$ and solvents were evaporated under reduced pressure. The resulting solid was triturated in water, then filtered and washed with water three times and dried to afford the title compound as a grey powder (5.6 g, 98%). ^{1}H NMR (300 MHz, $CDCl_3$): δ 8.35 (dd, *J* = 8.7, 1.2 Hz, 1H), 8.30 (s, 1H), 8.24 (dd, *J* = 7.5, 1.2 Hz, 1H), 7.92 (m, 1H), 4.08 (s, 3H), 1.57 (s, H_2O). ^{13}C{^{1}H}NMR (300 MHz, $CDCl_3$): δ 163.96, 153.55, 151.23, 140.88, 129.46, 126.06, 124.87, 123.25, 120.85, 116.60, 113.89, 53.91. HRMS: calcd. for $C_{12}H_8N_2O_7SF_3$ $[M + H]^+$ 381.0004; found 380.9990.

Compound 21: A mixture of compound **20** (2 g, 5.2 mmol, 1 equiv), KCN (0.68 g, 10.4 mmol, 2 equiv) and $Pd(PPh_3)_4$ (480 mg, 0.41 mmol, 0.08 equiv) in an anhydrous toluene/DMF (60 mL/6 mL) mixed solvent was heated at 100 ^{o}C for 2 h under N_2. Toluene was evaporated and the resulting mixture was diluted with ethyl acetate and washed three times with a saturated solution of $NaHCO_3$, once with water and once with brine. (**Note**: KCN is **Extremely Toxic**. It should be properly and carefully treated. For example, the reaction should be quenched with base **Not Acid**!) The organic layer was dried over $MgSO_4$ and then solvents were evaporated under reduced pressure. The resulting solid was triturated in methanol which was filtered and washed with methanol three times and dried to afford the title compound as a grey powder (1.25 g, 92%). ^{1}H NMR (300 MHz, $CDCl_3$): δ 8.64 (s, 1H), 8.49 (dd, *J* = 8.4, 1.2 Hz, 1H), 8.27 (dd, *J* = 7.5, 1.2 Hz, 1H), 7.98 (m, 1H), 4.09 (s, 3H), 1.55 (s, H_2O). ^{13}C{^{1}H}NMR (300 MHz, DMSO-d_6): δ 163.28, 149.32, 148.42, 137.58, 130.98, 128.50, 127.31, 126.67, 125.76, 120.08, 114.57, 53.34. HRMS: calcd. for $C_{12}H_8N_3O_4$ $[M + H]^+$ 258.0515; found 258.0526.

Compound 23: Compound **21** (1.54 g, 6 mmol, 1 equiv) was suspended in a AcOH/THF (50 mL/10 mL) mixed solvent. The flask was flushed with N_2 and 154 mg (10% by mass) 10% Pd/C was then added. N_2 was exchanged with H_2 and the mixture stirred under the H_2 atmosphere at room temperature overnight. The resulting

mixture was filtered over celite and solvents of the filtrate were evaporated under reduced pressure. The resulting solid was triturated in diethyl ether, filtered and dried, to yield compound **22** as, an acetic salt, a dark brown powder (quantitative) which was used directly in the next step without further purification. A mixture of the above compound **22** and DIPEA (2.1 mL, 12 mmol, 2 equiv) in DCM/CH_3CN (50 mL/30 mL) mixed solvent was cooled to 0 ^oC and followed by slowly adding a solution of Boc_2O (1.4 g, 6.6 mmol, 1.1 equiv) in DCM over 30 min. The reaction was allowed to stir at room temperature under N_2 overnight. The reaction mixture was washed three times with a saturated solution of NH_4Cl, once with water and once with brine. The organic layer was dried over $MgSO_4$ and then solvents were evaporated under reduced pressure. The resulting solid was triturated in acetonitrile. Then solid was isolated by filtration, washed with small amount of acetonitrile and dried to afford the title compound as a brown powder (1.8 g, 90%). ^1H NMR (300 MHz, $CDCl_3$): δ 8.08 (s, 1H), 7.45 (m, 1H), 7.28 (m, overlapped with C*H*Cl_3), 6.95 (dd, *J* = 7.5, 1.2 Hz, 1H), 4.99 (br, 1H), 4.80 (d, *J* = 5.7 Hz, 2H), 4.03 (s, 3H), 2.47 (br, H_2O), 1.49 (s, 9H). $^{13}C\{^1H\}$NMR (300 MHz, $CDCl_3$): δ 166.13, 155.96, 145.96, 145.28, 144.39, 137.47, 130.32, 128.20, 118.84, 110.48, 110.34, 80.24, 52.86, 41.77, 28.51. HRMS: calcd. for $C_{17}H_{22}N_3O_4$ $[M + H]^+$ 332.1605; found 332.1605.

Compound 25: Compound **23** (1.3 g, 4 mmol, 1 equiv) was dissolved in 125 mL of THF/H_2O (4:1) mixed solvent. LiOH ·H_2O (252 mg, 6 mmol, 1.5 equiv) was added and the reaction mixture was allowed to stir at room temperature for another hour. Citric acid hydrate (420 mg, 2 mmol, 0.5 equiv) was then added to neutralize the reaction and the solvents were evaporated under reduced pressure to afford a suspension. It was then filtered and the solid was dried to afford compound **24** as a light yellow powder (quantitative) which was used directly in the next step without further purification. The above compound **24** was dissolved in 21 mL dioxane, and 71 mL of a 10% *w/v* $NaHCO_3$ aqueous solution (84 mmol, 21 equiv) was added. To the resulting slurry was added a solution of Fmoc-Cl (1.34 g, 5.2 mmol, 1.3 equiv) in 75 mL dioxane dropwise at 0 ℃ over 1 h. The mixture was stirred at 0 ℃ for a further

hour, then at room temperature overnight. The reaction pH was brought to 4 by adding 5% *w/v* citric acid solution in water. The mixture was then extracted three times with CH_2Cl_2. The combined organic layers washed three times with brine, dried over $MgSO_4$ and solvents were evaporated under reduced pressure. To the resulting oily residue was added acetonitrile to allow full precipitation. The solid was isolated by filtration, washed with a small amount of acetonitrile and dried to afford the title compound as a white powder (1.98 g, 92%, purity by RP-HPLC: 99%). RP-HPLC (60-70% B, over 10 min) R_t =9.9 min. ^{1}H NMR (300 MHz, DMSO-d_6): δ 13.60 (br, 1H), 10.47 (s, 1H), 8.36 (br, 1H), 8.10 (br, 1H),7.93 (d, *J* = 7.2 Hz, 2H), 7.77 (m, 5H), 7.36 (m, 4H), 4.64 (m, 4H), 4.46 (t, *J* = 6.6 Hz, 1H), 3.32 (s, H_2O), 1.43 (s, 9H). ^{13}C{^{1}H}NMR (300 MHz, DMSO-d_6): δ 165.49, 155.87, 153.48, 148.30, 145.00, 143.69, 140.80, 136.54, 136.24, 129.48, 127.76, 127.23, 127.20, 125.13, 120.22, 117.65, 116.49, 116.03, 78.39, 66.42, 46.58, 40.79, 28.18. HRMS: calcd. for $C_{31}H_{30}N_3O_6$ $[M + H + Na]^{2+}$ 540.2129; found 540.2129.

Compound 26: 5-bromo-2-nitroaniline (40.6 g, 187 mmol, 1 equiv) was dissolved in 600 mL acetic acid at 70 ^{o}C. Ethylvinylether (55 mL, 560 mmol, 3 equiv), then concentrated H_2SO_4 (20 mL, 380 mmol, 2 equiv) were added to the solution. The mixture was stirred at 70 ^{o}C for 15 min, then another 15 min at 120 ^{o}C. After cooling down to room temperature, the reaction mixture was poured over ice and 1 L 30% *w/v* NaOH was added while stirring. The resulting suspension was stirred with ethyl acetate and then filtered through celite to eliminate a few tars. The organic phase was separated and dried over $MgSO_4$. Solvents were evaporated and the resulting solid was solubilised in 170 mL boiling isopropanol. After cooling down to room temperature, the mixture was sonicated to allow full precipitation. The solid was isolated by filtration, washed with cyclohexane, and dried to afford the title compound as a grey powder (22 g, 45%). ^{1}H NMR (300 MHz, DMSO-d_6): δ 8.53 (d, *J* = 8.7 Hz, 1H), 8.18 (d, *J* = 8.1 Hz, 1H), 8.07 (d, *J* = 8.1 Hz, 1H), 7.76 (d, *J* = 8.7 Hz, 1H), 3.32 (s, H_2O), 2.72 (s, 3H). ^{13}C{^{1}H}NMR (300 MHz, DMSO-d_6): δ 162.73, 147.23, 138.47, 135.31, 128.72, 126.00, 125.59, 124.49, 123.41, 24.91. HRMS: calcd. for

$C_{10}H_8BrN_2O_2$ $[M + H]^+$ 266.9764; found 266.9768.

Compound 27: compound **26** (22 g, 82 mmol, 1 equiv) and SeO_2 (18.3 g, 165 mmol, 2 equiv) were stirred in 300 mL pyridine at 80 ^oC for 48 hours. Pyridine was evaporated under reduce pressure. The resulting solid was stirred in boiling ethanol for 30 min. The hot mixture was filtered through celite and the filtrate was evaporated under reduce pressure. 1 L $KHSO_4/K_2SO_4$ buffer was added to the resulting oil and the flask was sonicated for 30 min. The resulting solid was isolated by filtration and dried to afford the title compound as a grey powder (23 g, 95%). ^1H NMR (300 MHz, DMSO-d_6): δ 13.90 (br, 1H), 8.83 (d, J = 8.7 Hz, 1H), 8.38 (d, J = 8.7 Hz, 1H), 8.30 (m, 2H), 3.32 (s, H_2O). $^{13}C\{^1H\}$NMR (300 MHz, DMSO-d_6): δ 165.15, 151.37, 147.92, 138.37, 137.47, 131.43, 128.31, 124.76, 124.62, 124.14. HRMS: calcd. for $C_{10}H_6BrN_2O_4$ $[M + H]^+$ 296.9506; found 296.9515.

Compound 28: compound **27** (22 g, 74 mmol, 1 equiv), K_2CO_3 (12 g, 89 mmol, 1.2 equiv) and benzyl bromide (11 mL, 89 mmol, 1.2 equiv) were stirred in 300 mL DMF at room temperature for 12 hours. DMF was evaporated under reduce pressure and water was added to the resulting solid. The mixture was extracted with ethyl acetate two times and the organic layer was dried over $MgSO_4$. After filtration, ethyl acetate was evaporated and the solid was triturated in ethanol. The resulting solid was isolated by filtration, washed with cyclohexane and dried to afford the title compound as a grey powder (18 g, 64%). ^1H NMR (300 MHz, DMSO-d_6): δ 8.87 (d, J = 9.0 Hz, 1H), 8.42 (d, J = 9.0 Hz, 1H), 8.32 (m, 2H), 7.43 (m, 5H), 5.49 (s, 2H), 3.32 (s, H_2O). $^{13}C\{^1H\}$NMR (300 MHz, DMSO-d_6): δ 163.30, 150.06, 147.82, 138.36, 137.76, 135.60, 131.70, 128.51, 128.42, 128.24, 128.01, 124.89, 124.86, 124.13, 67.19. HRMS: calcd. for $C_{17}H_{12}BrN_2O_4$ $[M + H]^+$ 386.9975; found 386.9982.

Compound 29: bis(dibenzylidene acetone)-palladium [0] (505 mg, 0.88 mmol, 0.02 equiv) and 1,2,3,4,5-pentaphenyl-1'-(di-*tert*-butylphosphino)ferrocene (624 mg, 0.88 mmol, 0.02 equiv) were added to a screw cap flask containing compound **28** (17 g, 44 mmol, 1 equiv) in 350 ml THF under nitrogen atmosphere. Then

2-*tert*-butoxy-2-oxoethyl zinc (II) bromide[39] (22.9 g, 88 mmol, 2 equiv) was added and the mixture was stirred at 70 ℃ for 12 h. The reaction vessel was allowed to cool to room temperature. The mixture was filtered and the filtrate was poured into 1.2 L water. Then $KHSO_4$ was added to bring the pH to approximately 3. The mixture was extracted with DCM three times. The combined organic layers was washed once with brine and dried over $MgSO_4$. The resulting solution was concentrated to around 50 mL and stirred with silica for 5 min, then filtered and washed with DCM. Solvent was evaporated and isopropanol was added to the resulting oil to allow precipitation occurred. The resulting solid was isolated by filtration and dried to afford the title compound as a white powder (8.4 g, 45%). ^{1}H NMR (300 MHz, $CDCl_3$): δ 8.58 (d, *J* = 9.0 Hz, 1H), 8.32 (d, *J* = 9.0 Hz, 1H), 8.08 (d, *J* = 7.8 Hz, 1H), 7.62 (d, *J* = 7.5 Hz, 1H), 7.52 (m, 2H), 7.41 (m, 3H), 5.50 (s, 2H), 4.04 (s, 2H), 1.59 (s, H_2O), 1.38 (s, 9H). ^{13}C{^{1}H}NMR (300 MHz, $CDCl_3$): δ 168.92, 164.49, 149.82, 148.24, 139.51, 136.74, 135.57, 134.36, 128.98, 128.79, 128.50, 128.28, 124.43, 122.63, 82.54, 67.86, 40.31, 28.04. HRMS: calcd. for $C_{23}H_{23}N_2O_6$ $[M + H]^+$ 423.1551; found 423.1559.

Compound 30: Compound **29** (8.86 g, 21 mmol, 1 equiv) was dissolved in 800 mL THF and the flask flushed with N_2. 886 mg (10% by mass) 10% Pd/C was then added. N_2 was exchanged with H_2 and the reaction was allowed to stir at room temperature under the H_2 atmosphere for one day. The mixture was filtered over celite and solvents were evaporated under reduced pressure to yield the title compound as an orange powder (6.16 g, 97%) which was used directly in the next step without further purification.

Compound 31: Compound **30** (4.72 g, 15.6 mmol, 1 equiv) was dissolved in 200 mL dioxane, and 265 mL of a 10% *w/v* $NaHCO_3$ aqueous solution (312 mmol, 20 equiv) was added. To the resulting slurry was added a solution of Fmoc-Cl (5.25 g, 20.3 mmol, 1.3 equiv) in 100 mL dioxane dropwise at 0 ℃ over 1 h. The reaction mixture was allowed to stir at 0 ℃ for one hour, then at room temperature overnight. The reaction pH was brought to 4 by adding 5% *w/v* citric acid solution in water. The

39. T. Hama, and J. F. Hartwig, *Org. Lett.*, **2008**, 10, 1549.

mixture was then extracted three times with CH_2Cl_2. The combined organic layers were washed three times with brine and dried over $MgSO_4$. Solvents were evaporated under reduced pressure. The resulting oily residue was purified by column chromatography (100% CH_2Cl_2 to CH_2Cl_2/MeOH = 99/1) to afford the title compound as a white powder (5.3 g, 65%, purity by RP-HPLC: 98%). RP-HPLC (40-100% B, over 5 min) R_t =18.7 min. ^{1}H NMR (300 MHz, $CDCl_3$): δ 8.77 (s, 1H), 8.37 (m, 3H), 7.79 (m, 4H), 7.42 (m, 5H), 5.30 (s, DCM), 4.53 (d, *J* = 7.2 Hz, 2H), 4.28 (t, *J* =7.2 Hz, 1H), 3.73 (s, 2H), 1.55 (s, H_2O), 1.31 (s, 9H). ^{13}C{^{1}H}NMR (300 MHz, $CDCl_3$): δ 170.06, 162.49, 153.40, 143.91, 143.85, 141.52, 137.48, 135.90, 135.03, 132.24, 128.67, 127.98, 127.36, 125.43, 124.67, 121.46, 120.19, 115.92, 81.76, 67.72, 47.18, 39.34, 28.03. HRMS: calcd. for $C_{31}H_{29}N_2O_6$ $[M + H]^+$ 525.2020; found 525.2018.

Compound 32: Methyl 4-bromo-8-nitroquinoline-2-carboxylate [15a] (11.8 g, 38 mmol, 1 equiv) was dissolved in 600 mL of THF/H_2O (3:1) mixed solvent. LiOH ⊣H_2O (2.41 g, 57 mmol, 1.5 equiv) was added and the reaction mixture was allowed to stir at room temperature for one hour. 1 M HCl was then added to acidify the reaction to approximately pH 3. The resulting mixture was filtered and the solid was washed with water and dried to afford the title compound as a light yellow powder (10.5 g, 94%). ^{1}H NMR (300 MHz, DMSO-d_6): δ 8.40 (m, 3H), 7.94 (m, 1H), 3.49 (s, H_2O). ^{13}C{^{1}H}NMR (300 MHz, DMSO-d_6): δ 165.32, 155.30, 148.40, 138.40, 134.06, 129.91, 128.42, 127.87, 126.69, 124.64. HRMS: calcd. for $C_{10}H_6BrN_2O_4$ $[M + H]^+$ 296.9506; found 296.9513.

Compound 33: Compound **32** (9.8 g, 33 mmol, 1 equiv), K_2CO_3 (5.34 g, 40 mmol, 1.2 equiv) and benzyl bromide (4.9 mL, 40 mmol, 1.2 equiv) were stirred in 200 mL DMF at room temperature for 12 hours. DMF was evaporated under reduce pressure and water was added to the resulting solid and filtered. The solid was washed once with water, once with ethanol, once with cyclohexane and dried to afford the title compound as a grey powder (12.3 g, 97%). ^{1}H NMR (300 MHz, $CDCl_3$): δ 8.57 (s, 1H), 8.48 (dd, *J* = 8.4, 1.2 Hz, 1H),8.15 (dd, *J* = 7.5, 1.2 Hz, 1H), 7.82 (m, 1H),7.51

(m, 2H), 7.41 (m, 3H), 5.50 (s, 2H), 1.56 (s, H_2O). $^{13}C\{^1H\}$NMR (300 MHz, $CDCl_3$): δ 163.48, 149.66, 149.04, 139.59, 135.53, 135.30, 130.76, 129.51, 128.81, 128.62, 128.58, 128.38, 126.78, 125.30, 68.17. HRMS: calcd. for $C_{17}H_{12}BrN_2O_4$ $[M + H]^+$ 386.9975; found 386.9981.

Compound 34: To a flask containing a solution of compound **33** (9 g, 23.3 mmol, 1 equiv), bis(dibenzylidene acetone)-palladium [0] (275 mg, 0.47 mmol, 0.02 equiv) and 1,2,3,4,5-pentaphenyl-1'-(di-*tert*-butylphosphino)ferrocene (330 mg, 0.47 mmol, 0.02 equiv) in 100 mL anhydrous THF under N_2 atmosphere was added slowly a suspension of 2-*tert*-butoxy-2-oxoethyl zinc (II) bromide (12.2 g, 47 mmol, 2 equiv) in 64 mL anhydrous THF. The reaction mixture was stirred at room temperature for 4 h. The resulting mixture was filtered and the filtrate was poured into 1 L water. Then $KHSO_4$ was added to bring the pH to approximately 3. The mixture was extracted with DCM three times. The combined organic layers was washed once with brine and dried over $MgSO_4$. The resulting solution was concentrated to around 50 mL and stirred with silica for 5 min. It was then filtered and washed with DCM. Solvents were evaporated and isopropanol was added to the resulting oil to allow precipitation occurred. The solid was isolated by filtration and dried to afford the title compound as a white powder (5.8 g, 59%). ^1H NMR (300 MHz, $CDCl_3$): δ 8.27 (dd, J = 8.7, 1.2 Hz, 1H), 8.20 (s, 1H), 8.09 (dd, J = 7.5, 1.2 Hz, 1H), 7.75 (m, 1H), 7.51 (m, 2H), 7.41 (m, 3H), 5.49 (s, 2H), 4.07 (s, 2H), 1.55 (s, H_2O), 1.39 (s, 9H). $^{13}C\{^1H\}$NMR (300 MHz, $CDCl_3$): δ 168.33, 164.49, 149.81, 149.54, 143.08, 139.46, 135.54, 129.45, 128.78, 128.51, 128.33, 127.95, 127.39, 124.27, 124.02, 82.71, 67.88, 40.34, 28.01. HRMS: calcd. for $C_{23}H_{23}N_2O_6$ $[M + H]^+$ 423.1551; found 423.1554.

Compound 35: Compound **34** (6 g, 14.2 mmol, 1 equiv) was dissolved in 300 mL THF and the flask flushed with N_2. 600 mg (10% by mass) 10% Pd/C was added and N_2 was exchanged with H_2. The reaction mixture was allowed to stir at room temperature under the H_2 atmosphere for one day. The resulting mixture was filtered over celite and solvents were evaporated under reduced pressure to afford the title compound as an yellow powder (4 g, 93%) which was used directly in the next step

without further purification. ^{1}H NMR (300 MHz, DMSO-d_6): δ 8.00 (s, 1H), 7.44 (m, 1H), 7.06 (dd, *J* = 8.4, 1.2 Hz, 1H), 6.89 (dd, *J* = 7.5, 1.2 Hz, 1H), 6.60 (br, 2H), 4.09 (s, 2H), 3.33 (br, H_2O), 1.38 (s, 9H). ^{13}C{^{1}H}NMR (300 MHz, DMSO-d_6): δ 169.36, 165.68, 147.19, 142.67, 142.61, 135.67, 130.53, 129.38, 121.18, 108.95, 108.69, 80.79, 39.01, 27.61. HRMS: calcd. for $C_{16}H_{19}N_2O_4$ $[M + H]^+$ 303.1339; found 303.1352.

Compound 36: compound **35** (3.6 g, 12 mmol, 1 equiv) was dissolved in 60 mL dioxane, and 211 mL of a 10% *w/v* $NaHCO_3$ aqueous solution (252 mmol, 21 equiv) was added. To the resulting slurry was added a solution of Fmoc-Cl (4.03 g, 15.6 mmol, 1.3 equiv) in dioxane (200 mL) dropwise at 0 ℃ over 1 h. The reaction mixture was allowed to stir at 0 ℃ for one hour, then at room temperature overnight. The reaction pH was brought to 4 by adding 5% *w/v* citric acid solution in water. The mixture was then extracted three times with CH_2Cl_2. The combined organic layers were washed three times with brine and dried over $MgSO_4$. Then solvents were evaporated under reduced pressure. The resulting oily residue was added diethyl ether to allow full precipitation. Solid was isolated by filtration, washed with diethyl ether and dried to afford the title compound as a white powder (3.9 g, 62%, purity by RP-HPLC: 97%). RP-HPLC (60-80% B, over 10 min) R_t =10.1 min. ^{1}H NMR (300 MHz, $CDCl_3$): δ 8.98 (br, 1H), 8.40 (br, 1H), 8.23 (s, 1H), 7.80 (d, *J* = 7.5 Hz, 2H), 7.68 (m, 4H),7.42 (m, 4H), 4.69 (d, *J* = 6.0 Hz, 2H), 4.40 (t, *J* = 6.3 Hz, 1H), 4.06 (s, 2H), 1.55 (br, H_2O), 1.41 (s, 9H). ^{13}C{^{1}H}NMR (300 MHz, $CDCl_3$): δ 168.97, 165.80, 154.35, 144.43, 143.85, 143.80, 141.49, 137.31, 135.61, 130.05, 129.28, 127.94, 127.34, 125.10, 122.34, 120.15, 117.28, 117.02, 82.47, 67.83, 47.15, 40.31, 28.05. HRMS: calcd. for $C_{31}H_{29}N_2O_6$ $[M + H]^+$ 525.2020; found 525.2022.

Chapter 4

Towards quaternary structure mimics: water-soluble aromatic helix bundles

Contributors:
Dr. Pradeep K. Mandal carried out crystallization, crystal structure determination and refinement.

Objectives:

- Establish rational designs for constructing self-assembled aromatic helix bundles in water.
- According to the design, synthesize related quinoline oligoamide helical foldamers and study their self-assembling behavior in water through NMR and crystallography.
- Study hydrophobic effects and electrostatic interactions between helically folded aromatic foldamers in water.
- Verify water solubility and crystal growth ability of those short side chains (see chapter three) when different side chains are combined into one quinoline oligoamide foldamer.
- Attempt to construct self-assembled helix bundles with α-amino acid/quinoline hybrid foldamers.

1. Introduction

Sophisticated protein structures and cellular processes are the result of regulation of highly ordered quaternary structures that are built from secondary and tertiary structures. It is important and meaningful for chemists to design and construct bio-mimics dedicated to learn, mimic, and surpass those structures and functionalities in biological systems. The resulting knowledge would be of help for understanding similar biological processes and developing new materials and functions.

Considerable numbers and a variety of artificial bio-inspired structures are achieved based on α-peptides.[1] One famous and well-understood class of them is coiled coil (Figure 1a). It is formed via assembly of α-helices in water and aimed to mimic protein quaternary structures. The driving forces of assembly mainly consist of hydrophobic effects based on the so-called knob-into-hole (KIH, Figure 1b)[2] mode and electrostatic interactions normally referred to as salt bridges. Through rational design and with the help of well-established computational models, coiled coils can reach different sized and shaped architectures (Figure 1c).[3] Despite many succeeded cases and reliable computational modes available, the discovery of new protein mimics based on natural polypeptides is not without its challenges. One of the main obstacles resides in the incomplete understanding of sequence-to-structure relations, especially in the connection between primary sequence and secondary structure. In this respect, non-natural oligomers, known as foldamers,[4] have their inherent

1. a) D. N. Woolfson, *Advances in protein chemistry*, **2005**, 70, 79; b) J. M. Fletcher, A. L. Boyle, M. Bruning, G. J. Bartlett, T. L. Vincent, N. R. Zaccai, C. T. Armstrong, E. H. C. Bromley, P. J. Booth, R. L. Brady, A. R. Thomson, and D. N. Woolfson, *ACS Synth. Biol.* **2012**, 1, 240; c) J. M. Fletcher, R. L. Harniman, F. R. H. Barnes, A. L. Boyle, A. Collins, J. Mantell, T. H. Sharp, M. Antognozzi, P. J. Booth, N. Linden, M. J. Miles, R. B. Sessions, P. Verkade, and D. N. Woolfson, *Science*, **2013**, 340, 595; d) A. G. Tebo, and V. L. Pecoraro, *Curr. Opin. Chem. Biol.* **2015**, 25, 65; e) E. H. C. Bromley, K. Channon, E. Moutevelis, and D. N. Woolfson, *ACS Chem. Biol.* **2008**, 3, 38.
2. a) F. H. C. Crick, *Acta Cryst.* **1953**, 6, 689; b) J. D. Steinkruger, G. J. Bartlett, D. N. Woolfson, and S. H. Gellman, *J. Am. Chem. Soc.* **2012**, 134, 15652
3. a) E. Moutevelis, and D. N. Woolfson, *J. Mol. Biol.* **2009**, 385, 726; b) D. E. Mortenson, J. D. Steinkruger, D. F. Kreitler, D. V. Perroni, G. P. Sorenson, L. Huang, R. Mittal, H. G. Yun, B. R. Travis, M. K. Mahanthappa, K. T. Forest, and S. H. Gellman, *Proc. Natl. Acad. Sci., USA*, **2015**, 112, 13144; c) D. N. Woolfson, G. J. Bartlett, A. J. Burton, J. W. Heal, A. Niitsu, A. R. Thomson and C. W. Wood, *Curr. Opin. Chem. Biol.* **2015**, 33, 16; d) A. R. Thomson, C. W. Wood, A. J. Burton, G. J. Bartlett, R. B. Sessions, R. L. Brady, and D. N. Woolfson, *Science*, **2014**, 346, 485.
4. S. Hecht, and I. Huc, editors. *Foldamers: structure, properties and applications.* John Wiley & Sons, **2007**.

advantages. They are structurally stable and predictable; they can form well-defined secondary structures akin to those in proteins; they are, in some cases, proteases resistant;[5] and there are many different folding rules to follow so that they could reach the architectures and functionalities similar to and beyond those of biopolymers.

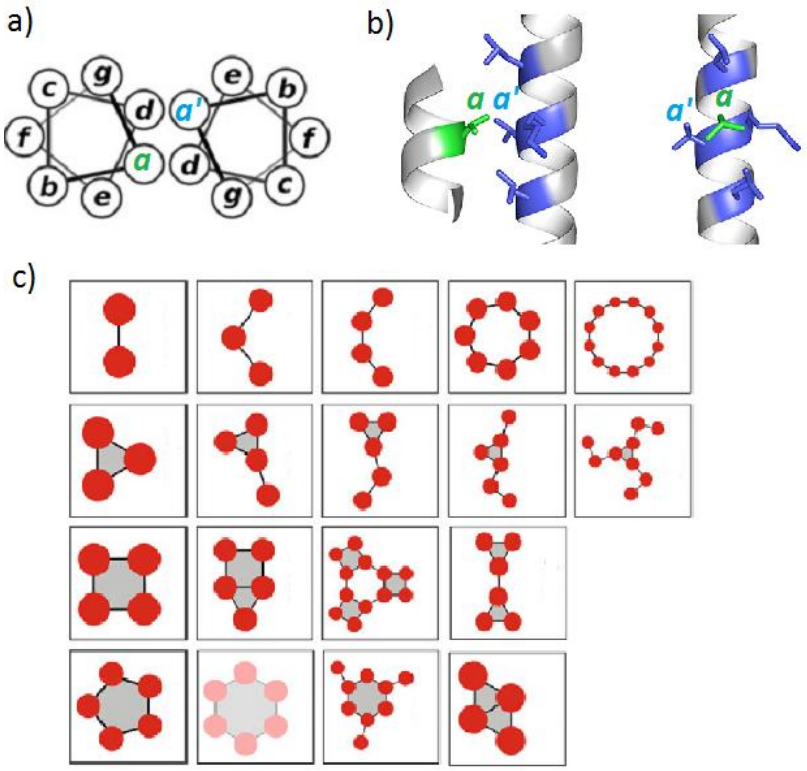

Figure 1. a) Helical wheel showing the repeated residues of an α-helix. b) An example showing knob(green)-into-hole(blue) mode. c) Various architectures based on coiled coils (red spots stands for α-helix derivatives) identified from proteins in nature. The highlighted residues (**a** in green and **a'** in blue) indicate where and how the KIH interaction normally takes place.

In foldamer chemistry, extensive efforts have been devoted to produce non-natural oligomers which in most of time only display a secondary structure.[6] Knowledge about and progress towards higher level of organization and assembling are limited. Quaternary structure mimics (here focus on helix bundles) established by assembly of amphiphilic helices based on α/β-peptide hybrid backbones from Samuel H.

5. a) L. M. Johnson and S. H. Gellman, *Methods Enzymol.* **2013**, 523, 407; b) J. Frackenpohl, P. I. Arvidsson, J. V. Schreiber, and D. Seebach, *ChemBioChem* **2001**, 2, 445; c) E. R. Gillies, F. Deiss, C. Staedel, J. M. Schmitter, and I. Huc, *Angew. Chem., Int. Ed.* **2007**, 46, 4081.
6. a) S. H. Gellman, *Acc. Chem. Res.* **1998**, 31, 173; b) D. J. Hill, M. J. Mio, R. B. Prince, T. S. Hughes, and J. S. Moore, *Chem. Rev.* **2001**, 101, 3893; c) I. Huc, *Eur. J. Org. Chem.* **2004**, 17; d) G. Guichard, and I. Huc, *Chem. Commun.* **2011**, 47, 5933; e) D.-W. Zhang, X. Zhao, J.-L. Hou, and Z.-T. Li, *Chem. Rev.* **2012**, 112, 5271.

Gellman's group[7] and homo-β-peptide backbones from Alanna Schepartz's group[8] represent the limited cases from peptide foldamers reported up to now. Recently, Gilles Guichard's group reported another case[9] via oligourea backbones which filled the blank of quaternary structure mimics in non-peptide foldamers. Guided by the *de novo* models, oligourea foldamers were designed and produced to show the ability of self-assembling into well-defined nanostructures in aqueous medium (Figure 2). Their crystal structures unambiguously indicated the oligourea foldamers in these nanostructures undergo quaternary assemblies. Moreover, the crystal structures also revealed that control of the final topology of these assemblies can be achieved by manipulation of their primary sequences. As a result, two different quaternary structure mimics, discrete helical bundle and non-discrete channel-type structure, were created via different oligourea sequences. It is noteworthy here that the resulting side chain organization of these oligourea helical foldamers is similar to quinoline oligoamide foldamers. Thus, some features of these oligourea bundles will be helpful of inspiring the helix bundle design based on quinoline oligoamide foldamers in water.

7. a) W. S. Horne, J. L. Price, J. L. Keck, and S. H. Gellman, *J. Am. Chem. Soc.* **2007**, 129, 4178; b) J. L. Price, W. S. Horne, and S. H. Gellman, *J. Am. Chem. Soc.* **2010**, 132, 12378; c) M. W. Giuliano, W. S. Horne, and S. H. Gellman, *J. Am. Chem. Soc.* **2009**, 131, 9860.
8. a) J. P. Miller, M. S. Melicher, and A. Schepartz, *J. Am. Chem. Soc.* **2014**, 136, 14726; b) J. L. Goodman, E. J. Petersson, D. S. Daniels, J. X. Qiu, and A. Schepartz, *J. Am. Chem. Soc.* **2007**, 129, 14746; c) M. A. Molski, J. L. Goodman, C. J. Craig, H. Meng, K. Kumar, and A. Schepartz, *J. Am. Chem. Soc.* **2010**, 132, 3658.
9. G. W. Collie, K. Pulka-Ziach, C. M. Lombardo, J. Fremaux, F. Rosu, M. Decossas, L. Mauran, O. Lambert, V. Gabelica, C. D. Mackereth, and G. Guichard, *Nat. Chem.* **2015**, 7, 871.

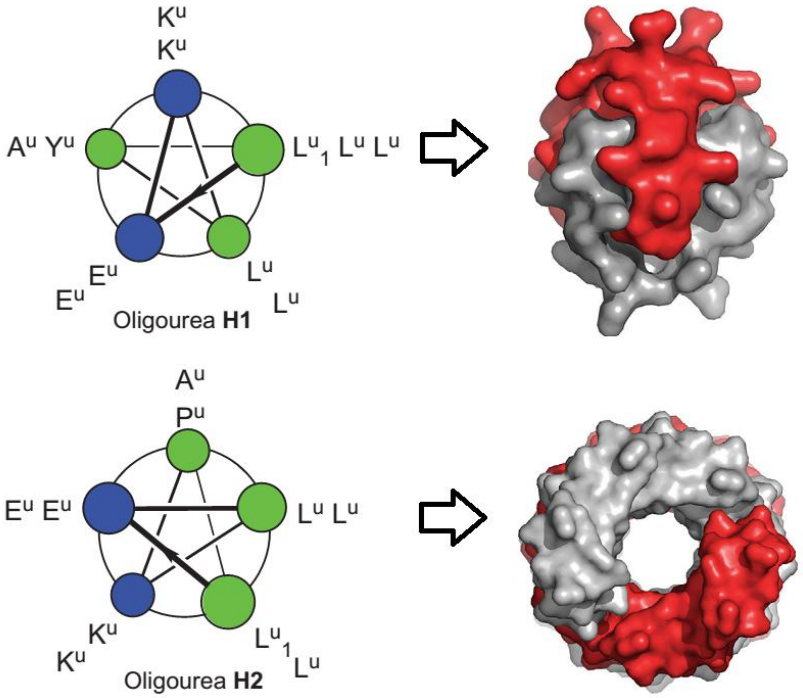

Figure 2. Quaternary assemblies formed from water-soluble oligourea foldamers. Left shows helical-wheel representations of oligoureas and their side chain distributions. Right shows crystal structures which are yielded from their corresponding oligourea sequences in water.

In general, except the challenge of design and synthesis, other factors restricting the discovery of higher level organization in foldamers could also include the paucity of high-resolution structural data and water-soluble foldamers, and the experimentally difficulty of structure elucidation in addition. Nevertheless, even with the limited examples and knowledge in hand, chemists were able to achieve some applications and functionalities of these protein mimics. For instance, Alanna Schepartz and coworkers were able to use their bundles to perform molecular recognition and chemical catalysis.[10] Through self-assembly of helically folded β^3-peptides, a series of protein-like thermodynamically stable bundles were constructed in water (Figure 3). Through kinetic analysis and high-resolution structural analysis, they found these protein mimics could realize a measurable catalytic function to carry out ester hydrolysis. Further study of this system revealed that the catalytic activity is relied on the geometric arrangement of histidine and arginine residues. This discovery also

10. P. S. P. Wang, J. B. Nguyen, and A. Schepartz, *J. Am. Chem. Soc.* **2014**, 136, 6810.

indicated that the catalytic activity of substrate-specific active sites can be optimized by structure-guided design. In the same group, other applications such as molecular recognition were also reported.[11] Besides, applications on construction of nanofibres[12] were reported by Samuel H. Gellman and co-workers.

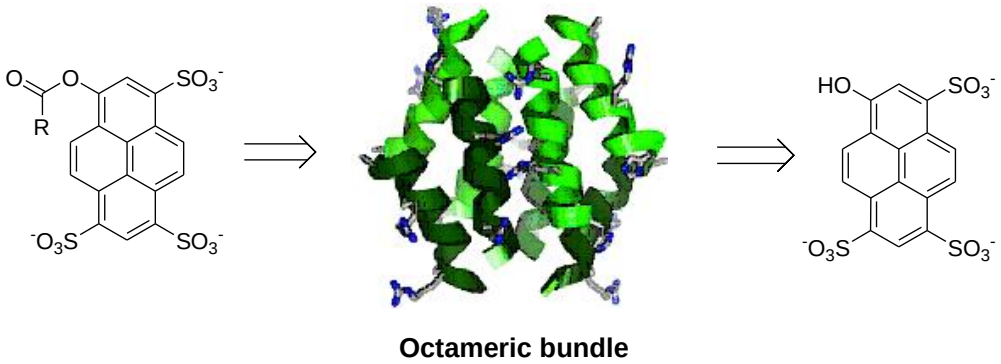

Figure 3. Helix bundle acted as a catalyst to perform ester hydrolysis.

We are interested in producing protein mimics based on aromatic oligoamide foldamers, the quinoline-based oligoamides here. This class of foldamers possesses some desired features which would potentially favor the formation of helix bundles. As mentioned in chapter one, these properties include: a) high stability of their resulting folded secondary structures (regardless of the change of their side chains) so that would favor crystallization and rational design of side chains in a predictable way; b) chemical accessibility and amenability to modification allowing the utilization of unlimited side chains beyond the twenty naturally occurring amino-acid side chains; c) the improved solubility and crystal growth ability in aqueous medium (referring to the cases with relatively short and rigid side chains, see chapter three); and d) the ability of folding into stable helical conformations as short as three residues in length. However, high stability and rigidity is a double-edged sword. It could also be an impediment of self-regulation to adapt the situation when the design is not good enough. In this case, the assembly of secondary structures with backbones like polypeptides in contrast would benefit from their inherent flexibility to automatically

11. a) M. S. Melicer, J. Chu, A. S. Walker, S. J. Miller, R. H. G. Baxter, and A. Schepartz, *Org. Lett.* **2013**, 15, 5048; b) M. S. Melicher, A. S. Walker, J. Shen, S. J. Miller, and A. Schepartz, *Org. Lett.* **2015**, 17, 4718.
12. W. C. Pomerantz, V. M. Yuwono, C. L. Pizzey, J. D. Hartgerink, N. L. Abbott, and S. H. Gellman, *Angew. Chem. Int. Ed.* **2008**, 47, 1241.

rectify the small error or mistake from a design and eventually achieve the desired conformation. Thus, to elaborate an ideal design with high accuracy represents another challenge in our studies.

This chapter mainly discusses our progress on design and constructing a helix bundle since up to now we have not yet obtained an ideal helix bundles.

2. Design

The strategy of constructing water-soluble aromatic helix bundles is based on firstly the formation of stable aromatic helical foldamers and secondly the rational arrangement of their side chains. To the great extent, these side chains enable intermolecular interactions and endow the resulting bundles with solubility. A wise choice of side chains would allow generating helix bundles through hydrophobic effect and/or electrostatic (usually salt bridges) interactions while retaining their water solubility. Thus, those side chains play a crucial role in our design towards water-soluble quaternary structure mimics. Meanwhile, a stable secondary structure, the helical foldamer, is also important since it allows us to place side chains in a predictable way. In general, we employ hydrophobic effects to bring helices together and salt bridges to enhance the formed helix bundles.

Learning from many failed trials, we now generally focused on the quinoline-based water-soluble oligoamides with their C-terminus and N-terminus capped with 2-aminoisobutyric acid residue (**Aib**) and diethylene glycol-like tail (**Tail**), respectively (Figure 4a). One feature of the quinoline-based helical foldamer is its relatively flat and large area of hydrophobic surfaces at the N- and C-terminus. They can undergo head-to-head stacking with each other by π-π interactions and solvophobic effects which make the situation complicated. In organic solvents, typically in chloroform, these solvophobic effects are minor. On the contrary, in aqueous medium they are maximized. These solvophobic effects in cooperation with π-π interactions may cause aggregation in and even precipitation from water impeding further studies of the conformations. Thus, a **Tail** and an **Aib** residue are attached at the N-terminus and C-terminus, respectively, for the purpose to disturb or ease aggregation.

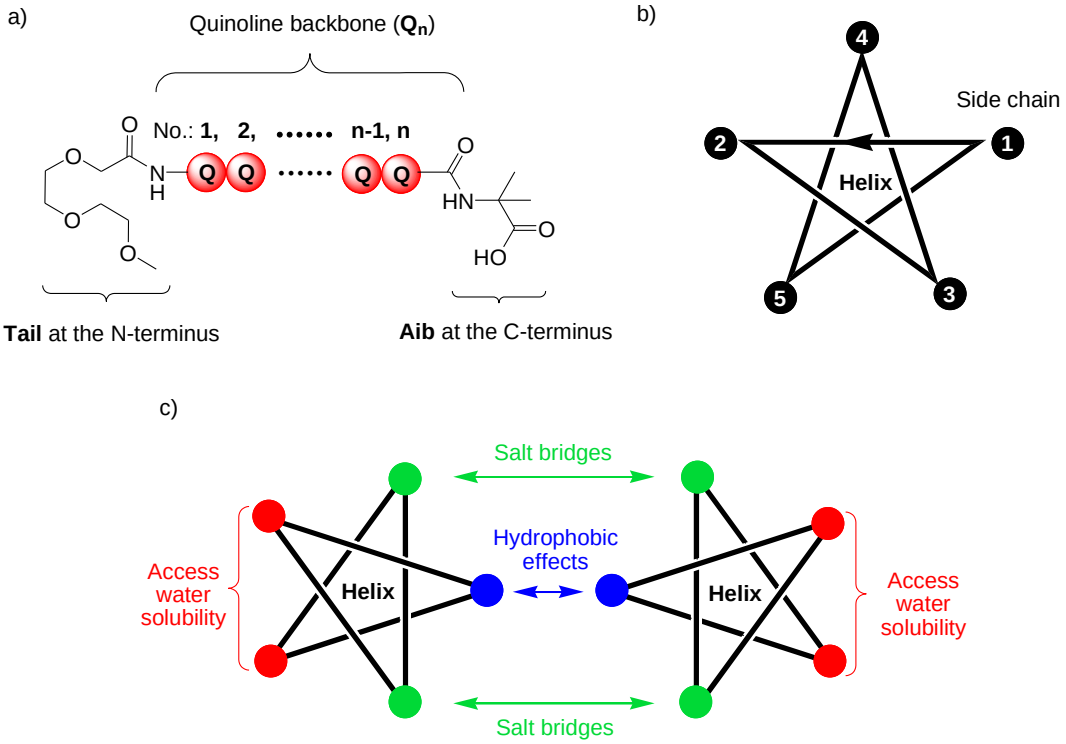

Figure 4. a) Quinoline-based oligoamide used for helix bundle design: structure of **Tail** residue at the N-terminus, simplified representation of quinoline backbone, and structure of **Aib** residue at the C-terminus. b) Five-pointed star showing the usual positions of side chains in quinoline-based helices counting monomers from 1 to 5 and so on. c) Simplified representation of the helix bundle design principle (showing a dimeric helix bundle as the example).

Another important feature of quinoline-based oligoamide foldamers is the high predictability of their side chains' position (Figure 4b). The well-defined and rigid canonical helical conformation enables the regular projection of their side chains in a five-pointed star mode.[13] In this way, we can place hydrophobic side chains to have hydrophobic effects at one branch of the star and arrange salt bridges at their nearby branches to enhance the bundle formation, while can still use the remaining two branches at the back to provide solubility by water-soluble side chains (Figure 4c).

Although the design looks straightforward, the way we have been on to produce and structurally elucidate helix bundle conformation is far more complicated. Many factors should be taken into account, for instance, the number and size of hydrophobic side chains. Too many and big-sized hydrophobic side chains could cause severe

13. a) H. Jiang, J.-M. Léger, and I. Huc, *J. Am. Chem. Soc.* **2003**, 125, 3448; b) H. Jiang, J.-M. Léger, C. Dolain, P. Guionneau, and I. Huc, *Tetrahedron* **2003**, 8365.

aggregation and hinder the nearby salt bridge formation, while too few and small size of which may not be hydrophobic enough to drive helices to get together. Even with a proper number of ideal-sized hydrophobic side chains, to address all the other issues is still not without challenges. The position and orientation of the charged side chains for salt bridge formation on the quinoline ring will affect the curvature and thus the size of the resulting bundle. Too large a curvature may cause a crush, i.e. no bundle formation, while too small will result in inefficient hydrophobic effects (or, in the other manner, inefficient salt bridges) and thus exposing a large area of hydrophobic surface to the aqueous medium. Moreover, for the latter case, it also means higher possibility of co-existence of several multiple helix bundles (e.g. large bundles consisting 8~10 helices may co-exist in water by using the same helix constituent). Other important factors also include solubility, crystal growth ability, and possibility of combination of parallel/anti-parallel and right/left-handed helices.

The above exemplified design is the one we have most frequently used up to now. The following text will also present other designs we used before or some of which we are going to use.

3. Results and discussion

3.1 Design based on quinoline oligoamide foldamers with one hydrophobic side chain per five residues

3.1.1 Sequences with acetyl group or Tail at N-terminus

Preliminary study was based on quinoline 12mers with N-terminus capped with acetyl group (Ac-Q_{12}-OH). The design principle is similar as the one presented above. However, at that time we had not yet developed building blocks with the side chains that could endow their foldamers with both good water solubility and crystal growth ability. Instead, we were mainly using monomers with aspartic acid-like (Asp) or ornthine-like (Orn) side chains to provide the helices with solubility in water and the ability to assemble via salt bridges. In addition, both ends of the sequences were not well protected. In other words, the resulting helices would have two relatively flat hydrophobic surfaces at their N- and C-terminus, which might undergo head-to-head stacking and cause aggregation. This situation would become even worse once they formed bundles because the hydrophobic surfaces would be accordingly enlarged.

As expected now (but disappointingly that time), the corresponding foldamers **1** - **5** (Figure 5a) were all failed to crystallize from water and showed broad ^{1}H NMR spectra in water (Figure 6). In foldamer **1** and **2**, we encoded the quinoline residues with hydrophobic side chains (methoxyl, OMe or leucine-like, Leu) at number 4 and 9, with negatively (Asp) and positively (Orn) charged side chains at number series 1-6-11 and 2-7-12, respectively, and with polar side chains (Diol) at number series 3-5-8-10. Thus, according to the folding rule and side chain arrangement principle showed in Figure 4b (also see Figure 5b), Asp and Orn side chains would locate, linearly and separately, at two sides of the hydrophobic core to form salt bridges when the assembling occurred. If the bundle formed, four Diol side chains would appear at the outer rim of the helix bundle to afford crystal growth ability and water solubility (Figure 5b). However, the resulting foldamers expressed disappointedly poor water

solubility regardless the change of hydrophobic side chains from Leu to methoxyl group. No (or extremely broad) signals of a foldamer was found on ^{1}H NMR spectra. We endeavored to crystallize foldamer **1** and **2** from aqueous/organic mixed solvents such as water/methanol and water/acetonitrile. All these trials were failed.

a)

	1 2 3 4 5 6 7 8 9 10 11 12
Foldamer **1**:	Ac-$Q^{Asp}Q^{Orn}Q^{diol}Q^{Leu}Q^{diol}Q^{Asp}Q^{Orn}Q^{diol}Q^{Leu}Q^{diol}Q^{Asp}Q^{Orn}$-OH
Foldamer **2**:	Ac-$Q^{Asp}Q^{Orn}Q^{diol}Q^{OMe}Q^{diol}Q^{Asp}Q^{Orn}Q^{diol}Q^{OMe}Q^{diol}Q^{Asp}Q^{Orn}$-OH
Foldamer **3**:	Ac-$Q^{Asp}Q^{Orn}Q^{Orn}Q^{OMe}Q^{Orn}Q^{Asp}Q^{Orn}Q^{Orn}Q^{OMe}Q^{Orn}Q^{Asp}Q^{Orn}$-OH
Foldamer **4**:	Tail-$Q^{Asp}Q^{Orn}Q^{Asp}Q^{OMe}Q^{Asp}Q^{Asp}Q^{Orn}Q^{Asp}Q^{OMe}Q^{Asp}Q^{Asp}Q^{Orn}$-OH
Foldamer **5**:	Ac-$Q^{diol}Q^{diol}Q^{Orn}Q^{OMe}Q^{Asp}Q^{Asp}Q^{Orn}Q^{Asp}Q^{OMe}Q^{Orn}Q^{diol}Q^{diol}$-OH

b)

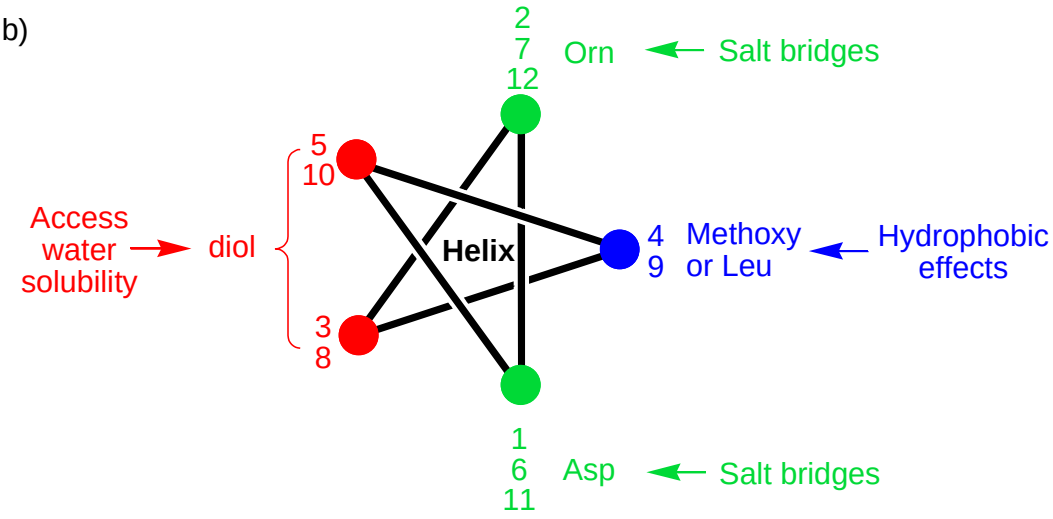

Figure 5. a) Sequences of foldamer **1** – **5**. b) Side chain arrangement of foldamer **1** and **2** on a five-pointed star model. The color in each sequence highlights the replaced residues comparing to its upper sequence. Different color of quinoline residues indicates their location on the five-pointed star model.

We assumed diol side chain was not good enough to play a role of providing water solubility. Therefore, all diol side chains were replaced by Orn side chains (foldamer **3**). Another benefit of this design is that, once they form bundles, there will be charge repulsions among bundles so that could ease the situation of aggregation. But the disadvantage is also obvious. The Orn side chains are too flexible to be compatible with crystallization. Indeed, foldamer **3** showed good solubility in acidic and neutral

water but no signs of crystal formation. Moreover, the ^{1}H NMR spectrum of foldamer **3** was broad indicating the existence of no specific aggregation (Figure 6a).

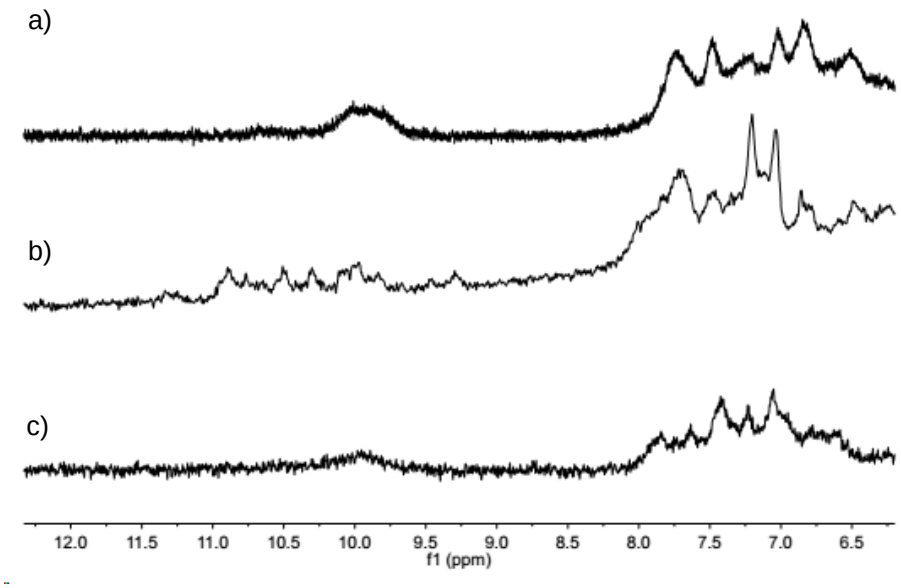

Figure 6. Part of the ^{1}H NMR spectra (300 MHz) of foldamers a) **3**, a) **4** and a) **5** showing aromatic amide (9 - 12 ppm) and aromatic (6.5 – 9 ppm) protons resonances in 10%D_2O/H_2O at 25 ^{o}C.

To address the issue of poor crystal growth ability, we designed and synthesized two new sequences (foldamers **4** and **5**), in parallel, following different principles. Foldamer **4** was a negatively charged version of foldamer **3**. We hope the relatively shorter length of Asp side chains could help improve the crystal growth ability. In addition, it is isosteric to the Leu side chain which provides great crystal growth ability from organic solvents. Meanwhile, we were aware that there was non-specific aggregation taking place in water by judging the broad appearance of ^{1}H NMR spectrum. Therefore, a **Tail** was attached to the N-terminus of foldamer **4**. However, the result from crystallography came out as usually bad as foldamers **1** – **3**. But the appearance of ^{1}H NMR spectrum did improve (Figure 6b). At least the region of aromatic amide and aromatic protons was not as broad as before although it was still not sharp and hard to identify a single set of signals. This implied to some extent the additional **Tail** may be of help for disturbing aggregation or helices stacking.

At the same time, foldamer **5** was synthesized. Instead of using homogeneous side chains at the 3-5-8-10 positions, Orn and Asp side chains were placed there alternately (Figure 5a and 7). This design was based on the principle that these side chains may form salt bridges or electrostatic interactions to restrict the freedom (to compensate the flexibility) of these side chains so that would eventually favor crystallization. However, we were also aware this design would disfavor its solubility in water and have the risk of cross linking helices by salt bridges. Thus, aggregation and precipitation may occur. Another change of the design was happened on position 1, 2, 11 and 12. Two Orn and two Asp side chains were replaced by Diol side chains. We assumed that if there were salt bridges formation, a small number of them should be strong enough to reinforce the hydrophobic effects and guide the assembly. On the contrary, if there were no salt bridges, then these flexible side chains would be a penalty for crystallization. Moreover, diol side chains could also form hydrogen bonds and hydrophobic interactions with themselves to enhance the assembly while remaining the ability of crystallization. As analyzed above, the results of NMR and crystallographic studies came out opposite to those of foldamer **4**. Foldamer **5** had limited solubility in water and its ^{1}H NMR spectrum in 10%D_2O/H_2O was also broad as expected (Figure 6c). But encouragingly, we obtained the first crystal of this series of foldamers despite the failure of collecting good-quality data that yields a crystal structure in the end.

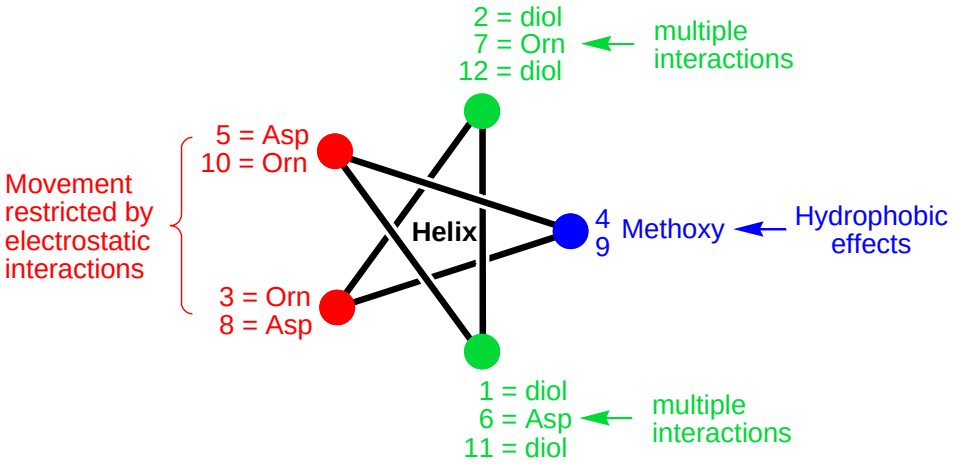

Figure 7. Side chain arrangement of foldamer **5** on a five-pointed star model.

To summarize this series of designs, we learned that: a) proper protections of N- and C-termini should be taken to ease complicated situations like stacking and aggregation; b) side chains that could provide both water solubility and crystal growth ability were urgently desired; c) putting constraints on flexible side chains, or making them rigid and shorter may increase the chance of getting crystals.

3.1.2 Sequences with Tail at N-terminus and Aib at C-terminus

Based on the preliminary results mentioned above, we experienced a long period to develop monomers with rigid side chains which were supposed to provide foldamers with both water solubility and crystal growth ability (see chapter three). Meanwhile, we envisioned the 2-aminoisobutyric acid residue (**Aib**) might help disturb the stacking happened at C-termini while remain the possibility of SPS from C-terminus and racemic crystallization of the resulting foldamers. Thus, new foldamers would comprise a **Tail** at the N-ternimus, an **Aib** at the C-ternimus, and relatively rigid side chains (Figure 8a). It is worth to mention here that introducing sulfonic acid side chain onto a foldamer remarkably improves its water solubility and thus makes otherwise impossible design in water become possible.

A molecular model of foldamer **6** indicated it was fit to form a trimeric bundle (Figure 8b). Initial model was built for an analogue of foldamer **6** in which the carboxymethyl side chain was on the 4^{th} position of the quinoline ring (not showed here). The model indicated a smaller curvature than foldamer **6** induced by salt bridges and thus several different sized helix bundles may form via self-assembling. This was not an ideal feature since it would complicate the further investigations. Nevertheless, the situation of self-assembly became simpler when the carboxymethyl side chain was moved to 5^{th} position. As shown in figure 8b, the model implied a well-defined trimeric bundle. The hydrophobic side chains were perfectly embedded into each other foldamer's hydrophobic cavity to form a compact yet comfortable hydrophobic core. The carboxymethyl and aminomethyl side chains adopted slightly

up-to-down pattern to meet each other to form salt bridges providing the resulting bundle structure with high rigidity. Since the length and angles of these salt bridges were well-fitted, the curvature of this helix bundle could hardly be changed and, therefore, a trimeric bundle should be the dominant species. Besides, the existed angles of these salt bridges also determined the tilted orientation of these helices so that resulted in a slightly coiled bundle resembling coiled coils in nature.

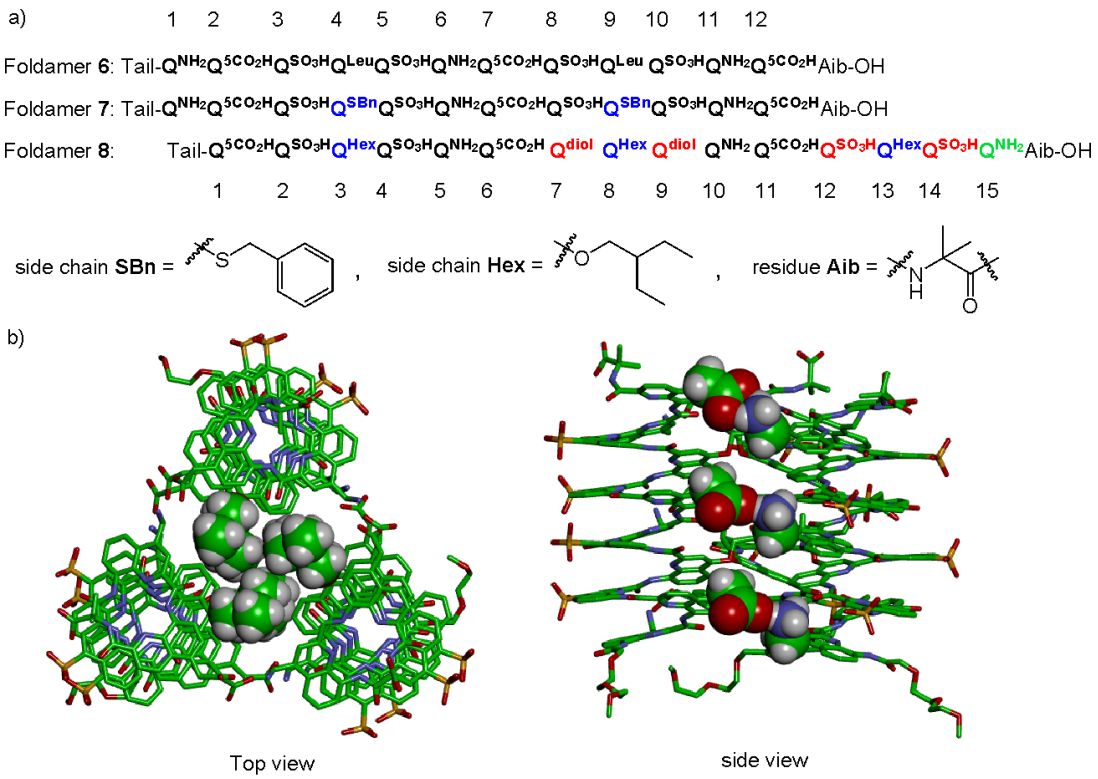

Figure 8. a) Sequences of foldamer **6** – **8** and structures of SBn and Hex side chains and **Aib** residue. b) Molecular model (energy minimization) of foldamer **6**. Hydrogen, carbon, nitrogen, oxygen and sulfur atoms are shown in white, green, blue, red and orange, respectively. Space-filling calotte models (also referred to CPK models) highlighted the volume occupied by hydrophobic side chains inside helix bundle and salt bridges between helices.

Foldamer **6** was synthesized through SPS method and purified by semiprep-HPLC. Qualitative solubility assays of this sequence revealed good solubility in basic and neutral water (pH > 6), fair in weak acidic water (pH > 4) and poor in acidic water with pH lower than 4. As expected, the NMR signals of foldamer **6** were sharp, which validated our assumption of incorporating **Tail** and **Aib** at N- and C-termini, respectively, to interrupt head-to-head staking. Good solubility of foldamer **6** allowed us to perform various solution phase studies via NMR technique. However, no matter

how the conditions were changed to favor the assembling (high concentration up to 11.0 mM; low temperature down to 5 ^{o}C; high salt concentration up to 250 mM of sodium chloride to favor hydrophobic effects; addition of organic solvent, acetonitrile, to favor salt bridge formation), the NMR spectra (Figure 9, also see experimental part) had been constantly showing a single set of peaks. This was an indication of either no self-assembly occurred, still to be as single helices, or a very well-defined self-assembling structure. Besides, there were also no obvious chemical shifts or dramatic changes of peak pattern indicating a very rigid and stable conformation.

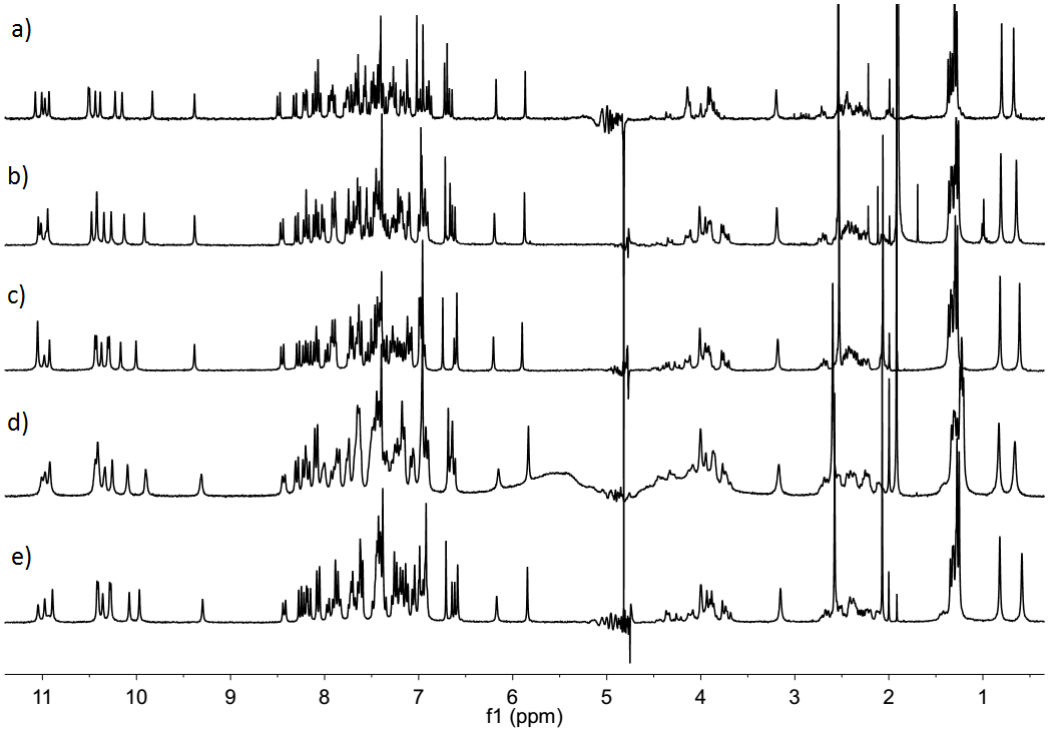

Figure 9. Variable concentration ^{1}H NMR (300 MHz) spectra of foldamer **6** in 10%D_2O/H_2O. a) 0.15 mM, b) 2.0 mM, c) 7.0 mM, and d) 11.0 mM of foldamer **6**. e) 7.0 mM **6** + 250 mM NaCl.

With no solid evidences of helix bundle formation from solution phase study, we turned to focus on solid state investigation. High quality crystals suitable for X-ray analysis were engendered soon from water via a standard hanging drop technique. The fast access of crystals for the quinoline foldamer displaying different side chains validated the high crystal growth ability of these short side chains developed in chapter three. However, instead of affording a desired trimeric bundle, a helix pair (or a pseudo dimeric bundle) was formed according to the crystal structure (Figure 10).

Indeed, there were hydrophobic effects between Leu side chains. But the Leu side chains intercalated into the hydrophobic cavities of each another helix guiding the formation of a pseudo dimeric bundle despite the possible chance to organize a trimeric bundle with the help of salt bridges or electrostatic interactions. The salt bridges also formed yet in an unexpected way. Instead of bridging with carboxymethyl side chains, these aminomethyl groups went with one line of sulfonic acid side chains. Thereby, the geometry of a planned bundle was disturbed and thus impossible for the further conversion of the pseudo dimeric bundle into a trimeric one. Similar results were also occurred to foldamer **7** which bore thiobenzyl (SBn) side chains instead of Leu side chains. This sequence was supposed to provide potentially more powerful solvophobic effects including π-π interactions to favor the assembly. However, both NMR and crystallography assays (see experimental part) showed similar results as those of foldamer **6**. (Thank Dr. Pradeep K. Mandal for crystallization and crystal structure determination and refinement.)

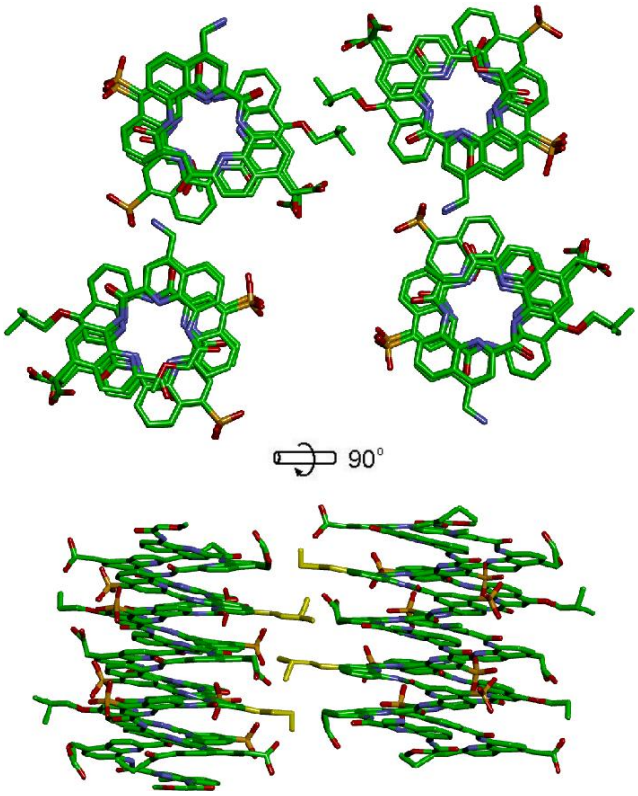

Figure 10. Crystal structure of foldamer **6**. Carbon, nitrogen, oxygen and sulfur atoms are shown in green, blue, red and orange, respectively. Hydrogen atoms have been omitted for clarity. In the bottom structure, these side chains (Leu) involved in hydrophobic effect are highlighted in yellow. This crystal structure has not been fully refined.

Having a lesson from the above failures, foldamer **8** was thus designed (Figure 8a). To interrupt the adherence between aminomethyl groups and sulfonic acid side chains, two Diol side chains were introduced to replace two sulfonic acid side chains in the middle of their arrays. The length of the foldamer and the hydrophobicity of the hydrophobic array were also increased to consist of fifteen quinoline residues and three hydrophobic side chains (Hex instead of Leu, and i.e. six carbons instead of four carbons), respectively.

The solution and solid phase studies again implied negative results of forming helix bundles. As usual, proton NMR showed there was only one set of peaks which might indicate well-defined assembly or single helices. But the crystal structure unambiguously exhibited a single helix arrangement in the solid state. The packing of this crystal structure was driven by some unusual forces which were hard to be understood. The enhanced hydrophobic core didn't result in better and stronger hydrophobic effects between two helices. Instead, these Hex side chains tended to interact with the newly incorporated diol side chains and exposed themselves to the surface with several sulfonic acid side chains. In contrast, all aminomethyl groups went together to act the role hydrophobic side chains should do. Thus, for foldamer **8**, there were no direct salt bridges between these side chains. Presumed reasons of these phenomena could be that a) Hex side chains were bulky and branched so that might disturb the nearby salt bridges formation; b) carboxymethyl and aminomethyl side chains were too short and too rigid to adapt the situation with certain restraints to form salt bridges; c) actually there were some weak interactions between hex and diol side chains (hydrophobic effects), and between these aminomethyl side chains (hydrogen bonding). Nevertheless, the recurrence of crystals of these foldamers bearing different side chains highly emphasizes the power of these newly developed short side chains to facilitate crystallization from water. (Thank Dr. Pradeep K. Mandal for crystallization and crystal structure determination and refinement.)

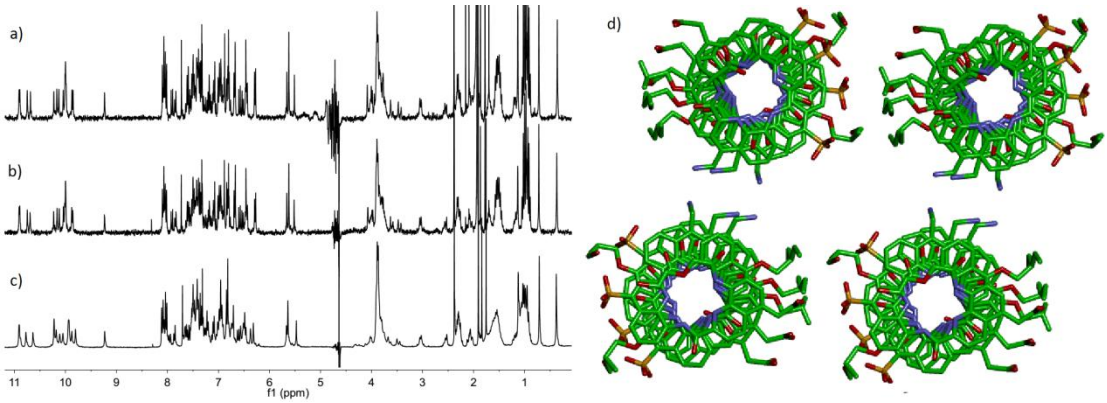

Figure 11. Variable concentration ^{1}H NMR (300 MHz) spectra of foldamer **8** in 10%D_2O/H_2O in a) 0.5 mM, b) 2.0 mM, and c) 8 mM. d) Crystal structure of foldamer **8**. Carbon, nitrogen, oxygen and sulfur atoms are shown in green, blue, red, and orange, respectively. Hydrogen atoms have been omitted for clarity. This crystal structure has not been fully refined.

From this series of designs, we were aware that the hydrophobic effect in water might be much weaker than we expected, in other words, the hydrophobic core should be further enlarged (by putting more hydrophobic side chains) or enhanced (in cooperation with other interactions). What's more, the aminomethyl and carboxymethyl may not be the ideal components of forming salt bridges in our cases. We may consider reusing Asp and Orn side chains if it is necessary. However, in order to gather enough intermolecular interaction information, temporarily, carboxymethyl and aminomethyl side chains will not be replaced since we still need them to provide foldamers with high possibility of crystallization from water.

3.2 Design based on quinoline oligoamide foldamers with more than one hydrophobic side chain per five residues

In general, this design was aimed to increase the hydrophobicity of foldamers and thus enhance the hydrophobic effects (Figure 12). However, different to the strategy of extending the length or the size of hydrophobic side chains as presented above (from leu to hex which might also cause stereohindrance), possessing more than one hydrophobic side chains per five residues on the helical foldamers means a smaller

curvature of the resulting bundles (if the hydrophobic effects take place in the desired way). In addition, there will be fewer positions left for the salt bridge design.

Foldamer **9** had four Leu side chains distributing on two branches of the five-pointed star model of a helix (Figure 12a-b). Nearby were the aminomethyl and carboxymethyl groups for electrostatic interactions as usual. As a consequence, there was only one branch remained for accommodating sulfonic acid side chains to provide water solubility. Thus foldamer **9** would have approximately 40% hydrophobic surface if simply against the five-pointed star model. However, the proton NMR in water was still able to detect a single set of sharp peaks at the concentration as high as 11 mM (see experimental part). Similar to foldamers **6** - **8**, playing with different concentration yielded similar (chemical shifts, the shape and number of the signals) proton NMR spectra indicating either a single helix, or a well-defined assembled structure (or different states exhibiting similar NMR spectra). Crystallization of foldamer **9** was easy and fast, however we have not yet obtain an X-ray analysis data with the resolution better than 1.4 Å to afford a crystal structure up to now.

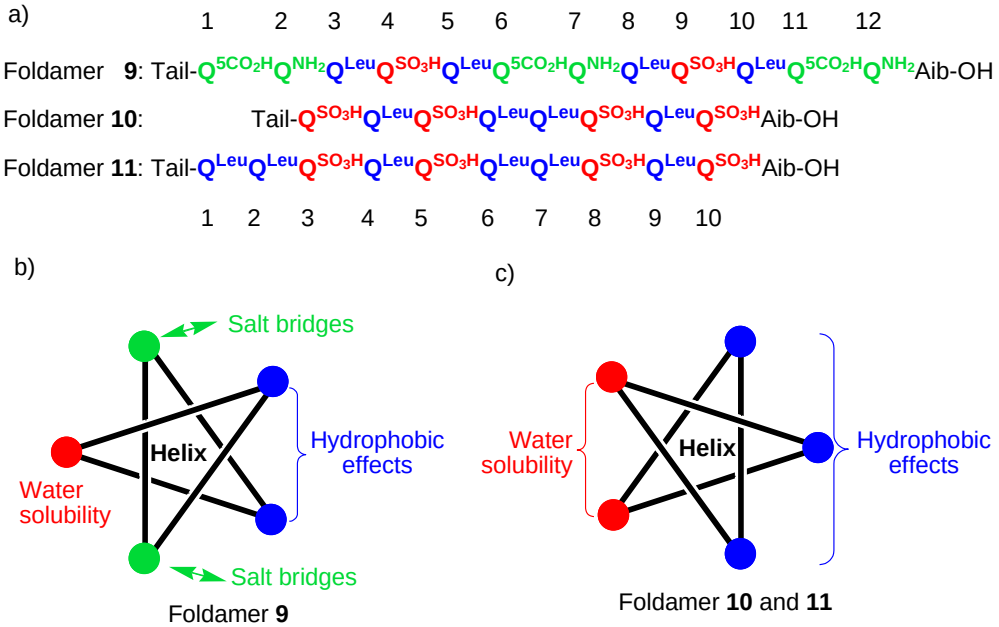

Figure 12. a) Sequences of foldamer **9** – **11**. b) Side chain arrangement of foldamer **9** - **11** on a five-pointed star model. Different color of the quinoline residues indicate their locations on the five-pointed star model.

Inspired by the constantly showed sharp NMR profile of foldamers **6 - 9**, we endeavored to reach the limitation of the sharp NMR profile by increasing the hydrophobicity of these amphiphilic foldamers (foldamers **10** and **11**, Figure 12a). The purpose of this assay was twofold: development of helix bundles with the driving forces purely relying on the hydrophobic effects (Figure 12c); otherwise in the scenario of single helix, examination of the sulfonic acid side chains its ability of accommodating hydrophobic side chains to allow the resulting foldamers being soluble in water. Foldamer **11** was two residues ($\mathbf{Q^{Leu}}$) longer than foldamer **10**. The other part of their sequences and side chain arrangement were the same. However, the proton NMR studies of foldamers **10** and **11** showed again incredibly a single set of sharp signals. Foldamer **10** expressed excellent water solubility in basic water (> 10 mM). Variable concentration ^{1}H NMR studies of foldamer **10** showed slightly up field shifts of the aromatic amide and aromatic proton signals when the concentration increased from 0.5 mM to 10 mM. This was probably because of enhanced stacking of the helix layers and thus a potentially assembled structure (Figure 13a-b). The 10 mM spectrum was slightly broader than the one at 0.5 mM, which was also pointed to the possibility of self-assembly. The solubility of foldamer **11** in basic water was limited to approximately 2 mM (cloudy solution). Higher concentration reaching 4 mM caused precipitation and a very broad NMR spectrum indicating severe aggregation (Figure 13e). Nevertheless, it was still hard to imagine a single set of sharp NMR signals at 2 mM (Figure 13d) and there was no difference of the spectrum comparing to the one at 0.5 mM (Figure 13c). It might be still single helices dominated in the solution. But then it really became an unprecedented discovery that a species could expose roughly 60% hydrophobic surface to water with its concentration remaining at as high as a millimolar level. Another feature of foldamer **10** and **11** is noteworthy. They can also be dissolved in organic solvents under acidic conditions, such as in chloroform with TFA. The ^{1}H NMR spectrum of foldamer **10** was extremely broad (not shown here), but the one of foldamer **11** was relatively distinguishable (see experimental part, Figure 22). They might have chances to form

helix bundles in organic solvents driving by hydrogen bonding, solvophobic effects or metal chelation.

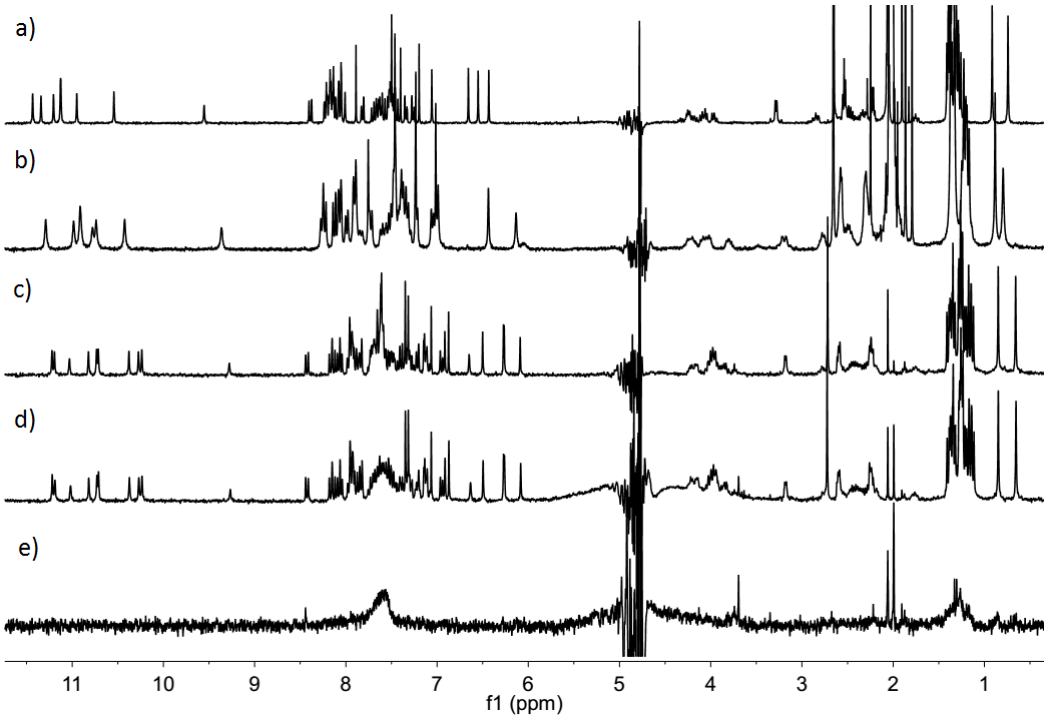

Figure 13. Variable concentration ^{1}H NMR (300 MHz) spectra of foldamer **10** and **11** in 10%D_2O/H_2O. a) 0.5 mM, and b) 10 mM of foldamer **10**; c) 0.5 mM, d) 2.0 mM, and e) 4.0 mM of foldamer **11**.

In line with the same design principle, there are two other strategies can be carried out in future. First one has the same side chain distribution as foldamers **6** – **8** but the hydrophobic core is further enhanced by incorporating a new quinoline residue bearing two hydrophobic side chains (Figure 14a). The second one is based on previous designs. One or two hydrophobic side chains are introduced to both sides of the hydrophobic core (Figure 14b). As a result, hydrophobic and electrostatic interactions will work cooperatively. The case that two hydrophobic side chains sandwich one charged side chain will enhance the salt bridges (by insulating them from surrounding water molecules) while in the other scenario the surrounding salt bridges will secure these covered hydrophobic effect to minimize the possible assembly with other hydrophobic side chains.

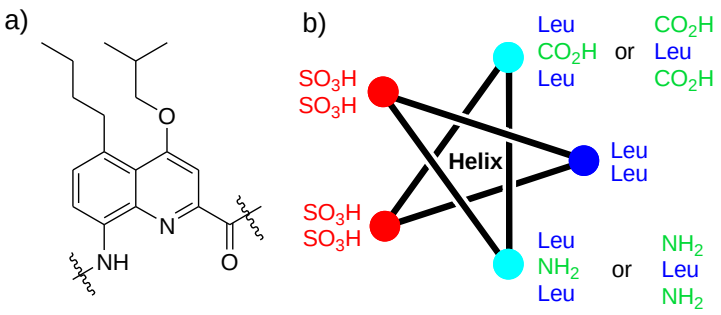

Figure 14. a) New hydrophobic residue bearing two hydrophobic side chains. b) Side chain arrangement of other designs on a five-pointed star model.

3.3 Design based on α-amino acid/quinoline hybrid oligoamide helical foldamers.

In parallel with those designs based on quinoline oligoamide helical foldamers, bundle construction via $\mathbf{(XQ_2)}_n$-type (**X** = α-amino acid, and **Q** = quinoline) hybrid foldamers were also carried out. The design principle also included hydrophobic effects, but in most cases without salt bridges. The reason is that the helical folded structure of $\mathbf{(XQ_2)}_n$-type hybrid foldamers has its side chains arranged in a triangle model (Figure 15). In order to have a proper curvature and water solubility of the resulting helix bundles, in most cases only one branch of the triangle was design to bear hydrophobic side chains. The remaining two branches were either aminomethyl or carboxymethyl side chains to access water solubility and crystal growth ability. However, we also tried one design with these two branches involved in salt bridge formation.

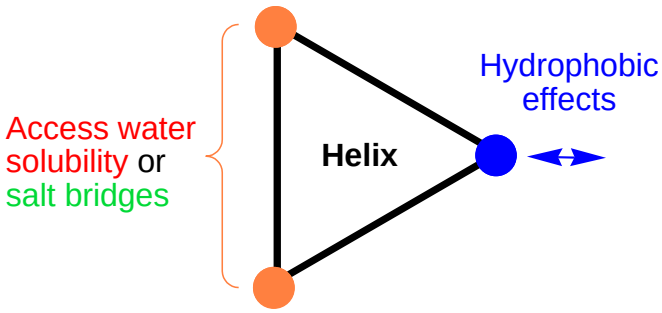

Figure 15. Designs based on $\mathbf{(XQ_2)}_n$-type hybrid foldamers. A triangle model shows side chain arrangement of these hybrid foldamers.

It was not long before we found these **$(XQ_2)_n$**-type hybrid foldamers might not suitable for the helix bundle design. The most fatal factor was its limited positions for hosting side chains for hydrophobic effects, electrostatic interactions and water solubility. As discussed above in the quinoline-based designs, actually one array of hydrophobic side chains were far not hydrophobic enough to induce the assembly consisting more than two helices (or at least not strong enough to maintain the resulting self-assembling structures for long). They either formed a single helix (an undecameric **FQ_2**-type foldamer in chapter two) or a pseudo dimeric bundle (foldamers **6** and **7**). It is also a truth that, if salt bridges are chosen to take place at the remaining two branches, there will be limited space for accessing water solubility and vise versa. Such cases either showed constantly a single set of sharp NMR signals or insoluble in water for NMR studies or crystallization. Another factor was its inherent flexibility comparing to the rigid quinoline oligoamide foldamers. We synthesized an undecameric **SQ_2**-type foldamer for the purpose of constructing helix bundles in organic solvents (not shown here). Its crystal structure from DCM indicated the folded helical structure could be interrupted by the hydrogen bond formation between a single amino acid side chain (serine) and the backbone to form a helix-turn-helix-like conformation.

4. Conclusion and perspectives

Various helix bundle designs based on quinoline and α-amino acid/quinoline hybrid oligoamide foldamers were proposed. The corresponding sequence-dependent foldamers of these designs were synthesized. Their solution phase and solid phase studies up to now indicated no desired (relatively stable and big-sized) helix bundles generated. However, some designs are promising. Compound **10** and **11** may have a potential assembly in water indicated by variable concentration proton NMR and crystallization of these foldamers is in progress. The upcoming new designs also have better chance to yield the desired helix bundle structure. The related synthesis and studies are also in progress. Nevertheless, the recurrence of crystals of these foldamers bearing different side chains validates our assumption in chapter three that shorter side chains can improve the crystal growth ability of aromatic foldamers from water. Once the desired helix bundle structures are obtained, further research emphasis will be placed on their applications, such as:

- Molecular channels (to mimic channel proteins). By constructing helix bundles or helix barrels with different cavities, transportation of molecules with different size and polarity may be achieved.

- Chemical catalysis (to mimic enzymes). Selectively mutation of some side chains on the inner face of helix bundles may create some active sites to catalyze some reactions, such as hydrolysis.

- Folding induction. The self-assembly process of forming a helix bundle in principle is the process of side chains recognition. Through rational design of these side chains on one side of a quinoline-based helical foldamer (targeting interactions with specific side chains on a peptide), induction of an otherwise randomly coiled peptide into a helical conformation may be achieved.

5. Experimental part

5.1 Methods for X-ray crystallography

For crystallization, lyophilized powders of foldamers **1 - 11** were dissolved using ultrapure water such that the foldamer solutions had a final concentration of 2 mM (or 1.0 mM for foldamer **11**). The other process is the same as previous (see chapter three, 5.1). Protocol of structure determination and refinement doesn't show here since all the presented crystal structures in this chapter are partially refined results.

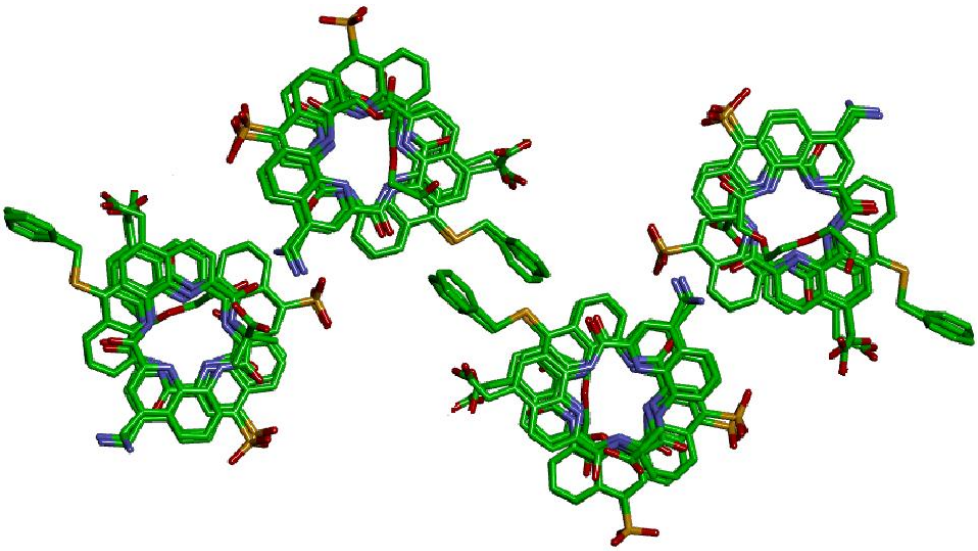

Figure 16. Crystal structure of foldamer **7**. Carbon, nitrogen, oxygen and sulfur atoms are shown in green, blue, red, and orange, respectively. Hydrogen atoms have been omitted for clarity. The crystal structure has not been fully refined yet.

5. 2 Solution phase studies via ^{1}H NMR

Methods for NMR spectroscopy refers to chapter two, 6.3.1.

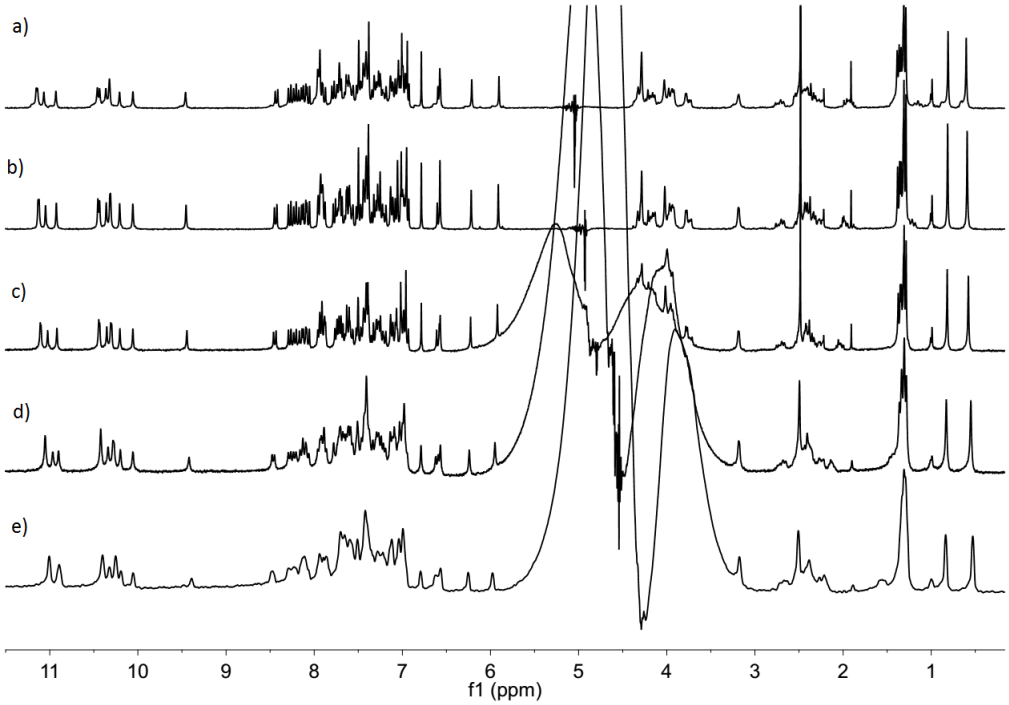

Figure 17. Variable temperature ^{1}H NMR (300 MHz) spectra of foldamer **6** in 10%D_2O/H_2O. a) 5 ^{o}C, b) 10 ^{o}C, c) 25 ^{o}C, d) 50 ^{o}C and e) 75 ^{o}C.

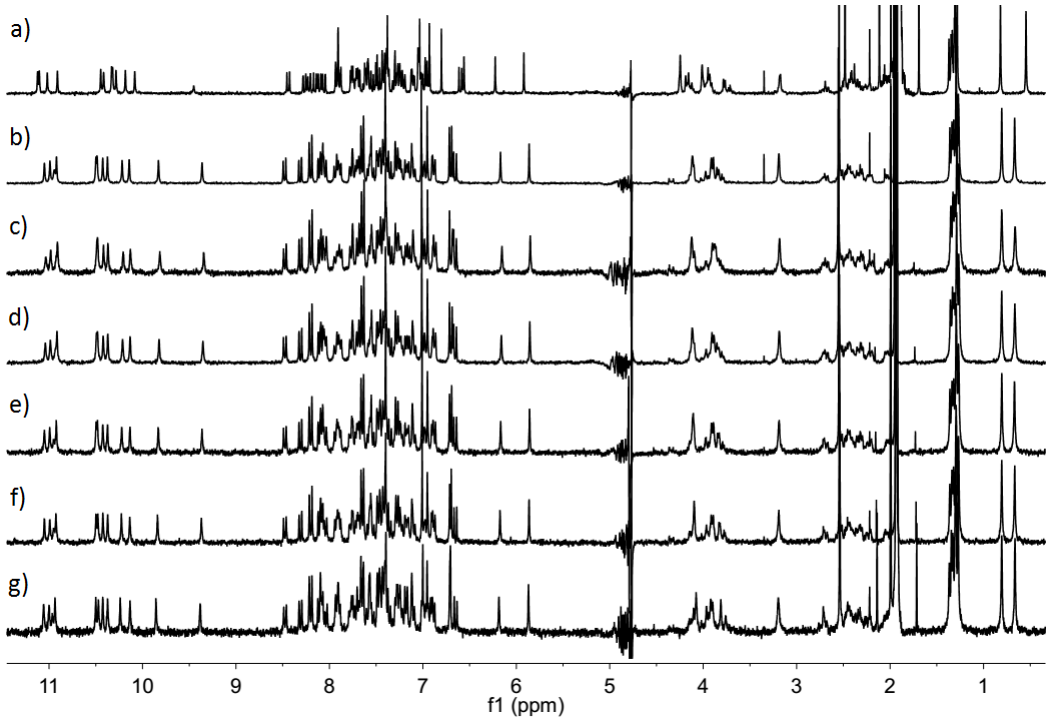

Figure 18. Variable pH ^{1}H NMR (300 MHz) spectra of foldamer **6** in 10%D_2O/H_2O. a) Addition of 0.2 M NH_4OH aqueous solution to reach pH around 9 and b) pure water (pH around 7). Addition of 0.5 M NH_4Ac-AcOH aqueous buffer (pH = 5.6): c) 1 equivalent, d) 3 equivalent, e) 6 equivalent, f) 12 equivalent, and g) 36 equivalent.

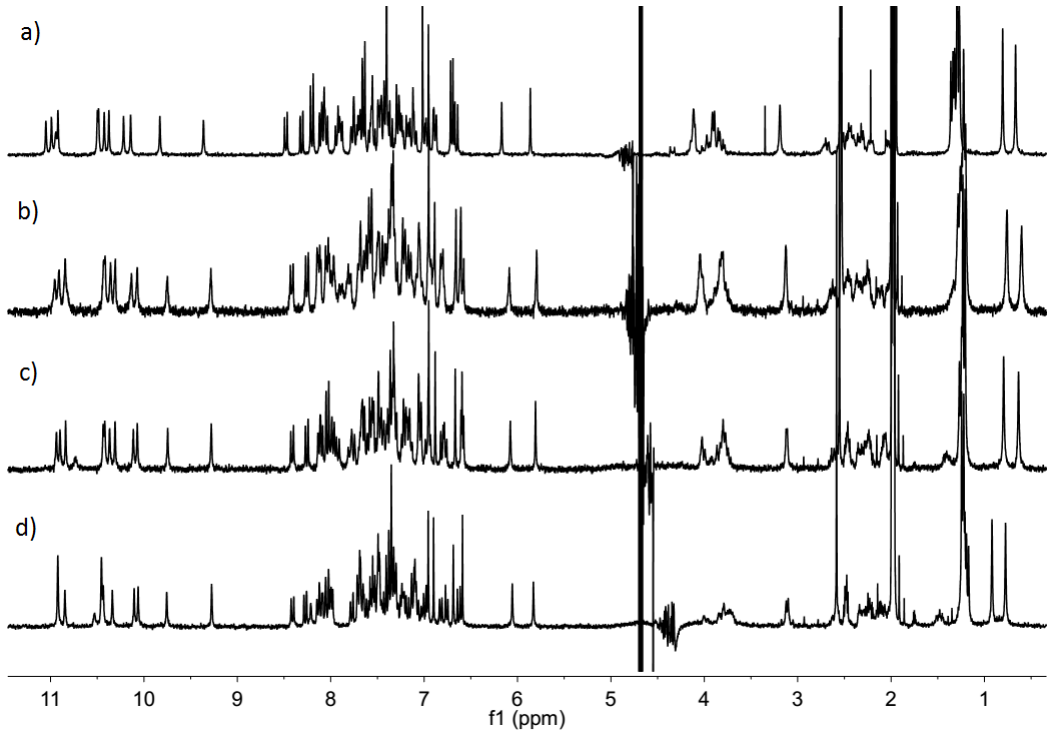

Figure 19. Variable solvent ^{1}H NMR (300 MHz) spectra of foldamer **6** in a) 10%D_2O/H_2O, b) 10%CD_3CN-d_3/H_2O, c) 20%CD_3CN-d_3/H_2O, and d) 40%CD_3CN-d_3/H_2O.

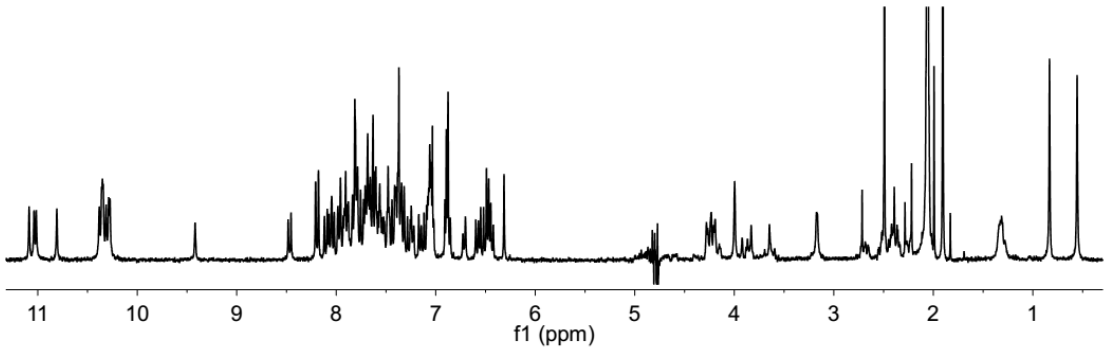

Figure 20. a) ^{1}H NMR (300 MHz) spectra of foldamer **7** in 10%D_2O/H_2O. b) Crystal structure of foldamer **7**. Carbon, nitrogen, oxygen and sulfur atoms are shown in green, blue, red, and orange, respectively. Hydrogen atoms have been omitted for clarity. The crystal structure has not been fully refined yet.

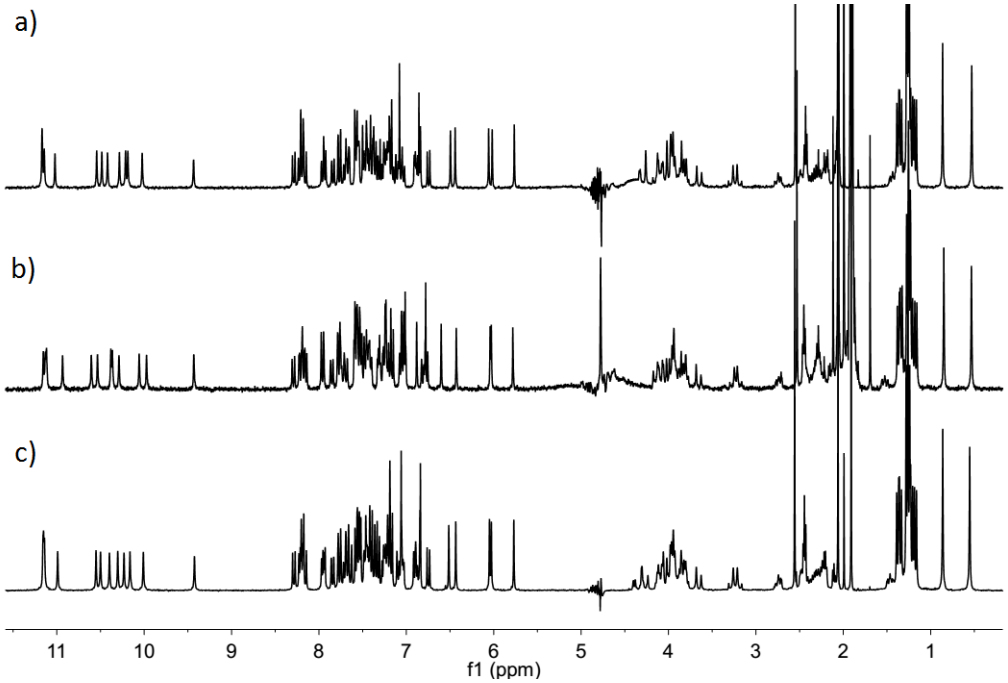

Figure 21. Variable concentration ^{1}H NMR (300 MHz) spectra of foldamer **9** in 10%D_2O/H_2O: a) 0.5 mM, b) 2 mM, and c) 11 mM.

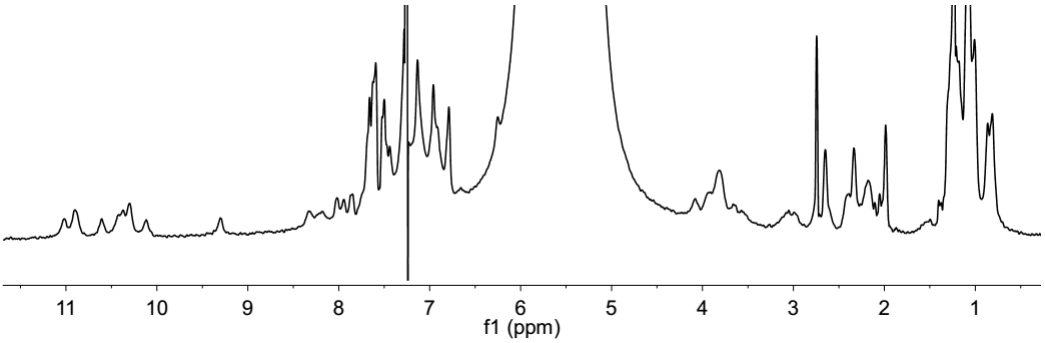

Figure 22. ^{1}H NMR (300 MHz) spectra of foldamer **11** (with TFA) in $CDCl_3$.

5.3 Molecular modeling

MacroModel version 8.6 (Schrödinger Inc.) was used for building the molecular models. The minimization conditions (force field: MMFFs; solvent: water; cutoff: extended; method: TNCG; and maximum iterations: 500) are constant throughout the calculations.

5.4 Methods for chemical synthesis

General procedures refer to chapter two, 6.5.1.

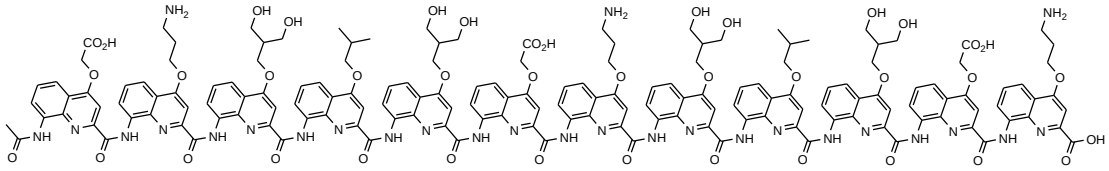

Foldamer **1**

Foldamer **1**: foldamer **1** was synthesized using the SPS procedures previously reported[14] on a 20.5 μmol scale (50 mg of Wang resin, manufacturer's loading 0.41 mmolg^{-1}). The crude product was purified by semi-preparative RP-HPLC (5-40% B, over 15 min) to afford the title compound as a yellow solid (12 mg, 19%, purity by RP-HPLC: > 99%). RP-HPLC (5-40% B, over 10 min) R_t =9.3 min. ^{1}H NMR (300 MHz, DMSO-d_6): δ 10.96 (s, 1H), 10.92 (s, 1H), 10.88 (s, 1H), 10.76 (s, 1H), 10.43 (s, 1H), 10.39 (s, 1H), 10.31 (s, 1H), 10.24 (s, 1H), 10.19 (s, 1H), 10.05 (s, 1H), 9.92 (s, 1H), 8.59 (m, 3H), 8.23 – 8.05 (m, 7H), 7.99 (d, J = 7.2 Hz, 1H), 7.82 (d, J = 7.5 Hz, 1H), 7.70 – 6.85 (m, overlapped with –NH_3^+ signals), 6.74 (s, 1H), 6.55 (s, 1H), 6.42 (s, 1H), 6.32 (s, 1H), 6.26 (s, 1H), 5.96 (s, 1H), 5.86 - 5.65 (m, 6H), 5.32 (m, 1H), 5.09 - 5.01 (m, 2H), 4.88 - 4.76 (m, 4H), 4.74 - 4.57 (m, 4H), 4.50 – 3.00 (m, overlapped with water peak), 2.60 – 2.00 (m, overlapped with DMSO peak), 1.35 - 1.20 (m, 15 H). HRMS: calcd. for $C_{161}H_{153}N_{27}O_{40}$ $[M + 2H]^{2+}$ 1552.5401; found 1552.5572.

14. a) B. Baptiste, C. Douat-Casassus, K. Laxmi-Reddy, F. Godde, and I. Huc, *J. Org. Chem.* **2010**, 75, 7175; b) S. J. Dawson, X. Hu, S. Claerhout, and I. Huc, *Meth. Enzym.* **2016**, 580, 279.

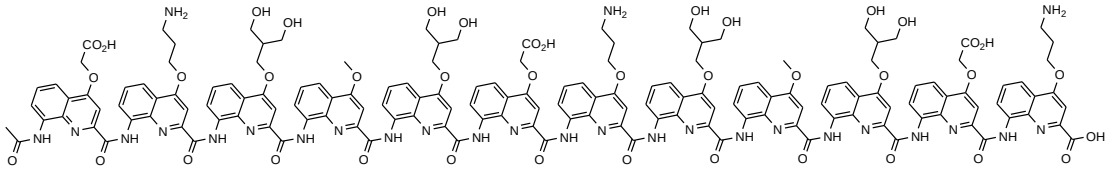

Foldamer **2**

Foldamer **2**: foldamer **2** was synthesized using the SPS procedures previously reported[14] on a 20.5 μmol scale (50 mg of Wang resin, manufacturer's loading 0.41 mmolg^{-1}). The crude product was purified by semi-preparative RP-HPLC (25-35% B, over 15 min) to afford the title compound as a yellow solid (15 mg, 24%, purity by RP-HPLC: 96%). RP-HPLC (25-35% B, over 10 min) R_t = 7.0 min. ^{1}H NMR (300 MHz, DMSO-d_6): δ 10.99 (s, 2H), 10.91 (s, 1H), 10.80 (s, 1H), 10.53 (s, 1H), 10.43 (s, 1H), 10.36 (s, 1H), 10.33 (s, 1H), 10.28 (s, 1H), 10.12 (s, 1H), 10.08 (s, 1H), 8.39 - 8.25 (m, 4H), 8.05 - 7.85 (m, 8H), 7.69 – 7.05 (m, overlapped with –NH_3^+ signals), 6.97 - 6.91 (m, 3H), 6.78 (s, 1H), 6.60 (s, 1H), 6.42 (s, 1H), 6.31 (s, 1H), 6.30 (s, 1H), 6.01 (s, 1H), 5.95 (s, 1H), 5.82 - 5.71 (m, 5H), 5.35 (m, 1H), 5.08 - 5.03 (m, 1H), 4.91 - 4.58 (m, 12H), 4.38 - 4.25 (m, 3H), 3.99 - 3.02 (m, overlapped with water peak), 2.50 - 2.00 (m, overlapped with DMSO peak), 1.26 (m, 3H). HRMS: calcd. for $C_{155}H_{141}N_{27}O_{40}$ $[M + 2H]^{2+}$ 1509.9909; found 1510.0121.

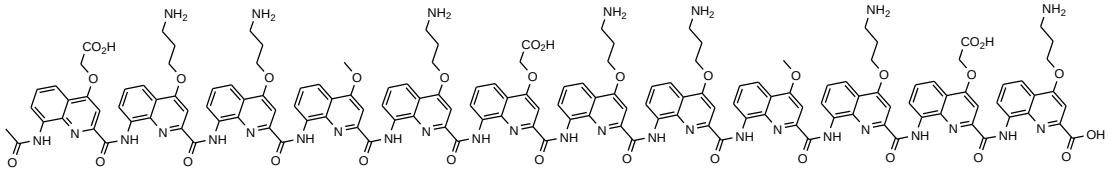

Foldamer **3**

Foldamer **3**: foldamer **3** was synthesized using the SPS procedures previously reported[14] on a 20.5 μmol scale (50 mg of Wang resin, manufacturer's loading 0.41 mmolg^{-1}). The crude product was purified by semi-preparative RP-HPLC (20-30% B, over 15 min) to afford the title compound as a yellow solid (18 mg, 30%, purity by RP-HPLC: 98%). RP-HPLC (20-28% B, over 10 min) R_t = 5.3 min. ^{1}H NMR (300 MHz, DMSO-d_6): δ 10.98 (s, 1H), 10.90 (s, 1H), 10.87 (s, 1H), 10.77 (s, 1H), 10.59 (s,

1H), 10.47 (s, 1H), 10.41 (s, 2H), 10.37 (s, 1H), 10.24 (s, 1H), 10.22 (s, 1H), 8.25 - 7.79 (m, overlapped with $-NH_3^+$ signals), 7.69 - 7.40 (m, overlapped with $-NH_3^+$ signals), 7.29 - 6.87 (m, 18H), 6.77 (s, 1H), 6.61 (s, 1H), 6.34 (s, 1H), 6.28 (s, 2H), 6.04 (s, 1H), 5.93 (s, 1H), 5.78 - 5.71 (m, 5H), 5.32 (m, 1H), 5.06 - 4.53 (m, 6H), 4.38 - 3.87 (m, 19H), 3.30 – 3.00 (m, overlapped with water peak), 2.50 – 2.00 (m, overlapped with DMSO peak), 0.98 (s, 3H). HRMS: calcd. for $C_{151}H_{137}N_{31}O_{32}$ [M + 2H]$^{2+}$ 1448.0017; found 1448.0089.

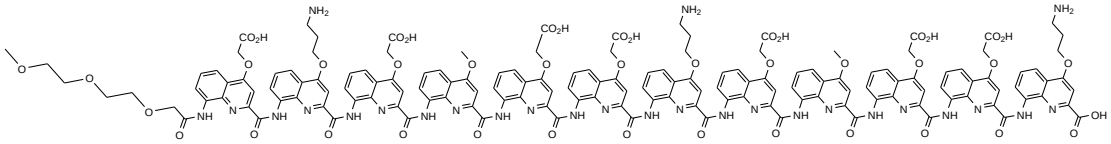

Foldamer **4**

Foldamer **4**: foldamer **4** was synthesized using the SPS procedures previously reported[14] on a 20.5 μmol scale (50 mg of Wang resin, manufacturer's loading 0.41 mmolg^{-1}). The crude product was purified by semi-preparative RP-HPLC (10 - 20% D, over 15 min) to afford the title compound as a yellow solid (14 mg, 23%, purity by RP-HPLC: 98%). RP-HPLC (13 - 19% D, over 10 min) R_t = 9.5 min. ^{1}H NMR (300 MHz, DMSO-d_6): δ 10.99 (s, 1H), 10.94 (s, 1H), 10.78 (s, 2H), 10.52 (s, 1H), 10.38 (s, 1H), 10.30 (s, 1H), 10.26 (s, 2H), 10.13 (s, 1H), 10.09 (s, 1H), 9.15 (s, 1H), 8.30 (br, 2H), 8.02 - 7.95 (m, 2H), 7.88 - 7.80 (m, 3H), 7.76 - 7.59 (m, 13H), 7.48 - 6.92 (m, overlapped with NH_4^+), 6.78 (s, 1H), 6.56 (s, 1H), 6.36 (s, 1H), 6.30 (s, 1H), 6.24 (s, 1H), 5.99 (s, 1H), 5.89 (s, 1H), 5.80 (s, 1H), 5.71 (s, 1H), 5.66 (s, 1H), 5.64 (s, 1H), 5.09 - 5.03 (m, 1H), 4.89 - 4.55 (m, 15H), 4.36 - 3.00 (m, overlapped with water peak), 2.55 - 2.00 (m, overlapped with DMSO peak). HRMS: calcd. for $C_{152}H_{127}N_{27}O_{43}$ [M + 2H]$^{2+}$ 1508.9285; found 1508.9353.

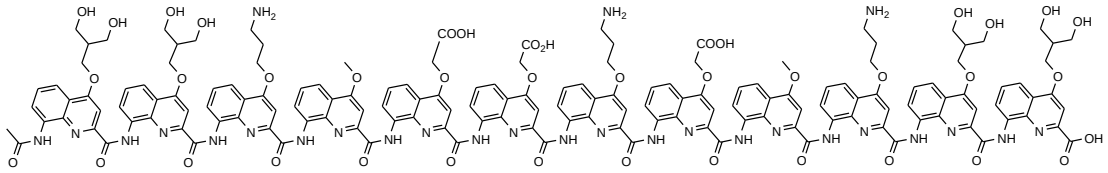

Foldamer **5**

Foldamer **5**: foldamer **5** was synthesized using the SPS procedures previously reported[14] on a 20.5 μmol scale (50 mg of Wang resin, manufacturer's loading 0.41 mmolg^{-1}). The crude product was purified by semi-preparative RP-HPLC (25 - 35% B, over 15 min) to afford the title compound as a yellow solid (15 mg, 24%, purity by RP-HPLC: 96%). RP-HPLC (25 - 35% B, over 10 min) R_t = 6.2 min. ^{1}H NMR (300 MHz, DMSO-d_6): δ 10.97 (s, 1H), 10.94 (s, 1H), 10.86 (s, 1H), 10.77 (s, 1H), 10.52 (s, 1H), 10.31 (s, 1H), 10.27 (s, 1H), 10.20 (s, 1H), 10.18 (s, 1H), 10.11 (s, 1H), 10.07 (s, 1H), 8.28 (br, 1H), 8.19 (br, 2H), 8.06 - 7.95 (m, 6H), 7.75 - 7.04 (m, overlapped with –NH_3^+), 6.96 - 6.85 (m, 3H), 6.75 (s, 1H), 6.72 (s, 1H), 6.41 (s, 1H), 6.38 (s, 1H), 6.26 (s, 1H), 5.95 (s, 1H), 5.93 (s, 1H), 5.84 (s, 1H), 5.77 (s, 1H), 5.74 (s, 1H), 5.73 (s, 1H), 5.67 (s, 1H), 4.87 - 4.59 (m, 9H), 4.36 - 3.93 (m, 17H), 3.75 - 3.00 (m, overlapped with water peak), 2.50 - 2.00 (m, overlapped with DMSO peak), 0.98 (s, 3H). HRMS: calcd. for $C_{155}H_{141}N_{27}O_{40}$ $[M + 2H]^{2+}$ 1510.4932; found 1510.4981.

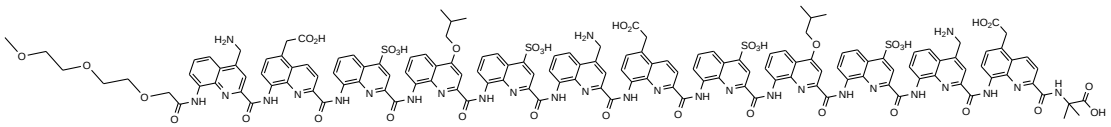

Foldamer **6**

Foldamer **6**: foldamer **6** was synthesized using the SPS procedures previously reported[14] on a 20.5 μmol scale (50 mg of Wang resin, manufacturer's loading 0.41 mmolg^{-1}). The crude product was purified by semi-preparative RP-HPLC (12 - 17% D, over 10 min) to afford the title compound as a yellow solid (10 mg, 16%, purity by RP-HPLC: > 99%). RP-HPLC (12 - 17% D, over 7 min) R_t = 7.4 min. ^{1}H NMR (300 MHz, 10%D_2O/H_2O, *v*/*v*%): δ 11.05 (s, 1H), 10.99 (s, 1H), 10.94 (br, 1H), 10.92 (s,

1H), 10.50 (s, 1H), 10.49 (s, 1H), 10.43 (s, 1H), 10.38 (s, 1H), 10.22 (s, 1H), 10.14 (s, 1H), 9.83 (s, 1H), 9.36 (s, 1H), 8.48 (d, *J* = 8.7, 1H), 8.31 (d, *J* = 7.8, 1H), 8.20 (d, *J* = 8.7, 2H), 8.12 - 8.03 (m, 4H), 7.95 - 7.88 (m, 3H), 7.78 - 7.08 (m, overlapped with $-NH_3^+$ peak, 29H), 7.02 - 6.87 (m, 6H), 6.72 - 6.64 (m, 3H), 6.17 (s, 1H), 5.86 (s, 1H), 4.15 - 3.77 (m, 6H), 3.19 (s, 1H), 2.74 - 2.01 (m, 12H), 1.36 - 1.27 (m, 12H), 0.81 (s, 3H), 0.67 (s, 3H). HRMS: calcd. for $C_{148}H_{126}N_{28}O_{38}S_4$ $[M + 2H]^{2+}$ 1515.3830; found 1515.3799.

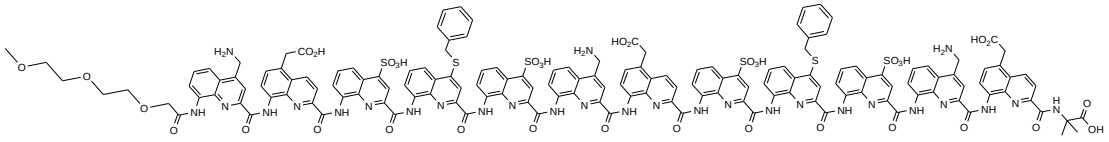

Foldamer **7**

Foldamer **7**: foldamer **7** was synthesized using the SPS procedures previously reported[14] on a 20.5 μmol scale (50 mg of Wang resin, manufacturer's loading 0.41 $mmolg^{-1}$). The crude product was purified by semi-preparative RP-HPLC (13 - 23% D, over 10 min) to afford the title compound as a yellow solid (12 mg, 19%, purity by RP-HPLC: 99%). RP-HPLC (13 - 23% D, over 7 min) R_t = 7.0 min. ^{1}H NMR (300 MHz, 10%D_2O/H_2O, *v*/*v*%): δ 11.09 (s, 1H), 11.04 (s, 1H), 11.01 (s, 1H), 10.81 (s, 1H), 10.38 - 10.27 (m, 7H), 9.42 (s, 1H), 8.47 (d, *J* = 9.0 Hz, 1H), 8.19 (d, *J* = 8.4 Hz, 2H), 8.12 - 7.22 (m, overlapped with $-NH_3^+$ peak), 7.17 - 7.02 (m, 7H), 6.91 - 6.85 (m, 4H), 6.73 - 6.70 (m, 1H), 6.60 - 6.42 (m, 5H), 6.31 (m, 1H), 4.28 - 3.66 (m, 7H), 3.17 (m, 1H), 2.72 - 2.22 (m, 9H), 0.83 (s, 3H), 0.56 (s, 3H). MS: calcd. for $C_{154}H_{122}N_{28}O_{36}S_6$ $[M + 2H]^{2+}$ 1566.3484; found 1566.2062.

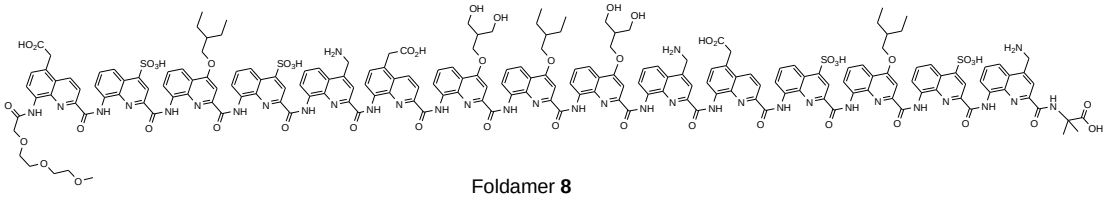

Foldamer **8**

Foldamer **8**: foldamer **8** was synthesized using the SPS procedures previously reported[14] on a 20.5 μmol scale (50 mg of Wang resin, manufacturer's loading 0.41 mmolg^{-1}). The crude product was purified by semi-preparative RP-HPLC (20 - 25% D, over 10 min) to afford the title compound as a yellow solid (11 mg, 14%, purity by RP-HPLC: 94%). RP-HPLC (20 - 25% D, over 7 min) R_t = 6.4 min. ^{1}H NMR (300 MHz, 10%D_2O/H_2O, *v*/*v*%): δ 10.91 (s, 2H), 10.78 (s, 1H), 10.64 (s, 1H), 10.22 (s, 2H), 10.18 (s, 1H), 10.11 (s, 1H), 10.05 (s, 1H), 9.94 (s, 3H), 9.88 (s, 1H), 9.80 (s, 1H), 9.23 (s, 1H), 8.11 - 7.85 (m, 8H), 7.71 - 6.46 (m, overlapped with –NH_3^+ peak), 6.37 (s, 1H), 6.32 (s, 1H), 5.67 - 5.62 (m, 2H), 5.48 (s, 1H), 4.31 - 3.44 (m, 19H), 3.08 - 3.01 (m, 1H), 2.58 - 2.51 (m, 1H), 2.38 - 2.26 (m, 7H), 2.13 - 2.02 (m, 2H), 1.72 - 1.43 (m, 9H), 1.13 - 0.93 (m, 17H), 0.71 (s, 3H), 0.38 (s, 3H). HRMS: calcd. for $C_{196}H_{180}N_{34}O_{48}S_4$ $[M + 2H]^{2+}$ 1952.5780; found 1952.5770.

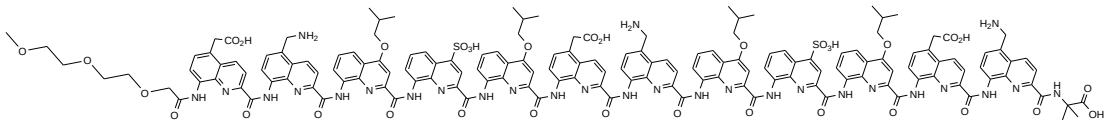

Foldamer **9**

Foldamer **9**: foldamer **9** was synthesized using the SPS procedures previously reported[14] on a 20.5 μmol scale (50 mg of Wang resin, manufacturer's loading 0.41 mmolg^{-1}). The crude product was purified by semi-preparative RP-HPLC (20 - 30% D, over 10 min) to afford the title compound as a yellow solid (11 mg, 18%, purity by RP-HPLC: > 99%). RP-HPLC (25 - 28% D, over 7 min) R_t = 7.1 min. ^{1}H NMR (300 MHz, 10%D_2O/H_2O, *v*/*v*%): δ 11.09 (m, 3H), 11.07 (s, 1H), 10.92 (s, 1H), 10.48 (s, 1H), 10.43 (s, 1H), 10.33 (s, 1H), 10.24 (s, 1H), 10.16 (s, 1H), 10.10 (s, 1H), 9.94 (s, 1H), 9.36 (s, 1H), 8.22 (d, *J* = 8.7 Hz, 1H), 8.16 - 8.08 (m, 4H), 7.90 - 7.86 (m, 2H), 7.78 (d, *J* = 8.7 Hz, 1H), 7.70 (d, *J* = 8.4 Hz, 2H), 7.65 - 7.09 (m, 25H), 7.04 - 6.96 (m, 4H), 6.85 - 6.77 (m, 4H), 6.68 (d, *J* = 8.7 Hz, 1H), 6.45 (s, 1H), 6.37 (s, 1H), 5.98 (s, 1H), 5.96 (s, 1H), 5.70 (s, 1H), 4.34 - 4.17 (m, 1H), 4.08 - 3.74 (m, 10H), 3.62 - 3.56 (m, 1H), 3.24 - 3.10 (m, 1H), 2.72 - 2.64 (m, 1H), 2.49 (m, 3H), 2.43 - 2.12 (m, 8H),

1.32 - 1.27 (m, 6H), 1.21 - 1.10 (m, 18H), 0.80 (s, 3H), 0.49 (s, 3H). HRMS: calcd. for $C_{156}H_{142}N_{28}O_{34}S_2$ $[M + 2H]^{2+}$ 1507.4837; found 1507.4903.

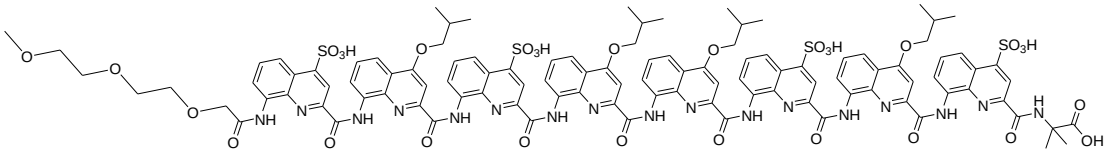

Foldamer **10**

Foldamer **10**: foldamer **10** was synthesized using the SPS procedures previously reported[14] on a 20.5 μmol scale (50 mg of Wang resin, manufacturer's loading 0.41 $mmolg^{-1}$). The crude product was purified by semi-preparative RP-HPLC (40 - 50% D, over 10 min) to afford the title compound as a yellow solid (10 mg, 22%, purity by RP-HPLC: 99%). RP-HPLC 42 - 47% D, over 7 min) R_t = 6.5 min. ^{1}H NMR (300 MHz, 10%D_2O/H_2O, *v*/*v*%): δ 11.43 (s, 1H), 11.34 (s, 1H), 11.21 (s, 1H), 11.13 (s, 2H), 10.95 (s, 1H), 10.54 (s, 1H), 9.55 (s, 1H), 8.39 (d, *J* = 9.0 Hz, 1H), 8.24 - 8.01 (m, 11H), 7.89 (s, 1H), 7.82 (d, *J* = 6.9 Hz, 1H), 7.72 – 7.40 (m, 12H), 7.34 (d, *J* = 6.9 Hz, 1H), 7.27 (d, *J* = 6.9 Hz, 1H), 7.20 (s, 1H), 7.06 (s, 1H), 6.66 (s, 1H), 6.55 (s, 1H), 6.43 (s, 1H), 4.36 - 3.94 (m, 3H), 3.34 - 3.24 (m, 1H), 2.65 (s, 3H), 2.55 - 2.20 (m, 7H), 1.41 - 1.26 (m, 24H), 0.92 (s, 3H), 0.74 (s, 3H). HRMS: calcd. for $C_{107}H_{99}N_{17}O_{30}S_4$ $[M - 2H]^{2-}$ 1114.7819; found 1114.7841.

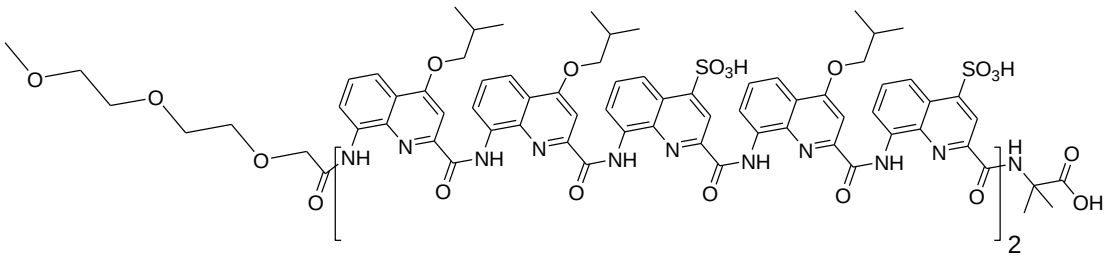

Foldamer **11**

Foldamer **11**: foldamer **11** was synthesized using the SPS procedures previously reported[14] on a 20.5 μmol scale (50 mg of Wang resin, manufacturer's loading 0.41 $mmolg^{-1}$). The crude product was purified by semi-preparative RP-HPLC (60 - 70% D, over 10 min) to afford the title compound as a yellow solid (9 mg, 16%, purity by

RP-HPLC: 94%). RP-HPLC 60 - 70% D, over 7 min) R_t = 6.3 min. ^{1}H NMR (300 MHz, 10%D_2O/H_2O, *v*/*v*%): δ 11.22 (s, 1H), 11.19 (s, 1H), 11.03 (s, 1H), 10.82 (s, 1H), 10.73 (s, 1H), 10.71 (s, 1H), 10.38 (s, 1H), 10.27 (s, 1H), 10.24 (s, 1H), 9.28 (s, 1H), 8.43 (d, *J* = 8.7 Hz, 1H), 8.18 - 8.04 (m, 4H), 7.98 - 7.83 (m, 8H), 7.76 - 7.25 (m, overlapped with NH_4^+ signals), 7.22 (d, *J* = 7.5 Hz, 1H), 7.14 - 7.11 (m, 3H), 7.06 (s, 1H), 6.97 – 6.92 (m, 2H), 6.87 (s, 1H), 6.65 (s, 1H), 6.50 (s, 1H), 6.27 (s, 1H), 6.27 (s, 1H), 6.09 (s, 1H), 4.25 - 3.73 (m, 7H), 3.24 - 3.12 (m, 2H), 2.72 (s, 3H), 2.61 - 2.19 (m, 11H), 1.41 - 1.12 (m, 36H), 0.85 (s, 3H), 0.66 (s, 3H). HRMS: calcd. for $C_{135}H_{127}N_{21}O_{34}S_4$ $[M - 2H]^{2-}$ 1356.8874; found 1356.8890.

Conclusion and perspectives

Aromatic oligoamide foldamers are a promising class of biological mimics considering not only their ability of mimicking protein secondary structures but also those biological applications achieved in this field, such as protein recognition, DNA recognition, cell-penetration and protein tertiary structure mimics. A series study of water-soluble aromatic oligoamide foldamers in this thesis uncovers their folding, crystallization and self-assembling behavior in water and, further, provides knowledge for the structure and assembly studies of other systems in water. The solid phase synthetic methodology and water-soluble short side chains developed here pave an avenue to fast access hybrid oligoamide foldamers and endow aromatic foldamers with crystal growth ability from water, respectively. Those designs for constructing helix bundles with water-soluble quinoline-related oligoamide foldamers described in the last chapter, together with those developed methods, represent a new strategy to study helix bundle architectures and a novel platform of constructing higher-level protein structure mimics.

Firstly, an efficient solid phase methodology was developed. This method allows the coupling of α-amino acid onto aromatic amine to take place while can still control the racemization of α-amino acid under negligible range, for what most coupling reagents and normal acyl halide protocols cannot serve. Together with the dimer strategy for addressing those difficult cases (e.g. Aib), fast access of α-amino acid/quinoline hybrid oligoamides was achieved. Afterwards solution phase studies of the water-soluble hybrid oligoamides by CD and NMR indicated the folding behavior and the resulting folded conformation of $(\mathbf{XQ})_n$-type foldamers in water are unpredictable while, in contrast, $(\mathbf{XQ_2})_n$-type foldamers can adopt stable helically folded conformation. The molecular model based on NOE correlations and the most recently single crystal structure of $(\mathbf{XQ_2})_n$-type foldamers unambiguously showed that α-amino acid side chains were arranged in a linear array on one side of the helix. Remarkably, they also demonstrated that these α-amino acid residues can indeed have the chance to adopt the different hydrogen bonding mode parallel to the helix axis as

showed in the proposed molecular model in chloroform previously shedding light on conformational preferences of these hybrid sequences under different conditions.

The identified short side chains in chapter three are promising for the purpose of improving solubility and crystal growth ability of aromatic foldamers in/from water. Six oligoamides displaying these side chains were synthesized to show their ability of endowing otherwise very hydrophobic aromatic foldamers with water solubility and also to validate our assumption that the shorter and more rigid side chains can favor the crystallization of aromatic foldamers from water. The difference in crystal growth ability of oligomers bearing carboxymethyl side chains on one hand, and those with aspartic acid-like side chains on the other hand, is striking considering that the side chains of the latter are just one atom longer than those of the former. The results in the case of helical aromatic amide foldamers may certainly be extrapolated to other aromatic molecular and supramolecular systems. Extrapolation to other short and rigid polar functionalities may also be considered.

At last, different strategies of constructing helix bundles using aromatic oligoamide helical foldamers were discussed. The corresponding quinoline-based or α-amino acid/quinoline hybrid oligoamide foldamers were synthesized to investigate their self-assembling behavior in water. NMR and crystallographic studies in water indicated hydrophobic effect is much weaker than expected and the electrostatic interactions (or salt bridges) take place in the undesired way. Nevertheless, the recurrence of crystals of these foldamers bearing different side chains validates again our assumption that crystal growth ability of aromatic foldamers could be improved by installing shorter and more rigid side chains. Moreover, the helix pair (or pseudo dimeric bundle) was able to form under the guide of simply hydrophobic effect. In the end, by continuously increasing the hydrophobicity of quinoline oligoamide foldamers, a striking situation was reached that a decamer with six isobutoxy side chains covering ~60% surface of the helix can still express one set of sharp NMR signals at the concentration as high as milli molar range in water.

Further researches of these aromatic oligoamide foldamers in water can be

envisioned. With the developed SPS method and the property of linear arrangement of α-amino acid side chains on one side of the helix, different $(\mathbf{XQ_2})_n$-type foldamers displaying diverse α-amino acid side chains can be synthesized targeting the applications on biological systems. Such applications could be protein recognition, cell-penetration, protein structure mimics, and so on. Those developed water-soluble shorter side chains will be certainly of particular use for constructing water-soluble aromatic architectures and facilitating the crucial structure elucidation process in solid state. Thus, for instance, manifestation of aromatic β-sheets structures from water could be envisioned. Moreover, solid state structural investigation of those aromatic foldamers with remarkable properties that have been observed in aqueous media, including endomolecular recognition and double helix formation, could also be planed. For the helix bundle studies, further enhancement of hydrophobic effect and more accurate or sophisticated designs will be considered. Afterwards, with the successful cases of helix bundles, some biological applications could be imagined. For example, these bundles with large cavities could serve as molecular channels and chemical catalyst after proper modifications.

Appendix I. List of abbreviations

Boc : *tert*-butyloxycarbonyl
Cbz : carboxybenzyl
CD : circular dichroism
COSY : correlation spectroscopy
C.P. : crude purity
CPK : Corey, Pauling, Koltune space filling
DBU : 1,8-Diazabicyclo[5.4.0]undec-7-ene
DCM : dichloromethane
DIAD : diisopropyl azodicarboxylate
DIPEA : diisopropylethylamine
DMF : *N*,*N*-dimethylformamide
DTBS : di-tert-butylsilylene
EtOAc : ethyl acetate
ESI : electrospray ionization
Fmoc : Fluorenylmethyloxycarbonyl
Ghosez reagent : 1-chloro-*N*,*N*,2-trimethyl propenylamine
HBTU : N,N,N',N'-Tetramethyl-O-(1H-benzotriazol-1-yl)uronium hexafluorophosphate
HMBC : heteronuclear multiple bond correlation
HOBt : 1-Hydroxybenzotriazole hydrate
RP-HPLC : Reversed-Phase High-Performance Liquid Chromatography
HRMS : high resolution mass spectroscopy
HSQC : heteronuclear single quantum coherence
Me : methyl
MeOH : methanol
MMFFs : Merck Molecular Force Field static
NMR : nuclear magnetic resonance
NOESY : Nuclear Overhauser Effect SpectroscopY
PPh_3 : triphenylphosphine
ppm : parts per million
ROESY : rotating-frame overhauser effect spectroscopy
r.t. : room temperature
SPS : Solid-Phase Synthesis
TBAF : tetra-n-butylammonium fluoride
TCAN : trichloroacetonitrile
TFA : trifluoroacetic acid
THF : tetrahydrofuran
TIS : triisopropylsilane
TLC : thin layer chromatography
TNCG : Truncated Newton Conjugate Gradient
TOCSY : total correlation spectroscopy

Appendix II. List of nomenclature

X: α-amino acid residue;

Q: 8-amino-2-quinolinecarboxylic acid residue;

Tail: 2-(2-(2-methoxyethoxy)ethoxy)acetic acid residue.

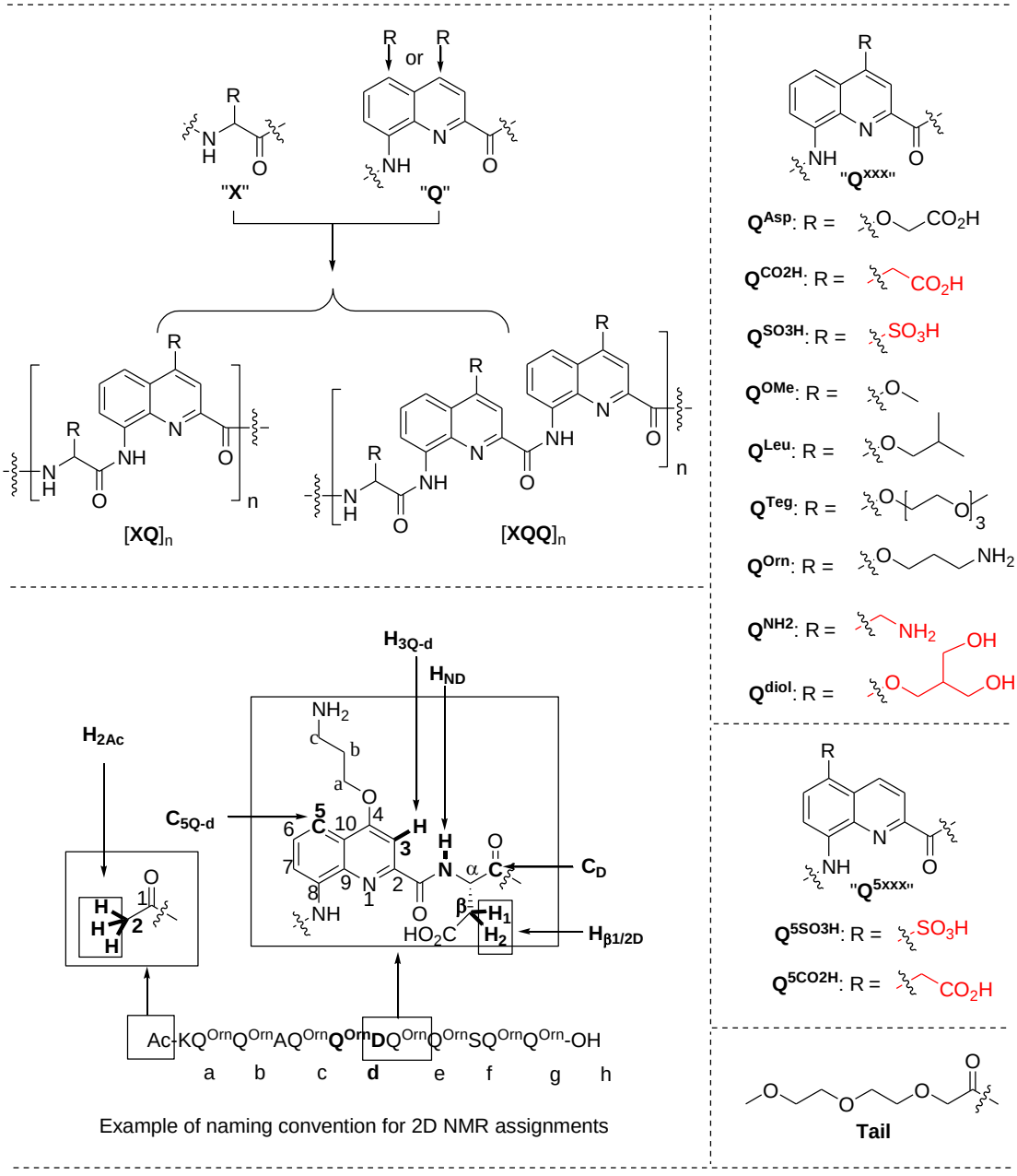

Synthèse, analyses structurales et assemblage de foldamères oligoamide hydrosolubles à base de quinolines

La chimie des foldamères est un domaine de recherche en pleine expansion où les chimistes explorent la construction d'architectures artificielles variées mimant les structures repliées des biopolymères naturels. Les foldamères d'oligoamides quinoline, constituent une branche importante des foldamères montrant de nombreuses caractéristiques attractives, incluant la stabilité et la prédictibilité de leurs conformations repliées, qui en font de bons candidats pour des applications biologiques. Jusqu'à présent, la plupart des études sur les foldamères d'oligoamides quinolines ont été menées dans des solvants organiques. Cette thèse a pour objectif d'étendre leur portée au milieu aqueux et présente plusieurs méthodologies pour parvenir à leur solubilité, leur repliement, la variation de leurs chaines latérales, leur agrégation et leur capacité à former des cristaux dans l'eau.

Tout d'abord, une méthode de synthèse en phase solide a été développée permettant l'accès rapide aux foldamères hybrides α-amino acide/quinoline (**X**/**Q**). Leur étude dans l'eau montre que contrairement aux foldamères hybrides de type $(\mathbf{XQ})_n$, ceux de type $(\mathbf{XQ_2})_n$ sont capables d'adopter une conformation hélicoïdale présentant un alignement des chaines α-amino acides dans l'espace. Ensuite, plusieurs chaines latérales courtes ont été identifiées pour doter les foldamères aromatiques d'une solubilité et d'une capacité à cristalliser dans l'eau. Six oligoamides quinoline ont ainsi été synthétisés pour une étude modèle. Des cristaux ont été obtenus pour toutes les séquences sauf une, présentant une excessive solubilité dans l'eau. Enfin, des efforts ont été faits pour construire des faisceaux d'hélices auto-assemblés dans l'eau à base d'effets hydrophobes et d'interactions électrostatiques. Les études RMN et cristallographiques ont indiqué que les effets hydrophobes étaient plus faibles qu'attendu et ne provoquaient pas d'agrégation forte.

Mots clés: foldamère, hélice, synthèse en phase solide, faisceaux d'hélices, foldamère hybride, auto-assemblage, cristallographie, assignation RMN, foldamère hydrosoluble, acide α-aminé.

Synthesis, structural analysis, and assembly of water soluble quinoline-based oligoamide foldamers

Foldamer chemistry is a rapidly expanding research field where chemists explore the construction of various artificial architectures that mimic the folded structures of biopolymers found in nature. Quinoline oligoamide foldamers, as an important branch of foldamers, have been shown to possess many desirable features, including stability and predictability of their folded conformations, and are promising candidates to achieve biological applications. Up to now, most investigations of quinoline oligoamide foldamers have been carried out in organic solvents. This thesis is aimed to expand their scope in aqueous medium and presents several methodologies to achieve solubility, folding, side-chain variation, aggregation and crystal growth ability in water.

First, a solid phase synthesis method was developed to enable the fast access to α-amino acid/quinoline (**X**/**Q**) hybrid oligoamide foldamers. The study of these hybrid foldamers in water showed that contrary to $(\mathbf{XQ})_n$-type foldamers the $(\mathbf{XQ_2})_n$-type foldamers could adopt aromatic helical conformations with α-amino acid side chains aligned in space. Then, several short side chains were identified to endow aromatic foldamers with both solubility in, and crystal growth ability from water. Six quinoline oligoamides displaying these side chains were synthesized as a case study. Crystals were obtained from aqueous medium in all cases but one, exceedingly soluble in water. At last, efforts were made to construct self-assembled aromatic helix bundles in water based on hydrophobic effects and electrostatic interactions. NMR and crystallographic studies indicated that hydrophobic effects are weaker than expected and not strongly conducive of aggregation.

Keywords: foldamer, helix, solid phase synthesis, helix bundle, hybrid foldamer, self-assembly, crystallography, NMR full assignment, water-soluble foldamer, α-amino acid.

UMR 5248 Chimie et Biologie des Membranes et Nanoobjets (CBMN)
Institut Européen de Chimie et Biologie (IECB)
2 rue Robert Escarpit 33607 PESSAC CEDEX